TRANSCRIPTOMIC ANALYSIS OF THE ROLE OF HDAC4 IN CARDIAC DIFFERENTIATION OF MOUSE EMBRYONIC STEM CELLS



Tasabeeh Mohamed

School of Life Sciences

University of Nottingham

This dissertation is submitted for the degree of Doctor of Philosophy

November 2023

DECLARATION

This dissertation is the result of my own work and includes nothing, which is the outcome of work done in collaboration except where specifically indicated in the text. It has not been previously submitted, in part or whole, to any university of institution for any degree, diploma, or other qualification.

ABSTRACT

Embryonic heart development is a complex process that is intricately controlled by various transcription factors and signalling pathways. Perturbations to this process can lead to congenital heart disease, the most common cause of infant mortality in the UK. In this project, cellular models of heart development were used to investigate the function of histone deacetylation in cardiac differentiation. P19CL6 murine embryonic carcinoma cells and murine embryonic stem cells were differentiated and mESCs were chosen for downstream analyses. RNA-Seq was employed to study genes involved in normal differentiation, in addition to the consequences of nonspecific Class II HDACs inhibition using Trichostatin A (TSA) and *Hdac4* knockout mediated by CRISPR/Cas9. Differentiated cells showed lower expression of pluripotency-associated genes such as *Nanog* and *Sox2*. Genes linked with processes like cytoskeletal assembly and extracellular matrix formation were upregulated. Results also suggested that Trichostatin A treatment and *Hdac4* knockout may have contributed to changes in gene expression. TSA was found to alleviate repression of *Tbx5* and *Hand2*. *Hdac4* knockout uncovered a possible role for methylation in cardiomyocyte gene regulation. Contractility genes were also investigated by comparing the transcriptional profiles of beating with non-beating differentiated cells. Genes associated with congenital heart disease, such as *Tnni3* and *Myh6* were identified. This analysis also revealed a newly-identified pathogenic gene, *Ryr2*, as well as the candidate gene *Sh3bgr*. While the results are not fully conclusive and require further validation, this study corroborated that HDACs play a regulatory role in cardiac differentiation and contractility and found an interesting similarity between the consequences of pan-HDAC inhibition and specific *Hdac4* knockout.

ACKNOWLEDGEMENTS

I would first like to thank the University of Nottingham International Office for making my PhD possible through the Vice Chancellor Scholarship. I would also like to show utmost gratitude to Professor Brook for his constant guidance, support and mentorship. Thank you for always reminding me of the value of my work and having faith in me as a scientist. I will forever be grateful.

I would also like to extend my thanks to everyone I met and worked with in the Brook Lab, Sarah, Kerry, Anna, Anjani, Reem, Marzena and Tushar. This would not have been possible without your constant help, support, coffee breaks and birthday cakes. I am immensely grateful to the team at DeepSeq, University of Nottingham, for their labour, time and expertise.

I would not have been where I am today if it was not for my wonderful support network of friends and family. I am appreciative of all my friends for always lending an ear to my constant complaints and helping through difficult times. I would especially like to thank Aalaa Haider, for going above and beyond what it means to be a friend, and being my family in Nottingham.

To my parents, Mohamed and Nahla, thank you for being a constant source of inspiration. Thank you for always being proud of me no matter what and for your endless love and hard work that got me through not just the PhD, but also life. My wonderful siblings, Khider and Tibyan, thank you for the jokes, the talks and for keeping me grounded. I truly could not have wished for a more loving family and I am blessed to have you.

I would like to thank Khalid, my best friend and his wonderful family. Thank you for being my biggest fan and not letting me give up on myself.

Finally I would like to dedicate this thesis to the revolutionaries and martyrs of the Sudanese Revolution. While this sacrifice is negligible compared to giving your life for a cause, your fight for freedom, peace and justice kept me going, and served as a constant reminder of why I embarked on this journey in the first place, for a better and prosperous Sudan.

CONTENTS

LIST OF ABBREVIATIONS XV
1 INTRODUCTION 1
1.1 MAMMALIAN HEART DEVELOPMENT 1
1.1.1 Embryonic cardiac morphogenesis 1
1.1.2 Chamber formation 4
1.1.3 Chamber septation 7
1.1.4 Outflow tract development 9
1.1.5 Valves formation 11
1.1.6 Genetics of heart development 12
1.1.7 Cardiomyocyte differentiation and development 18
1.1.8 Epigenetics in heart development 23
1.1.9 Histone deacetylases 33
1.1.10 HDACs in cardiac development 41
1.1.11 Background work leading to this project 44
1.1.12 HDAC inhibition 47
1.1.13 Congenital heart disease 47
1.1.14 Animal and cell-based models to study heart development 50
1.1.15 CRISPR/Cas9 genome editing technology 54
1.1.16 Transcriptomic analysis of stem cell differentiation into cardiomyocytes 55
1.1.17 RNA Sequencing 56
1.1.18 Transcriptional profiling of stem cell-derived cardiomyocytes 58
1.2 PROJECT AIMS 61
2 MATERIALS AND METHODS 63
2.1 MICROBIAL TECHNIQUES 63
2.1.1 Bacterial culture plates 63
2.1.2 Culturing colonies 64
2.1.3 MiniPrep: isolating plasmid DNA 64
2.1.4 MaxiPrep to isolate plasmid DNA 64
2.1.5 Glycerol stocks 65

2.2 MOLECULAR TECHNIQUES 65
2.2.1 Polymerase chain reaction *65*
2.2.2 Gel extraction *66*
2.2.3 PCR Clean-up *66*
2.3 CELL CULTURE AND MAINTENANCE 67
2.3.1 Thawing *67*
2.3.2 Freezing *67*
2.3.3 P19CL6 culture *67*
2.3.4 CGR8 mESCs culture *67*
2.3.5 Splitting *68*
2.3.6 P19CL6 cardiomyocyte differentiation *68*
2.3.7 Embryonic Stem Cell Differentiation *69*
2.3.8 Trichostatin A treatment *70*
2.4 IMAGING 71
2.5 BEATING ANALYSIS 71
2.6 IMMUNOFLUORESCENCE 71
2.6.1 Fluorescent imaging *72*
2.7 WESTERN BLOT 72
2.8 CRISPR/CAS9-MEDIATED KNOCK OUT OF *HDAC4* 74
2.8.1 Target site design *74*
2.8.2 sgRNA synthesis *74*
2.8.3 DNA Extraction from CGR8 cells *75*
2.8.4 Polymerase Chain Reaction *75*
2.8.5 In vitro assay *76*
2.8.6 Vector Design *77*
2.8.7 Nucleofection *78*
2.8.8 DNA Extraction *79*
2.8.9 Sequencing *79*
2.8.10 RNA extraction *80*
2.8.11 RNA Library Prep *80*
2.9 RNA SEQUENCING 82
2.9.1 1. Read Alignment *82*
2.9.2 Differential Expression *82*

3 HDAC INHIBITION AND CRISPR/CAS9-MEDIATED KNOCKOUT IN CELLULAR MODELS OF CARDIAC DIFFERENTIATION 84

3.1 INTRODUCTION 84

3.2 CHAPTER AIMS: 87

3.3 RESULTS 88

3.3.1 P19CL6 cells form embryoid bodies 88

3.3.2 P19CL6 differentiated EBs inefficiently form beating cardiomyocytes 90

3.3.3 Mouse embryonic stem cells are capable of forming EBs 91

3.3.4 Embryonic stem cells differentiate into cardiomyocytes more efficiently 94

3.3.5 Differentiating mESCs express cardiac markers 95

3.3.6 Differentiating mESCs express HDAC4 protein 98

3.4 TRICHOSTATIN A TREATMENT OF DIFFERENTIATING MESCS 100

3.4.1 TSA treatment affected EB morphology 100

3.4.2 TSA treatment did not significantly affect beating onset 102

3.5 CRISPR/CAS9-MEDIATED KNOCKOUT OF *HDAC4* 103

3.5.1 Target site design 103

3.5.2 Guide RNA quality check 104

3.5.3 Chosen guide RNA site is able to drive cleavage 106

3.5.4 Selection of hygromyocin- resistant colonies 107

3.5.5 Survival of cells harbouring Hdac4 mutations 111

3.5.6 Characterisation of the mutation in cell line B5 112

3.5.7 Western Blot to confirm the presence of a truncated protein. 119

3.5.8 Differentiation of the B5 mutant line. 120

3.5.9 Beating analysis and comparison of differentiated wild-types, TSA-treated and Hdac4 knockout cells 121

3.6 DISCUSSION 123

3.6.1 Comparing P19CL6 cells to embryonic stem cells as in vitro models of cardiac differentiation 124

4 CHAPTER 4: RNA-SEQ ANALYSIS OF CARDIAC DIFFERENTIATION .. 135

4.1 INTRODUCTION 135

4.2 CHAPTER AIMS 135

4.3 4.3 RESULTS: 139

4.3.1 RNA extraction and quality control 139

4.3.2 Sequencing reads and mapping 140

4.3.3 Stem cells undergo significant transcriptomic changes during differentiation *143*
4.3.4 Unsupervised Multiple pair-wise comparisons show that differentiation-related genes are upregulated *148*
4.3.5 Effect of TSA treatment and Hdac4 knockout on beating cells *159*
4.3.6 Contractility protein-coding genes are differentially expressed in the beating state *160*
4.3.7 Ingenuity Pathway Analysis *165*
4.3.8 IPA graphical summary suggests DNA methylation plays a role in cardiomyocyte beating *171*
4.3.9 Graphical summary of wild-type and Hdac4 KO stem cell-induced cardiomyocytes *174*
4.4 DISCUSSION 177
5 CHAPTER 5: GENERAL DISCUSSION 184
5.1.1 Embryonic stem cells are better models of heart development *186*
5.1.2 Effect of chemical HDAC inhibition on cardiac differentiation *186*
5.1.3 CRISPR/Cas9-mediated knock out of Hdac4 ..... *187*
5.1.4 Contractility proteins may be regulated by methylation *190*
5.1.5 Concluding remarks *190*
5.1.6 Study Limitations *191*
5.1.7 Future Work *192*
6 BIBLIOGRAPHY 194
7 APPENDICES 249
7.1 APPENDIX 1: FULL LIST OF CANONICAL PATHWAYS GENERATED BY IPA 249
7.2 APPENDIX 2: FULL LIST OF TOX FUNCTIONS GENERATED BY IPA 302

LIST OF TABLES

TABLE 1-1. BRIEF DEFINITIONS OF MOST COMMON CONGENITAL HEART DEFECTS. A BRIEF EXPLANATION OF THE PHYSIOLOGICAL ABNORMALITIES FOUND IN EACH ONE IS PROVIDED. 48

TABLE 2-1. PCR CONDITIONS USED. TM REPRESENTS ANNEALING TEMPERATURE AND WAS ADJUSTED AS REQUIRED FOR EACH PRIMER PAIR 65

TABLE 2-2. LIST OF ANTIBODIES USED FOR IMMUNOFLUORESCENCE EXPERIMENTS AND THEIR RESPECTIVE DILUTIONS. 72

TABLE 2-3. SEQUENCES FOR OLIGOS USED FOR SGRNA IN VITRO SYNTHESIS. THESE WERE THE SAME FOR ALL GUIDE RNAS GENERATED. 75

TABLE 2-4. LIST OF PRIMERS USED TO AMPLIFY REGIONS CONTAINING TARGET SITES GENERATED USING CRISPOR. 76

TABLE 2-5. LIST OF PRIMERS USED TO GENERATE LARGER PCR PRODUCTS USED TO CHARACTERISE MUTATIONS. 80

TABLE 3-1. SUMMARY OF P19CL6 DIFFERENTIATION EXPERIMENT DATA. EB COUNT DATA FOR EXPERIMENT 8 IS NOT AVAILABLE. EBS: EMBRYOID BODY. (Y/N): YES/NO. 90

TABLE 3-2. SUMMARY OF MESCS DIFFERENTIATION EXPERIMENT DATA. EB COUNTS WERE NOT PERFORMED FOR EXPERIMENTS 7-9. EBS: EMBRYOID BODY. (Y/N): YES/NO. 91

TABLE 3-3. TABLE OF FIRST BEATING OCCURRENCE IN TSA-TREATED DIFFERENTIATING MESCS AND UNTREATED CONTROLS. 102

TABLE 3-4. LIST OF TARGET SITES GENERATED BY CRISPOR, THEIR SEQUENCES, PAM SEQUENCES AND LOCATIONS ON *HDAC4* MOUSE GENE 104

TABLE 4-1 SAMPLES USED FOR RNA-SEQUENCING AND ANALYSIS 139

TABLE 4-2 DIFFERENTIAL GENE EXPRESSION ANALYSIS COMPARING WILD-TYPE UNDIFFERENTIATED CELLS TO EACH GROUP OF DIFFERENTIATED CELLS,

irrespective of beating. The threshold for statistical significance was p<0.05 144

Table 4-3. A summary of the functions of the upregulated genes in the beating cells. 161

Table 4-4. Canonical pathway analysis indicates that cardiac hypertrophy signalling is enhanced in the differentiated state. 167

Table 4-5. Tox function analysis showed an enrichment for congenital heart disease related pathway inhibition. 169

LIST OF FIGURES

FIGURE 1-1. MAMMALIAN HEART DEVELOPMENT TAKES PLACE IN SIMILAR STEPS IN HUMAN AND MOUSE EMBRYOS, BUT ON DIFFERENT TIMELINES. 3

FIGURE 1-2. VENTRICULAR TRABECULATION DURING EMBRYONIC DEVELOPMENT..... 5

FIGURE 1-3. ATRIAL SEPTATION TAKES PLACE IN STAGES INVOLVING CELLS OF MYOCARDIAL, MESENCHYMAL AND NEURAL CREST ORIGIN. 8

FIGURE 1-4. OUTFLOW TRACT SEPTATION. THE OFT BEGINS AS THE COMMON CONDUIT FORMED FROM THE TRUNCUS ARTERIOSUS AND BULBUS CORDIS OF THE LOOPING CARDIAC TUBE. 10

FIGURE 1-5. TIMELINE OF HUMAN AND MOUSE EMBRYONIC CARDIAC DEVELOPMENT. 12

FIGURE 1-6. A SARCOMERE IS FORMED OF THIN AND THICK FILAMENTOUS PROTEINS ARRANGED IN AN INTERLOCKING PATTERN 18

FIGURE 1-7. CARDIOMYOCYTE DIFFERENTIATION IS A COMPLEX PROCESS UNDER THE CONTROL OF STAGE-SPECIFIC GENE EXPRESSION. 21

FIGURE 1-8. STEP-WISE LINEAGE COMMITMENT AND DIFFERENTIATION OF CARDIOMYOCYTES IS CAREFULLY REGULATED BY A HOST OF TRANSCRIPTION FACTORS AND SIGNALLING MOLECULES. 22

FIGURE 1-9. SCHEMATIC OF DNA PACKAGING AROUND NUCLEOSOMES AND HISTONE-TAIL MODIFICATIONS..... 25

FIGURE 1-10. ILLUSTRATION OF THE EFFECT OF HISTONE ACETYLATION ON NUCLEOSOME (BLUE CYLINDERS)..... 27

FIGURE 1-11. WILD-TYPE, *TBX5*, *KAT2A* AND *KAT2B* MORPHANTS..... 32

FIGURE 1-12. CRISPR/CAS9-MEDIATED KNOCKOUT OF KAT2A AND KAT2B IN ZEBRAFISH PHENOCOPIES MORPHOLINO KNOCKDOWN, AND RESULTS IN A SIMILAR PHENOTYPE TO KNOCKING OUT TBX5. 33

FIGURE 1-13. SCHEMATIC OF HDAC PROTEIN CLASSES AND THEIR DOMAINS.. 35

FIGURE 1-14. HDACS 4 AND 5 INTERACT WITH THE SMRT/NCOR COMPLEX AND THEIR PHOSPHORYLATION 39

FIGURE 1-15. TBX5 IS ACETYLATED BY KAT2A AND KAT2B AND DEACETYLATED BY HDAC4 AND HDAC5..... 46

FIGURE 1-16. . A DIAGRAM OF THE ADULT HUMAN HEART SHOWING THE ANATOMICAL LOCATIONS OF VARIOUS CONGENITAL HEART ABNORMALITIES 50

FIGURE 1-17. A SCHEMATIC OF THE CRISPR/CAS9 SYSTEM AT WORK. GUIDE RNA DRIVES CAS9 CLEAVAGE AT A LOCUS IN THE DNA THAT LIES ADJACENT TO A PAM SEQUENCE (PURPLE). 55

FIGURE 1-18. AIMS AND OBJECTIVES OF THIS THESIS. 63

FIGURE 2-1. SCHEMATIC SUMMARY OF DIFFERENTIATION PROCEDURE 69

FIGURE 2-2. DIFFERENTIATING EMBRYOID BODIES WERE TREATED WITH 50 NM TSA FOR 8 DAYS, STARTING ON DAY 7. 71

FIGURE 2-3. MAP OF VECTOR CARRYING CAS9, SGRNA, AMPICILLIN AND HYGROMYCIN RESISTANCE GENES NUCLEOFECTED INTO CELLS..... 77

FIGURE 2-4. SCHEMATIC SUMMARY OF RESISTANT COLONY SELECTION AND EXPANSION FOLLOWING NUCLEOFECTION. 79

FIGURE 2-5. SCHEMATIC OF LIBRARY GENERATION PROCEDURE USING THE QUANTSEQ 3' RNA SEQUENCING KIT..... 81

FIGURE 3-1. STAGES OF P19CL6 CELL LINE DIFFERENTIATION INVOLVE THE FORMATION OF EMBRYOID BODIES IN HANGING DROPS, THEN IN SUSPENSION, FOLLOWED BY PLATING. 90

FIGURE 3-2. MESCS FORM EMBRYOID BODIES THAT WHEN PLATED, CAN DIFFERENTIATE INTO BEATING CARDIOMYOCYTES. 93

FIGURE 3-3. MOUSE EMBRYONIC STEM CELLS DIFFERENTIATE INTO CARDIOMYOCYTES EARLIER THAN P19CL6 CELLS.. 94

FIGURE 3-4. IMMUNOFLUORESCENCE SHOWED THE EXPRESSION OF PLURIPOTENCY ASSOCIATED MARKER AT START OF DIFFERENTIATION PROCEDURE..... 96

FIGURE 3-6. CONTRACTILITY-ASSOCIATED ALPHA-ACTININ PROTEIN WAS EXPRESSED IN BEATING REGIONS OF DIFFERENTIATED STEM CELLS. 98

FIGURE 3-7. IMMUNOFLUORESCENT STAINING OF HDAC4 EXPRESSION IN DIFFERENTIATING STEM CELLS INDICATES ITS PRESENCE THROUGHOUT DIFFERENTIATION, WITH HIGHER EXPRESSION DETECTED AT LATER STAGES. 99

FIGURE 3-8. TSA TREATMENT AFFECTS EB MORPHOLOGY. IMAGES OF AN EMBRYOID BODY FROM DIFFERENTIATING ES CELLS AT THE FIRST DAY OF TSA TREATMENT, DAY 7 IN (A) TO DAY 15 (G). 101

FIGURE 3-9. TSA TREATMENT DID NOT SIGNIFICANTLY AFFECT BEATING ONSET. 103

FIGURE 3-10. BIOANALYZER CHECK OF RNA INTEGRITY SHOWED THAT SGRNA10 WAS OF THE BEST RELATIVE QUALITY, WITH NO DEGRADATION. 105

FIGURE 3-11. THE SELECTED TARGET SITE IS LOCATED IN EXON 18 OF THE *HDAC4* GENE. 106

FIGURE 3-12. SELECTED GRNA 10 CAN DRIVE CAS9-MEDIATED CLEAVAGE AT THE GENOMIC TARGET SITE.. 107

FIGURE 3-13. CLEAVAGE BY CAS9 ENZYME AT THE TARGET SITE IN THE GENOME LEADS TO A DOUBLE STRAND BREAK. 107

FIGURE 3-14. 700-800 BP FRAGMENTS OF GENOMIC DNA WERE AMPLIFIED FOR EACH COLONY.. 108

FIGURE 3-15. SEQUENCE ALIGNMENT FROM COLONIES SHOWED DELETIONS OF DIFFERENT SIZES.. 110

FIGURE 3-16. KNOCKOUT MESCS EXHIBIT A DECREASE IN RAISED, DOME-LIKE MORPHOLOGY. 112

FIGURE 3-17. DNA EXTRACTED FROM COLONY B5 SHOWS A ~220-BP DELETION WHEN COMPARED TO WILD-TYPE.. 113

FIGURE 3-18 AN ILLUSTRATION OF THE RELATIVE LOCATIONS OF THE PRIMER PAIRS USED RELATIVE TO THE GENOMIC TARGET SITE AND THEIR ORIENTATIONS.. 115

FIGURE 3-19. SEQUENCE ALIGNMENTS OF DNA EXTRACTED FROM WILD-TYPE AND MUTANT CELLS USING DIFFERENT PRIMERS PAIRS CONSISTENTLY SHOWS 221-BP DELETION. 117

FIGURE 3-20. CLEAVAGE AT THE TARGET SITE IS PREDICTED TO RESULT IN A TRUNCATED PROTEIN. 118

FIGURE 3-21 . WESTERN BLOT RESULT USING ANTI-HDAC4 ANTIBODY WAS NOT CONCLUSIVE..... 119

FIGURE 3-22. COLONY B5 MESCS ARE ABLE TO DIFFERENTIATE VIA EBS..... 121

FIGURE 3-23. *HDAC4* KNOCKOUT DID NOT SIGNIFICANTLY AFFECT BEATING ONSET. 121

FIGURE 3-24. SCREENSHOTS FROM MYOCYTER OUTPUT SHOW WHAT THE PROGRAMME RECOGNISES AS BEATING REGIONS. 123

FIGURE 3-25. WILD-TYPE BEATING CELLS WERE COMPARED TO TSA-TREATED AND KNOCKOUTS USING MYOCYTER. 123

FIGURE 3-26. POSSIBLE EXON SKIPPING EVENT COULD HAVE TAKEN PLACE DUE TO CRISPR/CAS9 EDITING OF *HDAC4*..... 131

FIGURE 3-27. PHOSPHORYLATION OF HDAC4/5 LEADS TO THEIR NUCLEAR EXPORT AND ACTIVATION OF *TBX5* TARGETS. 133

FIGURE 4-1 RNA WAS EXTRACTED FROM UNDIFFERENTIATED AND DIFFERENTIATED CELLS FOR RNA-SEQ ANALYSIS..... 136

FIGURE 4-2. A SCHEMATIC EXPLAINING THE STEPS TAKEN TO ANALYSE RNA SAMPLES. 138

FIGURE 4-3. INITIAL QUALITY CONTROL CHECKS ON DATA FROM RNA-SEQ SHOWS THAT DNA WAS OF SUFFICIENT MAPPING QUALITY FOR DOWNSTREAM ANALYSES.. 142

FIGURE 4-4. HEAT MAP OF DIFFERENTIALLY EXPRESSED GENES SHOWS THAT REPLICATE SAMPLES CLUSTER TOGETHER.. 143

FIGURE 4-5 PRINCIPAL COMPONENT ANALYSIS OF COMPARISONS BETWEEN UNDIFFERENTIATED CELLS AND EACH OF THE DIFFERENTIATED GROUPS SHOWS THAT CONTROL REPLICATES CLUSTER TOGETHER.. 147

FIGURE 4-6 COMPARING UNDIFFERENTIATED "GROUND-STATE" STEM CELLS TO BEATING CELLS IN ALL TREATMENTS REVEALS A DYNAMIC CHANGE IN TRANSCRIPTION..... 150

FIGURE 4-7 UPREGULATED TERMS IN WILD-TYPE BEATERS ONLY DIFFER FROM THOSE FOUND IN THE *HDAC4* KOS OR TSA-TREATED BEATERS. 154

FIGURE 4-8. DOWNREGULATED GENES IN WILD-TYPE AND TSA-TREATED BEATERS BELONGED TO SIMILAR BIOLOGICAL PATHWAYS MOSTLY RELATED TO METABOLISM. 155

FIGURE 4-9. DIFFERENTIAL GENE EXPRESSION ANALYSIS OF WT UNDIFFERENTIATED AND DIFFERENTIATED BEATING CELLS SHOWS A SIGNIFICANT CHANGE IN GENE EXPRESSION.. 159

FIGURE 4-10. COMPARING DIFFERENTIALLY EXPRESSED GENES IN WT BEATING VS TSA TREATED OR HDAC4 KO SHOWED A SMALL NUMBER OF SIMILARLY REGULATED GENES. 159

FIGURE 4-11. COMPARISON OF WILD-TYPE DIFFERENTIATED BEATING AND NON-BEATING CELLS SHOWED AN UPREGULATION OF CONTRACTILITY PROTEIN-CODING GENES. 161

FIGURE 4-12 GRAPHICAL SUMMARY OF DGE RESULTS BETWEEN WILD-TYPE BEATING AND DIFFERENTIATED NON-BEATING CELLS REVEAL A POSSIBLE ROLE FOR DNA METHYLATION IN CARDIOMYOCYTE BIOLOGY 173

FIGURE 4-13. GRAPHICAL SUMMARY OF WILD-TYPE AND *HDAC4* KO BEATERS HINTS AT IMPLICATING *HDAC4* IN INTERFERON SIGNALLING IN CARDIOMYOCYTES 175

List of Abbreviations

Acronym	Definition
ADP	Adenosine diphosphate
ANOVA	Analysis of variance
ASD	Atrial septal defect
ATP	Adenosine triphosphate
AVC	Atrioventricular canal
AVSD	Atrioventricular septal defect
BAV	Bicuspid aortic valve
BHLH	Basic helix-loop-helix
BMP	Bone morphogenetic protein
BSA	Bovine serum albumin
CBP	CREB-binding protein
CHD	Congenital heart disease
CHIP	Chromatin immunoprecipitation
CREB	cAMP response element binding protein
CRISPR	Clustered regularly interspersed short palindromic repeats
CUGBP	CUG Triplet Repeat RNA-Binding Protein
DCM	Dilated cardiomyopathy
DEG	Differentially expressed gene

Acronym	Definition
DGE	Differential gene expression
DMEM	Dulbecco's Modified Eagle Medium
DMP	Dorsal mesenchymal protrusion
DMSO	Dimethyl sulfoxide
DORV	Double outlet right ventricle
DSN	Duplex-specific nuclease
EDTA	Ethylenediaminetetraacetic acid
EGFP	Enhanced green fluorescent protein
ELAV	Embryonic lethal, abnormal vision
ESC	Embryonic stem cell
FBS	Foetal bovine serum
FGF	Fibroblast growth factor
FHF	First heart field
FLOT	Flotillin
GAPDH	Glyceraldehyde 3-phosphate dehydrogenase
GATA	GATA Binding Protein
GFP	Green fluorescent protein
GMEM	Glasgow minimum essential media
HAND	Heart And Neural Crest Derivatives
HAT	Histone acetyltransferase

Acronym	Definition
HCM	Hypertrophic cardiomyopathy
HDAC	Histone deacetylase
HDR	Homology directed repair
HDRP	Histone Deacetylase-Related Protein
HEPES	4-(2-hydroxyethyl)-1-piperazineethanesulfonic acid
HLHS	hypoplastic left heart syndrome
HRHS	Hypoplastic right heart syndrome
IAA	Interrupted aortic arch
JAK	Janus kinase
LIF	Leukaemia inhibitory factor
LIM	Lin11, isl-1, and mec-3
LNA	Long non-coding RNA
MADS	Minichromosome Maintenance Factor 1, Agamous, Deficiens, Serum Response Factor
MAPQ	Mapping quality
MBD	Methyl-CpG-binding domain
MEF	Myocyte enhancer factor
MHC	Myosin heavy chain
MITR	Myocyte enhancer-binding factor 2-interacting transcriptional repressor

Acronym	Definition
MOPS	3-(N-morpholino)propanesulfonic acid
MOZ	Monocytic leukemia zinc finger protein
MYST	MOZ, Ybf2, Sas2 and Tip60
NAD	Nicotinamide
NAS	Nonsense-associated alternative splicing
NCOR	Nuclear receptor co-repressor
NES	Nuclear export signal
NGS	Next generation sequencing
NHEJ	Non-homologous end joining
NSR	Not-so-random
OFT	Outflow tract
PAGE	Polyacrylamide gel electrophoresis
PAM	Protospacer adjacent motif
PBS	Phosphate buffered saline
PCA	Principal component analysis
PCAF	P300/CBP-Associated Factor
PCR	Polymerase chain reaction
PDA	Patent ductus arteriosus
PDD	Probe-directed degradation
PVDF	Polyvinylidene fluoride

Acronym	Definition
PFA	Paraformaldehyde
PGC	peroxisome proliferator-activated receptor gamma co-activator
PHD	Plant homeodomain
PSC	Pluripotent stem cell
PTA	Persistent truncus arteriosus
PTC	Premature termination codon
PTM	Post-translational modification
PVC	Polyvinyl Chloride
RAS	Rat sarcoma
RCM	Restrictive cardiomyopathy
RIN	RNA integrity number
RIPA	Radioimmunoprecipitation assay
RPM	Revolutions per minute
SAGA	Spt-Ada-GCN5 acetyltransferase (AT) containing
SAGE	Serial Analysis of Gene Expression
SAHA	Suberanilohydroxamic acid
SDS	Sodium Dodecyl Sulfate
SHF	Second heart field
SMA	Smooth muscle actin

Acronym	Definition
SMRT	Silencing mediator of retinoic and thyroid receptors
SNF	Sucrose Non-Fermentable
SNP	Single nucleotide polymorphism
SOCS	Suppressor of cytokine signaling
SOGA	Sppressor of glucose by autophagy
STAR	Spliced Transcripts Alignment to a Reference
SWI	SWItch
TAE	Tris-acetate EDTA
TALENS	Transcription activator-like effector nucleases
TAPVR	Total anomalous pulmonary venous return
TBST	Tris Buffered Saline with Tween
TEX	Terminator 5’-phosphate-dependent exonuclease
TGA	Transposition of the great arteries
TMRM	Tetramethylrhodamine, methyl ester
TOF	Tetralogy of Fallot
TPM	Transcripts per million
TSA	Trichostatin A
UDG	Uracil DNA glycosylase
VEGFR	Vascular endothelial growth factor receptor
VPA	Valproic acid

Acronym	Definition
VSD	Ventricular septal defect

1 INTRODUCTION

1.1 Mammalian heart development

1.1.1 Embryonic cardiac morphogenesis

In mouse and man, heart development follows a parallel set of steps, though on different timelines due to longer gestation in man. This section will outline the anatomical stages involved in embryonic heart development, the following section will concentrate on cardiomyocyte differentiation and biology.

After fertilisation, a bilaminar embryonic disc made of two layers, the epiblast and hypoblast, forms. This structure is formed by the second week of development in humans. During the third week, a thickened groove, the primitive streak, is formed in the midline of the embryonic disc, towards the caudal end, determining the embryonic axes in the process (See Figure 1-1 for an illustration of the human embryo at 18 days, showing the primitive streak in the midline). Following the formation of the primitive streak, cells detach from the epiblast and start migrating towards the interior of the embryo, displacing the hypoblast. By the end of that process, a trilaminar embryonic disc with three germ layers has formed. The layers are the ectoderm, mesoderm and the endoderm. Cells of the ectoderm give rise to the future epidermis, nervous system and migratory neural crest cells. The endoderm gives rise to the gastrointestinal tract and the mesoderm forms the circulatory system and musculature (Sylva, van den Hoff and Moorman, 2014).

After the formation of the primitive streak the embryo undergoes embryonic folding, around three weeks of human development and 7.5 days post coitus (dpc) for mouse. The embryo's shape goes from a disc to cylinder-like as it folds horizontally and medially. Cardiac precursors in the splanchnopleuric layer are found symmetrically lateral to the future mouth (somatopharyngeal membrane). Due to folding, bilateral cardiac precursors are brought together to form an epithelial structure known as the cardiac crescent (Moorman *et al.*, 2003; Ivanovitch, Temiño and Torres, 2017; Rossi *et al.*, 2021). See Figure 1-1 B for a mouse embryo at embryonic day (E)7.5 showing the cardiac crescent relative to the primitive streak. The cardiac crescent fuses at the

midline to form the heart tube, which is composed of an inner layer of endocardium and an outer layer of myocardium, called the proepicardium (Saga *et al.*, 1999; Meilhac and Buckingham, 2018), see Figure B showing the heart tube at E8.5. The anterior end of the tube is the arterial pole and the venous pole lies at the posterior end (Ivanovitch, Temiño and Torres, 2017).

The heart tube grows further by the addition of newly differentiated cardiomyocytes from the adjacent mesoderm, rather than by proliferating cardiomyocytes of the tube itself (Devine *et al.*, 2014). Cells from nearby mesoderm migrate to the heart tube where they differentiate into cardiomyocytes. The identity of these cardiomyocytes is then determined by their location in the developing heart (Esteban et al., 2022). The heart tube is formed of three layers, which are also found in the adult heart. These are the endocardium, forming the endothelial lining of the tube, the myocardium, which makes up most of the heart's musculature, and the visceral pericardium, forming the outermost external surface (Ivanovitch, Temiño and Torres, 2017).

The cardiac precursor cell pool can be divided into two groups, those that are present in the heart tube and those that are added later from nearby mesoderm. These are known as the first and second heart fields (FHF and SHF), respectively (Esteban *et al.*, 2022). Lineage tracing experiments showed that the first heart field (FHF) gives rise to the left ventricle and parts of the atria (Zaffran *et al.*, 2004). The second heart field, on the other hand, gives rise to the right ventricle, outflow tract and parts of the atria (Lescroart *et al.*, 2010; Vincent and Buckingham, 2010). Schematics illustrating human and mouse heart development are shown in Figure 1-1 A and B, respectively.

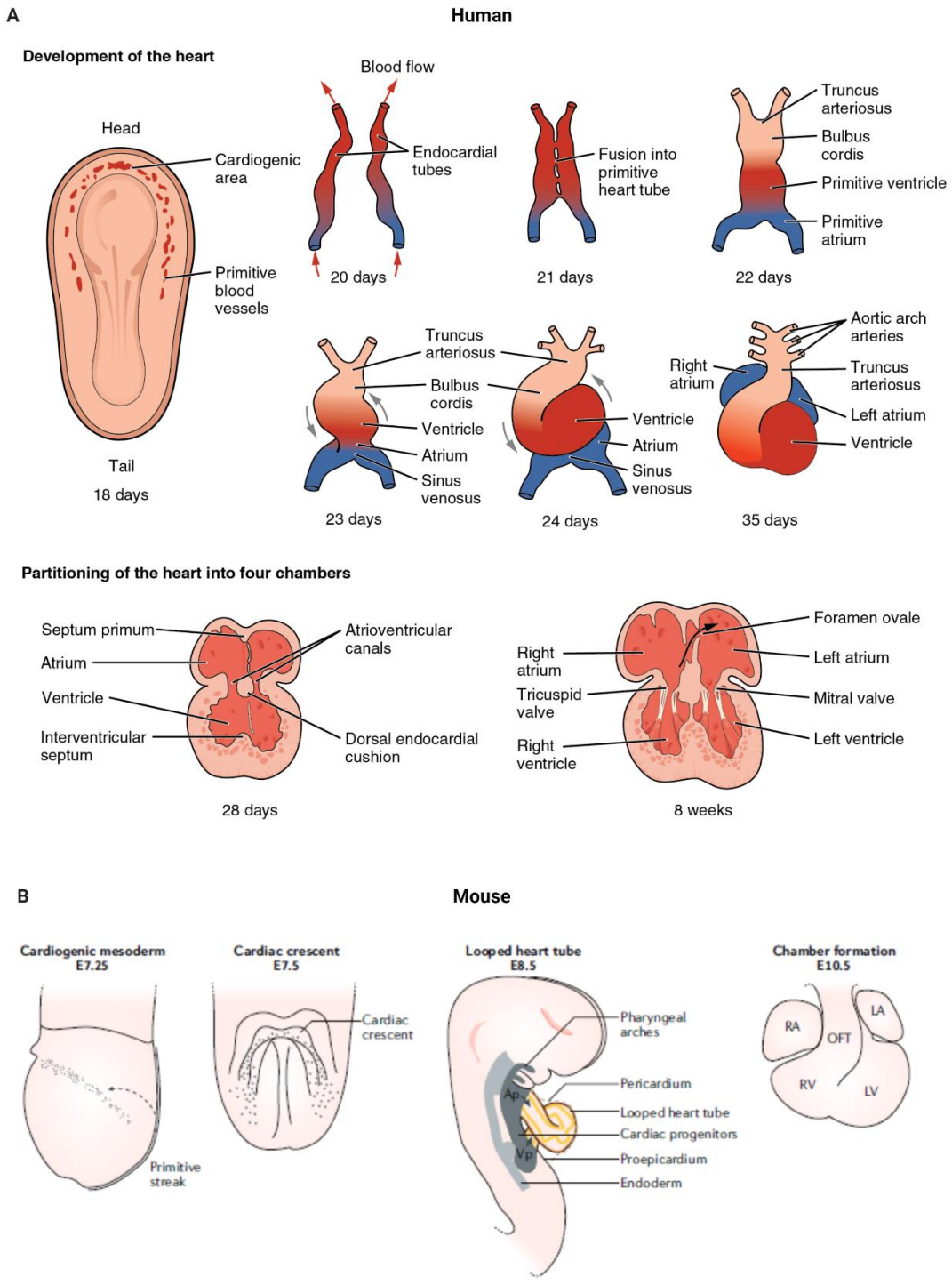


Figure 1-1. Mammalian heart development takes place in similar steps in human and mouse embryos, but on different timelines. (A) shows human heart development. After gastrulation and primitive streak formation, the cardiac crescent gives rise to cardiac tubes which fuse in the middle. The heart tube and its distinct areas are indicated. The tube undergoes rightward looping starting at 23 days and the process ends with the arteries being placed anterior to the ventricles. Septation occurs concurrently, starting at 28 days and continues to divide the heart into four chambers,

with the process completing fully at birth. The arrows show the direction of blood flow and embryonic age is indicated in numbers below the images. Illustration from Anatomy & Physiology, Connexions Web site **http://cnx.org/content/col11496/1.5/** (B) Mouse heart development in the mouse also starts with the specification of the cardiac crescent after gastrulation. Endocardial tubes fuse and undergo looping at E8.5. Atria take their place anterior to ventricles and chambers are clearly specified by E10.5. As in humans, septation also takes place concurrently. Figure taken from Meilhac and Buckingham, 2018

1.1.2 Chamber formation

The transition from a two-chambered heart to the four-chambered heart seen in mammals occurred as vertebrates adapted to life on land. The transition to land required greater oxygenation of the body, and the development of a four-chambered heart allowed for more efficient separation of oxygenated and deoxygenated blood. Partitioning the heart involves the development of septa and valves that ensure a unidirectional blood flow (Dong, Qian and Liu, 2021). This section will discuss the development of atria and ventricles, followed by valve development. It must be noted that while these structures are presented in this order, some developmental stages happen simultaneously or may overlap.

As the cardiac tube grows further, it undergoes significant morphological remodelling. This is orchestrated by various transcription factors such as *Nkx2.5*, *Tbx5* and *Gata4*, and various signalling pathways such as, Wnt, BMP, FGF and Notch. These work in concert to regulate the proliferation, differentiation and migration of cardiac progenitors, as noted previously (Mandrycky *et al.*, 2020). Next, the heart tube loops into an S-shape with inner and outer curvatures (Le Garrec *et al.*, 2017) (See figure 1-1, panel A, looping is depicted at days 23 and 24 for humans, and panel B, mouse cardiac looping at E8.5 and embryonic heart chambers shown at E10.5). As a result of this looping, the atria and sinus venosus end up behind the ventricles (Katano *et al.*, 2019) (see Figure 1-1).

The chambers begin forming in a process known as ballooning, characterised by proliferation and differentiation in localised areas of the heart tube (Christoffels *et al.*, 2000). Atria form symmetrically at the dorso-lateral sides of the heart tube. Local myocardium undergoes rapid proliferation, faster than surrounding myocardium,

leading to the formation of two pouches, which later become the embryonic atria (Günthel, Barnett and Christoffels, 2018). Broadly, atria are structurally formed of four components: the sinus venosus, the primary atrial septum (or septum primum), the arterial appendages and the atrioventricular canal (Moorman and Christoffels, 2003). The muscular bulk of the atria is formed of a complex network of subendocardial muscular bundles (Mantini *et al.*, 2023). Notably, atrial myocytes have secretory granules that produce the cardiac hormones atrial natriuretic peptide (ANP) and brain natriuretic peptides (BNP) (Galow, Brenmoehl and Hoeflich, 2023).

Concomitantly, the development of the ventricles also happens right after cardiac looping. This starts when ventricular myocytes form sheet-like projections into the extracellular matrix between the endocardium and the myocardium, known as the cardiac jelly (Figure 1-2 A) (Dong, Qian and Liu, 2021). These extrusions are known as trabeculae carneae, in a process named cardiac trabeculation, which involves morphological changes and the rearrangement of adhesion junctions. The expansion of these sheet-like muscles into the ventricular lumen increases surface area for oxygenation, and cardiac mass (Fatemifar *et al.*, 2019). This process entails the delamination of cardiomyocytes, where they extend their projections into the lumen (see Figure 1-2 B) This is followed by the constriction of their apical membranes by remodelling cell-cell junctions. As development progresses, the trabeculae gain structural complexity and radially-arranged trabecular projections form along the outer curvature of the ventricle (see Figure 1-2 C). As a result, two morphologically distinct layers appear in the ventricular myocardium, the inner trabecular layer and the outer compact layer (Jiménez-Amilburu *et al.*, 2016) (Figure 1-2 D).

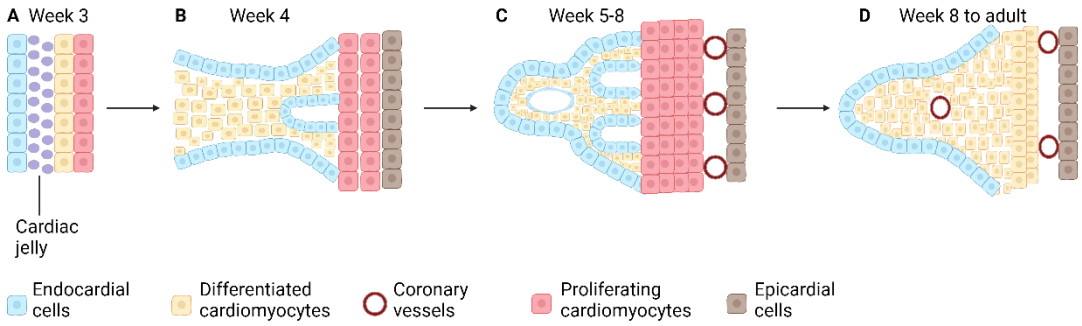


Figure 1-2. Ventricular trabeculation during embryonic development. (A) At week 3 of gestation, extracellular matrix known as cardiac jelly is sandwiched

between endocardial cells and layers of differentiated and proliferating cardiomyocytes. (B) At week 4, the cardiac tube undergoes looping and endocardial cells delaminate and form projections into the ventricular lumen. (C) During weeks 5-8, epicardial cells invade and contribute to the formation of coronary vasculature while trabecular myocardium undergoes compaction. (D) During later stages of gestation, the compact myocardium undergoes further thickening and compaction to form the mature, trabeculated ventricles. Figure redrawn from (Cherian *et al.*, 2016) using biorender.com.

Compact myocardium is more proliferative than trabecular myocardium and exhibits epithelial-like characteristics such as a cobblestone appearance and the expression of cell-cell adhesion proteins from the cadherin family (Cherian *et al.*, 2016; Jiménez-Amilburu *et al.*, 2016). Moreover, the two layers are characterised by different patterns of gene expression, where compact myocardium highly expresses *Tbx20, N-Myc* and *Hey2* and trabecular myocardium shows increased expression of *Bmp10, p57* and Sphingosine 1-phosphate receptor-1 (Wu, 2018).

Trabeculation involves epicardial cells (Figure 1-2), derived from coelomic epithelium, that are mesodermal in origin (Adrián Ruiz-Villalba and José M Pérez-Pomares, 2012). When the epicardium is specified, between E9.0 and E9.5 in the mouse, epicardial cells spread and adhere to the myocardium. They next undergo EMT, forming a population of invasive epithelia-derived cardiac cells (EPDCs). EPDCs migrate from the extracellular matrix between the myocardium and epicardial epithelium to the compact trabeculated ventricles, followed by the atrioventricular valves (Wolters *et al.*, 2021). This cell population also gives rise to cardiac fibroblasts, coronary endothelial and smooth muscle. EPDCs differentiation involves *Gata5, Tbx18, Wt1*, as well as BMP and FGF signalling (Wolters *et al.*, 2021).

The last final stages of ventricular development begin with the collapse of myocardium towards the base of the myocardial wall, resulting in the formation of a compact, solid ventricular wall. This process is regulated by the Notch signalling pathway (Grego-Bessa *et al.*, 2007). During late foetal and neonatal stages, ventricular myocytes form helical and spiral sheets, forming three-dimensional, multi-layered muscular bundles which take on the role of blood pumping during development (Wu, 2018).

1.1.3 Chamber septation

For the four chambers to carry out their functions properly in the fully-formed heart, direction of blood flow must be controlled. Septa form to divide the chambers, in addition to valves that ensure unidirectional blood flow. Septation takes place between the atria, in the middle of the ventricles, between the primary myocardium of the atrioventricular canal and primary foramen and in the outflow tract (Anderson *et al.*, 2014).

Atrial septation is a complex process and involves myocardial and mesenchyme cells of both endocardial and non-endocardial origin, including the neural crest. It broadly takes place in two stages, starting with the development of the primary septum, followed by the formation of the more solid secondary septum. The primary septum is a crescent-shaped structure growing from the atrial roof towards the atrioventricular cushions (Pustovit *et al.*, 2022) (see Figure 1-3). This growth is initiated from a mesenchymal cap in the atrial roof that lies adjacent to the dorsal mesenchymal protrusion (DMP) (see purple structure in Figure A). The primary septum, with the mesenchymal cap at the leading edge, does not reach the atrioventricular cushions and the gap between them is called the primary foramen (Jensen, Wang and Moorman, 2019). By the fifth week of gestation, the mesenchymal cap comes into contact with the atrioventricular cushions and these merge with the DMP to close the primary foramen. However, before closing, small perforations in the primary septum form by apoptosis (Jensen *et al.*, 2017; Jensen, Wang and Moorman, 2019). These merge and form a second opening named the secondary foramen. The secondary foramen allows right-left blood atrial shunting, which is needed for foetal blood oxygenation before the development of pulmonary circulation. The primary and secondary septa are marked by differential expression of *Tbx3, Tbx18, Isl2* and *Nkx2.5* (Pustovit et al., 2022).

Around weeks 6 to 8, the mesenchymal components that closed the primary foramen differentiate into myocardium, thus starting the formation of the secondary atrial septum (Jensen, Wang and Moorman, 2019). Inward folding of the atrial myocardium and subsequent growth towards the atrioventricular cushion follows. The secondary septum partially overlaps the secondary foramen, resulting in the formation of an oblique passage between the right and left atria, known as the foramen ovale (Jensen *et al.*, 2017). The foramen ovale becomes visible around week

12 of human gestation. In the foetus, blood can flow from right to left through the foramen ovale as the pressure is higher in the right atrium than the left. However, after birth, this pressure reverses, bringing the primary and secondary septa together, and closing the foramen ovale (Lindsey, Butcher and Yalcin, 2014). When closed, the remaining oval depression is called the fossa ovalis (Pustovit *et al.*, 2022).

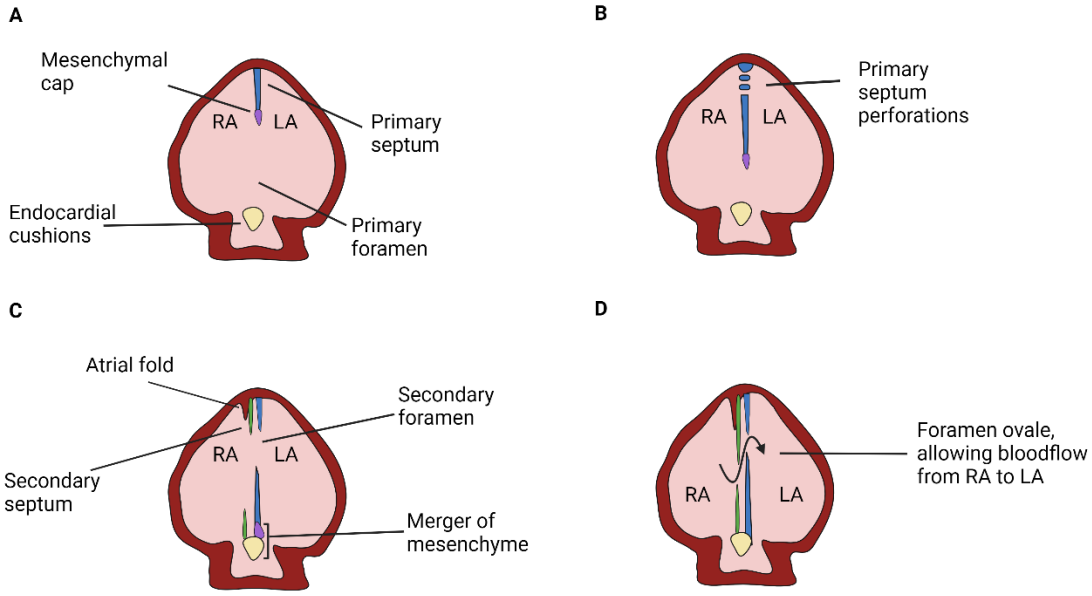


Figure 1-3. Atrial septation takes place in stages involving cells of myocardial, mesenchymal and neural crest origin. (A) The primary septum starts growing from the atrial roof, led by a mesenchymal cap. This structure grows towards the endocardial cushions and the space in between is called the primary foramen. (B) The primary septum continues to grow and cover the primary foramen. Concomitantly, secondary perforations appear due to apoptosis. (C) The primary septum and mesenchymal cap then fuse with the mesenchyme of the endocardial cushions, closing the primary foramen. A fold appears in the atrial roof as the atrium takes its shape and the secondary septum starts to form. The merged mesenchyme becomes muscularised and also contributes to the secondary septum. The perforations in the primary septum coalesce to form the secondary foramen, also known as the secondary foramen. This leads to the emergence of the secondary foramen. (D) The primary foramen is now closed, the septa continue to grow and mature and the foramen ovale allows blood shunting from the right to the left atrium. LA, left atrium; RA, right atrium. Figure created using biorender.com.

Ventricular septation takes place concurrently with atrial septation. The ventricular septum is formed from two populations of cells. The first population is of a myocardial origin and those grow upwards from the apex of the heart towards the endocardial cushion. The septum grows by a process called apposition, where cells are added from the adjacent left ventricular wall. The second population forms the membranous septum and those grow downwards from the endocardial cushion and connect the endocardial cushion to the myocardial septum (Sylva, van den Hoff and Moorman, 2014; Meilhac and Buckingham, 2018). The membranous septum develops to close the primary interventricular foramen, which forms as a result of the fusion of the primitive ventricle and the bulbus cordis (Goswami *et al.*, 2019). Unlike in atria, this foramen must be closed. The membranous septum develops from bulbar ridges in the outflow part of the developing ventricles, which fuse and form bulbar septum. The bulbar septum grows towards the interventricular septum, where the endocardial cushions proliferate to close the interventricular foramen (Poelmann *et al.*, 2016; Goswami *et al.*, 2019).

The muscular ventricular septum is divided into the inflow and outflow parts. The inflow septum is thick and rough, due to trabeculation. It also contains papillary muscles. The smaller outlet septum is smooth and leads to the pulmonary trunk on the right and the aorta on the left (Goswami *et al.*, 2019).

Cardiomyocytes in the muscular intraventricular septum are of both right- and left-ventricular origin. This was found using fate mapping where it was shown that they express *Mlc1v*, which is expressed in the right ventricular myocardium, and *Mlc3f*, which is expressed in left ventricular myocardium (Franco *et al.*, 2006).

In humans, ventricular septation is completed around 2 months after conception. The heart continues to mature for 7 months and atrial septation is completed by birth upon the initiation of pulmonary circulation. However, in murine embryos, septation completes only 2 weeks post conception, meaning less than a week is left for the foetus before birth. It can be argued, therefore, that some developmental processes that are completed at human birth are still ongoing in a neonatal mouse (Wessels and Sedmera, 2003).

1.1.4 Outflow tract development

At 26-30 dpc in human and 9.5 dpc in mouse, the outflow tract (OFT) is simply a myocardial tube that runs from the developing ventricles to the aortic sac and pulmonary sac (Sylva, van den Hoff and Moorman, 2014). The aortic sac in turn, is connected to the pharyngeal arch arteries (see Figure 1-4). The development of the OFT is a tightly regulated complex process, and perturbations its elongation or rotation during cardiac looping can give rise to congenital heart diseases (CHDs) (Roux *et al.*, 2015). OFT cardiomyocytes originate from a population of the anterior SHF that express *Fgf8* and *Mlc1v*, and a population of posterior SHF cells that express *Isl1*, but not *Fgf8* (Roux *et al.*, 2015).

Endocardial cushions, as well as neural crest-derived cells also contribute to OFT development. Endocardial cushions undergo EMT to give rise to valvular interstitial cells (DeLaughter *et al.*, 2013). These cells move towards each other and converge in the midline to separate the pulmonary and aortic outflow tracts (Figure 1-4). The aortic pulmonary septum is characterised by its spiral shape, ensuring separation between oxygenated and deoxygenated blood. The aorta and pulmonary trunk therefore spiral in opposite directions (see Figure).

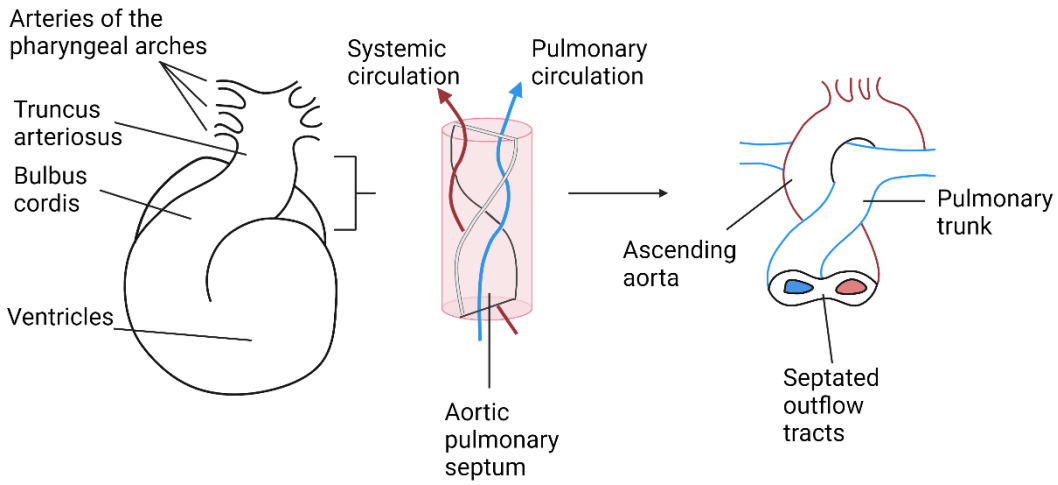


Figure 1-4. Outflow tract septation. The OFT begins as the common conduit formed from the truncus arteriosus and bulbus cordis of the looping cardiac tube. This channel allows blood to flow out of the heart and into the arteries of the pharyngeal arches. Neural crest cells on either side of the wall of the OFT proliferate and grow towards each other. They meet in the middle to form the spiral aortic pulmonary septum. Following further growth and maturation, this spiral septum separates the OFT into the ascending aorta and pulmonary trunk,

maintaining separation between oxygenated and deoxygenated blood. Figure redrawn from https://simplemed.co.uk/subjects/cardiovascular/embryology-of-the-cvs using Biorender.com.

Migratory neural crest cells also give rise to the pharyngeal arch arteries (Figure 1-4). These cells are characterise by their ability to coalesce upon reaching their destination and contribute to the development of that structure, or inducing differentiation in neighbouring cells. In the pharyngeal arches, neural crest cells populate the region, resulting in their remodelling. They contribute to the vascular smooth muscle of the brachiocephalic root of the internal carotid and pulmonary arteries, and the dorsal aorta (Bulatovic *et al.*, 2016). *Tgfb2*, *Bmp2*, *Wnt4* and retinoic acid are factors known to be expressed in cardiac neural crest cells (Yamagishi, 2021).

1.1.5 Valves formation

To control unidirectional blood-flow and ensure no back-flow occurs, valves form between atria and ventricles (atrioventricular valves) and between ventricles and the great atria (semilunar valves). The mitral valve controls blood flow from the left atrium to the left ventricle, while the tricuspid valve controls blood flow from the right atrium to the right ventricle (see Figure 1-1 A for the location of atrioventricular valves in a human embryonic heart at 8 weeks). The mitral valve is composed of two leaflets while the tricuspid valve has three. Cells from the inferior atrioventricular cushion give rise to the anterior mitral valve leaflet and the septal tricuspid leaflet (Bulatovic *et al.*, 2016). The posterior mitral leaflet and the anterior and posterior tricuspid leaflets originate from mesenchymal cells situated laterally to the atrioventricular canal. Atrioventricular valves form as a result of increased extracellular matrix complexity and lower endocardial cushion proliferation (Sylva, van den Hoff and Moorman, 2014).

Semilunar valves, on the other hand, only have a partial contribution from endocardial cushions. There are four endocardial cushions in the OFT, two of which give rise to the spiral septum and two that develop into the anterior cusp of the pulmonary valve, and the noncoronary cusp of the aortic valve. Aforementioned neural crest cells from the pharyngeal arches contribute to valve formation and

maturation (Mifflin *et al.*, 2018). To summarise cardiac development in human and mouse, please see Figure 1-5 for a timeline of key events.

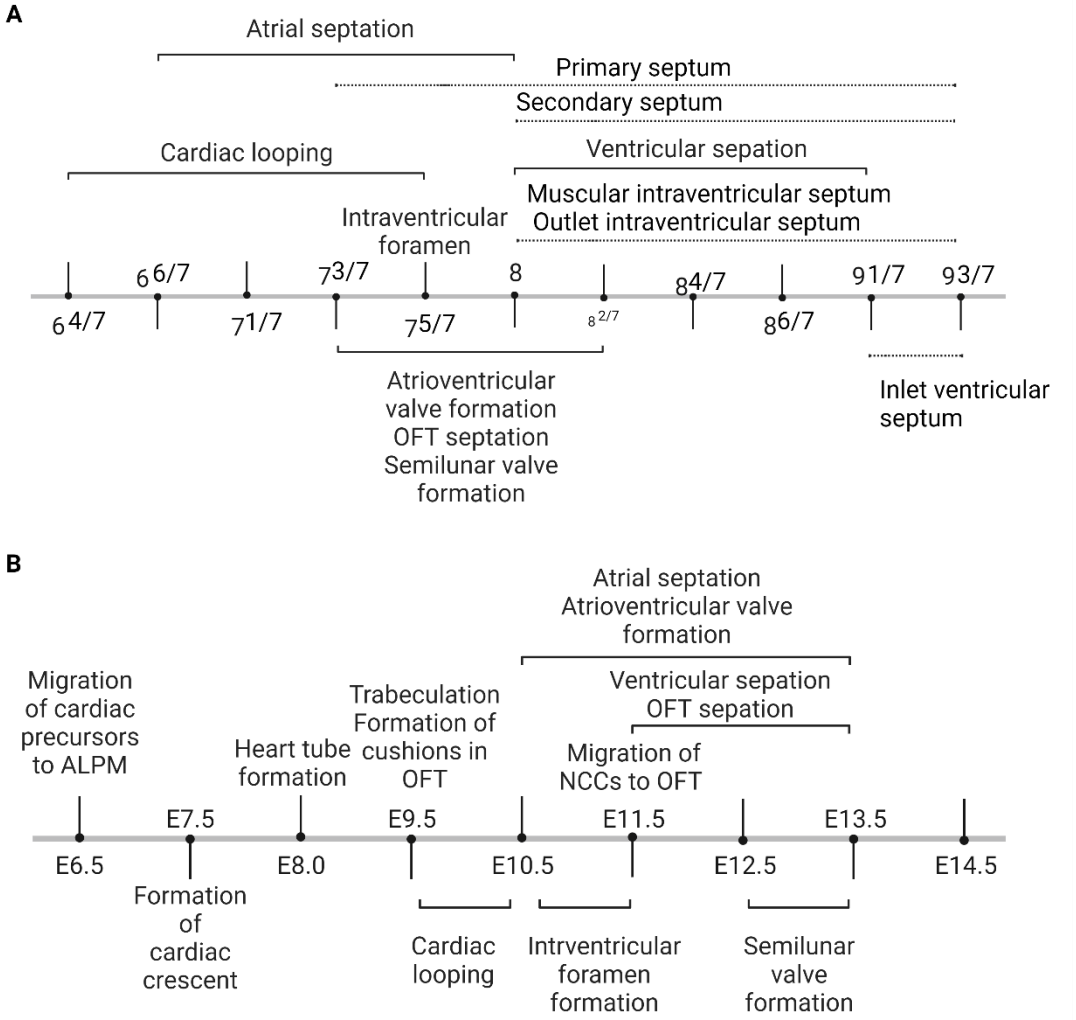


Figure 1-5. Timeline of human and mouse embryonic cardiac development. (A) Shows human heart development, initiation of developmental processes is plotted alongside corresponding days of gestation. (B) Depicts mouse cardiac developmental events relevant to embryonic days. In both timelines, the process can be summarised in the formation of the cardiac tube from mesodermal progenitors in the cardiac crescent, followed by looping and further expansion of the heart that involves chamber and OFT development followed by septation. ALPM, anterior lateral plate mesoderm; NCCs, neural crest cells; OFT, outflow tract. Figure created using biorender.com.

1.1.6 Genetics of heart development

Heart morphogenesis is strictly controlled by a network of transcription factors in addition to secreted molecules like bone morphogenetic protein (BMP), fibroblast growth factor (FGF) and Wnt proteins (Verhoeven *et al.*, 2011). These are expressed in gradients in a spatiotemporal-dependent manner, thus patterning the embryo and sending activating or inhibitory cues to underlying cells (Später *et al.*, 2014). These signals elicit a response in the form of gene expression which leads to cell proliferation, differentiation and structure formation. Cardiac-specific factors are thus only expressed in a defined sub-population of the mesoderm that gives rise to cardiac fields (Noseda *et al.*, 2011).

An evolutionarily conserved network of transcription factors and interacting signalling pathways regulate heart development. Four core conserved transcription factors contribute to heart development. These include NK2- (NK2 homeobox), MEF2- (myocyte enhancer factor), GATA- (GATA binding protein), TBX- (T-box) and HAND- (heart and neural crest-derived) type proteins, with species-specific variations. They control cell fate, contractile protein gene expression and cardiac structure morphogenesis (Olson, 2006; Akerberg *et al.*, 2019). Interestingly, these transcription factors also regulate each other's expression, thus stabilising the cardiac gene program (Buckingham, Meilhac and Zaffran, 2005; Kodo and Yamagishi, 2017). These core transcription factors have been found to function in cardiac development from drosophila to humans (Olson, 2006). Homologues of *NKX2.5* and *MEF2C* were even observed to be expressed in the rhythmically contracting pharynx muscle of the nematode *Caenorhabditis elegans*, possibly the most primitive heart (Sylva, van den Hoff and Moorman, 2014).

MEF2 is a MADS-box protein that is well conserved in all metazoans. It is the most ancient myogenic transcription factor. In cardiac cells, MEF2 interacts with other cardiac transcription factors to control the expression of genes encoding for contractile proteins (Schlesinger *et al.*, 2011). *Mef2* expression is enhanced by NK2-type homeodomain proteins (Deng *et al.*, 2017). There are four MEF2 proteins in vertebrates, and *Mef2c* in particular is needed for the induction of a subset of cardiac contractile protein genes, in addition to the development of cardiac structures that originate from the second heart field (Lin *et al.*, 1997). *Mef2c*-expressing cells can be detected as early as the late streak stage. *Mef2c* expression marks progenitors of the right ventricle and outflow tract myocardium (MP *et al.*, 2005). Additionally, *Mef2c*

knockout in mice is embryonic lethal at E9.5 due to severe cardiac defects (Lin *et al.*, 1997).

The gene *Nkx2.5* is expressed in cardiac progenitors and the associated endoderm in vertebrates (Zhang *et al.*, 2014), it is a homologue of Drosophila's *tinman*. Overexpressing *nkx2.5* in zebrafish and frogs led to the expansion of the heart field and promoted cardiac gene expression (Chen and Fishman, 1996). Moreover, a dominant-negative mutant *nkx2.5* protein blocked cardiogenesis in frog embryos (Fu *et al.*, 1998). In mouse embryos lacking *Nkx2.5*, early events in heart formation take place normally but embryos die from aberrant heart tube morphogenesis and perturbed left ventricle development (Lyons *et al.*, 1995). Cre-mediated deletion of *Nkx2.5* in mice led to the ablation of the outflow tract and a lack of ventricular compartmentalisation. In this experiment, a gene for Cre recombinase was inserted into the 3' untranslated region of *Nkx2.5*, leading to *Cre* expression under the control of *Nkx2.5* cis-regulatory control. Deletion was confirmed by crossing these mice with Cre-dependent reporter strains (Stanley *et al.*, 2002).

Nkx2.5 therefore is widely expressed in the second heart field and has a role in maintaining the role of SHF progenitors (Prall *et al.*, 2007; Chung and Rajakumar, 2016). *Nkx2.5* also plays a regulatory role and modulates the transcription of *Etv2*, required for endocardial development. *Etv2*-expressing cells only form endocardial cells and in its absence, these cells differentiate into other lineages (Ferdous *et al.*, 2009).

The GATA family of zinc finger transcription factors control the expression of numerous contractile protein genes, in addition to upstream genes such as *Nkx2.5*, *Mef2* and *Hand*. Six *Gata* genes are expressed in vertebrates, and three of those (*Gata4*, *-5* and *-6*) are expressed in the heart and are involved in heart development (Gallagher *et al.*, 2012). Overexpression of cardiac *gata* genes in frog and zebrafish embryos prematurely activates cardiac gene expression (Reiter *et al.*, 1999; Latinkić, Kotecha and Mohun, 2003). In the SHF, *Gata4*, along with *Tbx5* and the Hedgehog signalling pathway modulate the formation of the DMP and atrial septation. *Gata4* also activates the expression of *Gli1* in the posterior SHF to stimulate cell proliferation. *Gata4*-deficient mice exhibit atrial and atrioventricular septation defects which can interestingly be rescued by promoting constitutive Hedgehog signalling in the SHF (Zhou *et al.*, 2017).

The *Hand* genes regulate the development of ventricles (Buckingham, Meilhac and Zaffran, 2005). Notably, amphibians and fish have only one *hand* gene, which corresponds to them having only one ventricle. Zebrafish lacking this *hand* gene fail to develop ventricles (Yelon *et al.*, 2000). Mice have two *Hand* genes, *Hand1* and *Hand2*. Hand1 and Hand2 proteins are both involved in the formation of ventricles, albeit differently. *Hand2* also regulates the formation of the atrioventricular canal and cardiac valves (Laurent *et al.*, 2017). *Hand2* mutant mice develop a hypoplastic right ventricle while reduced *Hand1* activity results in failure of formation of the left ventricle (Vincentz, Barnes and Firulli, 2011) and mutations in *Hand1* have been shown to cause TOF (Wang *et al.*, 2017) and familial dilated cardiomyopathy (Zhou *et al.*, 2016). Additionally, knocking out *Hand1* in embryonic stem cells renders them unable to contribute to the outer curvature of the heart that later forms the left ventricle (Riley *et al.*, 2000). *Hand1* expression marks a domain of cells in the outflow tract and the epicardium, in addition to left ventricular myocardium (Barnes *et al.*, 2010).

Members of the T-box family are also pivotal players in this process as they function in myocardial proliferation and patterning. They are transcription factors that recognise a DNA sequence known as the T-half site through their highly conserved DNA-binding region (Steimle and Moskowitz, 2017). There can be a single, or multiple T-half sites with varying orientations and spacing in target gene promoters. Binding can then lead to transcriptional activation or repression (Tada and Smith, 2001). The T-box is also a conserved interaction domain for other transcription factors, histone-modifying enzymes and chromatin remodelling complexes that function in transcriptional control (Boogerd, Moorman and Barnett, 2009). 6 of the 17 members of the T-box family function in the development of the mammalian heart, namely *Tbx1*, *Tbx18* and *Tbx20* of the *Tbx1* subfamily, and *Tbx2*, *Tbx3* and *Tbx5* of the *Tbx2* subfamily (Zhu *et al.*, 2017). These work in concert and are expressed in different progenitor pools as well as different regions of the developing heart (Plageman and Yutzey, 2005; Hoogaars *et al.*, 2007). Interestingly, their role is also evolutionarily conserved in invertebrates, such as Drosophila, which have uncompartmentalised heart tubes (Stennard and Harvey, 2005). *Tbx2* and *Tbx3* are able to repress the myocardial gene programme to modulate the venous pole, atrioventricular canal and outflow tract formation. *Tbx1* expression is found in

outflow tract cardiac precursors and *Tbx18* expression is detected in the venous pole (Sylva, van den Hoff and Moorman, 2014).

Tbx5 is an important member of the T-box family in which mutations leads to Holt-Oram syndrome (Ghosh *et al.*, 2001; Vanlerberghe *et al.*, 2019). Holt-Oram syndrome is characterised by heart and upper limb defects (HOLT and ORAM, 1960). During development, *Tbx5* expression is detected in the first heart field (FHF) and its derivatives (Greulich, Rudat and Kispert, 2011), marking the left ventricular myocardium. This is shown by the fact that its expression is first detected in the bilateral wings of the cardiogenic mesoderm. Moreover, it is later found in the endocardium and myocardium of the inflow region, atria, the atrioventricular canal and the left ventricle. It is expressed in a gradient from the venous pole to the right ventricle (Sylva, van den Hoff and Moorman, 2014). However, *Tbx5* expression is not found in the outflow tract (OFT) of the looping, chambered heart tube (Bruneau *et al.*, 1999).

Tbx5 is a key regulator of the cardiac gene network. It is able to directly activate the expression of *Cdk6* to drive cardiac progenitor proliferation (L. Xie *et al.*, 2012). Moreover, it activates the expression of *Osr1*, encoding for a transcription factor needed for atrial septation. In addition, along, with the Sonic Hedgehog pathway, it plays a role in the formation of the DMP involved in atrial septation. It directly activates the expression of *Gas1*, the product of which is a Sonic Hedgehog signalling pathway component (L. Xie *et al.*, 2012).

Upstream factors controlling *Tbx5* expression have been debated. Retinoic acid signalling has been shown to limit *Tbx5* expression to the posterior region of the heart tube. Moreover, JAK-STAT3 signalling has been shown to be necessary and sufficient to drive *Tbx5* expression in P19CL6 cells, a cellular model of cardiomyocyte differentiation (Sirbu, Zhao and Duester, 2008; Snyder, Huang and Zhang, 2010). *Tbx5* interacts with other genes such as *Nkx2.5*, *Gata4* and *Mef2c* and they work cooperatively to drive and regulate cardiac development (Ghosh *et al.*, 2009, 2014; Waldron *et al.*, 2016). Interestingly, *Tbx5*, *Gata4* and *MEf2c* were able to rapidly and efficiently drive direct reprogramming of post-natal and dermal fibroblasts into cardiomyocyte-like cells (Ieda *et al.*, 2010). This can have immense implications for regenerative medicine and can be a leap in treatment options available for patients suffering from CHDs. One aim of elucidating the cardiac gene

network is to achieve efficient cell reprogramming of patients' own cells for applications in regenerative medicine and cardiac damage repair. Adding other factors, such as *Hand2*, *Mycod*, *Zfpm*, *Esrrg* and *Mesp1* enhanced the reprogramming efficiency of human embryonic stem cells and mouse tail tip and cardiac fibroblasts (Song *et al.*, 2012; Fu *et al.*, 2013)

Cardiomyocyte development involves the formation of sarcomeres, which is also governed by a specific set of genes. Sarcomeres (characterised by filamentous proteins) are the basic functional units of cardiac muscles and are crucial for the structure and function of cardiomyocytes (Gautel and Djinović-Carugo, 2016) (depicted in Figure 1-6). Two major types of filamentous proteins play a part in muscle contraction and relaxation. They are organised into thin and thick filaments that interlock (Teekakirikul, Ho and Seidman, 2013). Thin protein elements are Cardiac troponin complex members T (TNNT2), I (TNNI3), C (TNNC1), α-tropomyosin (TPM1) and α-cardiac actin (ACTC1). Thick protein elements are α/β-myosin heavy chain (MYH6/7), ventricular regulatory light chain (MYL3), ventricular essential light chain (MYL2) and cardiac myosin-binding protein C (MYBPC3). Titin-type and z-disc proteins, such as α-actinin are also found. These proteins use ATP hydrolysis to drive muscle shortening and lengthening (Morimoto, 2008), a process that requires precision as well as energy.

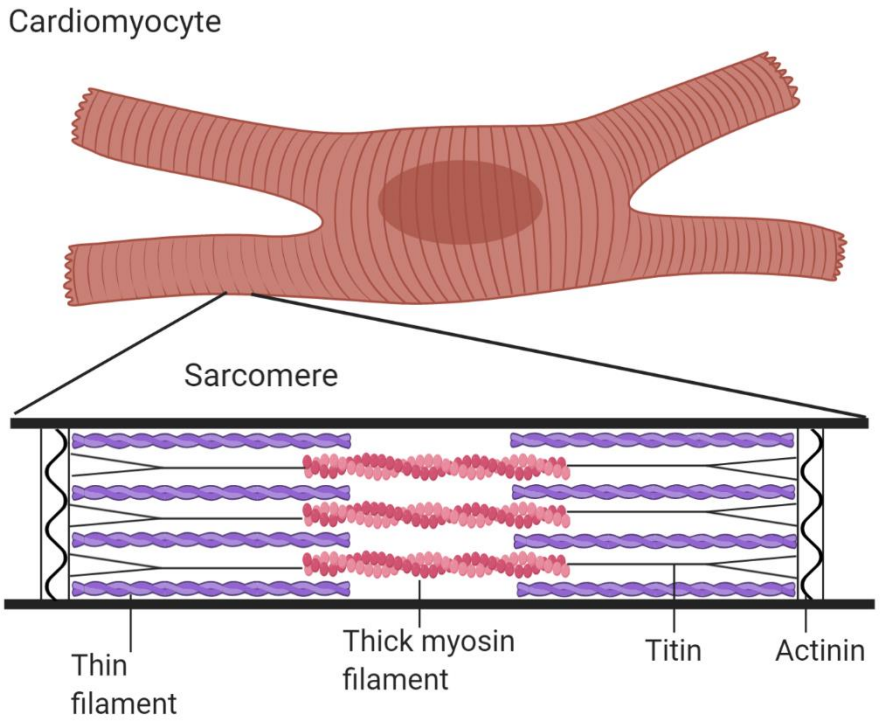


Figure 1-6. A sarcomere is formed of thin and thick filamentous proteins arranged in an interlocking pattern. It is the basic contractile unit of striated muscle. The thin filament is formed of a troponin, tropomyosin and actin complex. Myosin forms the thick filament. Figure created using Biorender.com.

Mutations in genes encoding for sarcomeric proteins can also lead to CHDs (Morimoto, 2008; Harris and de Tombe, 2019). α-myosin heavy chain (αMYH6) is a sarcomeric protein associated with cardiomyopathies. A mutation in *αMYH6* was found to cause a type of atrial septal defect (Ghosh et al., 2014) while *βMYH7* was the among the most frequently associated genes with dilated cardiomyopathy (McNally and Mestroni, 2017). Various mutations in the troponin complex, in addition to z-disc proteins have been found to cause a range of cardiomyopathies, such as hypertrophic cardiomyopathy (HCM), dilated cardiomyopathy (DCM) and restrictive cardiomyopathy (RCM) (Morimoto, 2008; McNally and Mestroni, 2017).

1.1.7 Cardiomyocyte differentiation and development

The heart contains several cell types, namely, cardiomyocytes, cardiac conduction cells, cardiac fibroblasts and vascular smooth muscle cells within the myocardium and endothelial cells in the myocardium and endocardium (Später *et al.*, 2014). Cardiomyocytes are a highly specialised cell type that undergoes a complex, step-wise differentiation process, outlined in **Error! Reference source not found.**. Cardiomyocytes of their various subtypes arise due the cooperation of a network of transcription factors and signalling pathways, defined by location and function. During differentiation, pluripotency-associated markers like *Oct4*, *Sox2*, and *Nanog* are downregulated while *T* (also known as *Brachyury*) is upregulated. *T* expression itself is regulated by Wnt signalling.

Pluripotent stem cells in the gastrulating mouse embryo transiently express *Oct4* in the epiblast before the emergence of the primitive streak (Figure 1-7). *Oct4* acts on *Sox17* to activate mesoendodermal/endodermal genes. *Sox2* is also expressed in the anterior epiblast (Van Vliet *et al.*, 2012). Oct4 and Sox2 transcription factors work in concert to activate a large number of genes by recognising and binding to chimeric motifs. They have also been shown to bind with Nanog at enhancers of multiple genes (Van Vliet *et al.*, 2012).

T was shown to be expressed throughout gastrulation (Figure 1-7), with the first cells exiting the epiblast were found to co-express *Gata6* and *T*. As cells differentiate down the mesodermal lineage and move proximally, the first cardiac-committed mesodermal population to emerge expresses *Flk1*, or human *KDR*. BMP4 secreted by the extraembryonic ectoderm drives posterior mesodermal differentiation (Van Vliet *et al.*, 2012). *Mesp1* drives the differentiation of cardiac progenitors (see Figure 1-7). Notably, *MESP1* and *ETS2* were found to be sufficient to reprogramme human dermal fibroblasts into cardiac progenitors (Islas *et al.*, 2012).

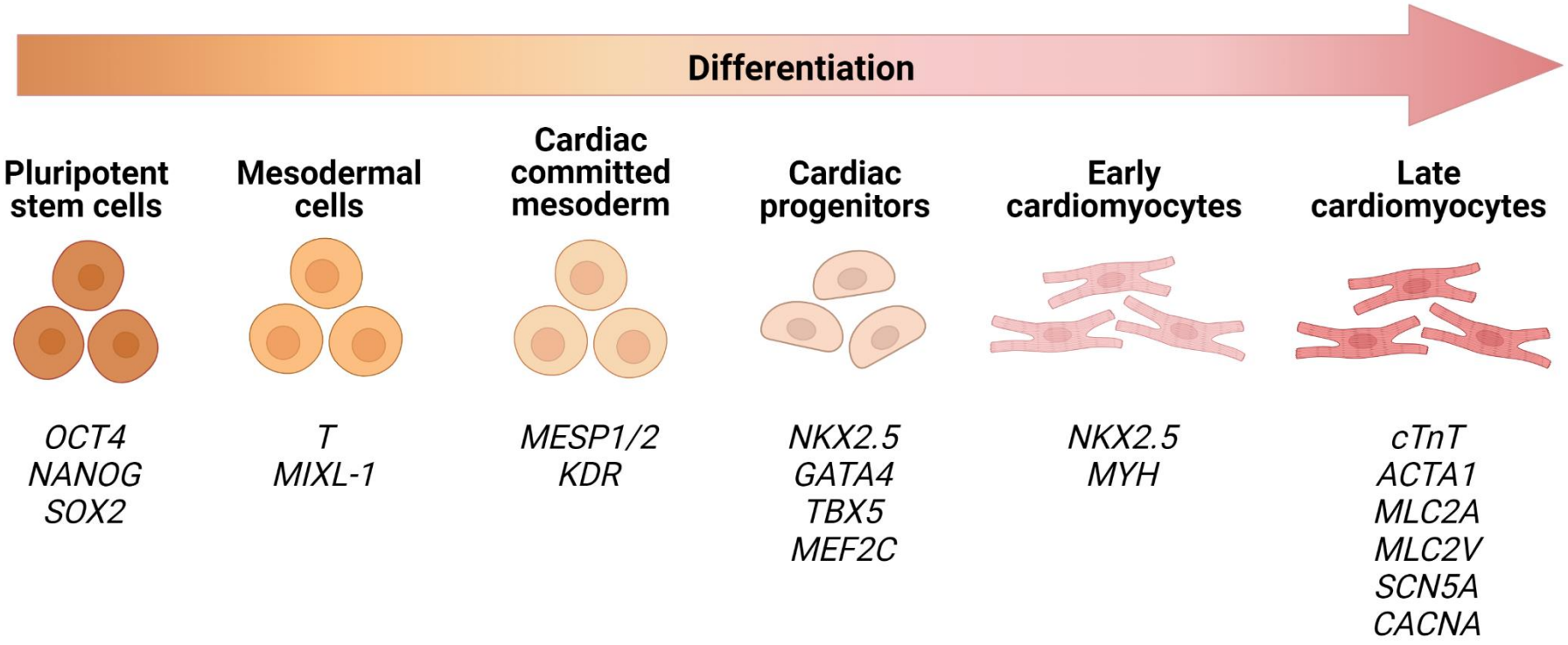

Differentiation
Pluripotent stem cells
OCT4
NANOG
SOX2
Mesodermal cells
T
MIXL-1
Cardiac committed mesoderm
MESP1/2
KDR
Cardiac progenitors
NKX2.5
GATA4
TBX5
MEF2C
Early cardiomyocytes
NKX2.5
MYH
Late cardiomyocytes
cTnT
ACTA1
MLC2A
MLC2V
SCN5A
CACNA

Figure 1-7. Cardiomyocyte differentiation is a complex process under the control of stage-specific gene expression. The figure shows markers of differentiation at each stage. Stem cells express pluripotency factors shown. Mesodermal lineage specification is driven by *T* and *MIXL-1*. Cardiac lineage commitment is marked by *MESP1, MESP2* and *KDR* expression. As differentiation progresses, cardiac progenitors express known cardiac genes *NKX2.5, GATA4, TBX5* and *MEF2C*. Mature myocytes express genes associated with contractility proteins such as *cTnT, ACTA1,* the sarcomeric proteins *MLC2A* and *MLC2V* and ion channels *SCN5A* and *CACNA*. Figure created with biorender.com

T also forms a negative feedback loop with the transcription factor *Mesp1*. *T* initially upregulates *Mesp1* expression but subsequently represses. *Mesp1* in turn supresses endodermal lineage commitment by downregulating *Sox17* and *Foxa2* and promotes the expression of *Mef2c*, *Gata4* and *Nkx2.5*, leading to the formation of cardiac progenitors (**Error! Reference source not found.**A). Concomitantly, *Isl1*, a secondary heart field marker, activates the expression of *Foxh1* and *Mef2c*, directing cells towards the right ventricle and secondary heart field (Wu *et al.*, 2006) (**Error! Reference source not found.**). *Nkx2.5* is one of the earliest genes expressed in cardiac progenitor cells and its downstream targets include *Anp, Hand1*, *Gata6* and cardiac α-actin. It also interacts with other transcription factors like *Tbx5* and *Gata4* to activate downstream cardiac targets such as cardiac-restricted ankyrin repeat protein (CARP) and natriuretic peptide precursor type A (Nppa) (A. Parikh *et al.*, 2015).

Cardiomyocytes also form specialised structures at their cell membranes to enable cell-cell adhesion and electrical coupling between adjacent cells. Desmosomes anchor adjacent cells together through the interaction of cadherin molecules and provide mechanical stability. Adherens junctions also contain cadherins, in addition to catenins, to mediate cell-cell adhesion (Karbassi et al., 2020). Gap junctions allow for electrical communication between cardiomyocytes, spreading action potentials and coordinating cardiac contraction. Propagation of action potential occurs via ion channels, where sodium channels open and potassium channels close to control depolarisation, which is maintained by the opening of calcium channels. Sodium and potassium channels are encoded by *SCN5A* and *KCNA5*, among others (Priest and

McDermott, 2015) (Figure 1-7). Calcium channels are encoded by *CACNA1C* and *CACNAB2* (Shah et al., 2022) (Figure 1-7).

In the next phase of foetal growth and during heart septation and formation of the outflow tract, differentiated cardiomyocytes undergo exponential proliferation. Cardiomyocytes contribute to hyperplasic (growth due to an increase in cell number) heart growth and undergo full cytokinesis (Padula, Velayutham and Yutzey, 2021).

Altogether, from initial lineage commitment to full contractile and electrophysiological functionality, cardiomyocyte growth and maturation involves multiple gene and signalling pathways. These are strictly regulated to confer cellular identity and function. Figure 1-8depicts a summary of the master genetic and molecular regulators of this process. Following mesodermal commitment, future regions of the heart are patterned via differential gene expression and signalling pathway-mediated induction/inhibition (Karbassi et al., 2020).

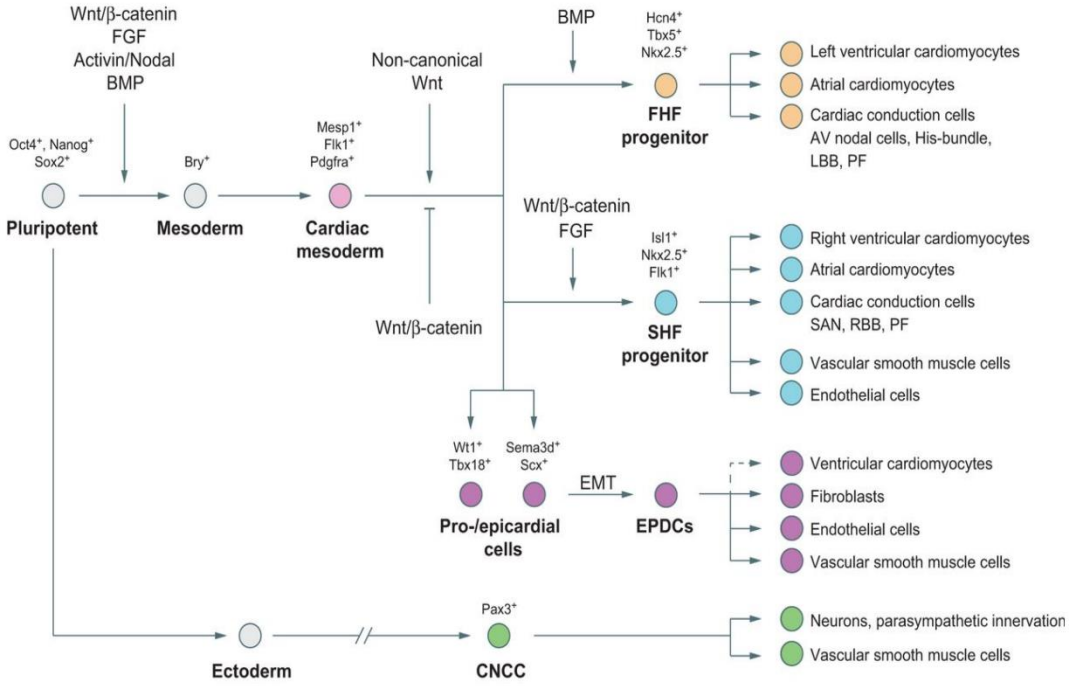


Figure 1-8. Step-wise lineage commitment and differentiation of cardiomyocytes is carefully regulated by a host of transcription factors and signalling molecules. Differentiation is driven by loss of *Oct4*, *Nanog* and *Sox2* expression and the induction of Wnt/β-catenin, FGF, Activin/Nodal and BMP pathways. Mesodermal cells expressing *Brachyury* (or *T*) commit to the cardiac lineage and

express *Mesp1*, *Flk1* (or *KDR*) and *Pdgfra*. These cells go on to form the FHF or SHF in response to BMP or Wnt/β-catenin and FGF signalling, respectively. *Hcn4*/*Tbx5*/*Nkx2.5*- expressing cells go on to form the FHF which contributes to the atrium, left ventricle, cardiac conduction cells and bundle cells. *Isl1*/*Nkx2.5*/*Flk1*- expressing cells differentiate into the SHF which forms the right ventricle, parts of the atria, conduction cells, vascular smooth cells and endothelial cells. Epicardium-derived cells emerge from cells expressing *Wt1*, *Tbx18*, *Sema3d* and *Scx*. These undergo EMT to generate ventricular myocytes, fibroblasts, endothelial cells and vascular smooth muscle cells. Cardiac neural crest cells are ectodermal in origin and contribute to cardiac innervation, vascular smooth muscle cells and valves. EPDCs, epicardium-derived cells; EMT, endothelial-to-mesenchymal transition; SAN, sinoatrial node; RBB, right bundle branch; LBB, left bundle branch; PF, Purkinje fibers; AV, atrioventricular. Adapted from (Später *et al.*, 2014).

1.1.7.1 Post-natal cardiomyocytes

After birth, heart growth switches from hyperplasic to hypertrophic (growth due to an increase in cell size) whereby cardiomyocytes go through mitosis without cytokinesis. This results in the binucleation of cardiomyocytes. Murine cardiomyocytes exit the cell cycle approximately one week after birth while that process lasts for several years in humans (Payan, Hubert and Rochais, 2020).

Cardiomyocytes continue to mature postnatally. The heart must adapt to various organismal conditions after birth, such as ambient oxygen levels and energy requirements. Energy is primarily produced by glycolysis in murine foetal hearts and rapidly transitions to fatty acid oxidation in the first few days post-birth (Lopaschuk and Jaswal, 2010; Payan, Hubert and Rochais, 2020). Additionally, sarcomeres in cardiomyocytes undergo switching from foetal contractile proteins such as Myh7, Tnni1 and Myl7 to adult isoforms Myh6, Tnni3 and Myl2 (Payan, Hubert and Rochais, 2020).

1.1.8 Epigenetics in heart development

Eukaryotes have evolved an efficient method of packaging DNA that also functions in gene regulation. Eukaryotic nuclei are able to contain up to billions of base pairs of DNA in their miniscule sizes because DNA is tightly packaged in nucleosomes.

Nucleosomes are the repeating basic unit of chromatin, a dynamic polymer that forms the 'genetic material' (Rudnizky *et al.*, 2017). Epigenetic regulation is crucial to control gene expression and this section will outline how epigenetic modifiers function in cardiac differentiation.

A nucleosome is a structure formed of approximately 147 base pairs of DNA spooled around an octamer of core histone proteins- 2 copies of each of histone proteins H2A, H2B, H3 and H4 (Rudnizky *et al.*, 2017). Histones are small basic proteins formed of a globular domain and an NH2 terminus that projects from the nucleosome forming the "tail" (Jenuwein and Allis, 2001). H1 is a linker histone linking nucleosomes together and stabilising the octameric core into higher-order structures (Verdone *et al.*, 2006). Chromatin fibre also contains a variety of other accessory proteins and different variants of histones that are expressed in a cell- and developmental stage-specific manner. A variant of H3, for example, is present in eukaryotic centromeres, necessary for their assembly and function (Watts, Kumar and Bhat, 2016). H2A.Z, a variant of H2A, facilitates chromatin compaction through promoting polycomb repressive complex 2(PRC2)-mediated silencing and is correlated with H3K27me3 (histone 3 lysine 27 trimethylation) in mouse embryonic stem cells. While H3.3 counteracts PRC2-dependent silencing by hindering chromatin compaction (Y. Wang *et al.*, 2018).

Chromatin is subject to a wide range of posttranslational modifications that mostly manifest on histone amino termini, regulating access to the underlying DNA (Jenuwein and Allis, 2001). A wide variety of histone-modifying enzymes work in concert to carry out post-translational modifications (PTMs) that include acetylation, methylation, phosphorylation (Strahl and Allis, 2000) and the more recently discovered succinylation (Z. Xie *et al.*, 2012) among others. Enzymes work individually or in ATP-dependent complexes to carry out their functions and modify chromatin (Owen-Hughes, 2003). Thus histones not only provide an elegant means of DNA packaging, but play an important role in regulating chromatin dynamics and gene expression.

Distinct modifications of histone amino-terminal domains, such as lysine acetylation and methylation, serine phosphorylation or arginine methylation can cause dynamic transition between transcriptionally active or silent chromatin. The enzymes carrying out these histone tail modifications are able to recognise designated amino acids at

particular positions (Strahl and Allis, 2000; Verdone et al., 2006) providing a controlled level of specificity. Figure 1-9 depicts the winding of DNA around nucleosome histones and shows the various histone tail modifications that may occur on amino acids on histone tails.

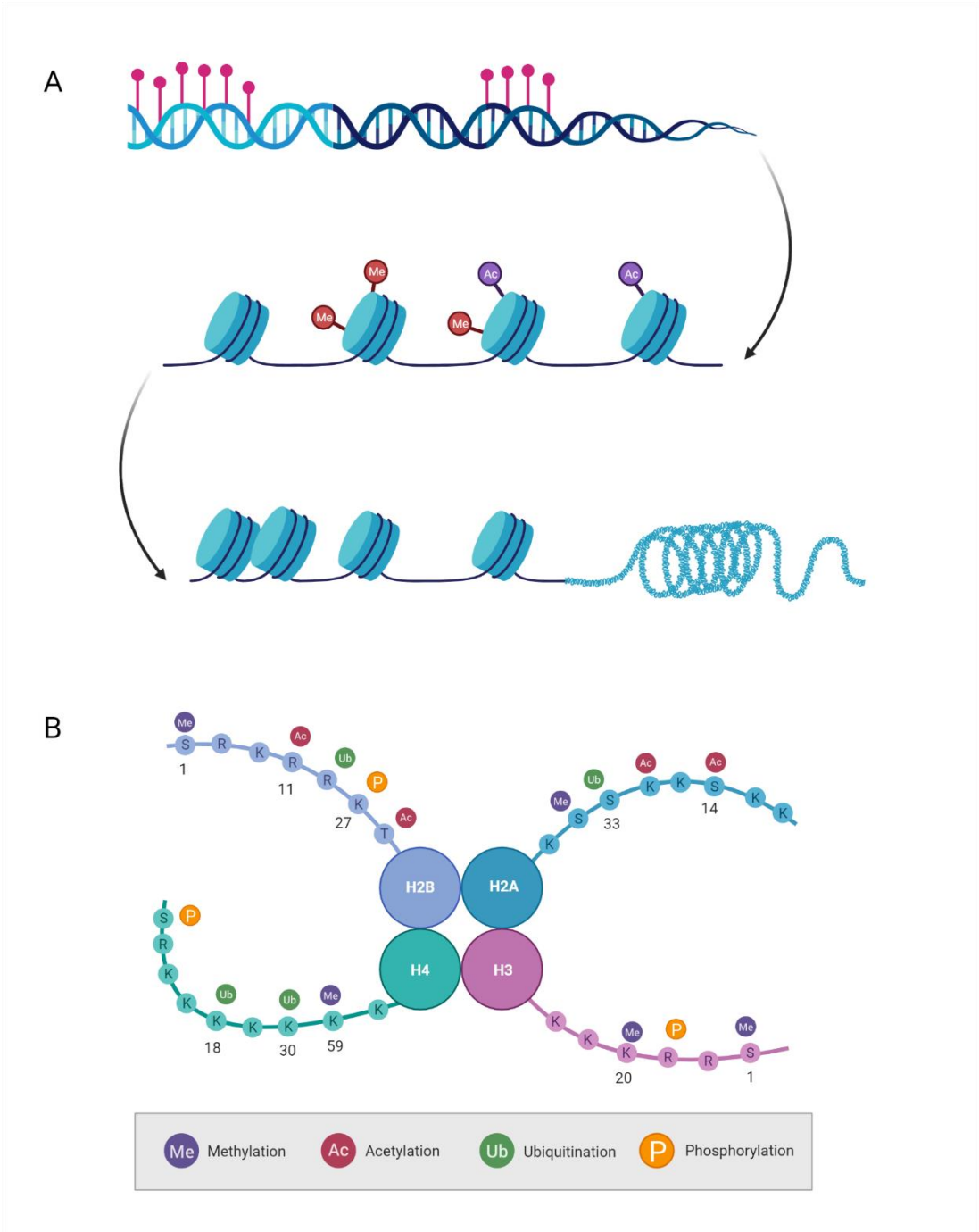


Figure 1-9. Schematic of DNA packaging around nucleosomes and histone-tail modifications. (A) Nucelosomes, represented by light blue cylinders, are the basic unit of chromatin and are made of histones. DNA winds around individual nucleosomes. Chromatin can be made more or less accessible via the

introduction of chemical modifications on histone tails. Examples of these modifications, methylation (Me) and acetylation (Ac) are shown in the figure. (B) Nucleosomes are octamers made of two of H2B, H2A, H4 and H3 proteins. DNA is wound around each nucleosome. Chemical marks are placed on specific amino acids on histone tails and those affect gene expression by controlling DNA polymerase and transcription factors' access to underlying DNA. The numbers indicate the position of amino acids. S, serine; K, lysine; R, arginine; T, threonine. Figure created with Biorender.com.

Condensation of nucleosomes, in addition to reducing the surface area for DNA storage, forms a physical barrier preventing transcription factors gaining access to the DNA and thus preventing gene expression. Three epigenetic processes and the interaction between them control this process. These are firstly, the involvement of ATP-dependent chromatin remodellers in the manipulation of histones and higher order chromatin structures. Secondly, post translational modifications of histone proteins by covalent labelling, and finally direct methylation of cytosine bases on the DNA (Zhu *et al.*, 2013; Quaife-Ryan *et al.*, 2016).

A major form of histone modification is methylation. Histone methylation can be associated with gene activation or repression, depending on the location of the lysine residue that is methylated and the number of methyl groups (mono-, bi- or trimethylation). Methyl groups are added by enzymes called methyl transferases (Quaife-Ryan et al., 2016). Methylation occurs on cytosine residues in CpG dinucleotides in the DNA sequence or on histone proteins around which the DNA is wound (Gilsbach *et al.*, 2014). Methylation marks at lysine 9 on Histones 1 and 3 are usually associated with transcriptionally silent heterochromatin (Xu and Jiang, 2020). On the other hand, methylation of lysine 4 on histone 3 is associated with transcriptional activation (Collins *et al.*, 2019).

Changes in DNA methylation patterns occur during the development and maturation of cardiomyocytes (Gilsbach et al., 2014). In ESCs, transcription factor binding sites for *Nanog* and *Oct4* are unmethylated (hallmark of gene activation in this case) contrary to the methylation of *Gata1* and *Mef2c* binding sites. As ESCs differentiate down the cardiac lineage, the pattern is reversed as pluripotency-related TF binding

sites become hypermethylated as opposed to the demethylation of cardiogenic TF binding sites (Gilsbach et al., 2014).

Another type of epigenetic change is histone acetylation, carried out by histone acetylases (HATs). HATs add acetyl (CH_3CO) groups to lysine residues on the tails of histone proteins. This adds a negative charge to histones, thus neutralising the lysine's positive charge and as a consequence, destabilising the electrostatic attraction between histones and the negatively charged DNA (Yang and Seto, 2007). This leads to a more relaxed chromatin structure, facilitating the access of gene transcription machinery and TFs and thus the consequent transcription of genes (Marmorstein and Zhou, 2014), see Figure 1-10. The "histone code" thus provides a means of controlling gene expression temporally, developmentally and spatially.

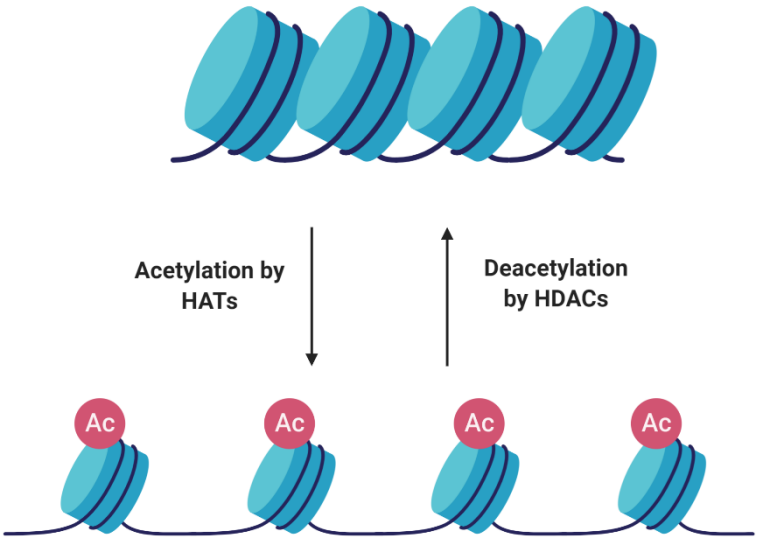


Figure 1-10. Illustration of the effect of histone acetylation on nucleosome (blue cylinders) compaction. DNA is tightly wound around nucleosomes. Acetylation/Deacetylation affects gene expression by strengthening or weakening the electrostatic charge between DNA and nucleosomes, respectively. A more 'open' chromatin structure leads to higher gene expression. Figure created using Biorender.com.

1.1.8.1 Histone acetylases

Acetylation of histone tails is an example of a post-translational modification (PTM) that modulates chromatin dynamics mediated by histone acetyltransferases (HATs). Acetylation is a prevalent protein modification found in both prokaryotes and

eukaryotes. More than 15,000 acetylation sites have been reported in some tissue types (reviewed in (Choudhary *et al.*, 2014)). Mutations affecting acetylation or acetyltransferase functions have been correlated with several human diseases. Most HATs are regulated by association with binding partners, through tethered domains or other PTMs. Acetylation occurs when an acetyl moiety is added to the ε-amino group of a lysine residue in a reversible reaction known as Nε-acetylation (Devaiah *et al.*, 2016) in an evolutionarily conserved manner that functions in a wide array of cellular pathways (De Luca *et al.*, 2014). This mechanism is not to be confused with N-terminal acetylation which is carried out by Nα-acetyltransferases (Linster and Wirtz, 2018). Protein acetylation was observed in all domains of life, playing roles in chromatin maintenance, protein stability, cell structure, cell metabolism and transcriptional regulation (Tucker *et al.*, 2014). Acetylation marks are placed on lysine residues usually located in N-terminal tails of core histones, examples are lysines 4, 9, 14 and 18 of histone H3 and lysines 5, 8 and 12 of histone H4 (Sun *et al.*, 2012). Acetylation of lysine residues by acetyltranferases is a reversible reaction (Tucker et al., 2014).

The idea that histone acetylation might play a part in gene regulation was first put forward by Allfrey and colleagues in 1964 (Allfrey, Faulkner and Mirsky, 1964). However, it was thirty years later that the first HAT, HAT1 was identified in yeast (Kleff *et al.*, 1995; Parthun, Widom and Gottschling, 1996). GCN5, more recently known as KAT2A, was then isolated from tetrahymena in 1996, and with it ushering in more discoveries of other HATs and histone PTMs (Brownell *et al.*, 1996). When early histone acetylases (HATs) were identified it was thought that they only acetylate histone tails but it was later discovered that these HATs themselves had non-histone substrates as well, such as p53 (Kouzarides, 2000). Acetylation marks are ‘read’ by well-conserved bromodomain-containing proteins that mediate downstream responses (Sanchez and Zhou, 2009). Bromodomains are present in HATs- and ATP-dependent chromatin remodelling complexes (Sun et al., 2012) such as the SWI/SNF complex. The latter contains bromodomains that function in recognising acetylated lysines which is followed by recruitment of the complex to the targeted region, changing its conformation to a more ‘open’ form to allow transcription machinery access (Hassan *et al.*, 2002).

There are at least five families of HATs, which act in larger protein complexes, thus enabling targeting of different enhancers and promoters. They are grouped into these families based on sequence and structural homology: HAT1, GCN5/PCAF, MYST (MOZ, Ybf2, Sas2 and Tip60), p300/CBP and Rtt109 (Yang and Seto, 2007). These HATs have a structurally conserved Acetyl Coenzyme A (AcCoA) binding core comprised of a three-stranded β-sheet and a helix that functions in AcCoA binding. Interestingly, while the structure of this core is conserved, there is little to no sequence homology among the different HAT families (Friedmann and Marmorstein, 2013). Many HATs like members of the p300/CBP and MYST families have been shown to acetylate both histone and non-histone proteins. Moreover, there are acetyltransferases such as α-tubulin acetyltransferase that only acetylate non-histone proteins (Spange *et al.*, 2009). As a matter of fact, thousands of proteins with different functions, such as kinases, transcription factors and ribosomal proteins are acetylated. Akin to phosphorylation and other PTMs, acetylation plays a part in regulating the function of these proteins in addition to taking part in cellular activities such as cell cycle control, cytoskeleton organisation, endocytosis and metabolism (McCullough and Marmorstein, 2016). Aberrant acetylation or deacetylation is thought to play a role in uncontrolled growth and division of tumour cells as cell-cycle checkpoints are disrupted (Sun et al., 2012).

Acetylation of lysine 27 on histone 3 (H3K27) is typically associated with enhancers of active genes, for example (Bannister and Kouzarides, 2011). Two of the most well-known HATs are p300 and CREB binding protein (CBP). Those are ubiquitously expressed and cooperate with many transcription factors to regulate gene expression in different cell types. Interestingly, p300 also directly acetylases cardiac transcription factors such as Mef2, Gata4 and serum response factor (Srf) to enhance DNA binding (Slepak *et al.*, 2001). Knocking out *p300* is embryonically lethal as it leads to proliferation defects, downregulation of cardiac structural genes (e.g. *Myh7*, α-actinin) and cardiac structural abnormalities (Shikama *et al.*, 2003).

1.1.8.2 KAT2A AND KAT2B

Human KAT2A (lysine acetyltransferase, also known as GCN5) and KAT2B (PCAF) are acetylases that share 70% sequence similarity. They are involved in a myriad of cellular processes such as chromatin remodelling, transcriptional regulation, DNA regulation and repair, cell cycle progression and cell death

(Fournier *et al.*, 2016). KAT2A/B acetylate lysine residues on mainly histone H3 and to a lesser extent, H4 to loosen chromatin compaction. However, KAT2A/B also have many non-histone targets. One example is the polo-like-kinase 4 (PLK4) protein that is a major regulator of centrosome assembly. PLK4 depletion leads to aberrant centriole formation while its overexpression leads to an abnormally high number of centrosomes, a hallmark of many cancers. Acetylating PLK4 inhibits its kinase activity (Fournier et al., 2016). Depleting KAT2A/B activity in mammalian cells has been shown to increase centrosome numbers (Orpinell *et al.*, 2010). KAT2A and KAT2B are expressed ubiquitously but KAT2A is highly abundant in the heart while KAT2B is highly expressed in the pancreas (Yang *et al.*, 1996).

Kat2a knockout is embryonic lethal, while *Kat2b*-null mice do not display an obvious phenotype. Double knockouts of *Kat2a* and *Kat2b*, however, result in severe developmental defects (Xu *et al.*, 2000). *Kat2a* and *Kat2b* show different expression patterns during embryogenesis, as *Kat2a* is expressed earlier (Yamauchi *et al.*, 2000).

1.1.8.3 KAT2A and KAT2B involvement in cardiac development

Protein acetylation adds a further level of complexity to the regulation of embryogenesis and heart development. Loss of function mutations in the *p300* gene in mice is embryonic lethal between E9.5 and E11.5 due to cardiac defects (Sartorelli *et al.*, 1997). Even in adult hearts, *p300* overexpression leads to hypertrophy and heart failure (Kawamura *et al.*, 2005). Gata4 and Mef2c are both acetylated in cardiomyocyte differentiation (Ma *et al.*, 2005; Shimizu *et al.*, 2018). Gata4 is acetylated by p300, leading to an increase in its transcriptional activity and the induction of the hypertrophy gene program (Takaya *et al.*, 2008). A dominant negative form of p300 was able to inhibit Gata4-mediated transcription in cardiac myocytes (Yanazume *et al.*, 2003). Moreover, overexpressing *p300* in mice increased Gata4 acetylation leading to myocardial hypertrophy and left ventricular remodelling in models of myocardial infarction (Miyamoto *et al.*, 2006). Hdac3 was found to participate in keeping Tbx5 acetylation levels in check to regulate cardiogenesis (Lewandowski et al., 2014).

In families with mutations in the *ADD3* gene, encoding for adducin-γ, a cytoskeletal protein, associated with some types of cerebral palsy, a homozygous pathogenic mutation *KAT2B* was found to be associated with kidney and heart disease. Synergistic knockdown of both *ADD3* and *KAT2B* were found to confer

susceptibility to heart and kidney disease in *ADD3*-associated diseases (Gonçalves *et al.*, 2018). Since KAT2B was shown to acetylate cytoskeletal regulators implicated in cardiomyopathies, like actinin-4 and myosin-7, it is possible that cardiac defects seen in patients with this genetic background are due to the loss of KAT2B-dependent acetylation of adducin-γ. Moreover, in a study looking at Chinese patients with congenital VSDs, two novel mutations were found in *TWIST1*. *Twist1* is required for cardiac neural crest cell migration, endocardial cushions formation and activates *Tbx20* expression (Chakraborty *et al.*, 2010). TWIST1 was also shown to interact with KAT2B, inhibiting its acetyltransferase activity (Hamamori *et al.*, 1999). The two mutations in the patients were found to impair this chemical interaction between TWIST1 and KAT2B, leading to the loss of TWIST1-mediated repression of E-cadherin (Deng *et al.*, 2015). These studies implicate *KAT2B* in cardiac development septal defects but the exact mechanism remains to be elucidated.

In a recent study conducted by our group investigating the role of KAT2A and KAT2B in cardiac development, it was found that they both acetylate TBX5. Meanwhile, P300 failed to do so. The presence of KAT2B also increased expression at downstream target promoter of *TBX5*, *Anf*. The acetylation site in TBX5 was mapped to lysine 339. Specific mutagenesis of the amino acid (K339R) abrogated KAT2A and KAT2B-mediated acetylation (Ghosh et al., 2018).

To validate the *in vitro* results, *in vivo* studies in zebrafish were also conducted. Morpholinos were used to knockdown both *kat2a* and *kat2b*. It was found that their knockdown led to cardiac and forelimb defects, reminiscent of those seen in Holt-Oram syndrome patients in freshly injected, F0 embryos. Cardiac looping was impaired, in addition to the presence of cardiac oedema. Pectoral fins were also short and stumpy (results shown in Figure 1-11). CRISPR/Cas9-mediated knockout of *kat2a* and *kat2b* recapitulated these results. *Kat2a* and *kat2b* knockout embryos also showed an absence of looping, cardiac oedema and stumpy fins. Moreover, chemical inhibition of Kat2b using Garcinol treatment resulted in similar cardiac and fin phenotypes. In all cases, morphant, knockout and chemically treated embryos displayed bradycardia (Ghosh et al., 2018)

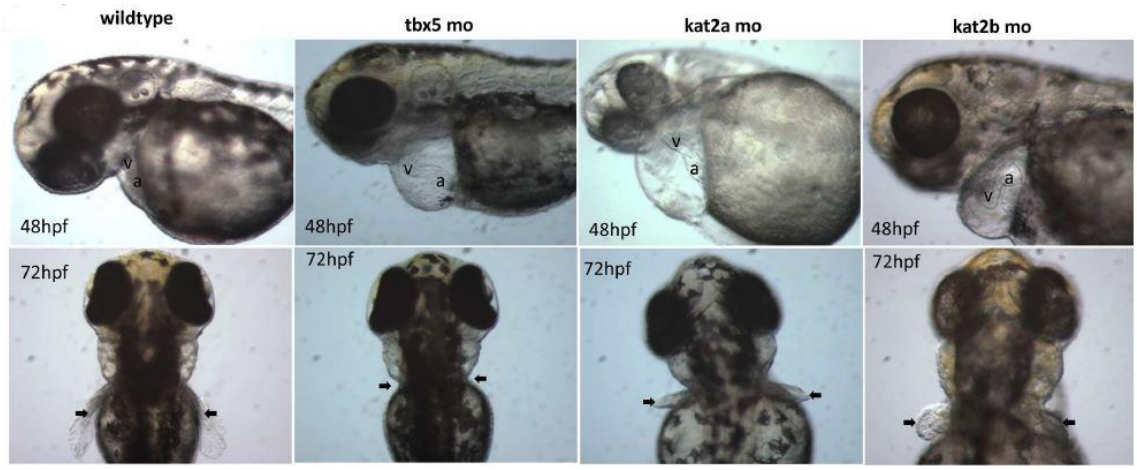


Figure 1-11. Wild-type, *Tbx5*, *kat2a* and *kat2b* morphants. Knocking down either *kat2a* or *kat2b* mirrors knocking down *tbx5* in that embryos show pericardial oedema, aberrant heart looping and stumpy or absent fins (Ghosh et al., 2018). Cardiac phenotypes are shown in the top row and fin phenotypes in the bottom row. The heart is compact in wild-type embryos. Morphants display a reduction in compaction and in looping, in addition to oedema around the heart. Arrows on bottom images point to pectoral fins at 72 hpf. In *tbx5* morphants, pectoral fins are severely affected. In both *kat2a* and *kat2b* morphants, fins are stumpy. A, atrium; hpf, hours post fertilisation; V, ventricle.

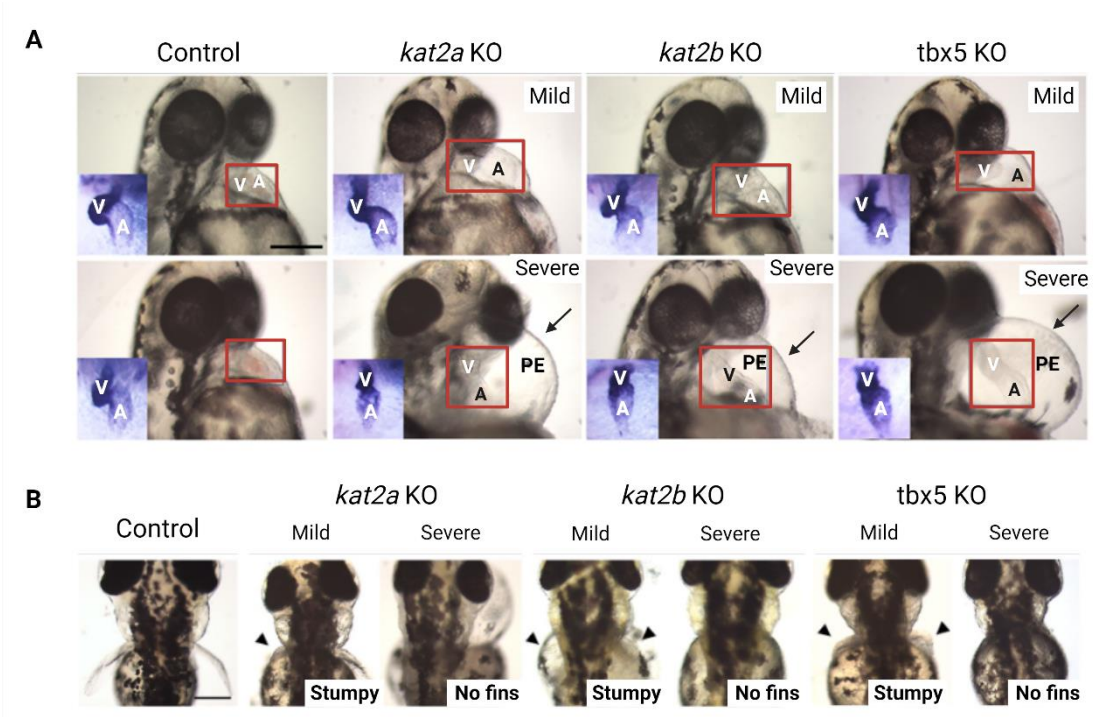


Figure 1-12. CRISPR/Cas9-mediated knockout of kat2a and kat2b in zebrafish phenocopies morpholino knockdown, and results in a similar phenotype to knocking out tbx5. Panel A shows the control embryo, with a normal looped heart, as evident by microscopy and in situ hybridisation using a cmlc2 probe, followed by mild and severe phenotypes for each knockout. Mild embryos showed reduced cardiac looping. Severe embryos showed a lack of looping and apparent cardiac oedema (black arrows). Panel B shows the pectoral fin phenotype in the control and knockout embryos. Mild embryos showed stumpy fins whole severe embryos lacked fins (black arrowheads). A, atrium; PE, pericardial oedema; V, ventricle. Scale bars= 200 µm.

Downstream target genes of *tbx5* were also reduced in *kat2a* and *kat2b* knockouts. Attempts using a *tbx5* acetyl-mimic transcript was successful in rescuing *kat2a* CRISPR/Cas9-mediated knockout. Morphant embryos were also rescued by injected mRNA of a downstream target of *tbx5*, *camk2d1* (unpublished data).

1.1.9 Histone deacetylases

Keeping the acetylation state in check requires both adding acetyl groups as well as removing them. The removal process is performed by histone deacetylases (HDACs). Traditionally, it was thought that deacetylation exclusively takes place on histones leading to gene repression through strengthening the electrostatic attraction between histones and DNA and thus reducing TFs' access to DNA. However, deacetylation of many non-histone proteins has now been shown and there have been calls to rename them acetyl-lysine deacetylases (acKDACs), but for simplicity, they will be referred to as HDACs in this thesis. HDACs remove acetylation marks through catalysing their hydrolysis, producing lysine and a free acetate (López, Sullivan and Fierke, 2016). Deacetylation of non-histone substrates has been shown to play a significant role in the regulation of many cellular processes (Seto and Yoshida, 2014).

HDACs are classified into 4 subclasses (Figure 1-13). Class I and Class III are ubiquitously expressed while Class II members are more enriched in the brain, muscles and T cells (Backs and Olson, 2005). Class I HDACs include HDACs 1, 2, 3 and 8 and are predominantly located in the nucleus (Milazzo *et al.*, 2020). They have a serine-binding domains and nuclear localisation sequences, with the exception of

HDAC2. Class II can be further subdivided into IIa and IIb. The former includes HDACs 4, 5, 7 and 9 while the latter is comprised of HDACs 6 and 10. Class IIa HDACs have nuclear localisation domains, serine-binding motifs and MEF2-binding domains. HDAC6 features a zinc finger protein-binding domain and a serine-glutamate tetradecapeptide sequence(Wang, Qin and Yi, 2015). Class II HDACs are able to shuttle between the nucleus and cytoplasm. Class III HDACs are members of the Sirtuins family (Sirt1-7). These are more involved in metabolic functions and contain zinc binding domains (Yang et al., 2015).

Class IV's lone member is HDAC11 (Voelter-Mahlknecht, Ho and Mahlknecht, 2005). Members of Classes I, II and IV depend on the metal zinc for their catalytic activity. While Class III, the sirtuins, need NAD (nicotine adenine dinucleotide) as a cofactor. HDACs often work in multi-subunit complexes. Class I HDACs, like HDAC1 and 2, are found in the NuRD (nucleosome remodelling and deacetylating), Sin3 and CoREST (co-repressor for element-1-silencing transcription factor) nuclear complexes (Yang and Seto, 2007). Another Class I member, HDAC3 functions in either the NCOR (nuclear receptor corepressor) or its homologue SMRT (silencing mediator of retinoic and thyroid receptors) (Sun et al., 2013). Most members of Class I are ubiquitously expressed in various tissues while members of Class IIa show a more restricted expression pattern. HDACs 4, 5 and 9 show highest expression in the heart, skeletal muscles and brain. The highest expression of HDAC7 was observed to be in CD4/CD8 double positive thymocytes (Verdin, Dequiedt and Kasler, 2003).

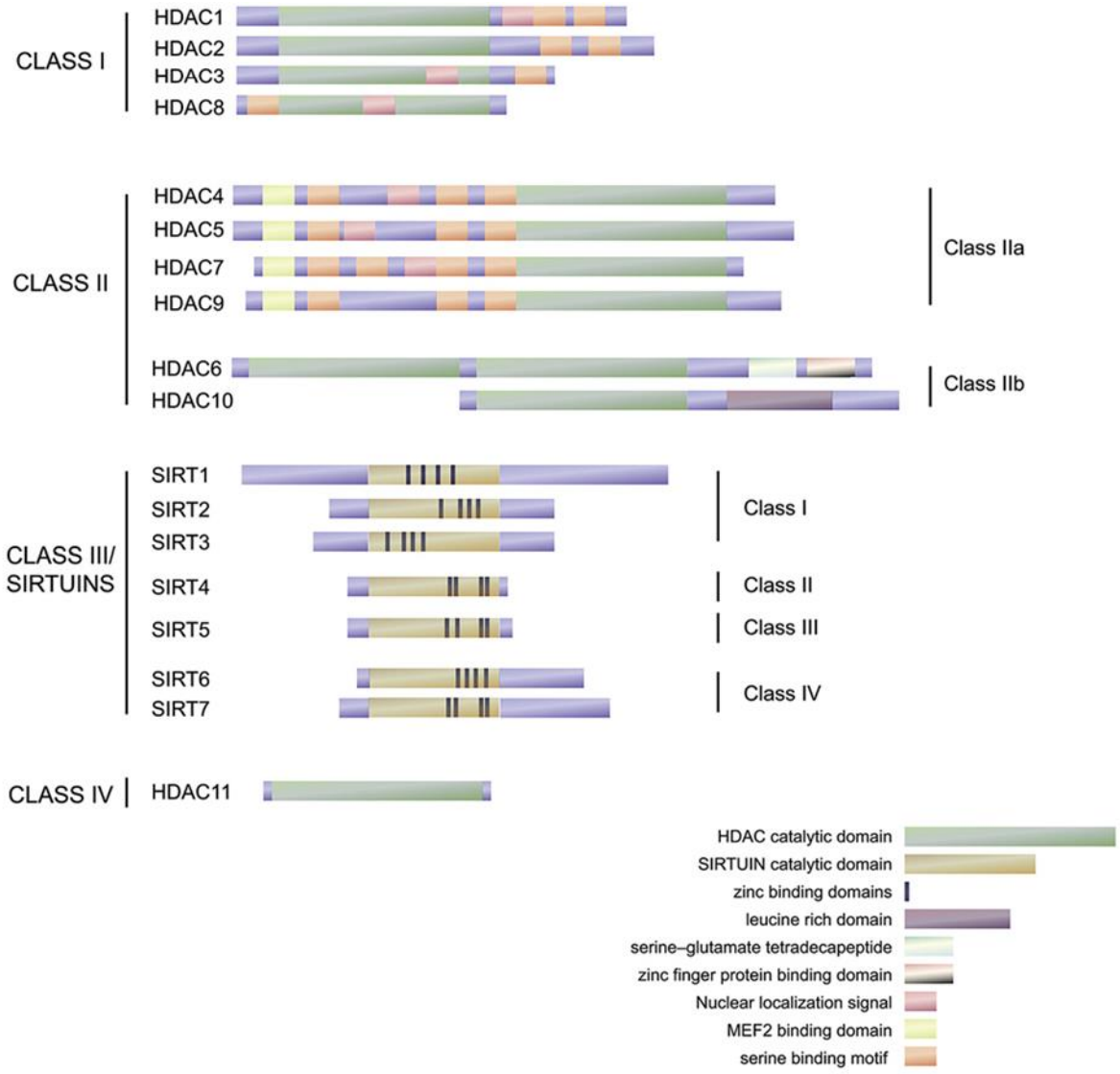


Figure 1-13. Schematic of HDAC protein classes and their domains. Class I contains 4 members with homologous architecture. Class II can be further divided into Class IIa containing HDACs 4, 5, 7 and 9 and Class IIb with HDACs 6 and 10. Class III are also known as sirtuins and Class IV has a single member HDAC11. The protein domains, motifs and localisation signals are indicated and shown in the colour key on the bottom right. Figure adapted from (Barneda-Zahonero and Parra, 2012).

The removal of the acetyl moiety from lysines does not only affect transcription. It also takes part in the regulation of other posttranslational lysine modifications of non-histone proteins, such as ubiquitination, methylation and sumoylation. The establishment or removal of an acetyl group can then ‘free’ that lysine for further

modifications with varying consequences. For example, HDAC2 was shown to shield a fusion oncoprotein from ubiquitination in synovial sarcoma cells (Patel *et al.*, 2019). Moreover, HDAC inhibition resulted in the protection of p53 from ubiquitination, allowing the acetyltransferase p300 to bind to its target genes and activate their transcription in human lung cancer cells (Zhao *et al.*, 2006). The microtubule-associated protein, α-tubulin is another target of HDAC-mediated regulation, where deacetylation by HDAC6 regulates cell motility (Hubbert *et al.*, 2002). HDACs may also take part in histone "cross talk". They are themselves tightly regulated and are controlled via protein-protein interactions and various posttranslational modifications. Phosphorylation is an example of post-translational modification and it activates HDACs 1, 2 and 3 but represses HDAC8. Aberrant HDAC activity was found to be a hallmark of various human diseases, including cancer (Seto and Yoshida, 2014).

HDACs do not directly bind to DNA to exert their functions, as they do not contain DNA-binding domains. Instead they bind directly to DNA-binding transcription factors and are recruited to promoters in this manner (Haberland, Montgomery and Olson, 2009).

Sequence homology was the route used to discover and isolate HDACs in various organisms. Results from a phylogenetic analysis of all HDAC family proteins from all available fully sequenced organisms indicated that the common ancestor of metazoans harboured 2 Class I, 2 Class II and a lone Class IV HDAC (Gregoretti, Lee and Goodson, 2004). Notably, the aforementioned HDAC classes evolved before histone proteins did, strongly suggesting that prime substrates may have not been histones (Seto and Yoshida, 2014).

1.1.9.1 Class I HDACs

Class I HDACs 1, 2, 3 and 8, contain highly conserved deacetylase domains and share significant homology with each other. Sequence similarities between them range from 45% to 94%. HDACs 1, 2, 3 and 8 are known transcriptional repressors and they can be localised to the nucleus, cytoplasm or specialised subcellular organelles (Seto and Yoshida, 2014).

Class I HDACs are often found in protein complexes. Studies where HDAC1 and HDAC2 were isolated individually showed they had very low intrinsic enzymatic

activity. Follow-up studies showed that HDAC1 and HDAC2 can be found together in at least three different multiprotein complexes namely the Sin3, the NuRD and the CoREST complexes. Sin3 and NuRD have a common core formed of HDAC1, HDAC2, RbAp46 and RbAp48. In addition, each of those complexes contains additional polypeptides such as Sin3, SAP18 in the Sin3 complex and Mi2 and MBD3 in the NuRD complex, among others. In experiments isolating individual subunits of the NuRD complex it was shown that the catalytic core on its own had a greatly reduced HDAC activity compared to the native holo-complex (Ayer, 1999). HDAC1 and HDAC2 are highly homologous and show widespread functional redundancy, except during embryonic development, the brain and the heart (Jamaladdin *et al.*, 2014).

1.1.9.2 Class IIa: HDAC4, 5, 7 and 9.

HDACs 4, 5 and 6 were discovered together by querying the GenBank database for homologues of yeast Hda1 (Grozinger, Hassig and Schreiber, 1999). They were found to contain conserved catalytic domains akin to those found in Class I HDACs, in addition to unique domains indicating that their divergence form Class I HDACs occurred early in evolution. HDAC7 was isolated as a silencing mediator that interacts with the SMRT complex (Kao *et al.*, 2000). HDAC7 has 3 silencing domains including a histone deacetylase domain. The other 2 possess autonomous independent repression function. Not a long time after HDAC7, HDRP (HDAC-related protein) was identified by studying human HDAC4 homologues. HDRP had 50% sequence identity with the noncatalytic amino-terminal domain of HDACs 4 and 5 (Zhou *et al.*, 2000). HDAC9 was also identified by its sequence homology to HDAC4 and was later found to have multiple isoforms, including HDRP, also known as myocyte enhancer-binding factor 2-interacting transcriptional repressor (MITR). Class IIa HDACs share 48-57% overall sequence identity between them (Seto and Yoshida, 2014).

Phosphorylation of a Class II HDAC, HDAC4 promotes its interaction with the 14-3-3 protein and subsequently changes its localisation. Multiple residues (S246, S467 and S632) on HDAC4 and corresponding conserved sites on HDAC5, HDAC7 and HDAC9 confer the HDAC-14-3-3 interactions (Seto and Yoshida, 2014). Members of the highly conserved acidic 14-3-3 family and Ca2+/CaM-dependent kinases (CaMKs) phosphorylate serine residues in the N-terminal. The phosphorylation event

leads to their sequestration in the cytoplasm, preventing nuclear localisation. Mutations in these residues was also shown to prevent their export to the cytoplasm (Li *et al.*, 2004; Williams *et al.*, 2013). Controlling nucleo-cytoplasmic shuttling of Class IIa HDACs regulates their repressive activities. Overexpressing CamKs leads to the cytoplasmic export of Class IIa HDACs and represses their transcriptional silencing activities (Karamboulas et al., 2006). Upon export, the HDACs are separated from their substrates.

Peculiarly, Class IIa HDACs have limited intrinsic de facto enzymatic activity. This is due to a Tyrosine to Histidine substitution within its catalytic deacetylase core. The substitution destabilises the transition state complex formed during an enzymatic reaction (Clocchiatti *et al.*, 2013). An experiment that generated a gain-of-function histidine to tyrosine mutation in HDAC4 showed that the protein was able to repress MEF2-dependent transcription in levels compared to the wild-type (Lahm *et al.*, 2007).

Class IIa HDACs are also often found in multi-subunit protein complexes (Figure 1-14) They do not bind DNA directly and interact within these complexes (or individually) with other DNA-binding proteins to exert their function. One of the most well-known targets of this subtype of HDACs is the MEF2 family of transcription factors. Other targets include CtBP (E1A C-terminal binding protein), heterochromatin protein HP1a and calmodulin (CaM). They also interact with the SMRT and NCoR (Verdin, Dequiedt and Kasler, 2003). MEF2 transcription factors are known to play a significant role in the transcriptional regulation of myogenesis. HDACs bind to MEF2 to supress myogenesis at various promoters of genes required for muscle differentiation (Ginnan *et al.*, 2012).

HDACs 4, 5, 7 and 9 were found to contain a conserved 17-amino acid motif in their N-termini that recognises and binds MEF2. HDAC4 was shown to interact with and repress MEF2-D which is expressed in thymocytes, a process regulated by calcium signalling (Youn, Grozinger and Liu, 2000). HDACs4 and 5 are also involved in muscle differentiation through their repression of members of the MEF2 family. Through repressing MEF2, *MyoD* expression is blocked. *MyoD* is a known activator of muscle-differentiation gene programme. The repression could be overcome by

CamK-mediated signalling (Lu *et al.*, 2000).

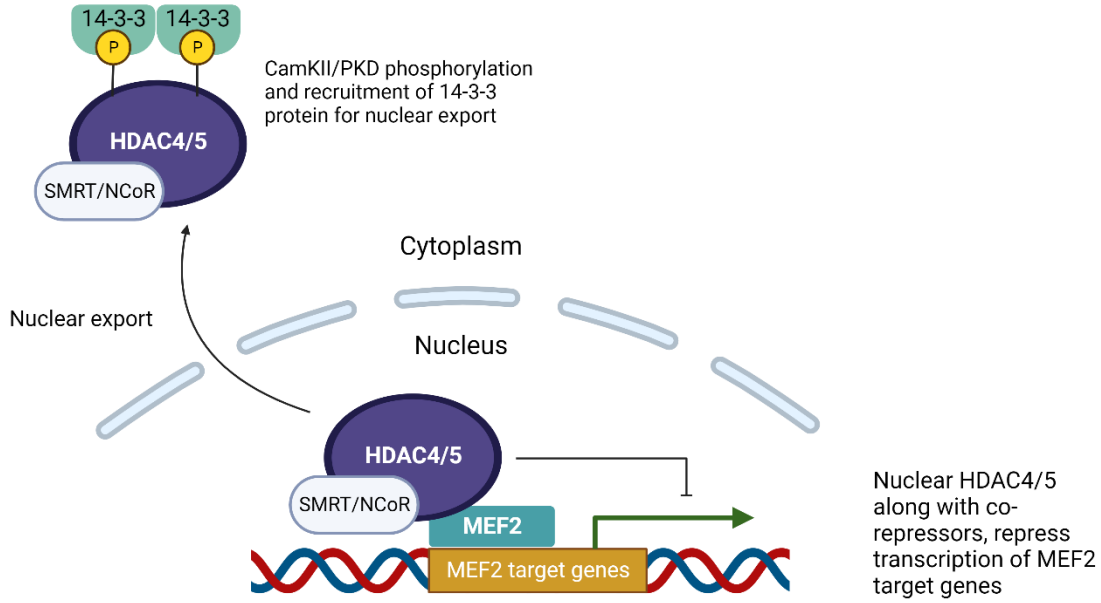


Figure 1-14. HDACs 4 and 5 interact with the SMRT/NCoR complex and their phosphorylation. Phosphorylation of HDAC4 and HDAC5 serine residues by CamK or PRKD recruits 14-3-3 proteins and sequesters them to the cytoplasm. Non-phosphorylated HDACs 4 and 5 are able to localise to the nucleus and, bind to MEF2 and repress the expression of MEF2 target genes. Figure created with biorender.com.

Class IIa HDACs take part in important processes such as B-cell activation and differentiation, inflammation and cell-cycle regulation. Through their repression of BCL6 either directly via their N-terminal domain or by being recruited to the promoter by SMRT they regulate BCL6 protein activity. Dysfunction in this protein is associated with B-cell lymphomas (López, Sullivan and Fierke, 2016). HDACs 4 and 5 also take part in heterochromatin maintenance by interacting with HP1a via another specific domain in the N-terminus (Wang, Qin and Zhao, 2014).

1.1.9.3 Class IIb: HDAC6 and HDAC10.

Class IIb HDACs are more closely related to each other than to other HDACs (de Ruijter *et al.*, 2003). They are characterised by having duplicated HDAC domains, although it is partial in HDAC10. Interestingly, site-directed mutagenesis of the catalytic HDAC domains in HDAC6 indicate that they might function independently despite their proximity to each other (Hai and Christianson, 2016) while separating them leads to loss of enzymatic activity (Fischle, Wang and Allis, 2003). HDAC6

also has a ubiquitination signal on the C-terminus domain (Ferreira De Freitas *et al.*, 2018). Members of Class IIb also show a more restricted expression pattern, and are less well understood than Class IIa HDACs (Park and Kim, 2020). HDAC6 is the most significant deacetylase for tubulin (Miyake *et al.*, 2016). It is noteworthy that HDAC6 also has a role in oncogenic transformation and cancer metastasis, making it an interesting target for drug design (Hai and Christianson, 2016).

HDAC10 is predominantly expressed in the liver, spleen and kidney (Fischer *et al.*, 2002; Tong *et al.*, 2002). *Hdac10* also demonstrates alternative splicing, with two different mRNA species being reported (Fischer et al., 2002). This is evidence of a further level of regulation by modulating RNA processing. HDAC10 has a catalytic domain on the N-terminus and an NES and a catalytic domain on its C-terminus. HDAC10 has been shown to interact with HDACs 1, 2, 3, the SMRT complex, in addition to HDACs 4, 5 and 7 but not 6. HDAC10 has been shown to be involved in deacetylating sperimidine, a polyamine whose aberrant regulation could lead to cancers of the colon, prostate and neuroblastoma (Hai *et al.*, 2017).

Class IIb HDACs are more resistant to wide scale HDAC inhibitors like trapoxin and sodium butyrate and are less sensitive than Class I and Class IIa HDACs (Furumai, 2001; Guardiola and Yao, 2002). Interestingly, deleting the partially duplicated HDAC domain in HDAC10 depletes their inhibitor resistance and restores their sensitivity (Furumai, 2001).

1.1.9.4 Class III (Sirtuins)

Sirtuins are also known as the Sir2 (silent mating-type information regulation 2) family, named for their function in yeast. There are 7 members in this class (SIRT1-7). Class III HDACs differ from other members of the HDAC superfamily in that they require NAD+ as a cofactor, as opposed to the zinc ion found in the catalytic core of conventional HDACs. Their catalytic mechanism is also different in that they do not simply hydrolyse acetyl-line like other HDACs. Instead, lysine deacetylation is coupled with NAD hydrolysis, yielding O-acetyl-ADP-ribose, nicotinamide and the deacetylated substrate. Interestingly, nicotinamide itself is an inhibitor of sirtuin activity, meaning a self-feedback loop is employed to regulate their functions. Sirtuins are divided into subgroups based on phylogenetic analysis or their localisation in mammalian cells between the nucleus, cytoplasm or mitochondria (Houtkooper, Pirinen and Auwerx, 2012). Sirtuins exhibit diverse expression patterns

and have distinct substrates and that lends them to take part in a wide variety of cellular processes. Despite being the third class of HDACs, Sirtuins are not exclusive histone or non-histone deacetylases. They possess other PTM-related functions such as ADP-ribosyltransferase, desuccinylation and demalonylation. They have been shown to be involved in cellular metabolism, the maintenance of 'stemness' and differentiation in mESCs and cancer stem cells. In addition, sirtuins take part in various cellular signalling pathways such as Hedgehog, Notch and Wnt (reviewed in (O'Callaghan and Vassilopoulos, 2017)

1.1.9.5 Class IV (HDAC11)

HDAC11 is particularly interesting due to its role as an immunoregulator. It interacts with the promoter of the interleukin 10 (IL-10), repressing its expression leading to the activation of immune function. HDAC11 depletion through genetic knockouts or treatment with small molecular inhibitors increases the immunosuppressive functions of Foxp3+ T-cells leading to immune tolerance (Huang *et al.*, 2017). HDAC11 was found to be localised to both the nucleus and cytoplasm. It is equally nuclear and cytoplasmic in immature astrocytes and oligodendrocytes and is predominantly cytoplasmic in embryonic astrocyte precursors (Milazzo *et al.*, 2020). It was shown to change localisation in response to stimuli, such as in stimulated Treg cells, where it changes from both nuclear and cytoplasmic location to mainly nuclear. HDAC11 lacks the nuclear localisation signals and phosphorylable serines that enable class II HDACs to shuttle between the cytoplasm and nucleus. However, its small size renders it able to move through nuclear pores by passive diffusion (Milazzo *et al.*, 2020).

1.1.10 HDACs in cardiac development

HDACs are needed for normal cardiac development as demonstrated by global and heart-specific knockout experiments. Widespread deletion of *Hdac1* is embryonic lethal before E9.5 (Lagger *et al.*, 2002). However, *Hdac1* expression is not detected in the heart at that point but *Hdac2* activity is increased in response (Lagger *et al.*, 2002). *Hdac2* knockout results in extensive perinatal cardiac anomalies including cardiomyocyte hyperplasia and apoptosis (Montgomery *et al.*, 2007). Double *Hdac1*/*Hdac2* KO results in female infertility, aberrant gene transcription. In the

heart, double KO results in arrhythmias, dilated cardiomyopathy and neonatal lethality (Montgomery *et al.*, 2007; Ma *et al.*, 2012).

Intriguingly, HDAC2 interacts with a small homeodomain factor, Hopx, to deacetylate Gata4, a major cardiac TF. Deletion of both *Hdac2* and *Hopx* causes an increase in the expression of *Gata4* targets, higher cardiomyocyte proliferation and eventually perinatal lethality (Trivedi *et al.*, 2010). *Hdac2* was also shown to have a role in cardiac hypertrophy by regulating GSK3β-mediated signalling (Trivedi *et al.*, 2007). Cardiac hypertrophy occurs as a response to normal mechanical or neurohormonal stimuli but if perturbed, can lead to congestive heart failure. This manifests in altering gene expression patterns and signalling pathways. These genetic changes include the reactivation of the foetal gene programme in cardiomyocytes (Carreño *et al.*, 2006). In heart failure, cardiomyocytes metabolism reverts from fatty acid oxidation to produce ATP, to glycolysis by increasing HIF-1α expression, which regulates the switch from fatty acid oxidation to glycolysis. Another example is the switch from the foetal, slow-twitch MHC-β to the fast-twitch MHC-α upon cardiac injury in mice (van der Pol *et al.*, 2020; Hong and Zhang, 2022). *Hdac2* is involved in regulating the expression of *Inpp5f*, which encodes for a phosphatase that modulates the PI3K/Akt/GSK3β pathway, the signalling pathway that transmits hypertrophic signals (Trivedi *et al.*, 2007). Homozygous *hdac2* mutant mice showed increased GSK3β signalling and an increased resistance to induced hypertrophy (Trivedi *et al.*, 2007).

HDACs 1 and 2 were shown to be major mediators of cardiac hypertrophy through a different mechanism, by increasing autophagy in cardiomyocytes in response to stress. Autophagy is a hallmark feature of pathological remodelling. These results were obtained by treating neonatal cardiomyocytes with hypertrophic agonists in the presence of HDAC inhibitors (Cao *et al.*, 2011).

It is thought that *Hdac1* and *Hdac2* have redundant roles in cardiac development, as the deletion of either gene does not lead to an extreme phenotype (Montgomery et al., 2007). However, knocking out both of them results in severe cardiac malfunction,. (Montgomery et al., 2007). Double knockouts also exhibit an increase in the expression of cardiac contractile and calcium handling genes. Despite their clearly crucial role in cardiac development, it is unclear whether they exert their functions by direct deacetylation of histones or other core cardiac factors such as

Gata4 (Quaife-Ryan et al., 2016). Furthermore, *Sirt1*-deficient mice display developmental defects that include cardiac, bone and retinal abnormalities (McBurney *et al.*, 2003). KO mice were smaller, and had cranio-facial and eye defects (Gabay *et al.*, 2013). Moreover, Sirt1 protein acts as a cardioprotective molecule, inhibiting cardiomyocyte apoptosis, regulates cardiac energy metabolism and confers protection against aging and hypertrophic stresses (L. Wang *et al.*, 2018). Consequently, cardiomyocyte-specific *Sirt1* KO mice had impaired responses to ischaemic injury as the metabolic switch between fatty acid and glucose oxidation was perturbed (Gabay *et al.*, 2013).

Global deletion of *Hdac3* is embryonic lethal at E9.5 while heart-specific knockouts survive for 3-4 months, before dying of severe cardiac hypertrophy and abnormalities in fatty acid oxidation pathways. This demonstrates the involvement of *Hdac3* in postnatal cardiomyocyte development and metabolism (Montgomery *et al.*, 2008). Moreover, knocking out either *Hdac5* or *Hdac9* results in cardiac hypertrophy by the virtue of the activation of *Mef2* targets and subsequent activation of the foetal hypertrophic gene programme. A double knockout of both Hdacs is perinatally lethal (Chang *et al.*, 2004). *Hdac9*-KO mice also show a higher propensity to stress-induced cardiac hypertrophy as well as stress-dependent cardiomegaly. Cardiomyocyte-specific mutations in phosphorylation sites in HDAC5 also leads to the activation of hypertrophy-associated genes in response to phenylephrine (Zhang *et al.*, 2002). *Hdac5*-null mice also display cardiomegaly in response to pressure overload. These phenotypes suggest possible redundancy in *Hdac5* and *Hdac9* functions in the heart (Chang et al., 2004). Interestingly, a study showed that expressing a mutant form of *Hdac9* could block the induction of the foetal cardiomyocyte gene programme in the presence of potent inhibitors (Zhang *et al.*, 2002).

HDAC3 has been shown to interact physically with Tbx5 modulating its acetylation level. Mutant mice lacking *Hdac3* in their cardiac progenitors showed premature cardiomyocyte differentiation in addition to severe cardiac developments. These phenotypes were accompanied by an upregulation in the expression of *Tbx5* targets and embryonic lethality. HDAC3 functions in repressing *Tbx5* activity thus preventing the activation of cardiomyocyte lineage-specific genes (Lewandowski et al., 2014). Interestingly, another study showed that Hdac3 is able to repress cardiac

differentiation of cardiac progenitors independent of its catalytic deacetylase activity. It was demonstrated that Hdac3 regulates differentiation by organising heterochromatin at the nuclear periphery (Poleshko *et al.*, 2017). A third study showed that Hdac3 represses Fgf9 and Igf2, via miR-322 and miR-503 through its deacetylase activity, resulting in disrupted epicardial formation, compromised ventricular compaction and hypoplastic ventricular wall. Additionally, Hdac3 was reported to also act as a gene activator. Altogether, these results suggest that Hdac3 is a dynamic protein , able of performing different functions in response to stimuli, interacting partners and cellular context (Jang *et al.*, 2022). Therefore, it can be concluded that Hdac3's activation of foetal gene programmes involved in cardiomyocyte differentiation upon myocardial stress can lead to hypertrophy.

1.1.11 Background work leading to this project

More relevant to this project is the member of Class IIa, HDAC4. Work conducted by our group indicate the interaction and functional relationship between HDAC4 and TBX5. HDAC4 and 5 were both found to remove acetylation of lysine 339 mediated by KAT2A and KAT2B. In these studies, TBX5 was found to be acetylated specifically by KAT2A and KAT2B, but not P300 in Cos7 cells. This acetylation was enhanced by the addition of TSA. Transcription of *MYH6* target genes was enhanced when analysed using promoter-reporter assays. Acetylation also increased the expression of another TBX5 target promoter, *ANF*. The acetylation motif was mapped using protein sequence homology followed by site-directed mutagenesis in the candidate region. Mutation of K339R resulted in complete loss of acetylation by both KAT2A and KAT2B, demonstrating that it is a the key lysine residue target (see Figure 1-15). Interestingly, this lysine residue is located within the nuclear localisation signal domain. In K339R mutant cells, only 17% showed nuclear TBX5 localisation, where 94% of the wild-types did. 83% of the mutant cells showed cytoplasmic localisation. This process is mediated by CRM1 nuclear export protein and was confirmed by treating K339R mutants with a chemical inhibitor of CRM1, leptomycin B. Following treatment, TBX5 remained in the nucleus in 96% of Cos7 cells and 85% of C2C12 cells. Altogether these results demonstrate that acetylation indeed activates expression of TBX5 target genes and that TBX5 acetylation is important for its nucleocytoplasmic shuttling.

Following on from identifying acetylases of TBX5, our group sought to study the link between TBX5 and deacetylases. Building on the knowledge that TBX5 is acetylated by KAT2B (Ghosh et al., 2018), Cos7 cells were co-transfected with tagged TBX5 and KAT2B expression plasmids, and either HDAC4 or HDAC5. Acetylation levels were analysed using an anti-acetylated lysine antibody. It was found that HDAC4 or HDAC5 overexpression significantly reduced TBX5 acetylation. Moreover, it was shown that the presence of HDAC4 or HDAC5 affected the cellular localisation of TBX5. TBX5 was nuclear in 100% of the wild-type cells but overexpressing HDAC4 or HDAC5 resulted in cytoplasmic localisation in 20-30% of the cells, thereby reducing TBX-mediated gene expression (Ghosh *et al.*, 2019).

To query the effect of the change in cellular localisation and based on the observation that acetylation regulates TBX5 via nucleocytoplasmic shuttling, reporter assays were conducted using the acetyl-deficient K339R mutant. Another objective of this experiment was to investigate whether HDAC4 and 5-mediated repression of TBX5 also occurred by chromatin remodelling and promoter recruitment at the transcriptional level. Promoter-reporter assays showed that the mutant TBX5 retained a significant level of transcriptional activity in activating the *MYH6* promoter. Co-transfection of the mutated protein with either HDAC4 or HDAC5 significantly reduced transcriptional activity. Notably, mutant proteins retained their binding abilities. Therefore, these results show that HDAC4 and HDAC5 can repress TBX through the structural modification of chromatin (Ghosh *et al.*, 2019).

Since HDAC4 and HDAC5 associate with MEF2-directed cardiac genes, the association between MEF2C and TBX5 was investigated. Moreover, domain mapping studies suggested that TBX5 interacts with MEF2C at the MADS box (Figure 1-15), a region present in both HDAC4 and HDAC5. Since HDAC4 resulted in a greater reduction in TBX5 transcriptional activity, pull-down assays were performed to study its interaction with MEF2C. Radiolabelled HDAC4 or MEF2C proteins were incubated with a fusion TBX5 protein in the first series of experiments, and radiolabelled HDAC4 and TBX5 were incubated with fusion MEF2C protein in the second. These showed that HDAC4 had a higher affinity for TBX5 than MEF2C. Follow-up experiments showed that increasing HDAC4 concentrations inhibited the

TBX5-MEF2C complex formation, while increasing concentrations of TBX5 failed to outcompete HDAC4 for MEF2C binding. This resulted in a decreased fold activation of the MYH6 promoter.

Taken together, these studies demonstrate the mechanisms by which acetylation levels of TBX5 are maintained by the synergistic effects of KAT2A, KAT2B, HDAC4 and HDAC5. They demonstrate that acetylation has a direct effect on protein localisation and on its transcriptional activation ability at the DNA target (see Figure 1-15). Therefore, the role of *Hdac4* in cardiomyocyte biology was chosen to study further and assess whether these interactions had any consequences on differentiation.

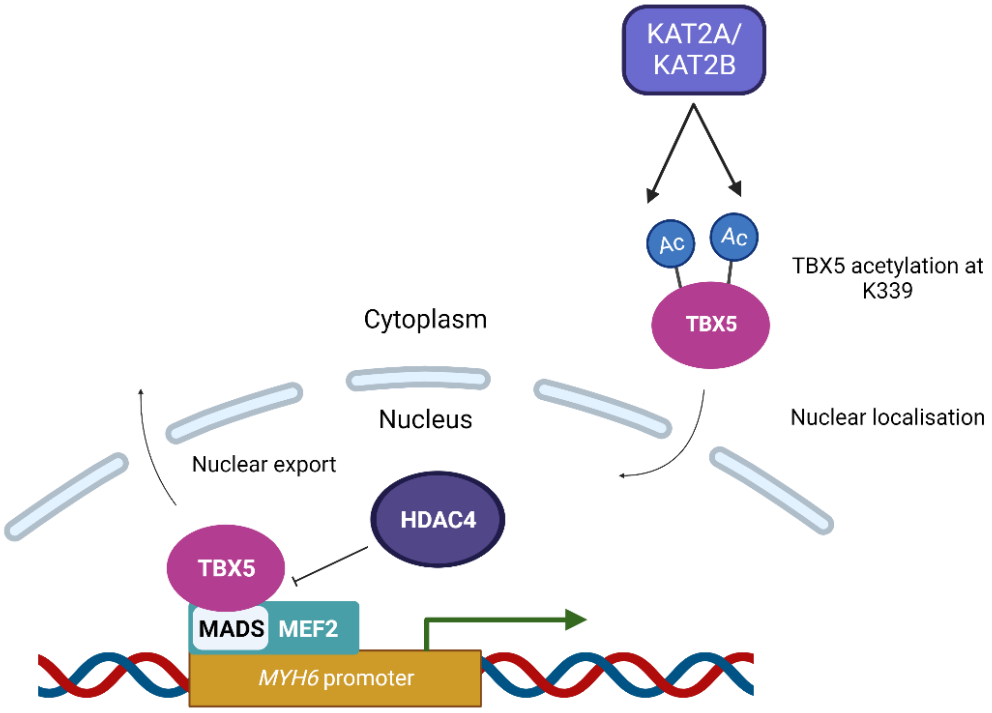


Figure 1-15. TBX5 is acetylated by KAT2A and KAT2B and deacetylated by HDAC4 and HDAC5. Acetylated TBX5 localises in the nucleus where it forms a complex with MEF2 via its MADS domain and activates the expression of MEF2 target promoters, like MYH6. Deacetylation by HDAC4 disrupts the interaction between TBX5 and MEF2, thus repressing TBX5-mediated gene expression. Moreover, deacetylation by HDAC4 results in the nuclear export of TBX5. Figure created using Biorender.com.

Additionally, HDAC4 inhibition was shown to play a role in controlling cardiac commitment of cardiac stem cells (Zhang et al., 2014). *Hdac4*-deficient mice also

show skeletal defects (Seto and Yoshida, 2014). Interestingly, HDAC4 is a target of miRNA-1, one of four miRNAs shown to be sufficient to reprogram fibroblasts into cardiomyocytes (Jayawardena *et al.*, 2012; Di Giorgio and Brancolini, 2016). Class II HDACs were implicated in heart failure signalling (Kronlage, Katus and Backs, 2016). Moreover, HDAC4 and HDAC5 function in cardiac hypertrophy by controlling *Mef2* expression (Ghosh *et al.*, 2019).

1.1.12 HDAC inhibition

Since their discovery in the late 1970s (Riggs *et al.*, 1977; Candido, Reeves and Davie, 1978), HDAC inhibitors have been of great interest to researchers. HDAC inhibitors are classified according to their chemical structure: hydroxamate, short-chain fatty acid (carboxylate), benzamide, and cyclic peptide. The most studied type of inhibitor is the hydroxamates, to which Trichostatin A (TSA) belongs. Hydroxamates inhibit HDACs by inserting a long aliphatic chain into the catalytic pockets of HDACs, binding with the zinc ion and forming a chelate complex (Seto and Yoshida, 2014). HDAC inhibitors have been gaining traction for being potential anti-cancer drugs (Eckschlager *et al.*, 2017), with some undergoing clinical trials (Romero, 2019).

Trichostatin A is a wide-scale Class I and II HDAC inhibitor. It has been shown to affect apoptosis (Deng *et al.*, 2016), gene expression (Schnur *et al.*, 2007; Bui *et al.*, 2010; Pufahl *et al.*, 2012; Gurgul *et al.*, 2017), differentiation of stem cells (Hosseinkhani *et al.*, 2007; Maalouf *et al.*, 2009; Yang *et al.*, 2012; Lim *et al.*, 2013) and the cell cycle (Kim *et al.*, 2005), among other processes, due to its far-reaching inhibitory abilities. In the context of heart development and disease, TSA has been found to ameliorate cardiac hypertrophy (Cao *et al.*, 2011; Ooi *et al.*, 2015) and to prevent pathological cardiac remodelling after myocardial infarction (Zhang et al., 2012).

1.1.13 Congenital heart disease

Congenital heart diseases (CHD) are one of the most common types of birth defects. They affect approximately 9 in every 1000 babies born in the UK and are among the top causes of infant mortality (NHS UK). CHDs can be defined as “a gross structural abnormality of the heart or intrathoracic great vessels that is actually or potentially of

functional significance" (Mitchell, Korones and Berendes, 1971). This definition excludes defects of the great veins, aortic branches or congenital arrhythmias (Hoffman and Kaplan, 2002).

CHDs manifest in most structures of the heart. Those can be divided into three wide categories: septation defects, left-sided obstruction defects and cyanotic heart disease. Babies born with the latter category appear blue due to the mixing of oxygenated and deoxygenated blood in the circulation and are commonly known as 'blue babies'. Blue babies can have one of several conditions including tetralogy of Fallot (TOF), tricuspid atresia, transposition of the great arteries (TGA), pulmonary atresia, Ebstein's anomaly of the tricuspid valve, double outlet right ventricle (DORV), persistent truncus arteriosus (PTA) and total anomalous pulmonary venous connection. Septation defects can affect atria (atrial septal defects – ASDs) or ventricles (ventricular septal defects – VSDs). Left-sided obstructions include mitral stenosis, hypoplastic left heart syndrome (HLHS), aortic coarctation, aortic stenosis and interrupted aortic arch (IAA). Other congenital heart abnormalities that do not fit into any category include patent ductus arteriosus (PDA) and bicuspid aortic valve (BAV). The latter is the most common CHD, with septation defects coming next (Bruneau, 2008). These CHDs are defined in **Error! Reference source not found. Error! Reference source not found.**and Figure 1-16 shows the heart structures affected by various congenital heart defects.

Table 1-1. Brief definitions of most common congenital heart defects. A brief explanation of the physiological abnormalities found in each one is provided.

Congenital heart abnormality	**Definition**	**Reference**
Atrial septation defect	A heart anomaly where blood flows between atria when they are normally separated by a septum	(Geva, Martins and Wald, 2014)
Ventricular septation defect	Abnormal blood flow between ventricles due to a 'hole' between ventricles	(Spicer et al., 2014)
Tetralogy of Fallot	A congenital heart defect involving 4 symptoms: narrowing of right ventricle outflow tract (pulmonary stenosis), overriding aorta, VSD, right ventricular hypertrophy	(Apitz, Webb and Redington, 2009)
Tricuspid atresia	An abnormality or absence of the tricuspid valve that is located between the right atrium and ventricle, blood flow is thus blocked	(Thiene and Anderson, 1981)

Transposition of the great arteries	It is when the pulmonary artery is where the aorta should be and vice versa	(Marathe and Talwar, 2015)
Pulmonary atresia	An abnormality in the pulmonary valve between the right ventricle and the lungs	(El Louali et al., 2011)
Ebstein's anomaly of the tricuspid valve	An anomaly of the tricuspid valve where it is located lower than normal the leaflets forming it are abnormally formed	(Geerdink and Kapusta, 2014)
Double outlet right ventricle	A CHD where both great arteries are both connected to the right ventricle	(Obler et al., 2008)
Persistent truncus arteriosus	A condition where the truncus arteriosus fails to divide into the pulmonary trunk and aorta during development	(Mavroudis, Jonas and Bove, 2015)
Total anomalous pulmonary venous connection	A defect in which the pulmonary veins form abnormal connections to the systemic venous circulation	(Katre et al., 2012)
Mitral stenosis	It is the narrowing of the mitral valve, which lies between the left atrium and left ventricle	(del Nido and Baird, 2012)
Hypoplastic left heart syndrome	A condition characterised by the significant underdevelopment of the left side of the heart	(Ciocca et al., 2015)
Aortic coarctation	A narrowing in the aorta	(Cardoso et al., 2014)
Aortic stenosis	A narrowing of the aortic valve, between the left ventricle and the aorta, often causes by abnormal valve leaflet formation	(Jashari et al., 2015)
Interrupted aortic arch	Incomplete development of the aorta with loss of continuity between ascending and descending portions of the aortic arch	(Messner et al., 2002)
Patent ductus arteriosus	The failure of a foetal blood vessel, the ductus arteriosus, to close after birth, affecting the flow of blood between the aorta and the pulmonary artery	(Anilkumar, 2013)
Bicuspid aortic valve	An anomaly of the aortic valve, where two of the three leaflets forming the valve fuse	(Cripe et al., 2004)

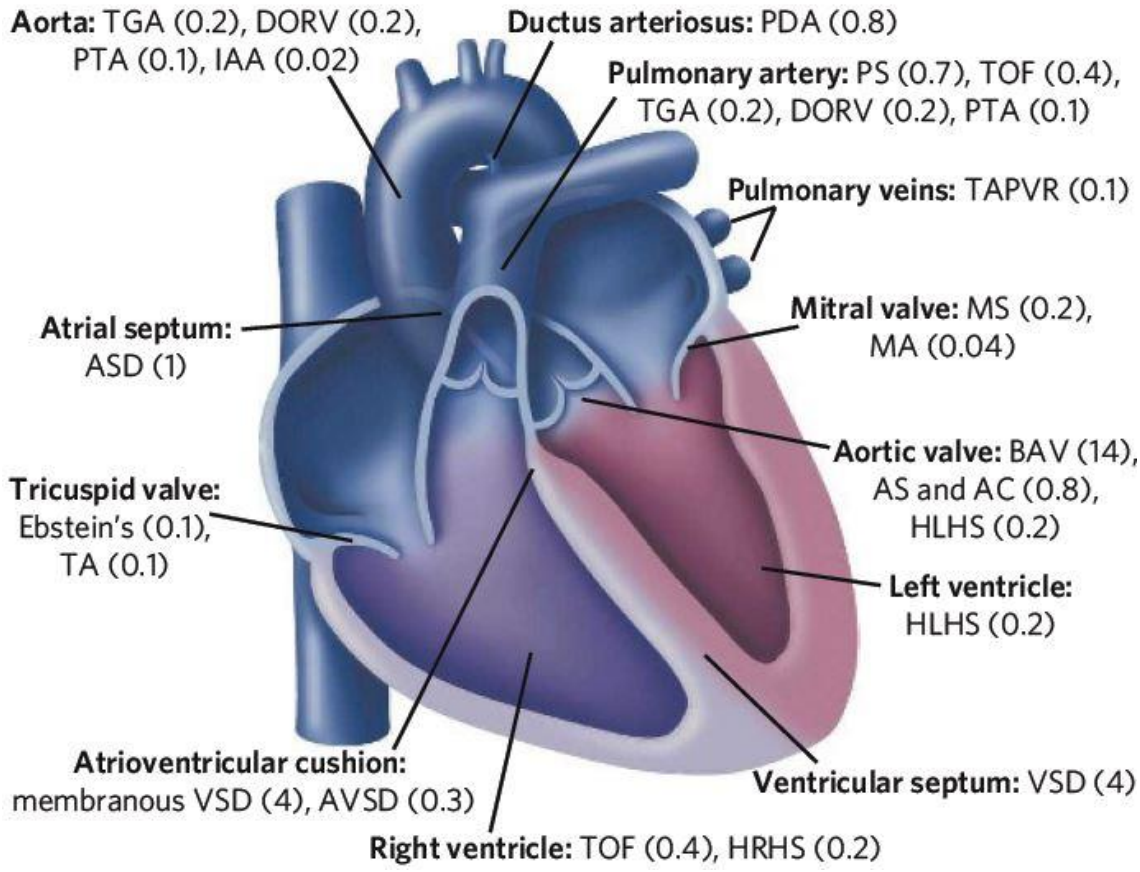


Figure 1-16. . A diagram of the adult human heart showing the anatomical locations of various congenital heart abnormalities. The numbers in brackets indicate the estimated incidence per 1000 live births. TAPVR: Total anomalous pulmonary venous return; MA: mitral atresia; HRHS: hypoplastic right heart syndrome; AVSD: atrioventricular septal defects. Adapted from Bruneau et al 2008.

Mortality and morbidity vary with the severity of the defect. A common consequence is neurological disorders, due to aberrant brain development and maturation *in utero* (Miller *et al.*, 2007). Corrective surgeries babies must undergo are risky and can greatly reduce quality of life (Bruneau, 2008). It is therefore vital to understand the underlying aetiology and mechanisms of CHDs. CHDs can also manifest on their own or as part of a genetic syndrome (Sifrim *et al.*, 2016).

1.1.14 Animal and cell-based models to study heart development

Vertebrates such as zebrafish and mice provide great *in vivo* models for heart development and congenital heart diseases. The zebrafish's ease to work with,

manipulate and its retention of cardiac regeneration throughout adulthood make it a particularly interesting animal to study (Tu and Chi, 2012).

1.1.14.1 Mouse models

There are many similarities in heart development between human and murine embryos. When heart development in human and mouse embryos were compared, it was found that developmental events were parallel, with small differences in atrial and ventricular morphology. These, however, are inconsequential to the appropriateness of using mice to model human development and subsequently, human disease (Krishnan *et al.*, 2014).

1.1.14.2 Cellular models of heart development

While they are incredibly useful, animals normally come with the need for ethical approvals, expenses and experience needed to maintain them. Cells in culture, while they may not exactly recapitulate developmental events, are invaluable for discerning the genes at work during cardiac differentiation (Tompkins *et al.*, 2016). During the course of this project, two types of cell lines were used in attempt to study cardiomyocyte differentiation: P19CL6 cells and mouse embryonic stem cells.

1.1.14.3 P19CL6 cells

P19 cells were originally obtained from the ectopic transplantation of a 7.5 day embryo into the testis of an adult mouse. The resulting tumour, a teratoma, grew rapidly and the undifferentiated cells from it were acquired and cultured. The embryonic carcinoma cell line was thus established. It has stem cell-like characteristics in that it can maintain an undifferentiated state, divide continuously and differentiate into cells from all three embryonic germ layers. P19 cells have a stable euploid male karyotype (McBurney, 1993). They can be easily cultured and maintained in an undifferentiated state without feeder cells (Yang et al., 2009). These properties allow them to be ideal for experiments involving the introduction of ectopic genes and/or those requiring a large number of cells. Additionally, it has been found that P19 cells can easily be induced to differentiate into different cell types. For example, treatment with retinoic acid can stimulate P19 cells to differentiate into derivatives of the neuroectoderm, namely neurons, astroglia and microglia (McBurney, 1993). More importantly, P19 cells can be stimulated to form endodermal and mesodermal derivatives including cardiac and skeletal muscle by

exposing cell aggregates to dimethyl sulfoxide (DMSO). The formation of P19-derived cardiomyocytes by DMSO induction is the focal point of this project.

P19 cells can form embryoid bodies (EBs), which are three-dimensional aggregates of pluripotent stem cells, capable of differentiating into cells from all three germ layers (Itskovitz-Eldor *et al.*, 2000). EBs resemble blastocysts in viable embryos. The formation of EBs in the presence of 0.5%-1% DMSO can induce cardiomyogenic differentiation of P19 cells (McBurney *et al.*, 1982). It has been hypothesised that DMSO can do so by stimulating the release of calcium from intracellular stores, consequently inducing various signal transduction pathways leading to the initiation of gene expression (Morley and Whitfield, 1993). 5-azacytidine, a global DNA demethylase, can also induce cardiac differentiation of P19 cells in a monolayer without the need for the formation of EBs or presence of DMSO (Choi *et al.*, 2004).

A derivative of the P19 line, able to differentiate into cardiomyocytes with a high efficiency after long term culture in mesoderm promoting conditions was isolated, named P19CL6. This subline differentiated into neuron with poor outgrowth and into cardiomyocytes with a higher efficiency than the P19 line (Habara-Ohkubo, 1996).

The capability of the P19CL6 line to differentiate into cardiomyocytes has made it an invaluable source for heart development as an *in vitro* model and cardiac regenerative therapy (Ohtsu et al., 2005). The ease with which it can be cultured and maintained meant that it was a promising model system. Novel factors involved in cardiac development were discovered using this line, such as *Midori* and *Cal*. Overexpression of *Midori* was found to enhance cardiac differentiation and cells expressing antisense *Midori* did not differentiate into cardiomyocytes as efficiently (Hosoda *et al.*, 2001). Cal is also a novel LIM-domain protein that interacts with Nkx2.5 and increases its expression therefore promoting myocardial differentiation (Yang et al., 2009).

The P19CL6 cell line has also been instrumental in finding signalling pathways that function in cardiac development, such as FGF and BMP signalling. For example, a sub-line expressing noggin, a BMP antagonist, was made and the cells did not differentiate into cardiomyocytes, consequently demonstrating that BMP is necessary for cardiac differentiation (Yang et al., 2009).

Interestingly, P19CL6 cells were found to function *in vivo* as well. P19CL6-derived cardiomyocytes were transplanted into the retroperitoneal area, on the omentum and around the femoral artery of mice. The cells adhered to the surfaces and grew to form masses in the transplanted area. These masses then began to pulsate albeit irregularly and slower than the host heart (Ohtsu et al., 2005). Taken together, these properties show the P19CL6 cell line's propensity to be used as a model system to investigate the effect certain genetic manipulations can have on cardiomyocyte differentiation.

1.1.14.4 Embryonic stem cells

Embryonic stem cells (ESCs) were first isolated from the inner cell mass of a 3.5 dpc mouse embryo at the blastocyst stage (Evans and Kaufman, 1981). Ever since then, they have been cultured and studied extensively. They are pluripotent and have the ability to proliferate indefinitely (Pauklin, Pedersen and Vallier, 2011). Since their derivation, a plethora of cell lines has been made available and their culture conditions have been optimised.

ESC 'stemness' can easily be preserved and they can be expanded in culture in self-renewing state through the modulation of culture conditions, through the introduction of the cytokine LIF (leukaemia inhibitory factor) and two inhibitors named Gsk3 and Mek.3 (a condition known as 2i/LIF) or growing them on feeder layers (Brickman and Serup, 2017). The pluripotency of mouse ESCs (mESCs) was truly established when they were injected into early blastocysts and these were implanted into pseudo-pregnant females and allowing the resultant embryos to develop to term. The ESCs were found to contribute to cells of all lineages, including the germ line (Bradley *et al.*, 1984).

Like the aforementioned P19 cells, mESCs can form EBs. These EBs are able to recapitulate some of the cell-cell interactions that take place in an embryo (Brickman and Serup, 2017). They mimic to some extent, events taking place in a 6 dpc embryo, including having an embryonic axis (Spangler et al., 2018). EBs can be differentiated *in vitro* into different lineages, by removing LIF and utilising the cells' ability to spontaneously differentiate, or directed differentiation by adjusting culture conditions. The addition of activin, for example, to EBs formed at low density can encourage endoderm differentiation (Livigni *et al.*, 2009). Retinoic acid can enhance neural differentiation (Guan *et al.*, 2001).

In the context of heart development and disease, mESCs provided a crucial accessible model system to study it. Protocols have been devised to derive beating cardiomyocytes from mESCs. These have been found to have similar properties to embryonic cardiomyocytes and to show sinusoidal, atrial and ventricular cell types (Maltsev *et al.*, 1993; Guan, Rohwedel and Wobus, 1999). They were shown to display the same genetic signatures as developing embryonic cardiomyocytes and improved understanding of lineage tracing studies (Meilhac and Buckingham, 2018). These have aided our understanding of embryonic cardiac development. Nearly 30 years later, we are closer than ever to utilising stem cell-derived cardiomyocytes for repair in patients with heart failure (Abdelwahid *et al.*, 2016; Park *et al.*, 2019; Kishino *et al.*, 2020). While work still remains to be done to fully elucidate the consequences of stem cell transplant into patient hearts, the outlook is positive.

1.1.15 CRISPR/Cas9 genome editing technology

Microbes have evolved their own defence systems to protect them from viral infections and invading nucleic acids. In many bacteria and most archaea, clustered regularly interspaced short palindromic repeats (CRISPR) exist for distinct genomic loci and provide a type of acquired immunity against viruses and foreign nucleic acids in a sequence-specific way (Barrangou *et al.*, 2007). This naturally occurring defence mechanism in microbes can be exploited and engineered to efficiently edit genomes. The CRISPR/Cas9 system can facilitate RNA-guided-site-specific- DNA cleavage (Cong *et al.*, 2013). The *S. pyogenes* Cas9 enzyme, an endonuclease, uses the CRISPR RNA to direct cleavage through its complementarity to 20 bases of genomic DNA and a transactivating RNA that induces sequence-specific double strand breaks in its target site in the DNA, which in turn is adjacent to an NGG trinucleotide known as the protospacer adjacent motif (PAM) (Gagnon et al., 2014). The CRISPR RNA and the transactivating RNA can be annealed to form a single guide RNA (sgRNA) sufficient for site-directed cleavage of target DNA (Jinek *et al.*, 2014)(Figure 1-10).

The CRISPR/Cas9 system has been applied in various *in vivo* settings, such as human cells, mice, *C. elegans* and zebrafish (Cong *et al.*, 2013; Friedland *et al.*, 2013; Hwang *et al.*, 2013; Mali *et al.*, 2013; Wang *et al.*, 2013). The result was efficient mutagenesis by non-homologous end joining (NHEJ)-mediated small

insertions or deletions (see Figure 1-17). The latter is a way of repairing double strand breaks in DNA that does not require a homologous template; it is often prone to errors (Bibikova *et al.*, 2002). The ability to choose and design sgRNAs provides a level of specificity and flexibility not offered by other genome editing methods, such as zinc finger nucleases or TALENS (Gagnon et al., 2014). CRISPR/Cas9 system can also be used to introduce specific nucleotide changes, or repair pathological mutations by introducing donor DNA as a repair template and utilising homology-directed repair mechanisms (Redman *et al.*, 2016).

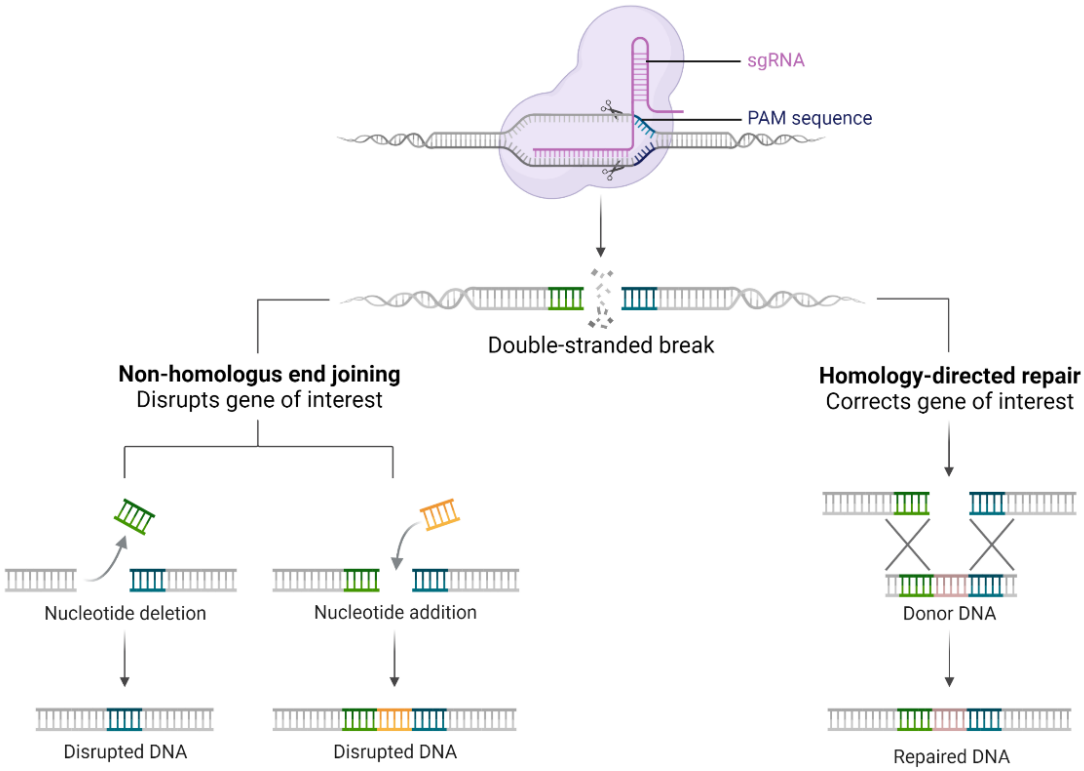


Figure 1-17. A schematic of the CRISPR/Cas9 system at work. Guide RNA drives Cas9 cleavage at a locus in the DNA that lies adjacent to a PAM sequence (purple). In the absence of a repair template, non-homologous end joining takes place, whereby random insertions or deletions are introduced. Alternatively, a donor DNA template can be provided, to achieve specific gene editing via homology-directed repair. Figure created with Biorender.com.

1.1.16 Transcriptomic analysis of stem cell differentiation into cardiomyocytes

The advent of high throughput sequencing techniques can only be described as revolutionary. From Sanger sequencing, through the Human Genome Project and

single cell genomic analysis, significant progress has been achieved. While studying the whole DNA sequence of a cell population or individual might tell us a lot about features and biological identity, studying the transcriptome at a point in time can be like taking a snapshot of cellular activities at that moment. It can provide a wealth of information about gene expression and provide a quantitative method to measure that level of expression without having to tread through entire genomes where the majority of the sequence is not translated and expressed. The interest in transcriptomics has exploded in the past 20 years or so. That can be highly attributed to the vast improvements in available technologies, bioinformatics tools, leading to more economical options and thus more user interest.

1.1.17 RNA Sequencing

RNA Sequencing has become the main method of choice for whole transcriptome analysis. Current popular techniques are microarrays and RNA-Seq, developed in the 1990s and 2000s, respectively (Miller *et al.*, 2013; Van Dijk, Jaszczyszyn and Thermes, 2014). Gene expression analysis using microarrays is based on hybridisation of fluorescently labelled targets derived from transcripts to a set of probes attached to a solid surface. While this method provides an efficient way of interrogating genome-wide transcripts at a relatively low cost, the requirement that a priori sequence information or reference genomes/transcriptomes be available for designing the microarray probes limited the development and application of this technology for discovery purposes. Moreover, technical concerns like cross-hybridisation and background signals often result in low specificity or low sensitivity for some genes (Hrdlickova, Toloue and Tian, 2017).

The new millennium brought with it the introduction of massive parallel sequencing, also known as deep sequencing or Next Generation Sequencing (NGS). NGS ushered in a new era for RNA research as we were now capable of acquiring an unprecedented amount of data in a short time, at lower costs. RNA-Seq became the primary method of choice to quantitatively study gene expression and identify novel RNA species. When compared to DNA microarray-based technology, RNA-Seq offers reduced background noise and a greater dynamic range for detection. Notably, RNA-Seq can be used to reveal sequence identity and removes the need for prior

knowledge of the sequence. The technology therefore lends itself well to analysing unknown genes and novel transcript isoforms. Several different technologies have been established for RNA-Seq (Nookaew *et al.*, 2012; Adiconis *et al.*, 2013; Han *et al.*, 2015).

1.1.17.1 3’ Sequencing

Since its inception, many RNA-Seq library preparation methods have been developed, increasing the number of choices for investigators. In classic whole transcriptome RNA-Seq, mRNAs are fragmented before being reverse transcribed into cDNA. Fragmentation and the library construction method of choice can possibly introduce biases in results. As cDNA fragments are sequenced on a platform, the number of reads generated from each transcript is proportional to the number of cDNA fragments making up the transcript rather than the number of transcripts. Intuitively, longer transcripts that generate more fragments will be assigned more reads. This can confound differential gene expression analyses as differentially expressed genes will consequently contain longer transcripts, as the statistical power of longer transcripts will be higher due to having a higher read count than shorter transcripts (Oshlack and Wakefield, 2009). Recently, 3’ RNA Sequencing methods have been established, such as Tag-Seq (Meyer, Aglyamova and Matz, 2011) and QuantSeq (Moll et al., 2014) to reduce the effects of this bias. In 3’ RNA-Seq, mRNAs are not fragmented prior to reverse transcription. What happens instead is that cDNAs are reverse transcribed only from the 3’ ends of mRNAs, and only one copy of cDNA is produced per transcript. This rids us of transcript length bias that arises in traditional RNA-Seq methods, as the number of reads generated is a direct reflection of the number of transcripts and short and long transcripts theoretically have the same coverage of reads (Ma *et al.*, 2019).

3’ RNA Seq has been used in many studies to profile and quantify gene expression. Tag-Seq was used by Meyer et al to investigate coral larvae. Quant-Seq was used to study gene expression in the human brain (Barbash *et al.*, 2017) and in transposon analysis in *Arabidopsis* (Oberlin *et al.*, 2017). These studies involved organisms with well-characterised genomes and it has been shown that 3’ RNA Sequencing is not ideal when little or no genomic information is available for the organism of interest. Classic RNA-Seq methods work better in these cases (Tandonnet and Torres, 2017). In a study comparing classic and 3’ library preparation for sequencing, Ma et al used

the KAPA Stranded mRNA-Seq Kit to prepare libraries using the whole transcript method and the Lexogen Quant-Seq 3' mRNA-Seq Library Prep Kit to generate 3' libraries. Libraries produced by both methods were then sequenced on an Illumina platform. Both methods had high reproducibility between biological replicates. They found that the whole transcriptome method did indeed assign more reads to longer transcripts while the 3' method was better at detecting shorter transcripts. However, Trad-KAPA was able to detect more differentially expressed transcripts. The authors concluded that no method had a clear advantage over the other and selecting one should depend on the goal of the study and the biological questions being answered (Ma et al., 2019). For this project, 3' RNA-Seq was chosen as the method is capable of addressing the biological questions being asked with a relatively cheaper price tag.

In 3' Quant-Seq RNA-Seq, libraries are generated starting with oligo-dT primed reverse transcription to synthesise the first strand. No polyA enrichment or ribosomal RNA depletion is required. The RNA template is then removed following first strand synthesis and random primers are used to prime second strand synthesis. At this stage the primers can be used to introduce sequencing platform-specific adapters. The double-stranded cDNA product is then purified with magnetic beads before being subjected to amplification by PCR where index sequences can be introduced as they are needed for cluster generation. Libraries generated can be sequenced on Illumina or IonTorrent platforms, with the protocol modified accordingly. For data analysis, another advantage of Quant-Seq is that there is no need for length normalisation, as only one fragment is generated per transcript and gene expression quantification is read-count-based (Moll et al., 2014).

1.1.18 Transcriptional profiling of stem cell-derived cardiomyocytes

The potential for stem cells to be a resource for generating various cell types for use in repair in disease contexts has long been a goal of stem cell researchers. With CHDs being relatively common disorders in infants and heart failure being a major cause of death in developed countries, developing cell based therapies to repair the heart has garnered a lot of interest. That makes it imperative to understand the dynamics of gene expression taking place during differentiation and development. RNA-Seq has been an invaluable tool. Along with great leaps forward in bioinformatics tool development, it has become very possible to generate gene

regulatory networks (GRNs) from expression profiles (McKinney-Freeman *et al.*, 2012; Cahan *et al.*, 2014; Miller *et al.*, 2014).

Cardiomyocytes obtained from developing mouse hearts were used to construct the gene network thought to control heart differentiation and development. Uosaki and colleagues produced an atlas of gene expression, pathways and transcriptional regulators and reconstructed GRNs during CM maturation. They used a microarray-based program to index CM maturation status. Using this program they were able to show that pluripotent-stem-cell (PSC)-derived CMs undergo maturation early but become arrested at a late embryonic stage even after long-term culture. They intriguingly identified transcriptional regulators defective in PSC-CMs that could cause this maturation arrest (Uosaki *et al.*, 2015).

Many studies over the years used the embryonic stem cell model to generate functional cardiomyocytes in attempts to elucidate the cardiac genetic network. Stem cells are first differentiated using standard methods and the cardiomyocytes are subsequently purified and profiled.

In 2007, Doss et al generated a stem cell line wherein puromycin resistance and enhanced green fluorescent protein (EGFP) expression were driven under the control of a cardiac-specific α-myosin heavy chain (MHC) promoter. The authors utilised the CGR8 murine stem cell model to differentiate into functional cardiomyocytes using the hanging drop method with favourable efficiency. The selectable markers were then used to select cardiomyocytes and RNA was extracted from those to obtain a transcriptional profile that was studied using Affymetrix expression microarrays covering all transcripts known at the time (Doss *et al.*, 2007). This was the first report of a transcriptome analysis of pure cardiomyocytes derived from mouse embryonic fibroblasts (MEF)-free ES cells. While they reported an expected increase in genes necessary for cardiomyocyte physiology, they also reported a downregulation in genes required for cell proliferation and apoptotic processes. The stem cell derived cardiomyocytes obtained by Doss et al exhibited a variety of electrophysiological morphologies, including atrial- and ventricular-like action potentials (APs), in addition to pacemaker-like APs. However, in most cases, APs did not match those of any particular cell type. Notably, in another study investigating stem cell derived cardiomyocytes selected using GFP expression under the control of α-MHC, GFP was restricted to pacemaker-like and atrial-like cells

(Kolossov *et al.*, 2005). The inconsistency between the two studies may be attributed to the fact that both sets of authors investigated differentiating cardiomyocytes at different stages, day 15 in the case of Doss and colleagues and 9 to 11-day old cells in the latter study by Kolossov at al.

Obtaining a pure, synchronised phenotype of stem cell derived cardiomyocytes still remains a major challenge in the field. Current differentiation methods give rise to cardiomyocytes with various specific phenotypes. Lab-to-lab differences, variations in media components, differentiation methods, stem cell line differences and cardiomyocyte purification methods are all possible explanations for that issue. There is still no direct and efficient method to obtain a fully pure population of cardiomyocytes from ESCs (Das and Fernandez, 2020; Sakamoto *et al.*, 2020). Enriching for cardiomyocytes using selectable markers or resistance genes is a way to circumvent that.

As interest in genetic profiling of stem cell derived cardiomyocytes grew, a wealth of data became available (Lee *et al.*, 2010; Palmer *et al.*, 2012; Pashai *et al.*, 2012). With increasing attention being paid to expression patterns themselves, interest also grew in the regulation of these expressed genes in accordance with the differentiation process, i.e. the trigger, maintenance and coordination of gene expression. The reduction in the expression of stem cell markers like *Sox2* and *Pou5f1* takes place concomitantly with the upregulation of cardiac differentiation markers such as *Nkx2.5* and *Gata4*.

A study by Gan, Schwengberg and Denecke found that several heart related genes as *Nppa*, *Nppb*, *Gata4* and *Gata6* were significantly upregulated during cardiomyocyte differentiation, as well as cardiomyocyte-specific genes like *Myh6*, *Myh7*, *Myl1* and *Myl2* (Gan, Schwengberg and Denecke, 2014).

Expression patterns of various transcription factors along with their targets can then be used to infer possible interaction networks and important regulation module elements in these networks. Based on their expression profile data for different transcription factors and differentially expressed genes during cardiomyocyte differentiation, the authors were able to deduce regulation networks. These networks also identify crucial central regulator transcription factors with roles in differentiation. *Mef2c*, *Nkx2.5* and *Gata4* are important elements of the network and

are upregulated. *Nkx2.5*, the 'trigger' in these networks, activates the transcription of *Mef2c*, *Gata4* and *Tbx5* (Gan, Schwengberg and Denecke, 2014).

Studying populations of cells and attaining transcriptional profiles is proving to be a powerful tool to pick apart various genetic events taking place during differentiation and inferences may be made to parallel events that may take place during natural development of a mammalian embryo. Interestingly, as technology improves, it is now possible to study transcriptional events to an exceptional level of detail, that of a single cell (Li et al., 2015). Single cell transcriptomics have been gaining popularity for the invaluable insights provided, as population purity is not an issue.

Cardiomyocytes derived from ESCs/iPSCs have great potential for therapy and disease modelling *in vitro* in addition to drug and toxicity screenings. A major caveat that must be considered however, is that their phenotype has largely been described as immature (Lieu *et al.*, 2009; Feinberg *et al.*, 2013; Robertson, Tran and George, 2013). By analysing cardiac sarcomeric genes and transcription factors at distinct points in development, Li et al found that mESC-derived CMs bear a great resemblance to CMs derived from the embryonic mouse heart up to the neonatal stage (Li et al., 2015).

Adult heart CMs, on the other hand, displayed moderate differences compared to neonatal heart CMs, especially in sarcomeric gene expression where some are more highly expressed in the adult. This finding was confirmed by performing qPCR on purified cell populations obtained from adult atrial and ventricular cells and comparing them to atrial and ventricular cells from neonates. The results suggested that the process of maturation that normally takes place in the neonatal stage is absent when deriving CMs from mESCs *in vitro* (Li et al., 2015).

Overall these studies show the potential of transcriptomic profiling. It can lead to a closer understanding of the genetic networks governing differentiation, what might go wrong in the context of disease and aid in providing us with a practically limitless resource of cells for drug screening and repair.

1.2 Project Aims

Great advances have been in studying the genetic mechanisms of heart development and how their dysregulation contributes to CHDs. However, the picture is far from

complete. Mapping out these pathways can have translational applications towards a potential, albeit ambitious, curative treatment. Ideally, these gene pathways can be leveraged *in vitro* to generate reprogrammed patient cells that can be transplanted to repair the damage, with no fear of immune rejection. This can also be utilised in gene therapy where a healthy cardiac gene is delivered to the cardiomyocytes.

With that broad goal in mind, and the specific goal of elucidating the regulators of *Tbx5* expression, this project aimed to expand our knowledge of cardiac differentiation models, the role of histone deacetylation and *hdac4* and cardiomyocyte contractility. Figure 1-18 lists the aims, experiments and relevance of this project using a Why-How-For What framework.

This project set out to compare two cellular models of heart development and optimise their differentiation, namely the P19CL6 embryonic carcinoma cell line and the CGR8 mouse embryonic stem cell line. This was done to find an optimal cellular differentiation model.

After developing a robust differentiation model, this study aimed to query the effects of wide-scale HDAC inhibition using TSA and specific *Hdac4* CRISPR/Cas9-mediated knockout on cardiac differentiation. The study aimed to use the two treatments to explore the roles of HDACs and *Hdac4* in cardiogenesis.

Moreover, this project set out to conduct transcriptomic profiling of stem cell-derived cardiomyocytes, and to examine the effects of HDAC inhibition and *Hdac4* knockout on gene expression. The overall hypothesis, therefore, of this exploratory study is that histone deacetylation inhibition and/or hdac4 KO would lead to significant changes in cardiomyocyte differentiation and gene expression.

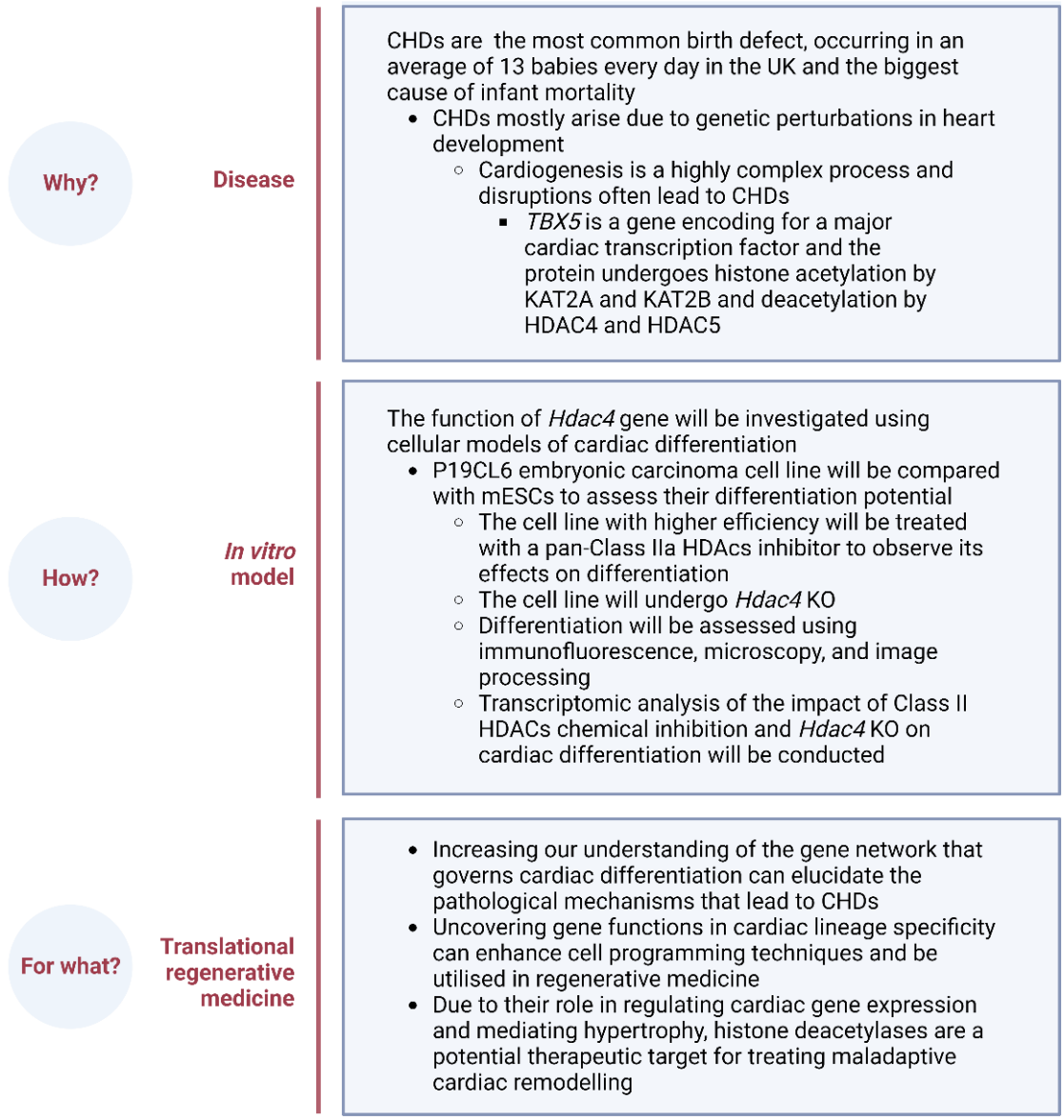


Figure 1-18. Aims and objectives of this thesis.

2 MATERIALS AND METHODS

2.1 Microbial Techniques

2.1.1 Bacterial culture plates

LB broth was made by combining 5g Bacto-tryptone, 2.5g yeast extract, 5g NaCl, 7.5g agar and 500mL of sterile distilled water. It was sterilised by autoclaving. To

make the plates, it was heated in a microwave until completely melted. It was then incubated at 50°C for an hour. Ampicillin (50 µg/ml stock) was then added at a 1:1000 dilution. Molten LB was then poured onto plates and those were left to dry. Aseptic techniques were used throughout.

2.1.2 Culturing colonies

A single, non-overgrown colony was picked with a sterile toothpick using aseptic techniques. The toothpick was then placed in a glass tube containing 5 ml LB with 5 µl Ampicillin. Those were cultured in a shaking incubator overnight at 37° at 200 rpm (revolutions per minute).

2.1.3 MiniPrep: isolating plasmid DNA

Cells were transferred from overnight cultures to Eppendorf tubes and centrifuged at 12000 g for 1 minute twice, disposing off the supernatant. DNA was isolated using Thermo Scientific MiniPrep kit (Thermo Fisher Scientific, MA, USA) following the manufacturer's instructions. In brief cells were resuspended in resuspension fluid, lysed for 5 minutes and then neutralised. 500 µl of column binding solution were added followed by a centrifugation step at 12000 g. wash solution was then added followed by another centrifugation. DNA was eluted in sterile distilled water and quantified using a NanoDrop® ND-1000 spectrophotometer (Thermo Fisher Scientific, MA, USA).

2.1.4 MaxiPrep to isolate plasmid DNA

Day cultures of single colonies in 5 ml LB broth containing 5 µl Ampicillin (50 µg/ml stock) were performed for 8 hours in a shaking incubator at 37°C at 200 rpm. These cultures were diluted 1/500 in Ampicillin-containing LB media and cultured overnight in a shaking incubator at 37°C at 200 rpm.

Following overnight cultures, bacterial cultures were poured into 50 ml Falcon tubes and centrifuged at 4°C at maximum speed (4498 g) for 5 minutes and the supernatant was disposed. Plasmids were isolated using Sigma Aldrich, MS, USA) GenElute HP Plasmid MaxiPrep Kit (Sigma Aldrich, MS, USA) using the manufacturer's instructions. Briefly, cells were resuspended in Resuspension solution followed by lysis using Lysis solution. Lysis was neutralised, followed by addition of Binding solution. The mixture was passed through filter syringes and the filtrate was

centrifuged at 3000 g. Wash solution was then added followed by a centrifugation step at 3000 g and eluted in sterile diluted water. DNA was quantified using a NanoDrop® ND-1000 spectrophotometer (Thermo Fisher Scientific, MA, USA).

2.1.5 Glycerol stocks

200 µl of glycerol were added to 800 µl fresh overnight culture (final concentration 20%). Samples were mixed and stored at -80 ·C.

2.2 Molecular Techniques

2.2.1 Polymerase chain reaction

PCR reactions were assembled using 2X MasterMix (Promega, WI, USA) which contain Taq polymerase, dNTPs, MgCl2 and PCR buffer. PCR reactions were cycled as follows using a G-Storm thermal cycler (Agilegene Technologies).

Table 2-1. PCR conditions used. Tm represents annealing temperature and was adjusted as required for each primer pair

	Stage	**Reps**	**Temperature (°C)**	**Time**
Initial denaturation	1	1	94-95	2 minutes
Amplification	2	30	94 Tm 72	30 seconds 30 seconds 1 minute
Final extension	3	1	72	5 minutes

PCR products were electrophoresed on 1.5% agarose gel at 70V for an hour. Agarose gel was made by dissolving agarose (Sigma Aldrich, MS, USA) in 1xTAE buffer (50x stock made by combining 50mM EDTA disodium salt, 2M Tris and 1M glacial acetic acid). Ethidium bromide (Sigma Aldrich, MS, USA) was added by diluting a 0.5 mg/ml stock solution 1:1000 in the agarose/buffer mix.

2.2.2 Gel extraction

Bands were excised from agarose gels using a blade in a UV box. They were then weighed and DNA was extracted using the QIAQuick® Gel Extraction Kit (Qiagen, Hilden, Germany) following the manufacturer's instructions. In short, the gel band was dissolved in 3x its weight of QG buffer and incubated at 50°C for 10 minutes. A volume of isopropanol was then added and the sample was centrifuged. The column was then washed using QG and PE buffers, then eluted in water. DNA was then quantified using a NanoDrop® ND-1000 (Thermo Fisher Scientific, MA, USA).

2.2.3 PCR Clean-up

DNA was extracted from PCR reactions using a QIAQuick® PCR Clean-up Kit (Qiagen, Hilden, Germany) following manufacturer's instructions.

2.3 Cell culture and maintenance

2.3.1 Thawing

P19CL6 cells and mESCs were thawed similarly. Cryovials containing frozen cells were warmed at 37°C for 1 minute. The cell solution was then transferred to a 15 ml Falcon tube containing 9 ml of fresh complete media and spun at 200 G for 5 minutes. The cell pellet was then resuspended in fresh media and seeded on to cell culture flasks.

2.3.2 Freezing

To freeze and maintain stocks of cells, they were first washed with PBS and trypsinised using 0.05% trypsin-EDTA (Gibco™, Thermo Fisher Scientific, MA, USA). Trypsin was inactivated by adding 7 ml of complete media and spinning the cell suspension at 200 G for 5 minutes. For P19CL6 cells, the pellet was resuspended in 10% DMSO in complete media and stored in cryovials (Nalgene, Thermo Fisher Scientific, MA, USA) at -80°C. Embryonic stem cell pellets were resuspended in a cryopreservation solution composed of 10% DMSO in Foetal Bovine Serum and stored in a CoolCell™ cell freezing container (Corning, New York, NY, USA) to achieve a cooling rate of 1°/minute for 24 hours. Cryovials were then transferred to the gaseous phase of liquid nitrogen for long term storage.

2.3.3 P19CL6 culture

The P19CL6 cell line used was originally obtained from The Department of Cardiovascular Medicine, The University of Tokyo Graduate School of Medicine, Tokyo. The cells were grown in Dulbecco's Modified Eagle Medium (DMEM, Gibco™, Thermo Fisher Scientific, MA, USA) supplemented with 10% (v/v) foetal bovine serum (FBS) EU approved origin (Gibco™, Thermo Fisher Scientific, MA, USA) and 2% (v/v) Penicillin-Streptomycin.

2.3.4 CGR8 mESCs culture

CGR8 mouse embryonic stem cells (Merck, NJ, USA, Dorset, United Kingdom) were cultured in Glasgow's Minimal Essential Medium (GMEM, Gibco™, Thermo Fisher Scientific, MA, USA) supplemented with 2 mM L-Glutamine (Merck, NJ, USA), 0.05 mM 2-Mercaptoethanol (2ME) (Merck, NJ, USA), 10% Foetal Bovine

Serum and 1000 units/ml ESGRO mouse Leukaemia Inhibiting Factor (LIF) (Merck, NJ, USA) on 0.2% gelatine (Merck, NJ, USA) in PBS-covered flasks. The cells were incubated at 37 °C, 5% CO2. The media was changed every day and the cells were passaged when they reached 70-80% confluence.

2.3.5 Splitting

0.05% trypsin-EDTA (Gibco™, Thermo Fisher Scientific, MA, USA) was used to remove adherent cells from the surface of the tissue culture flasks and dishes. Dulbecco's phosphate buffered saline (DPBS) (Gibco™, Thermo Fisher Scientific, MA, USA) was used to wash the cells before trypsinisation. Culture media was used to deactivate trypsin and obtain a cell suspension. Cells were split 1:10 into new flasks.

2.3.6 P19CL6 cardiomyocyte differentiation

The first day of the differentiation procedure was taken to be day 0. The cells were grown until near confluency, they were then washed twice with PBS and trypsinised by adding 3 ml trypsin and incubating at 37°C for 5 minutes. They were then resuspended in 10 ml of fresh media. A cell count was performed by transferring 200 µl of cells in media to a haemocytometer. A cell count was obtained and multiplied by 5000 to give the number of cells per ml. The cells were then diluted to 50,000 cells/ml. An equal volume of 1% DMSO in media was then added to give a solution containing 0.5% DMSO. A bacterial petri dish was filled with 20 ml of PBS. The lid was inverted and 12 drops of 20 µl containing the cells in 0.5% DMSO were pipetted. The lid was then turned over slowly and the hanging drops were placed above the PBS. The dish was then incubated at 37°C.

At day 2, 5 ml of 0.5% DMSO in media solution were added to small bacterial petri dishes. The hanging drops were gently washed from the lids with 2 ml of 0.5% DMSO solution. They were transferred to the small petri dishes and incubated at 37° C.

At day 5, the media containing embryoid bodies was transferred to a 50 ml Falcon tube. The embryoid bodies were left to sink and settle at the bottom. The media was then removed and discarded. 20 ml of fresh media were added to a tissue culture plate to which the embryoid bodies were transferred. They were spread around the

plate by swirling and then incubated at 37° C. Figure 2-1 summarises differentiation procedure used for both cell lines.

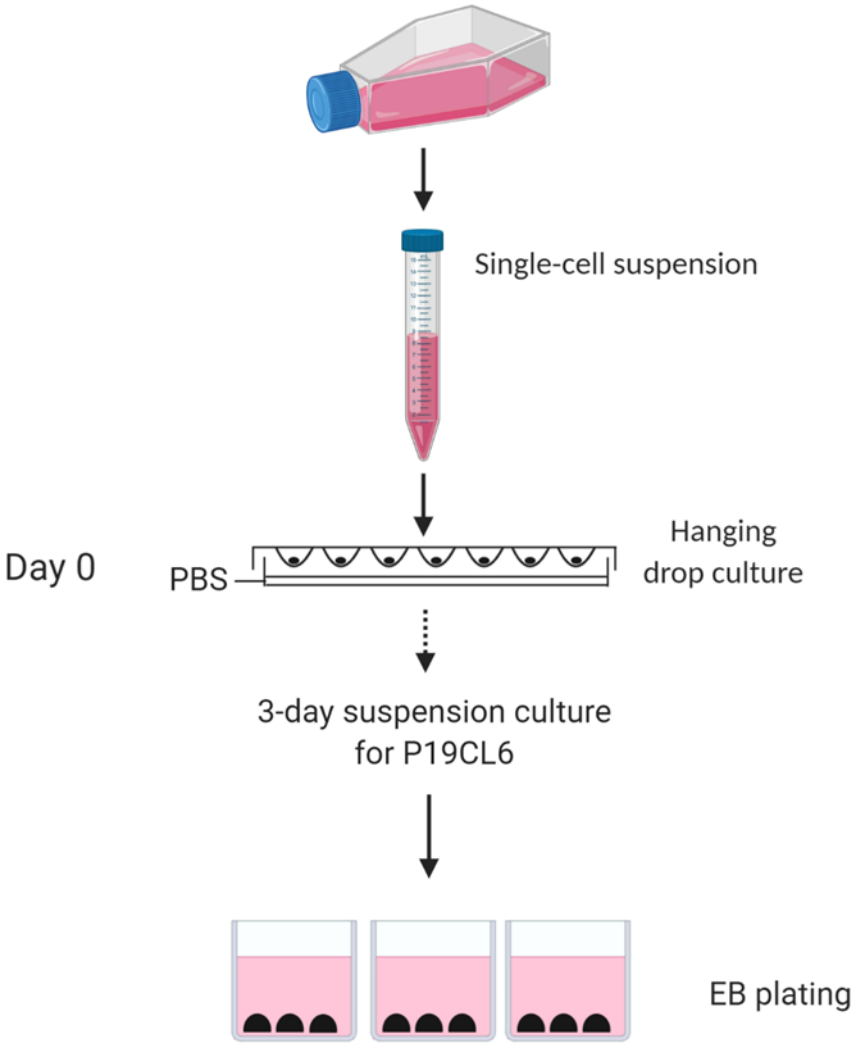


Figure 2-1. Schematic summary of differentiation procedure. Hanging drops were similarly produced for both cell lines at designated day 0. P19s were cultured in hanging drops for 2 days then in suspension for 3 days. ESCs were cultured in hanging drops for 3 days followed by plating. The bottom panel shows a side view of wells in culture plates. Figure created with Biorender.com

2.3.7 Embryonic Stem Cell Differentiation

To induce cardiomyocyte differentiation, the cells were harvested using trypsin-EDTA. Trypsin was applied to cells, followed by a 5-minute incubation at 37° C for 5 minutes. Serum-containing media without LIF (LIF- media) was added to

inactivate trypsin followed by gentle pipetting to ensure there was a fine suspension of cells. The number of cells was counted and the hanging drop method was used to induce the formation of embryoid bodies. Cells were diluted to a concentration of 20,000 cells/ml in LIF- media and 20 µl drops were dotted on the inside of a Petri dish lid. 10 ml of PBS were added to Petri dishes to prevent the hanging drops from drying. The lid was gently and swiftly inverted and placed on the dish, this was assigned Day 0. These were incubated at 37° C 5% CO2 for 3 days.

At day 3, the lids of the dishes were tilted and the drops were gently flushed with media and transferred using a serological pipette to 0.2% gelatine-covered 6-well plates, as can be seen in Figure 2 1. They were then counted and allowed to attach and differentiate while being observed, with daily media changes.

2.3.8 Trichostatin A treatment

The cells were maintained as previously stated. The hanging drop method was used to generate EBs. On day 2 of differentiation, the EBs were gently flushed from the lids. There were then cultured for 4 days in suspension in bacterial dishes. On day 6, the EBs were plated on gelatinised 6-well plates (with an average of 16 EBs per well). On day 7, after the EBs have attached to the plates, 50 nM Trichostatin A (Merck, NJ, USA) in LIF- media was applied. The media was changed every day. The process is summarised in Figure 2-2.

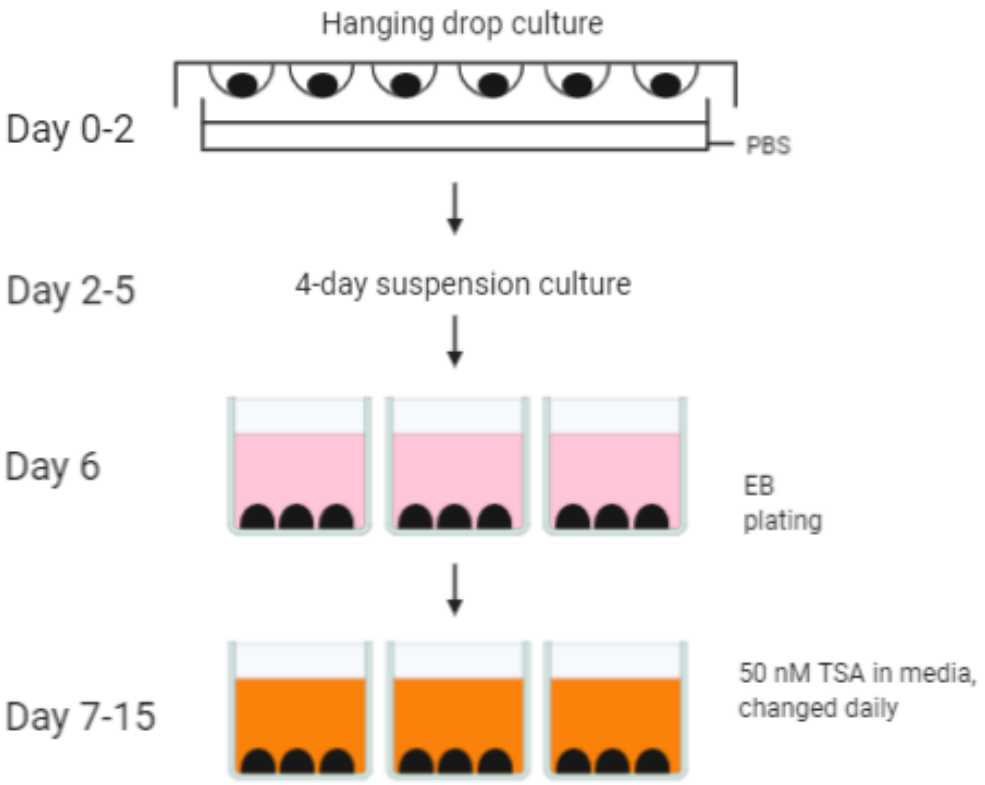


Figure 2-2. Differentiating embryoid bodies were treated with 50 nM TSA for 8 days, starting on day 7.

2.4 Imaging

Daily monitoring and imaging of embryoid bodies and differentiating cells were performed on an inverted microscope with an attached Nikon DS camera (Nikon, Tokyo, Japan).

Beating cardiomyocytes were recorded using a Zeiss LSM880 Exciter Microscope in wide-field setting at 100 frames-per-second.

2.5 Beating analysis

Recorded videos of beating cells were analysed using the MYOCYTER macro on ImageJ as described in (Grune *et al.*, 2019).

2.6 Immunofluorescence

Cells were cultured on gelatinised coverslips in 6-well plates. They were fixed in 4% PFA for 15 minutes, rinsed in PBS then blocked for 30 minutes at room temperature. Blocking buffer contained 5% Goat serum (Gibco™, Thermo Fisher Scientific, MA,

USA), 3% 1% Triton-X (Thermo Fisher Scientific, MA, USA), 20% 50mg/ml BSA (Fisher Scientific, Loughborough, UK) in DPBS. Primary antibodies used, dilutions and manufacturers are in the Table 2-2. Coverslips were incubated with primary antibodies in blocking buffer at 4°C overnight.

Table 2-2. List of antibodies used for immunofluorescence experiments and their respective dilutions.

Antibody	Dilution	Manufacturer	Product Code
Oct-3/4 Antibody (C-10)	1:200	Santa Cruz Biotechnology (TX, USA)	sc-5279
Nkx-2.5 antibody (A-3)	1:250	Santa Cruz Biotechnology (TX, USA)	sc-376565
TBX5 monoclonal antibody (M01), clone 1G10	1:250	Abnova (Taipei, Taiwan)	H00006910-M01
HDAC4	1:250	Santa Cruz Biotechnology (TX, USA)	sc-46672
Monoclonal anti-α-actinin (sarcomeric)	1:400	Sigma Aldrich (MS, USA)	A7811-100UL

Coverslips were washed with PBS 3 times for 10 minutes and incubated with secondary antibody Alexa Fluor Goat Anti-Mouse 488 (Thermo Fisher Scientific, MA, USA) in blocking buffer (1:1000 dilution) for 30 minutes at room temperature.

They were then washed with PBS again, VECTASHIELD® Antifade mounting media (Vector Laboratories, Peterborough, UK) was added and they were mounted on slides for imaging.

2.6.1 Fluorescent imaging

Imaging was performed on a Zeiss LSM880 microscope and viewed using ImageJ. Figures were compiled using Adobe Photoshop CS6.

2.7 Western Blot

A cell pellet was obtained by washing cells with PBS then trypsining. Trypsin was inactivated by resuspending the cells in complete media. Cell suspension was then spun at 200 g for 5 minutes to obtain a pellet. The pellet was then lysed with RIPA buffer (50 mM Tris-HCl pH 8.0, 150 mM NaCl, 1% NP-40, 0.5% sodium deoxycholate, 0.1% sodium dodecyl sulphate, 5 mM EDTA) in distilled water with 1x protease inhibitor cocktail added fresh at the time of use. Cells in lysis buffer were subjected to three cycles of freezing at -80° C and thawing on ice. The amount of protein in the lysate was then quantified using the Bradford Quick Assay, using reagents from BioRad (CA, USA). 20 µl of standard solutions containing 0µg, 1µg, 2µg, 5µg, 10µg and 20 µg bovine serum albumin in water were incubated with 980µl BioRad Dye reagent for 5 minutes. After which their optical density was measured on spectrophotometer at wavelength of 595 nm. Values were plotted to obtain a standard curve. 2 µl of sample lysate in 20µl sterile distilled water were then incubated with BioRad reagent and measured as previously. O.D values obtained were used to calculate protein amounts based on extrapolating the standard curve.

10µl of sample used for quantification above was mixed with 4 µl 4x SDS buffer (Invitrogen, CA, USA), 1.5 µl 10x reducing agent (Invitrogen, CA, USA) and incubated at 95°C for 5 minutes. Running buffer was prepared by mixing 40 ml 20x MOPS buffer (Sigma Aldrich, MS, USA) with 760 ml distilled water. Pre-cast 10% Bris-Tris gel were prepared by removing the comb and washing with running buffer 3 times. 10 µl of SeeBlue pre-stained marker (Invitrogen, CA, USA), 10 µl of MagicMarker XP (Invitrogen, CA, USA) and 10 µl of the protein sample were loaded onto the gel and run in an electrophoresis chamber for 55 minutes at 200V.

Transfer buffer was prepared by mixing 25 ml 20x transfer buffer (Sigma Aldrich, MS, USA), 50 ml 100% methanol and 425 distilled water. 4 sponges were soaked in transfer buffer. PDVF membrane (Invitrogen, CA, USA) was washed in 100% methanol for 5 minutes then with distilled water and finally in transfer buffer for 5 minutes. The gel was removed from the plastic casing and sandwiched between two buffer-soaked filter papers that were in turn sandwiched between two soaked sponged on either side. The sandwich was placed in a transfer cuvette and run in an electrophoresis chamber for 1.5 hours at 25V.

After transfer was completed, the membrane was washed twice with distilled water for 5 minutes. It was then blocked in 5% dry milk in TBST (150 mM NaCl, 20 mM

Tris, 0.05% Tween-20 (Sigma Aldrich, MS, USA)) for two hours. Following blocking, the membrane was washed in TBST 3 times for 5 minutes. The membrane was then incubated with the primary antibody dissolved in 3% bovine serum albumin in TBST at 4°C overnight.

On the second day, the membrane was washed with TBST 3 times. It was then incubated with secondary antibody in 3% in TBST for an hour at room temperature. Detection buffer was prepared by mixing equal volumes of Clarity Western Peroxide and Clarity Western Luminol/Enhancer reagents (BioRad, CA, USA). The membrane was then imaged using a Fuji LAS-3000 MINI scanner.

2.8 CRISPR/Cas9-mediated knock out of *Hdac4*

2.8.1 Target site design

To choose target sites in the *Hdac4* gene in mouse, the online tool CRISPOR (http://crispor.tefor.net/crispor.py) was used. The sequence for *Hdac4* was obtained from Ensembl (ENSMUSG00000026313). Exons from the gene were plugged into the tool and targets were generated. Single Guide (SG) sequences generated and tested were

SG7: CGTACATTCCCAAGACGGGG

SG8: GGGCGAGGTGCTCAGGTACG

SG9: TGAGAGGATTTGTGCCGTAG

SG10: CAGACGAGTGCACCTCATTC

SG11: CCCATCGTCATAGCGGTGCA

SG12: TTTGACGCCTACAGACAGCG

2.8.2 sgRNA synthesis

The sgRNA were synthesised using a non-cloning method using a T7 MAXIscript kit (Ambion, Thermo Fisher Scientific, Waltham, MA, USA) following the manufacturer's instructions according to the protocol published in (Gagnon *et al.*, 2014). Briefly, a 60-bp oligo was ordered that was comprised of the T7 promoter sequence, the target sequence and an overlap region that is complementary to the constant oligo and is needed for in vitro transcription. The constant oligo remains the

same for all sgRNA templates and form the tracRNA. The sequences were as shown in Table 2-3. Therefore, target specific oligos containing the T7 sequence and overlap region with the target-specific sequence in between looked like this

TAATACGACTCACTATA-N_{20}-GTTTTAGAGCTAGAAATAGCAAG with N representing target RNA sequence.

Table 2-3. Sequences for oligos used for sgRNA in vitro synthesis. These were the same for all guide RNAs generated.

T7	**TAATACGACTCACTATA**
Overlap region	GTTTTAGAGCTAGAAATAGCAAG
Constant oligo	AAAAGCACCGACTCGGTGCCACTTTTTCAAGTTGATAACGGACTAGCCTTATTTTAACTTGCTATTTCTAGCTCTAAAAC

2.8.3 DNA Extraction from CGR8 cells

Whole genomic DNA was extracted from confluent cells. They were first centrifuged at 150 G for 5 minutes to obtain a pellet. Next, the Blood and Tissue Kit (Qiagen, Hilden, Germany) was used to lyse the cells and extract DNA according to the manufacturer's instructions. Briefly, the cell pellet was resuspended in PBS and proteinase K was added. Lysis buffer AL was added and the mixture was incubated at 56°C for 10 minutes. Ethanol was then added and the mixture was centrifuged through a DNeasy Mini spin column at 8000 g for 1 minute. Buffer AW1 was then added followed by centrifugation at 8000 g, discarding the supernatant in both cases. Buffer AW2 was then added and the sample spun at 20,000 g for 3 minutes. DNA was then eluted into sterile distilled water and spun at 8000 g for 1 minute. DNA was quantified on a NanoDrop® ND-1000 (Thermo Fisher Scientific, MA, USA).

2.8.4 Polymerase Chain Reaction

Primers were designed using Primer3 (http://primer3.ut.ee/) from mouse genomic DNA flanking the target sites. 700-800-bp regions containing the target sites were amplified using PCR with the programme described in Table 2-4.

Table 2-4. List of primers used to amplify regions containing target sites generated using CRISPOR.

Primer name	Primer sequence	Tm (°C)	Product Size (bp)
*Hdac4*_SG7_700_F	AGGTATTGTGGGGATGAGGC	59.2	774
*Hdac4*_SG7_700_R	ACGAGTGGTGGACATGTTCT	59.0	
*Hdac4*_SG8_700_F	ACTGGCACTGACTGGTACTC	59.0	708
*Hdac4*_SG8_700_R	CCACACATCAGCACCTCATG	58.9	
*Hdac4*_SG9_700_F	CACTCAAAGGGCCCACTAGA	59.0	794
*Hdac4*_SG9_700_R	ATGTTCTCCCCTTGTGTCCC	59.3	
*Hdac4*_SG10_700_F	GGGCCACATGAACAAAACCT	59.0	749
*Hdac4*_SG10_700_R	GGCCCTGCTTTCTGTTTTGA	59.0	
*Hdac4*_SG11_700_F	ACTGTGGGACCATCTTCAGG	59.0	861
*Hdac4*_SG11_700_R	CGTGCCTGTAAGTAGCCAAC	58.9	
*Hdac4*_SG12_700_F	TGGCTGAGCTTCAAGACAGA	59.0	761
*Hdac4*_SG12_700_R	GATGCCAGCAAGTCTCCATG	59.0	

The PCR products were then subject to agarose gel electrophoresis to confirm they were of the expected size. The products were then cleaned using a Qiagen PCR Clean-up Kit (Qiagen, Hilden, Germany, Hilden, Germany) following the manufacturer's instructions.

2.8.5 In vitro assay

To assess the specificity and efficiency of the guide RNAs, a Cas9 *in vitro* assay was conducted. A reaction containing 3 µl Cas9 protein (New England Biolabs, Hertfordshire, UK), 3 µl Cas9 reaction buffer (New England Biolabs, Hertfordshire, UK), 1 µl guide RNA (approximately 300 ng) and RNAse free water up to 30 µl was assembled. The reaction was then incubated at 37° C for 15 minutes. 200 ng of the

cleaned PCR product were then added and that was put back in the incubator for 1 hour 30 minutes. After incubation, 1.5 µl 10mg/ml Proteinase K (Sigma Aldrich, MS, USA) was added. The reaction tube was incubated at 65° C for 15 minutes. The reactions were then run on a 2% agarose gel to analyse fragments.

2.8.6 Vector Design

The guide RNAs able to drive Cas9 cleavage were inserted into a mammalian expression vector along with Cas9 sequence. The vector was designed using www.vectorbuilder.com and purchased (Cyagen Biosciences GmbH, Germany). Figure 2-3 below shows a diagram of the plasmid used.

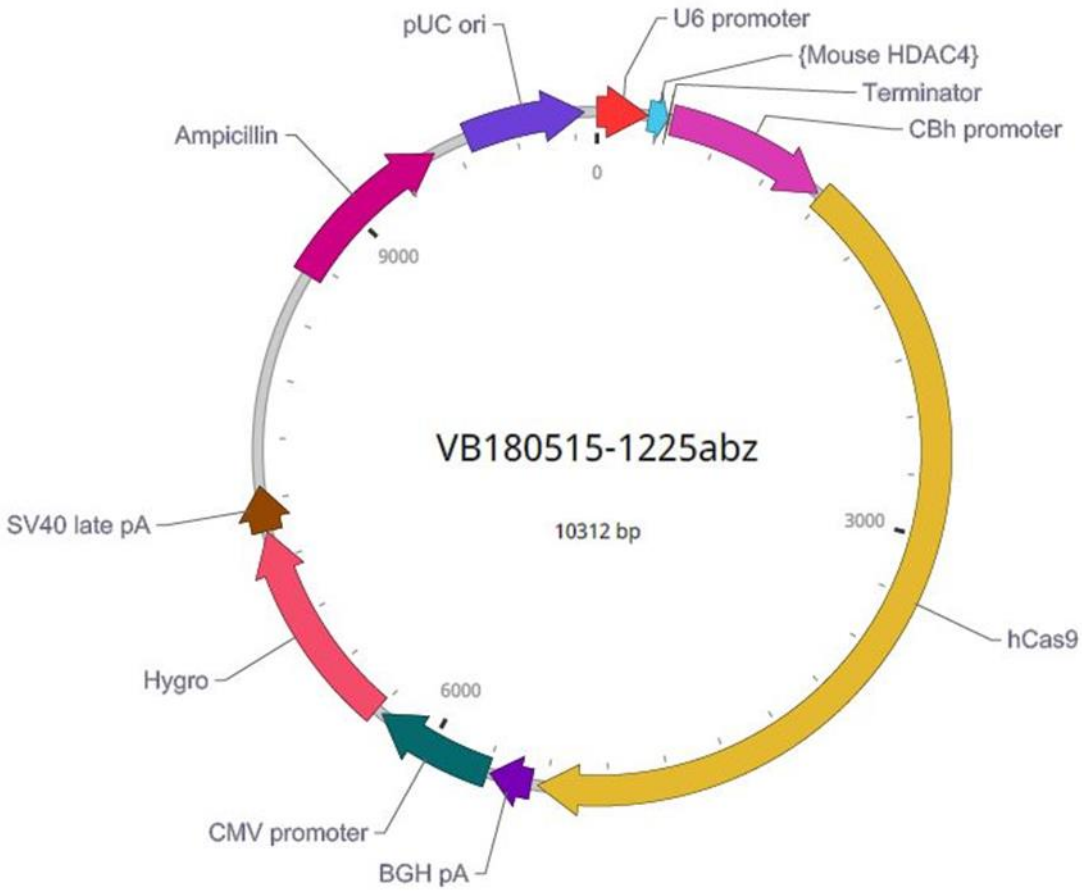


Figure 2-3. Map of vector carrying Cas9, sgRNA, ampicillin and hygromycin resistance genes nucleofected into cells. The vector was obtained from Cyagen Biosciences and designed using their online tools. It was 10.3 kb in size and contained the elements necessary for CRISPR/Cas9-mediated gene editing as

well as a replication origin, promoter regions and elements required for its incorporation.

2.8.6.1 Preparing the vector

The obtained glycerol stock was streaked on agar plates with ampicillin. Single colonies were picked and cultured for a day then overnight. To purify the DNA, a MaxiPrep kit was used and DNA was extracted as described above.

The vector was then linearised with EcoRI (New England Biolabs, Hertfordshire, UK) and electrophoresed on an agarose gel to assess its quality.

2.8.7 Nucleofection

The cells were electroporated using a Nucleofector® I device and the Mouse ES Cell Nucleofector® Kit (Lonza, Basel, Switzerland). The cells were maintained in supplemented GMEM media as previously, with daily media changes. They were harvested by trypsinisation for nucleofection when they were in early growth phase with well-formed domed colonies. 10 ug of the vector were nucleofected into approximately 2 million cells using pre-set programme A-23.

The cells were cultured for a further 48 hours to allow them to recover. For selection, the cells were treated with 100 μg Hygromycin (Thermo Fisher Scientific, MA, USA) for 14 days. Surviving single colonies were harvested using cloning rings. Rings were placed around each colony and petroleum jelly was used to form a seal. Trypsin was pipetted into the cloning ring and incubated for 5 minutes at 37˚C. Media was added to deactivate the trypsin and the cell suspension was obtained. Single colonies were expanded in 24-well plates, followed by T-25 flaks until they reached confluence after which they were further expanded in T-75 flasks. Frozen stocks were obtained at a regular basis. The process is summarised in Figure 2-4.

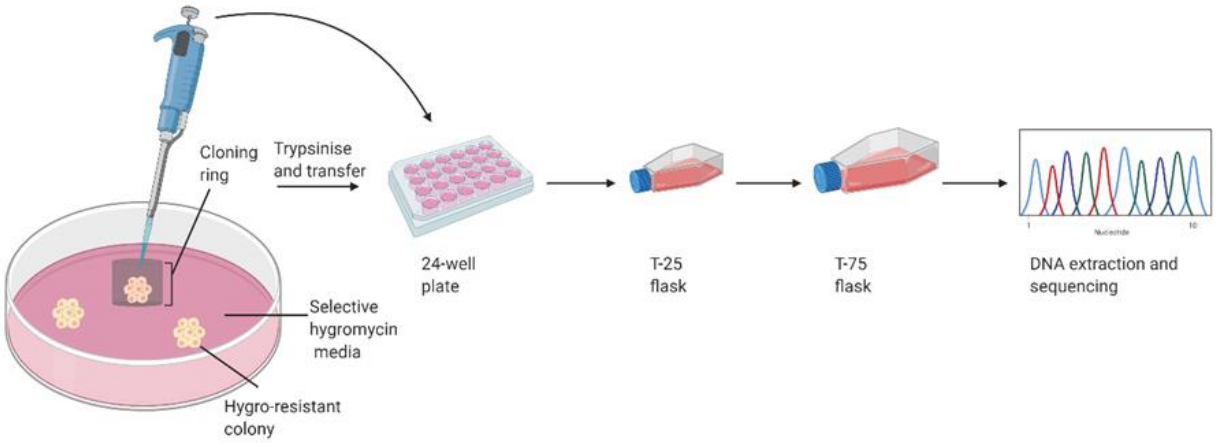


Figure 2-4. Schematic summary of resistant colony selection and expansion following nucleofection. Cells were grown in media containing Hygromycin B after they were allowed to recover post-transfection. They were observed daily and resistant colonies were picked at 14 days using cloning rings placed around single colonies. Cells were trypsinised and expanded in 24-well plates first. They were allowed to grow then expanded further in T-25 flasks, followed by T-75 flasks. When cells reached confluence, DNA was extracted and Sanger sequencing was conducted to investigate whether gene editing has taken place. Figure created with Biorender.com

2.8.8 DNA Extraction

Cells were washed with PBS, trypsinised and a maximum of $5x10^6$ cells were pelleted as previously. To extract DNA, the DNeasy Blood and Tissue kit (Qiagen, Hilden, Germany) was used following the manufacturer's instructions.

2.8.9 Sequencing

To assess whether the *Hdac4* gene was modified, DNA was extracted from confluent flasks expanded form individual colonies using the Blood and Tissue Kit (Qiagen, Hilden, Germany). Primers *Hdac4*_SG10_700_F and *Hdac4*_SG10_700_R used previously to generate 700-800 bp regions containing the target site were used again to generate fragments that were sequenced. Primers amplifying larger products were subsequently used as needed to characterise genotypes and are listed in Table 2-5.

Table 2-5. List of primers used to generate larger PCR products used to characterise mutations.

Primer name	Sequence	Tm (°C)	Product Size
*Hdac4*_1000_F	AAGTAGGAGGCTGCAAGGTT	58.9	1091
*Hdac4*_1000_R	CACGGACACACACACACATG	59.7	
*Hdac4*_1000_F	AAGTAGGAGGCTGCAAGGTT	58.9	1637
*Hdac4*_1600_R	AGGCTAGGCTCACAACCAAA	59.2	

2.8.10 RNA extraction

RNA from undifferentiated cells was extracted using the Rneasy Mini Kit (Qiagen, Hilden, Germany). RNA was extracted from wells with beating zones using cloning rings using the Rneasy Micro Kit (Qiagen, Hilden, Germany) according to the manufacturer's instructions. Extracted RNA was subjected to Dnase treatment using TURBO DNA-free™ Kit (Ambion, Thermo Fisher Scientific, Waltham, MA, USA) following manufacturer's instructions. In short 1 µl TURBO Dnase and 0.1 volume of 10x TURBO Dnase buffer were added to the RNA. The reaction was incubated at 37° C for 30 minutes then inactivated using 0.1 volumes of inactivation reagent. The reaction was incubated at room temperature for 5 minutes then centrifuged at 10,000 g for 5 minutes to obtain the supernatant.

Total RNA was quantified using a NanoDrop® ND-1000 (Thermo Fisher Scientific, MA, USA) (ThermoFisher). Quality was checked by measuring A260/A280 absorbance and using the Agilent BioAnalyzer.

2.8.11 RNA Library Prep

Library generation for RNA sequencing and bioinformatics analysis were performed at DeepSeq laboratory at the University of Nottingham. To generate sequencing libraries, 3' Quant-Seq kits were used (Lexogen, Vienna, Austria). Briefly, oligo-dT primers are used to prime first-strand cDNA synthesis from total RNA. The RNA

template is then degraded. Second strand synthesis is then primed with Illumina-compatible primers containing linker sequences. Next amplification takes place using primers that add barcodes to cDNA fragments. The process is depicted in Figure 2-5. Sequencing was performed on an Illumina NextSeq 500 platform.

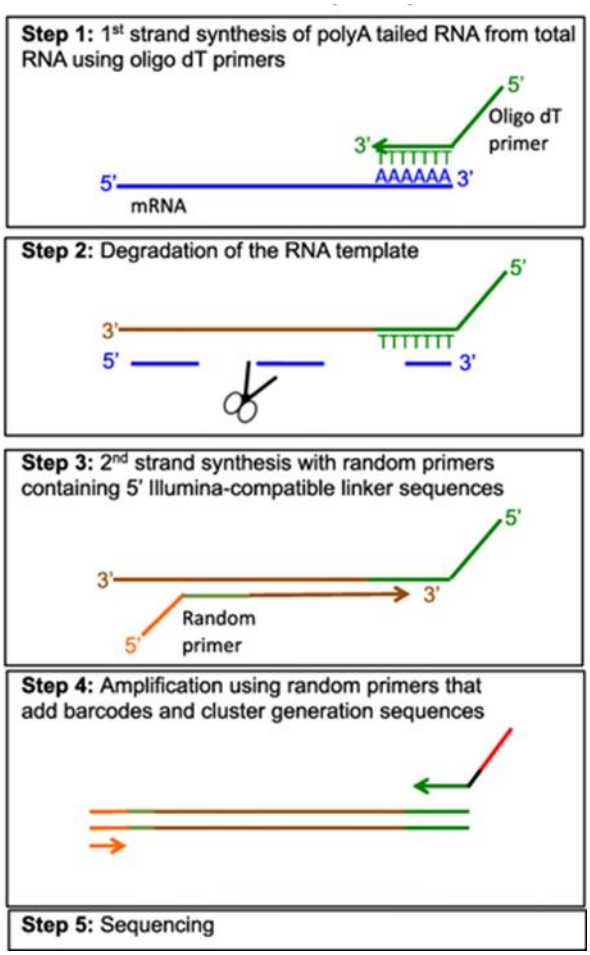


Figure 2-5. Schematic of library generation procedure using the QuantSeq 3' RNA Sequencing kit. In step 1, first-strand cDNA synthesis from total RNA is primed using oligo-dT primers. The RNA template is degraded and removed in step 2. The complementary, second strand is then synthesised using random primers tagged with Illumina-compatible linker sequences in step 3. Double stranded cDNA is then purified using magnetic beads and amplified in step 4. Libraries are amplified using PCR with random primers. This step introduces sequences required for barcoding and cluster generation. Libraries are then ready to be loaded onto the Illumina sequencing platform. Figure from (Moll *et al.*, 2014).

2.9 RNA Sequencing

2.9.1 1. Read Alignment

2.9.1.1 1.1. Trimming

A trimming pipeline was used to filter reads with low sequencing score as well as reads aligned to adaptor sequences. First, raw reads were trimmed against adaptors, and then reads were quality trimmed by Bluebee software

(https://www.bluebee.com/?gclid=EAIaIQobChMIvqDK9oCp5gIVBbTtCh3GeQCnEAAYASAAEgLyaPD_BwE).

2.9.1.2 Mapping

Trimmed reads were mapped onto the reference genome in the context of known gene exon coordinates by STAR mapping tool (Dobin *et al.*, 2013). The genome reference used was GRCm38 (mm10). Annotation source used was Ensembl (www.ensembl.org).

2.9.1.3 Mapping Quality (MAPQ)

Read alignments, both primary and unique, were filtered further according to their mapping quality score (MAPQ) which was generated by STAR. This is a probabilistic metric the accuracy of the read mapping.

2.9.2 Differential Expression

2.9.2.1 Bioinformatics

RNA-Seq bioinformatic analysis was conducted using the Galaxy platform described in (Afgan *et al.*, 2016) and SeqMonk (www.bioinformatics.babraham.ac.uk/projects/seqmonk/).

2.9.2.2 Differential Gene Expression

The differential gene expression R package DESeq2 in Galaxy, which is based on the negative binomial distribution was used. DESeq2 was used to detect the differentially expressed genes for each comparison, and padj < 0.05 was used as a threshold for statistical significance.

2.9.2.3 GO Analysis

GO (Gene Ontology) analysis was conducted using the g:Profiler web tool (https://biit.cs.ut.ee/gprofiler/gost) where gene lists were inputted into the interface and GO: Biological Process analysis was performed (Raudvere *et al.*, 2019).

2.9.2.4 Ingenuity Pathway Analysis

Ingenuity Pathway Analysis (IPA, Qiagen, Heidelberg, Germany) was performed on the results from DESeq2. Gene fold changes from different comparisons were input into the software to query enriched biological themes that may be driving the observed difference in gene expression. Statistical significance cut-off values of $p<0.05$ and z-score $\geq|2|$ were assigned.

3 HDAC INHIBITION AND CRISPR/CAS9-MEDIATED KNOCKOUT IN CELLULAR MODELS OF CARDIAC DIFFERENTIATION

3.1 Introduction

For a wide variety of reasons, cellular models are chosen as *in vitro* models of heart development in place of animal models. The specific research question being asked determines the model chosen. Maintaining cells in culture is far less labour intensive than caring for live animals, and clearly does not require as much space, breeding or feeding costs. Ethical issues associated with animal research and the need for additional trained experienced personnel are also important factors to consider. For this project, a comparison was conducted between the P19CL6 cell line and murine embryonic stem cells to choose the better model for the study's purposes.

Both cell lines are pluripotent and are capable of forming embryoid bodies (EBs). EBs were initially derived from embryonic carcinoma cells and later were formed from pluripotent stem cells from blastocysts (Brickman and Serup, 2017). In fact, EB formation was used as a means to show the similarities between embryonic carcinoma and embryonic stem cells, justifying their use for pluripotency and differentiation studies (Evans and Kaufman, 1981; Martin, 1981). A more accurate method of showing pluripotency is the injection of ESCs in pseudo-pregnant females and studying the embryos. Truly pluripotent cells will contribute to cells of all lineages, including the germ line. This assessment however, is beyond the scope of this study.

Upon plating, EBs are capable of spontaneously differentiating. In intricate experiments performed in the early 1980s, mouse ESCs were shown to spontaneously differentiate into visceral yolk sac, myocardium and blood islands. It was noticed that the process of yolk sac differentiation and organisation highly recapitulated embryonic development, providing important insights and justifications for their use as models (Doetschman *et al.*, 1985). Using RNA-Seq, Spangler et al were able to analyse EB differentiation and found broad similarities in gene expression patterns between EBs and mouse embryos (Spangler *et al.*, 2018)

This differentiation can be modulated and controlled through the addition of various factors, cytokines, inhibitors etc. For this project, the inherent ability of the cells to form beating cardiomyocytes was the focus. Differentiation and cellular properties were monitored over time with an ease not possible in live mammals.

The cardiac genetic network is of great interest to both those wanting to understand how cardiac differentiation occurs in an embryo and those studying congenital heart disease. *Tbx5* is often described as a 'master regulator' of heart development. It plays a part in activating other transcription factors as well as directly binding to DNA (Ghosh *et al.*, 2001). It is also the target of post-translational modifications by other proteins such as acetylases and deacetylases, which are of interest to this project. It is hypothesised that acetylation marks laid down by KAT2A and KAT2B are then removed by HDAC4 and HDAC5. Acetylation was shown to increase TBX5 activity (Gilda *et al.*, 2015). These results align with those found by Lewandowski and colleagues where Tbx5 activity in cardiac development increased upon silencing of Hdac3 (Lewandowski *et al.*, 2014).

Moreover, TBX5 has been shown to interact with TIP60, a member of the MYST histone acetyltransferase family to drive transcription at the *Srf* promoter (Barron *et al.*, 2005) (Barron *et al.*, 2005). PCAF and HDAC4 also regulate contractile activity in myofibrils of primary and adult heart cardiomyocytes (Gupta *et al.*, 2008).

Hdac4 is mainly expressed in the brain, heart and skeletal growth plates in mouse embryos (Vega *et al.*, 2004). *Hdac4* was found to be expressed in the heart at every developmental stage from early embryo to the neonatal phase. It has also been shown to be involved in regulating gene expression in mature cardiomyocytes (Karppinen *et al.*, 2018). It has been posited that *Hdac4* plays a critical role in cardiac differentiation of P19 cells induced to form EBs with hydrogen peroxide. It was shown that *Nanog* and *Hdac4* played a critical part in maintaining transcriptional silence of *Gata4* and *Nkx2.5* (Li *et al.*, 2018). Previous studies have demonstrated that Hdac4 and Hdac5 proteins regulate the cardiac gene programme upon nuclear [Ca2+] changes during development (Frey and Olson, 2003; Wu *et al.*, 2006; Zima *et al.*, 2007). Changes in [Ca2+] mediated by the sarcoplasmic reticulum of cardiomyocytes can change expression of cardiac specific transcription factors (Molkentin, 2004; Kook and Kee, 2011). It was demonstrated that changes in [Ca2+]

induce changes in Hdac4 and Hdac5 cellular localisation in embryonic cardiomyocytes, regulating cardiac gene expression (Karppinen *et al.*, 2018).

Furthermore, *Hdac4* was shown to play a role in heart failure. It was demonstrated that it plays a cardioprotective role in myocardial infarction (MI)-induced heart failure (HF) (Jebessa *et al.*, 2019). In a study aiming to investigate the effect of exercise on glucose metabolism and cardiac function in mice with MI-induced HF, it was shown that exercise activated myocardial AMP-activated protein kinase (AMPK), which phosphorylates Hdac4 consequently regulating *Glut1* expression through repressing *Mef2a*. *Glut1* knockdown impaired cardiomyocyte contractility (Jiang *et al.*, 2020). Inhibition of Hdac4 with TSA was also shown to induce the nuclear translocation of GRK4 (G protein-coupled receptor kinase 4) which phosphorylated Hdac4 and inhibited autophagy and promoted cardiomyocyte apoptosis (Li *et al.*, 2020). In diabetic cardiomyopathy, overexpression of mir-140-5p or silencing of *Hdac4* rescued cardiomyocyte apoptosis induced by *Neat1*, a long noncoding RNA induced by high glucose (Zou *et al.*, 2019).

Additionally, in patients with HF, the reactivation of the foetal gene programme including *ANP* and *BNP* in the left ventricle is indicative of maladaptive cardiac remodelling. The mechanism behind this process is not fully elucidated. Using human ventricular myocardium, it was found that increase of *ANP* and *BNP* expression did not occur via an increase in histone acetylation at their promoters. It was demonstrated that Hdac4 regulates *ANP* and *BNP* expression via di and trimethylation at their promoters, resulting in an increase in expression. In mouse hearts with cardiomyocyte-specific deletions of *Hdac4*, this process was reversed (Hohl *et al.*, 2013).

Class IIa HDACs in general, and HDAC4 in particular has been shown to be play a role in cardiac hypertrophy (Wei *et al.*, 2017). In response to stress, they HDACs phosphorylation and nuclear export, relieving their repression of *Mef2* transcription factors (Travers, Hu and McKinsey, 2020).

Cardiac hypertrophy contributes to the overall HF burden. The natural sweetener isosteviol sodium (STVNa) is known to have pharmacological benefits including cardioprotection. It was demonstrated that it inhibits myocardial ischaemia-reperfusion injury via restoring HDAC4 activity in the nucleus. In another study, it

was shown that preventing MEF2 acetylation prevented hypertrophy in cultured cardiomyocytes (Wei *et al.*, 2017).

In addition transgenic overexpression of *Hdac4* aggravated MIs and myocyte-specific overexpression of *Hdac4* promoted myocardial ischaemia/reperfusion injury (Zhang *et al.*, 2018). Interestingly, HDAC4 was shown to regulate cardiac development in postnatal mouse hearts but to drive cardiac dysfunction at 6 months of age. In infarcted hearts, HDAC4 enhanced cardiac dysfunction, promoted maladaptive remodelling and increased apoptosis (Zhang *et al.*, 2018).

It is clear that HDAC4 is involved in cardiac development, cardiac response to stress, hypertrophy and remodelling. It has also been suggested as a potential therapeutic target in cardiac hypertrophy and vascular inflammation (Kate L Weeks and Avkiran, 2015; Tarun and Antoniades, 2018; Liu *et al.*, 2020). It is also an important regulator of TBX5 activity. It is for these reasons that it garnered interest and why it was chosen for further analysis in this thesis.

3.2 Chapter Aims:

The main aim of this project is to investigate the role of *Hdac4* and its involvement in cardiac differentiation. For this purpose, cellular models lend themselves well. The objective of the study conducted and reported herein was to compare the cardiomyocyte differentiation ability of P19CL6 cells compared to murine embryonic stem cells. That was done to determine the best model for further analysis.

To analyse the role of *Hdac4* in the cardiac differentiation process, I initially established appropriate differentiation protocols (described in the previous section) and tested two different treatments on the differentiating cells. The first involved exposure to 50 nM of Trichostatin A for 7 days and the second was to genetically modify *Hdac4* and observe the consequences of both. Cells were treated with TSA to examine the general effect of inactivating Class II HDACs, whereas the CRISPR/Cas9-mediated knockout would give a more specific idea of the role *Hdac4* might play in the differentiation process.

The null hypothesis would predict for there to be no statistically significant difference in differentiation efficiency between untreated stem cells and TSA-treated

cells. It would also predict for there to be no difference between wild-type and *Hdac4* knockout cells. The experiments described herein used embryoid bodies to induce cardiac differentiation, study differentiating cells for the occurrence of beating and visually analyse beating to investigate a potential role of *Hdac4*. Due to its involvement in cardiogenesis in mammalian embryos, one would expect that there would be a significant difference.

3.3 Results

3.3.1 P19CL6 cells form embryoid bodies

To differentiate P19CL6 cells into cardiomyocytes, the classic hanging drop method was used, as described in (Smith *et al.*, 1987). Cells were aggregated in the hanging drops to form EBs. Due to the action of gravity, cells at the bottom of the drop congregate and form three-dimensional embryoid bodies. Upon culturing using this method, P19CL6 cells were efficiently able to form three-dimensional embryoid bodies of uniform sizes. The percentage of EBs formed from hanging drops in all attempts was 73.0%. Number of hanging drops and corresponding EBs generated is summarised in Table 3-1. At day 2 EBs were relatively small and grew bigger when in suspension. Upon plating at day 5, EBs attached to the bottom of the plate and grew. Epithelial-like cells were seen on the outer edge of the expanding EBs, forming a ‘halo’. Centre of EBs appeared darker, thicker and necrotic compared to the rest of the structure. They showed a starkly different morphology compared to undifferentiated cells (Figure 3-1). Therefore, P19CL6 cells used were capable of efficiently forming embryoid bodies.

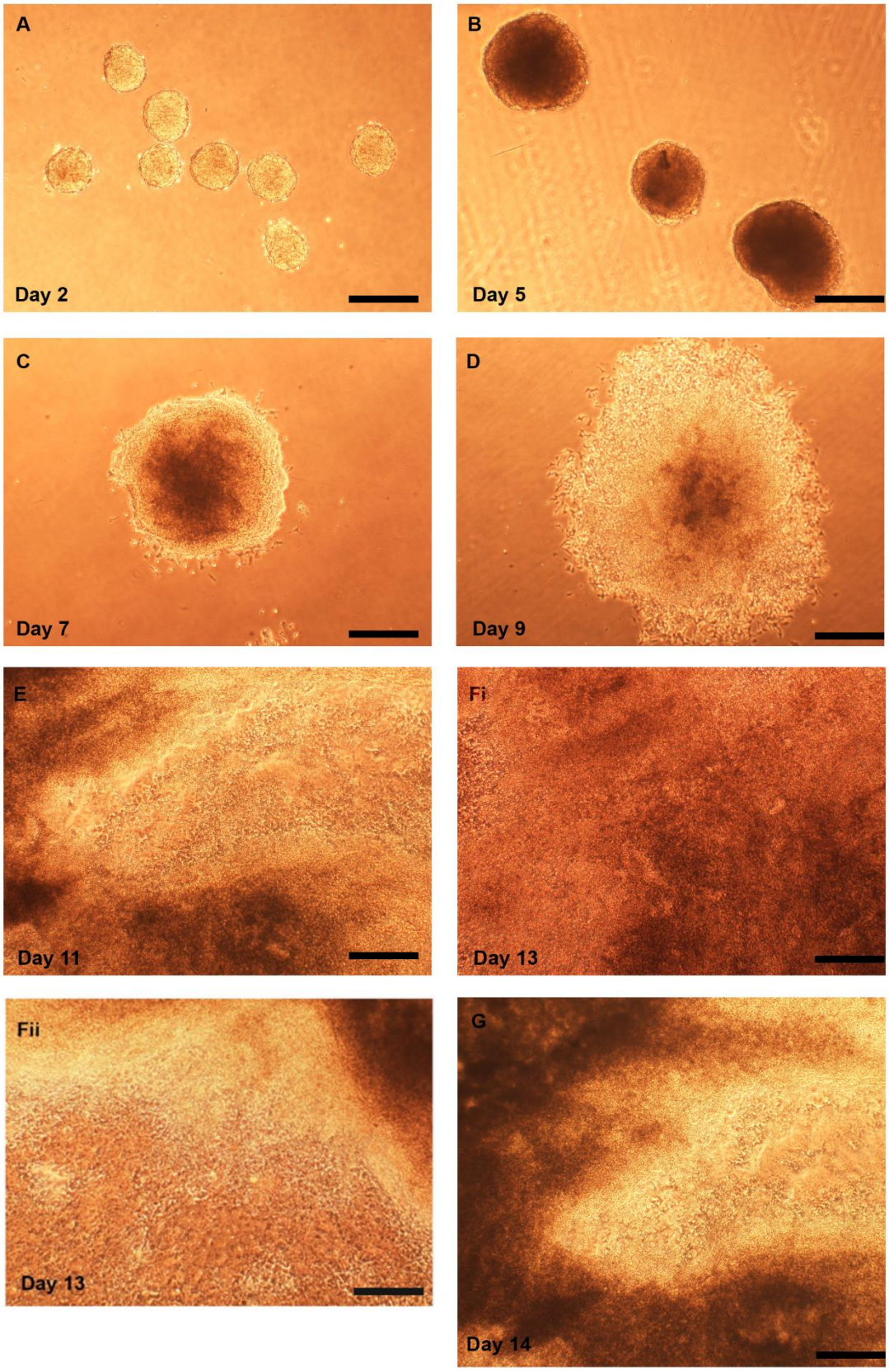

A
Day 2
B
Day 5
C
Day 7
D
Day 9
E
Day 11
Fi
Day 13
Fii
Day 13
G
Day 14

Figure 3-1. Stages of P19CL6 cell line differentiation involve the formation of embryoid bodies in hanging drops, then in suspension, followed by plating. Representative sample of n=1, EBs were imaged throughout. Panels A and B show embryoid body formation 2 days after hanging drop culture (A) and after 3 days in suspension culture (B), respectively. Panels C-G show the same EB over the course of differentiation. Panel C shows EB morphology 2 days after plating at 7 days post-differentiation. Panels D-G show the growth of the EB and the cells around it, forming a distinct 'halo', with image (D) being taken at day 9, image (E) at day 11. (Fi) and (Fii) show the top and bottom of the EB at day 13, respectively. (G) shows image of the EB taken at day 14. 100X magnification. Scale bars = 300 µm. EB, embryoid body.

3.3.2 P19CL6 differentiated EBs inefficiently form beating cardiomyocytes

After plating, the EBs were observed daily to look for pulsating or beating foci. Beating clusters were observed in 54.5% (n=11) of all experimental attempts. Within these experimental setups, these beating foci appeared in an average of 36% of observed plates. The earliest beating onset observed was at day 11 and observed in 2 plates to stop by day 20. Table 3-1 shows beating occurrence and onset from experiments. Results from these experiments therefore indicated that P19CL6 cells did not differentiate into cardiomyocytes with the efficiency required for further studies.

Table 3-1. Summary of P19CL6 differentiation experiment data. EB count data for experiment 8 is not available. EBs: embryoid body. (Y/N): yes/no.

Experiment	Number of hanging drops	Number of EBs	Beating (Y/N)	Beating onset day
1	46	32	N	
2	120	91	Y	14
3	239	154	N	
4	200	134	Y	11

5	200	169	Y	11
6	200	146	Y	16
7	232	156	N	
8	200	-	Y	16
9	200	166	Y	15
10	241	138	N	
11	181	171	N	

3.3.3 Mouse embryonic stem cells are capable of forming EBs

To compare EB-forming abilities of both cell lines, undifferentiated mESCs were also cultured in hanging drops to induce cardiogenic differentiation. Those can be clearly seen in panel B of Figure 3-2. The ability to form EBs is a measure of 'stemness' or pluripotency of the cells. Embryonic stem cells used in this project were able to form embryoid bodies with approximately 60% efficiency. To assess that, individual hanging drops (with any newly formed EBs) were seeded individually onto gelatinised 24-well plates. EBs counts were performed for 6 experiments and compared to the number of starting hanging drops. Data collected is shown in Table 3-2. The data collated showed that the CGR8 cells used had the ability to form embryoid bodies.

Table 3-2. Summary of mESCs differentiation experiment data. EB counts were not performed for experiments 7-9. EBs: embryoid body. (Y/N): yes/no.

Experiment	Number of hanging drops	Number of EBs	Beating (Y/N)	Beating onset day
1	92	20	Y	13
2	96	61	Y	12
3	400	239	Y	10
4	800	347	Y	8
5	397	241	Y	7

6	312	198	Y	8
7	-	-	Y	13
8	-	-	Y	11
9	-	-	Y	7

For differentiation purposes, hanging drops from Petri dish lids were washed onto 6-well plates. Each well had approximately 16 EBs. EBs formed as expected, and looked like small spheres of cells. When plated, the EB centre remains thick and slightly necrotic. Similarly to P19CL6 EBs, mESC EBs also form epithelial cell-like outgrowths or 'halos'. These are apparent even one day after plating at day 5, which can be seen in panel C of Figure 3-2. Growth of the EBs was closely monitored and imaged. EB centres remained thicker and more dense that surrounding areas. They were darker and more necrotic than the halo of cells around it. This change in appearance is indicative of differentiation.

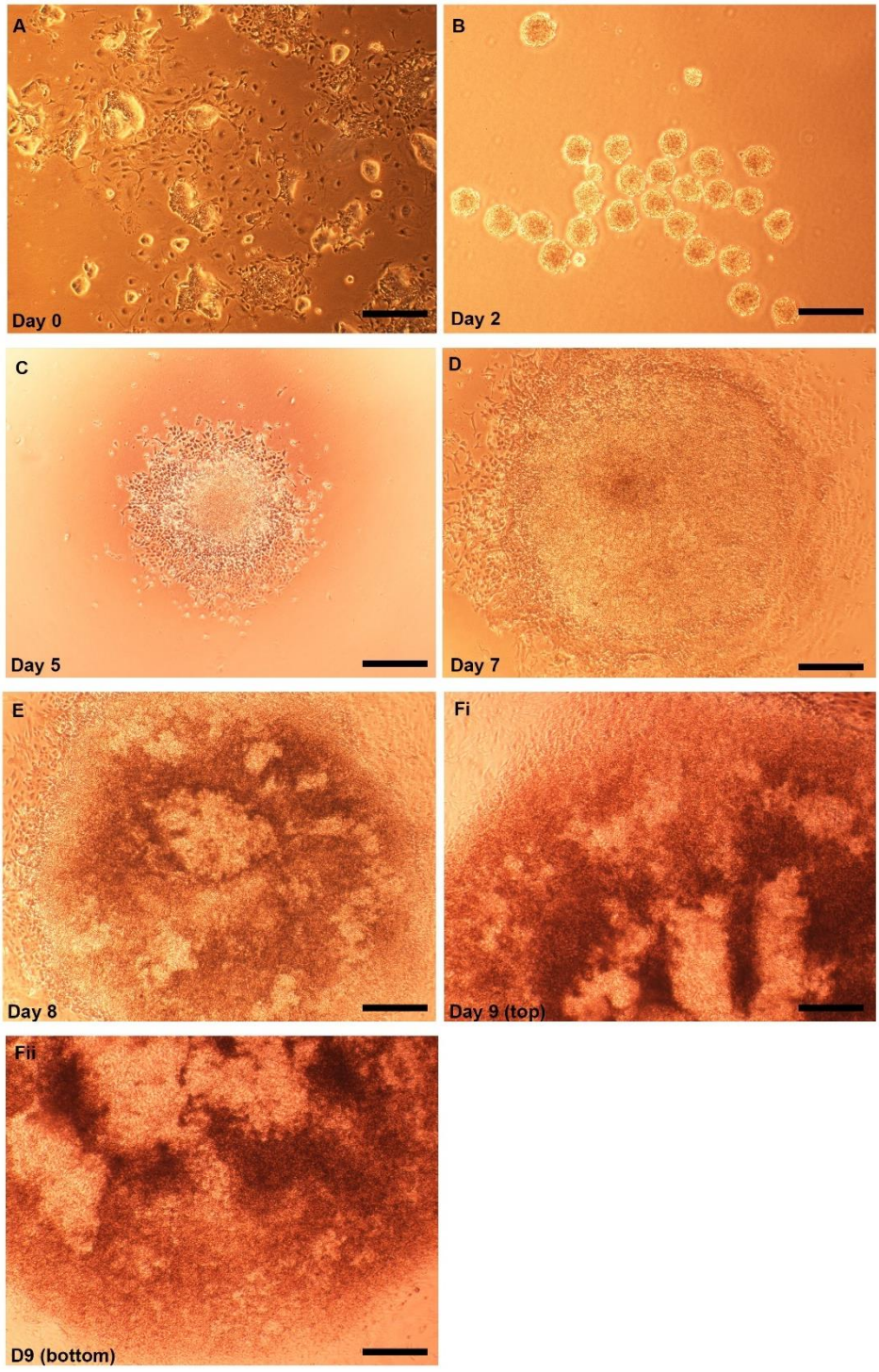


Figure 3-2. mESCs form embryoid bodies that when plated, can differentiate into beating cardiomyocytes. Representative sample of n=1, EBs were imaged throughout. Days are indicated at the bottom left of each panel, starting with undifferentiated cells at Day 0 (A). Panel B shows formed embryoid bodies after 2 days of hanging drop culture. For differentiation they were cultured in

hanging drops for 3 days then plated. Panels C-F show an embryoid body whose growth was monitored over time. Panel (C) shows the image taken at day 5. Panel (D) shows the image taken at day 7 and panel E at day 8. (Fi) and (Fii) show the top and bottom of the embryoid body at 9 days post differentiation. 100X magnification. Scale bars = 300 µm. EB, embryoid body.

3.3.4 Embryonic stem cells differentiate into cardiomyocytes more efficiently

To assess cardiogenic differentiation ability, beating onset was used as a measure of differentiation. The first day of the observance of a beating focus was noted for every experiment. Beating was observed as early as day 7 and was seen in 100% of differentiation experiments. The values were plotted in the graph presented in Figure 3-3. An unpaired t-test analysing the averages indicated a significant difference between the two cell types, with $p=0.0084$ ($p<0.05$). Having an earlier beating onset, in addition to seeing beating in all experiments led to mESCs being the cell model of choice for further study.

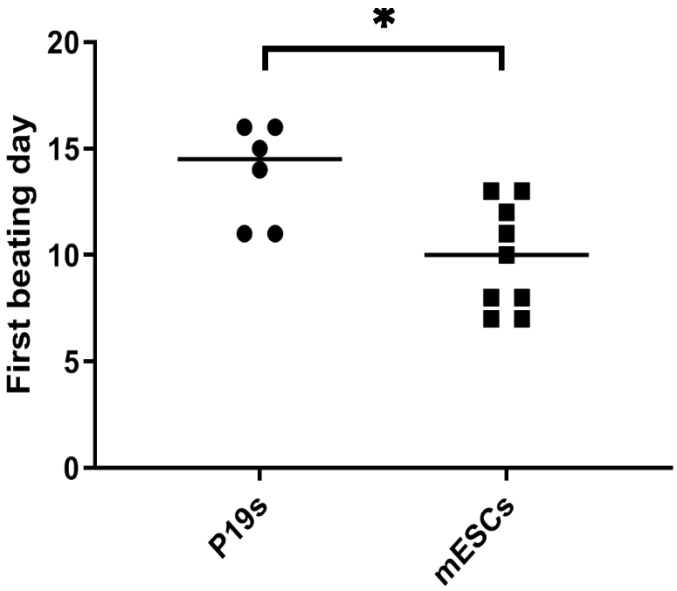


Figure 3-3. Mouse embryonic stem cells differentiate into cardiomyocytes earlier than P19CL6 cells. Initiation of beating was taken as a measure of differentiation and was plotted for each experiment. The horizontal line on the graph shows indicates the mean (13.8 for P19s and 9.9 for mESCs). The asterisk indicates a statistically significant difference between means ($p<0.05$).

Beating foci also varied in sizes and strength of contraction between mESCs and P19CL6s. Beating was easier to visualise with the mESCs and was more robust. It also lasted for longer and foci kept beating until disposal, as far as day 32. Beating from differentiated mESCs was photographed and time-lapse videos are shown in Movies 1-3.

3.3.5 Differentiating mESCs express cardiac markers

After establishing their better differentiation ability, an immunofluorescence assay was used to probe for and visualise the expression of known pluripotency-associated factor OCT4, in addition to cardiac markers NKX2.5, TBX5 and sarcomeric marker α-actinin in mESCs. Nuclei were labelled with Hoechst stain. OCT4 expression was monitored on days 4, 7 and 15. It showed a consistent decrease in intensity as can be seen in Figure 3-4. NKX2.5 expression was looked at the same ime points and TBX5 expression was probed at days 7 and 15, shown in Figure 3-5. The expression of NKX2.5 over time remained high. At day 15, it could be seen that NKX2.5 expression was highest near the centre of the EB and less so towards to outgrowing halo. The cardiac factor TBX5 was also looked at. Its expression appeared more widespread at day 7 while being the highest towards the centre at day 15, similarly to NKX2.5. This suggests that the cells forming the outgrowing halo can may going down differentiation routes different than cardiac lineages. This fits in with the observation that beating foci are usually found closer to the centre, in denser areas. As a marker of beating sarcomeres, the unit of striated muscle, α-actinin expression was probed (Figure 3-6). It can be seen from the image taken at day 15 that its expression is consistent with that expected of cardiomyocytes. Organised actinin filaments can be seen in the image and are indicated with a white arrow. Experiments with negative controls were not conducted to completely rule out non-specific staining. The results obtained from immunofluorescence can therefore be described as suggestive of cardiac differentiation protein marker expression.

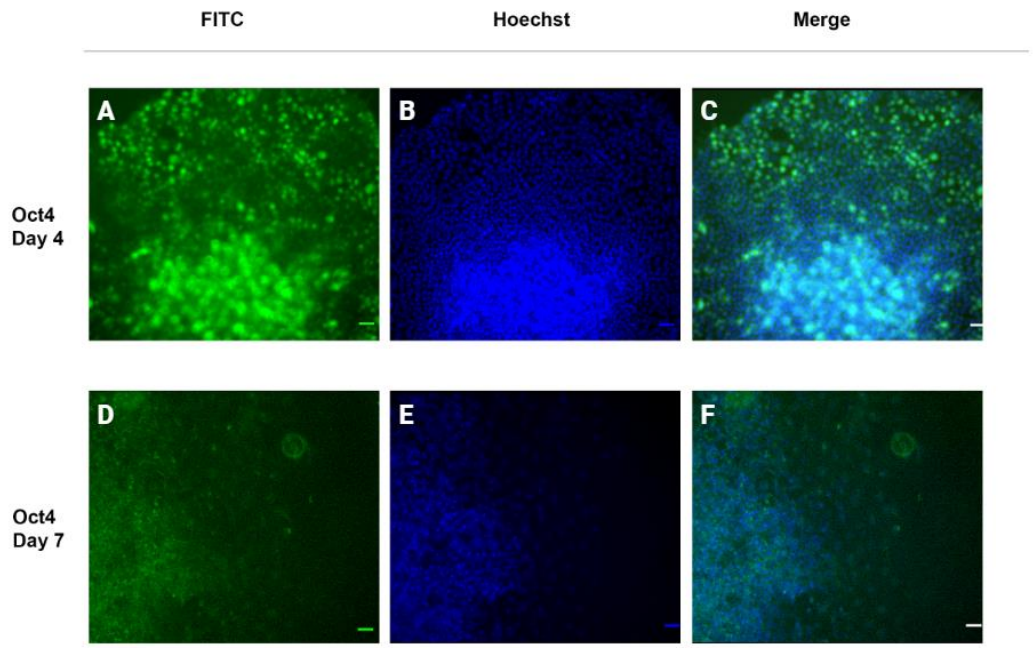


Figure 3-4. Immunofluorescence showed the expression of pluripotency associated marker at start of differentiation procedure. Nuclei were labelled with Hoechst stains and indicated proteins are labelled in green. Days post differentiation and proteins are indicated at the left. Oct4 expression was present at day 4 (A-C) and could still be seen at day 7 (D-F). Scale bars=115 µm.

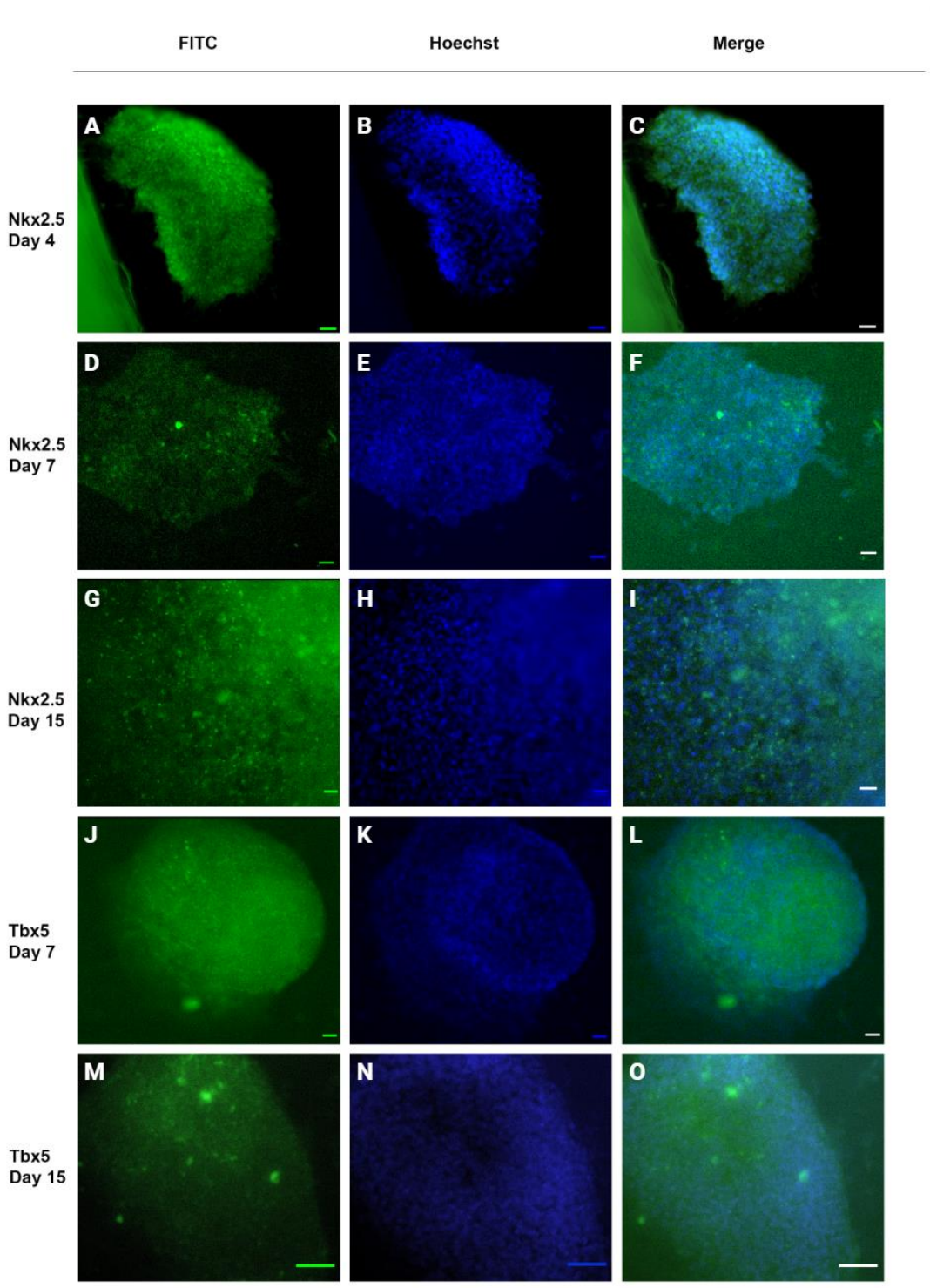


Figure 3-5. Cardiac markers were expressed in differentiating stem cells as indicated by immunofluorescence. Using antibodies against Nkx2.5 and Tbx5, fluorescence was seen at days 4, 5 and 15. Nuclei were labelled with Hoechst stains and indicated proteins are labelled in green. Days post differentiation and proteins are indicated at the left. Nkx2.5 expression was present at day 4 (A-C),

day 7 (D-F) and day 15 (G-I). Tbx5 was also present in differentiating mESCs, at day 7 (J-L) and day 15 (M-O). Scale bars A-L= 137 µm, M-O = 320 µm.

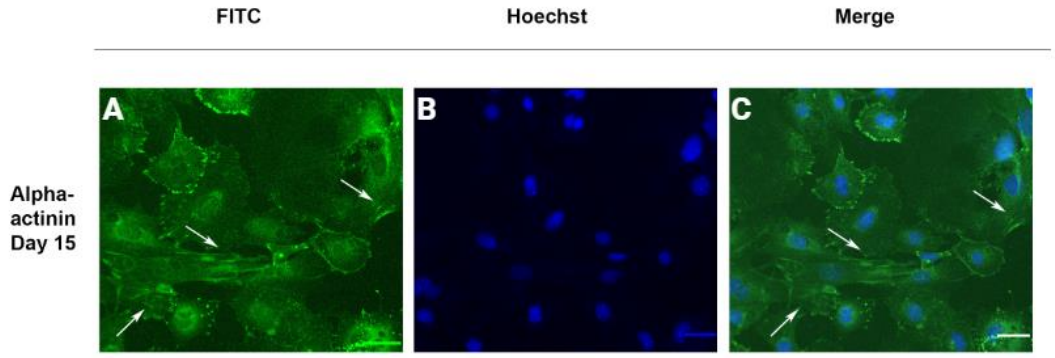


Figure 3-6. Contractility-associated alpha-actinin protein was expressed in beating regions of differentiated stem cells. White arrows point to actinin striations in beating cardiomyocytes (A) and (C). Anit-α-actinin antibody showed fluorescence at day 15 (A), nuclei were stained with Hoechst (B) and merged in (C). Scale bars = 235 µm.

3.3.6 Differentiating mESCs express HDAC4 protein

Embryonic stem cells were differentiated as previously described. The expression of HDAC4 was investigated using immunofluorescence to detect the presence of the protein, using an anti-HDAC4 antibody. Immunofluorescence assays were conducted at day 4, day 7, day 15 and day 21 and are shown in Figure 3-7. In general, results suggested that HDAC4 was expressed steadily at all time points investigated. Attempts at optimising Western blot experiments to quantify HDAC4 expression were made but were not successful. It was clear from the images obtained that HDAC4 was present in the cytoplasm as well as the nucleus, appearing to form a bright ‘ring’ around it at day 15. Experiments with negative controls were not performed to rule out non-specific staining or autofluorescence. However, attempts were made to confirm HDAC4 protein expression using Western blotting.

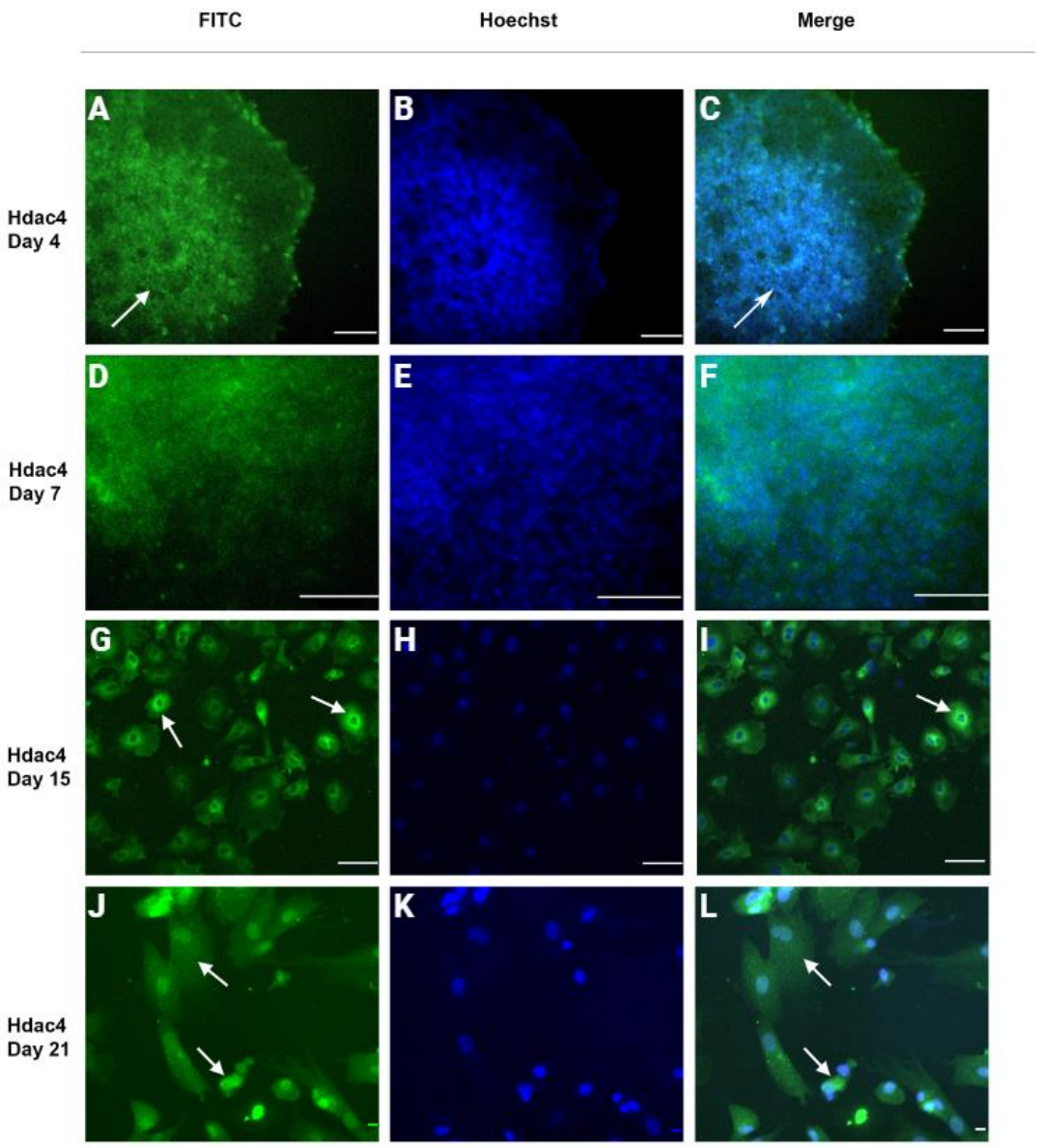


Figure 3-7. Immunofluorescent staining of HDAC4 expression in differentiating stem cells indicates its presence throughout differentiation, with higher expression detected at later stages. (A-C) Show HDAC4 expression at differentiation day 4. White arrows point to protein cellular location. Scale bars = 319 µm. (D-F) indicate HDAC4 expression at differentiation day 7. Image taken using 10x objective. Scale bars = 596 µm. (G-I) show HDAC4 expression at differentiation day 15. White arrows point to more visible fluorescence at the nuclear periphery. Scale bars = 293 µm. (J-L) Show expression at

differentiation day 21. Top white arrow points to cytoplasmic localisation of Hdac4 and bottom arrow indicates nuclear fluorescence. Scale bars = 64 µm.

3.4 Trichostatin A treatment of differentiating mESCs

3.4.1 TSA treatment affected EB morphology

Having established the baseline expression of *Hdac4* in differentiating mES cells I sought to establish the effect of Trichostatin A treatment (wide-scale inhibition of Class I and II HDACs) on the cells and their differentiation ability. 50 nM TSA in differentiation media treatment was applied on differentiation day 7 for 8 days to day 15 of differentiation (see Figure 2-2). TSA-containing media was changed every 24 hours. Treated cells were observed and imaged every day. Figure 3-8 shows images taken every day of a single EB for 8 days. Visual inspection of the cells was conducted. Had time permitted, morphometric analysis of cellular morphology would have been conducted to quantify the morphological changes. From visual inspection, it was seen that EB outgrowths spread across a larger area and were thinner. Central EB structures that are normally dense also were smaller and thinner. Cell debris was observed in all plates, indicating a degree of cell death caused by drug toxicity. Therefore, TSA had apparent, promptly visible effects on cell health and appearance.

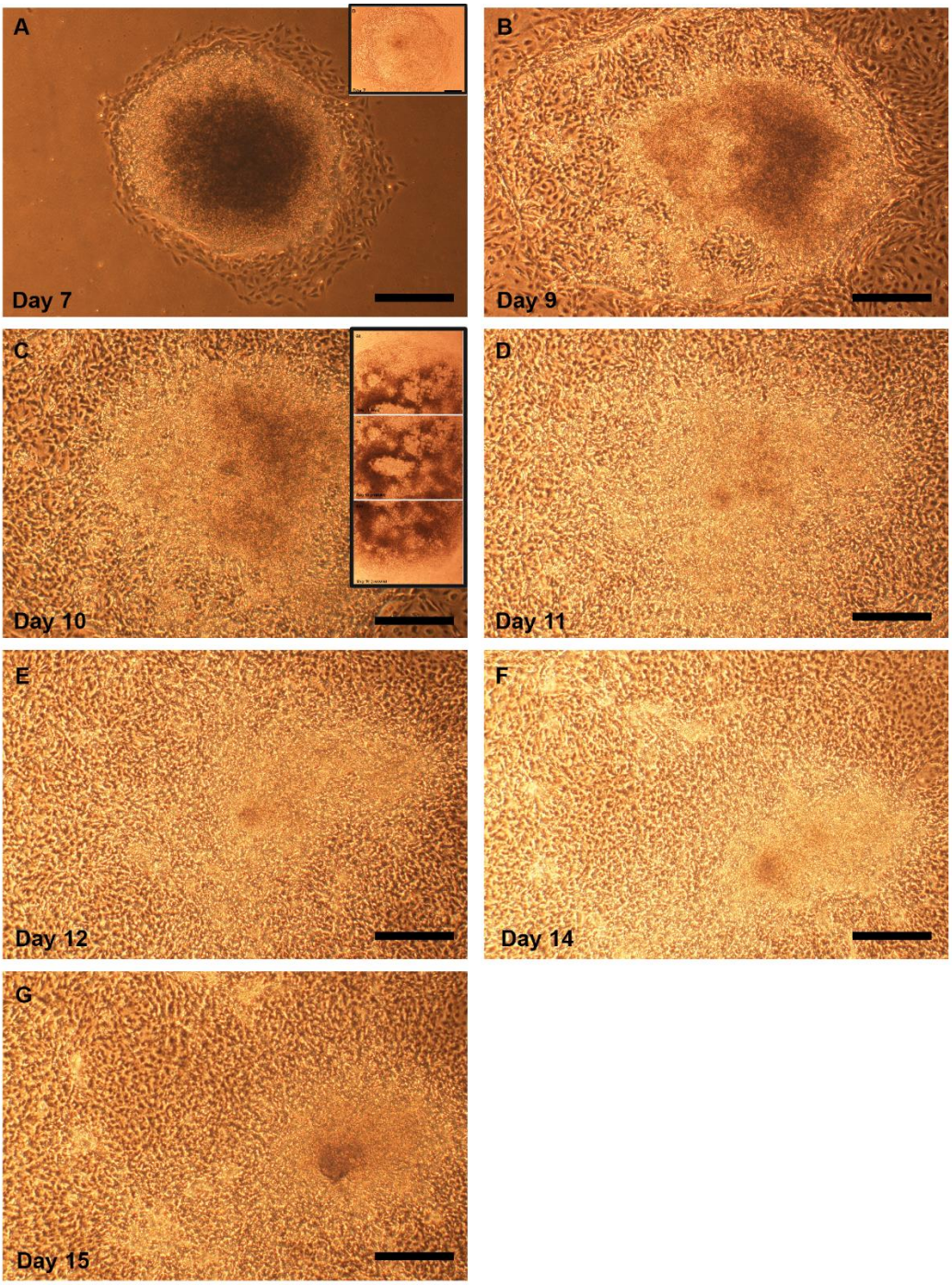


Figure 3-8. TSA treatment affects EB morphology. Images of an embryoid body from differentiating ES cells at the first day of TSA treatment, day 7 in (A) to day 15 (G). Differentiation day is indicated in the bottom left corner of every image. Insets in (A) and (C) show untreated mESCs at the same differentiation day. (C) shows how the EBs display thinner outgrowths while the untreated cells maintain a more solid core. The inset shows top, middle and bottom of an

untreated day 10 EB. Scale bars= 300 µm. Images were taken at 100X magnification.

3.4.2 TSA treatment did not significantly affect beating onset

To investigate the effect of TSA on cardiac differentiation, differentiating EBs were observed every day for the appearance of beating clusters. Similarly to differentiating wild-type untreated mESCs, beating foci were present in 100% of experimental attempts (n=13). The earliest beating onset observed in treated cells was on the same day as the treatment, day 7. TSA treatment was performed in the morning and beating was observed in the afternoon. However, there is no indication that TSA could have greatly accelerated cardiac differentiation. Day 7 was also the earliest day on which beating was noted for untreated wild-type differentiated mESCs. The first day beating was observed and plotted for TSA treated cells vs untreated counterparts that came from the same original flask and underwent the same differentiation procedure. Beating onset days were recorded and tabulated, the data is presented in Table 3-3 and the plotted graph is shown in Figure 3-9. While the average start-of-beating day for TSA-treated cells was 10.15 (n=13) and 11.11 (n=9) for untreated controls, an unpaired t-test did not indicate a statistically significant difference at the $p<0.05$ threshold. Notably, the beating pattern in TSA-treated cells differed from that seen in wild-type differentiated cells, see Movies 4-6. TSA-treated cells produced beating foci with a more wave-like form, as compared to the more twitch-like pulsating beating seen in wild-types. All in all, while TSA affected beating patterns, it did not significantly lead to earlier beating onset.

Table 3-3. Table of first beating occurrence in TSA-treated differentiating mESCs and untreated controls.

TSA treated cells		**Untreated controls**	
Experiment	Beating onset day	Experiment	Beating onset day
1	7	1	13
2	11	2	12
3	7	3	13
4	7	4	10

5	8	5	11
6	8	6	14
7	11	7	10
8	10	8	7
9	12	9	10
10	12		
11	12		
12	12		
13	15		

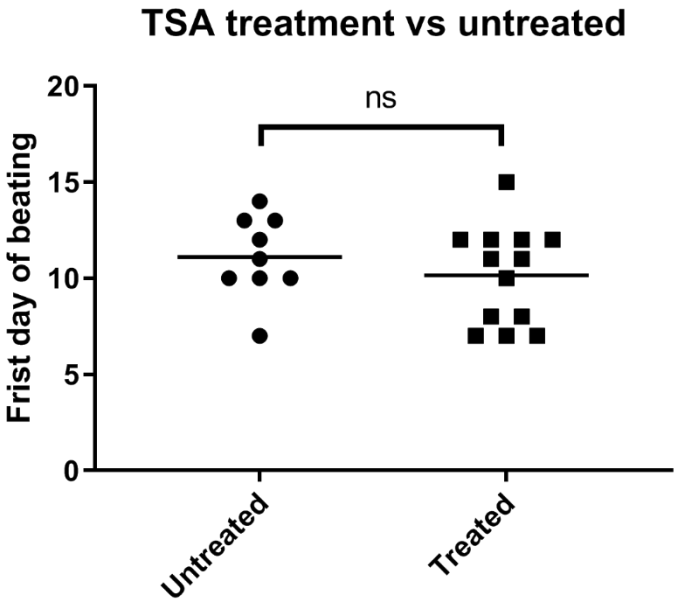


Figure 3-9. TSA treatment did not significantly affect beating onset. The graph shows a scatter plot of first day of beating observed for each experiment (N=9 for untreated controls and n=13 for TSA treated cells). The horizontal lines indicate the mean.

3.5 CRISPR/Cas9-mediated knockout of *Hdac4*

3.5.1 Target site design

To knockout *Hdac4* in mESCs, CRISPR/Cas9 technology was employed. First, to find appropriate target sites in the *Hdac4* gene, online predictor CRISPOR was used. Upon inputting *Hdac4* sequence, a list of potential guide RNAs was generated, shown in Table 3-4. These guide RNAs were then synthesised by *in vitro* transcription to test for Cas9 cleavage *in vitro*.

Table 3-4. List of target sites generated by CRISPOR, their sequences, PAM sequences and locations on *Hdac4* mouse gene.

Guide name	Sequence	PAM	Location
sgRNA7	CGTACATTCCCAAGACGGGG	TGG	Exon 7
sgRNA8	GGGCGAGGTGCTCAGGTACG	GGG	Exon 11
sgRNA9	TGAGAGGATTTGTGCCGTAG	AGG	Exon 16
sgRNA10	GAATGAGGTGCACTCGTCTG	GGG	Exon 18
sgRNA11	CCCATCGTCATAGCGGTGCA	GGG	Exon 21
sgRNA12	TTTGACGCCTACAGACAGCG	AGG	Exon 26

3.5.2 Guide RNA quality check

To check if Cas9 can drive cleavage at these target sites, the guide RNAs were synthesised via *in vitro* transcription. Resultant RNAs the guide RNAs were assessed for their size and integrity using an Agilent BioAnalyzer, expected size is approximately 90 bp. Good quality RNA results in defined bands and the absence of smearing. In Figure 3-10 resulting from the analysis, sgRNA10 was chosen for downstream analysis. The electrophoretogram traces in panel A show that sgRNA10 had a defined peak at the expected size. It had produced the most distinct band at the expected size and no smearing as seen in panel B, the band seen at >150 bp is likely from secondary RNA structures. These samples were run against an RNA ladder with the marker bands shown in the leftmost lane in panel B and the electrophoretogram trace in panel C. Figure 3-11 shows the location of the selected guide and the PAM sequence in exon 18 of *Hdac4*. The figure also shows the exon translation.

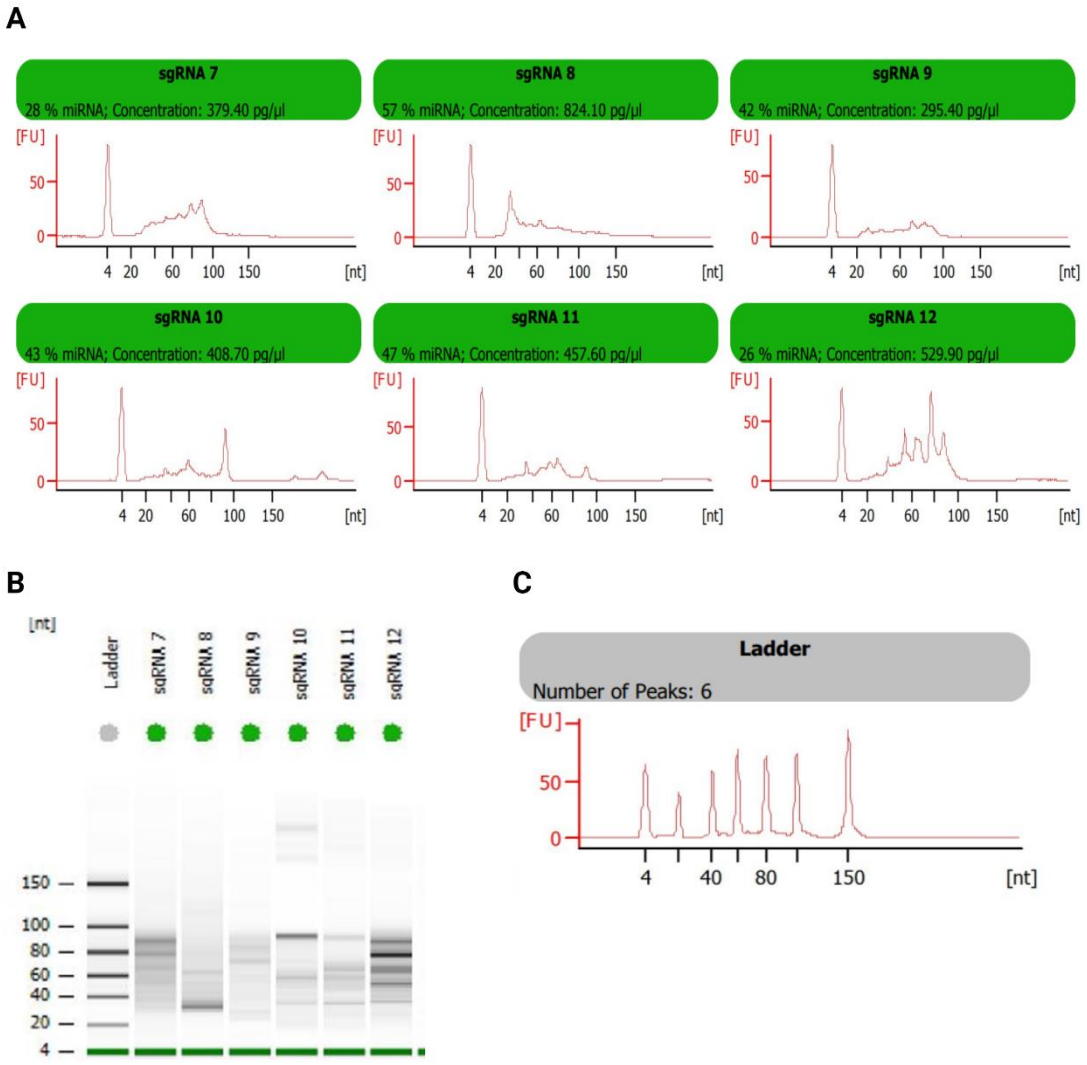


Figure 3-10. BioAnalyzer check of RNA integrity showed that sgRNA10 was of the best relative quality, with no degradation. (A) Electrophoretogram traces of all samples show several peaks at different sizes, while sgRNA10 resulted in a peak at the expected ~90 bp. (B) The samples were run against the manufacturer provided ladder with approximate sizes shown on the left, sgRNA10 resulted in the most distinct band at ~90 bp. (C) Shows the peaks expected corresponding to the ladder.



Figure 3-11. The selected target site is located in exon 18 of the *Hdac4* gene. Exon 18 sequence is highlighted in blue with target sequence indicated in red box. Green box indicates the PAM sequence. Image taken from Benchling.com

3.5.3 Chosen guide RNA site is able to drive cleavage

To test the ability of the guide RNA to drive cleavage, it was tested *in vitro*. A ~750 bp fragment was generated from genomic DNA that contains the potential target site. Figure 3-12, panel A shows the location of the target site in exon 18 of *Hdac4*. The PCR fragment was incubated with Cas9 protein and the guide RNA at 37°C. The protein was then digested with proteinase k and the resulting reaction run on a 2% agarose gel. Figure 3-12 shows that this guide RNA was able to drive Cas9 to cleave the DNA fragment at the predicted target site. This is evident in the presence of two smaller bands than the whole fragment. This experiment demonstrated the efficiency of the chosen guide RNA to drive Cas9-mediated cleavage at the genomic target site. Figure 3-13 is a schematic depiction of the process during the reaction. Since the reaction is carried out *in vitro*, the absence of any repair mechanism results in the appearance of two separate bands. These bands appeared at approximately ~200 and ~400 bp. Later investigations showed that this guide RNA is capable of driving a large deletion of ~221 bp. The bands are likely to be results of smaller DNA fragments that were present as a result. The wild-type copy can also be seen in Lane 1 (see Figure 3-12).

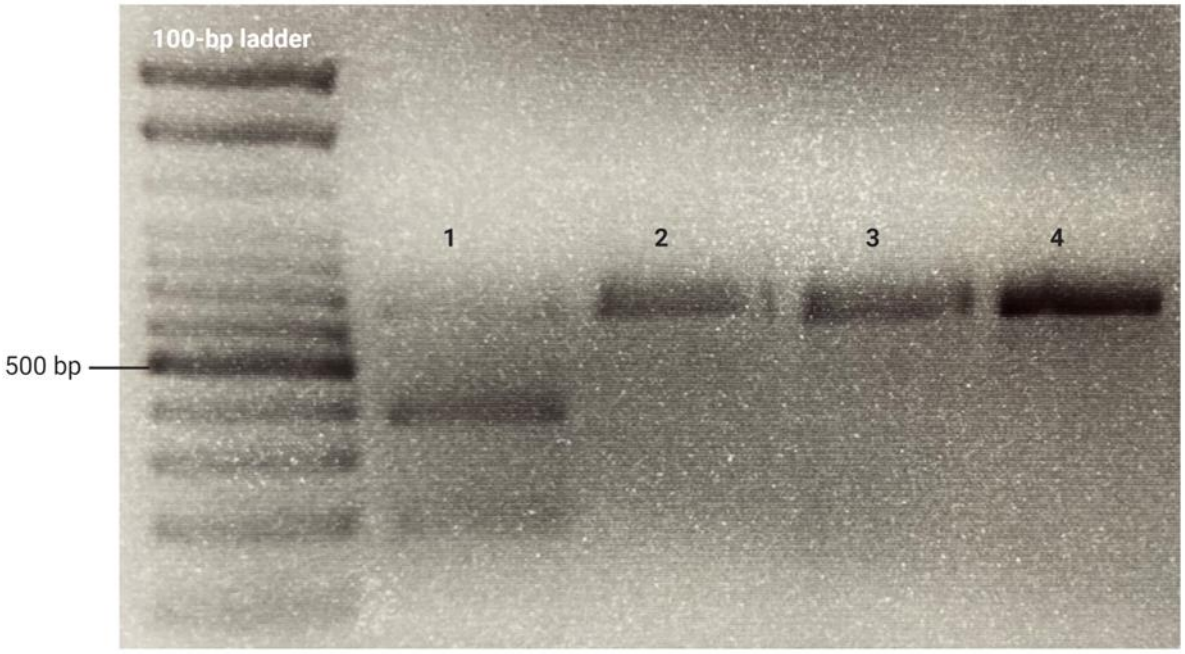


Figure 3-12. Selected gRNA 10 can drive Cas9-mediated cleavage at the genomic target site. Gel image shows result of the *in vitro* assay testing the efficacy of the guide RNA. Lane 1 shows the result of running the reaction including all components, with bands appearing at ~200 and ~400 bp. Lanes 2-4 are negative controls. 2: *in vitro* cleavage reaction without guide RNA. 3: *in vitro* cleavage reaction without Cas9 enzyme. 4: PCR template only.

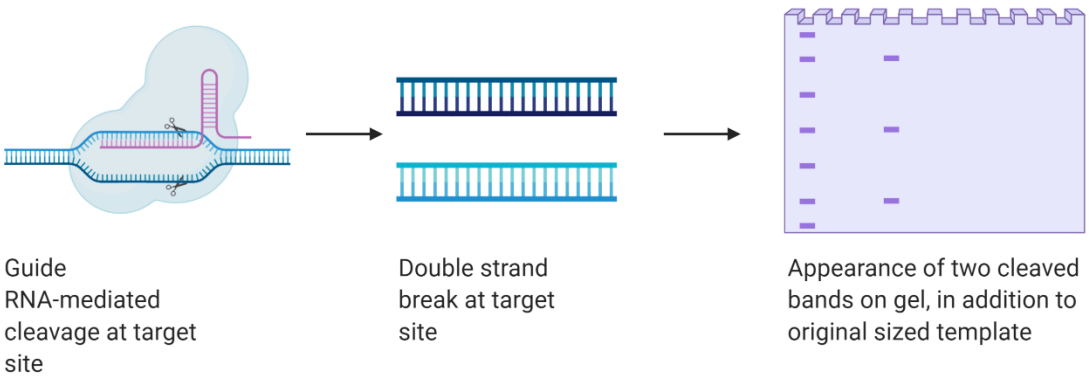


Figure 3-13. Cleavage by Cas9 enzyme at the target site in the genome leads to a double strand break. The two strands then appear as two bands on the agarose gel.

3.5.4 Selection of hygromyocin- resistant colonies

To perform CRISPR/Cas9-mediated knockout of *Hdac4*, a mammalian expression vector containing Cas9 mRNA, guide sequence and selectable markers was designed and purchased from Vector Builder. The vector contained a hygromycin B resistance gene to use as a selectable marker in cells after transfection. Prior to nucleofection, stem cells were treated with different concentrations of hygromycin B to discern the least concentration needed to kill all cells in 2 weeks. That was determined to be 100 μg/ml.

The vector was electroporated into cells and after recovery, they were propagated in selection media for 15 days. Plates were observed every day and on day 15, colonies that were at least one field-of-view apart were picked using cloning rings. These were expanded and their DNA extracted and PCR amplified using the primer pair "*Hdac4*_SG10_700_F" and "*Hdac4*_SG10_700_R", shown in Figure 3-14. Amplification from colony A6 was attempted twice and was not successful. On the whole, for all other colonies, the Cas9-mediated cleavage had not affected primer binding sites and PCR amplicons were obtained successfully.

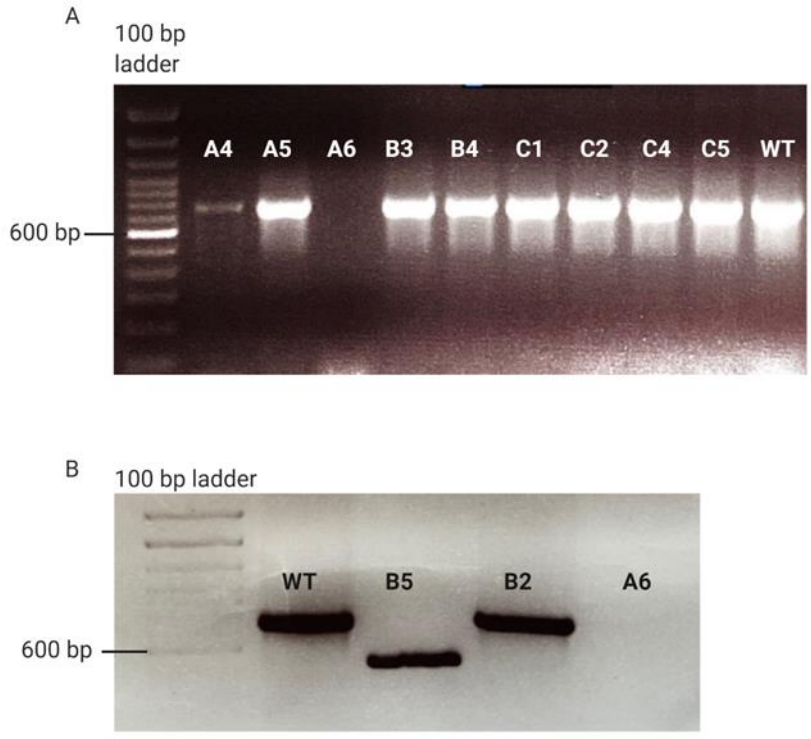


Figure 3-14. 700-800 bp fragments of genomic DNA were amplified for each colony. Attempts at amplifying DNA from colony A6 were not successful. (A) and (B) show gel images obtained from PCR amplification using the primer pair

"*Hdac4*_SG10_700_F" and "*Hdac4*_SG10_700_R". Lanes are labelled with the name of the colony. WT: wild-type.

Hdac4 sequence was compared in the DNA from the obtained colonies. Several clones showed a variety of mutations occurring near the target site. Of the colonies analysed with alignments shown in Figure 3-15, 5 samples showed deletions of different sizes, from a single base to a 221-base pair deletion in one of the colonies. Therefore, genome editing had successfully occurred for at least one allele for each of the colonies sequenced.

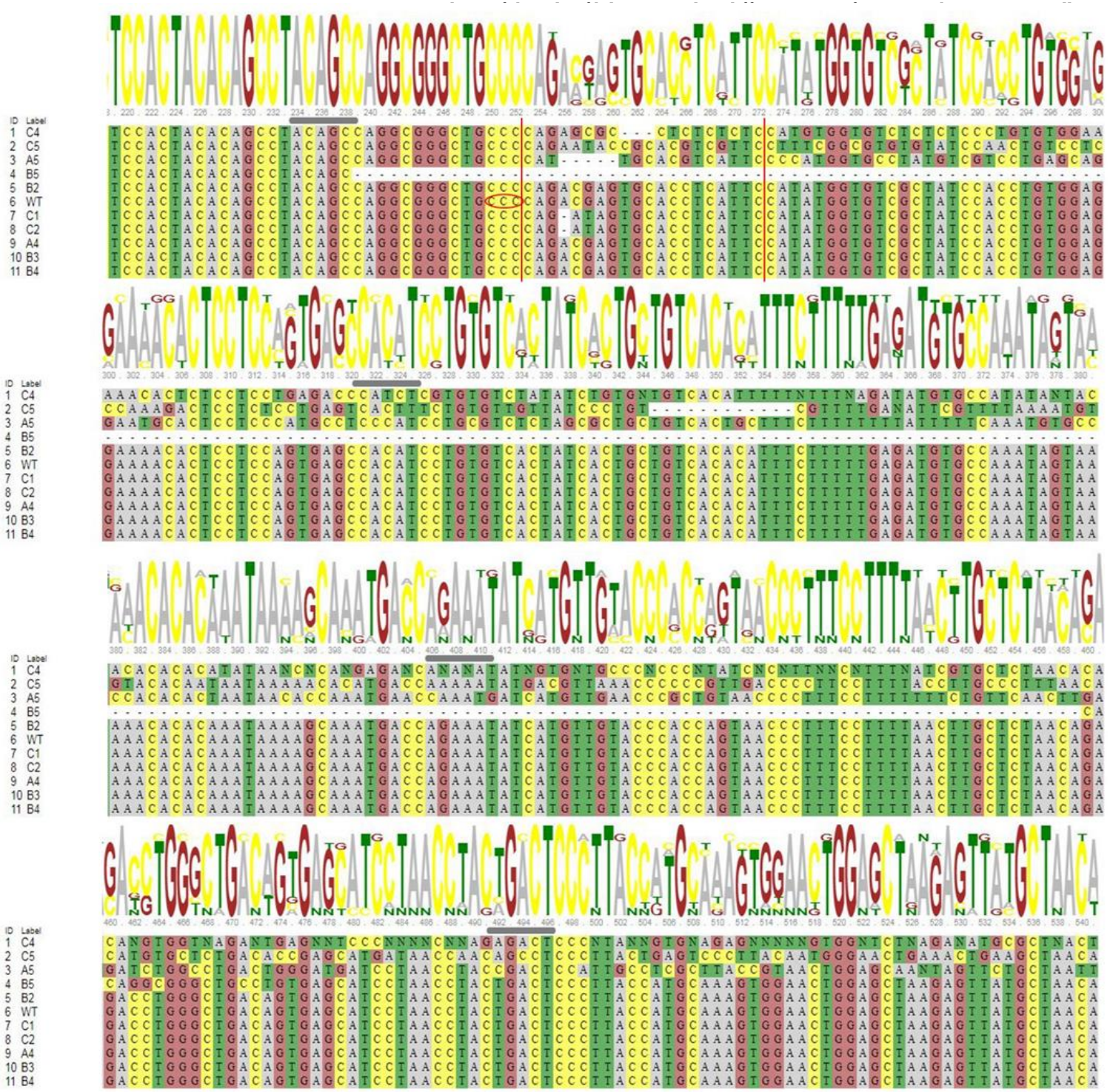


Figure 3-15. Sequence alignment from colonies showed deletions of different sizes. The two red lines show where the target site is and the red circle surrounds the PAM site (GGG on the complementary strand). The colony name is indicated on the left. WT: wild-type.

3.5.5 Survival of cells harbouring *Hdac4* mutations

The sequencing readouts showed the guide RNA could drive Cas9-mediated cleavage in or near the target site. From the alignments shown in Figure 3-15, it is evident that more than one type of mutation was randomly introduced. Cas9 cleavage can be repaired in cells by homology directed repair (HDR) or non-homologous end joining (NHEJ). Since no repair template was provided, the error-prone NHEJ pathway would have been used, introducing random mutations that varied in size.

To see if these mutations affected cell survival, the cells were expanded in small flasks and into large flasks when they reached confluence. Figure 3-16 shows photographs taken of 5 of the expanded colonies. They did not show a significant decrease in viability. However, a notable amount of cell debris was obvious in C1 and C2, with most in C1. Despite their apparent ability to grow, divide and reach confluence along the same timeline as other mutants and wild-types, cell-debris was often a common sight, suggesting apoptosis or cell death. Compared to wild-type mESCs, mutated mESCs showed less of the characteristic dome-shaped colonies. Raised, dome-shaped colonies were rarely seen as most cell colonies were flattened and appeared ‘epithelial-like’. Other colonies can be described as having intermediate phenotypes (see Figure 3-16).

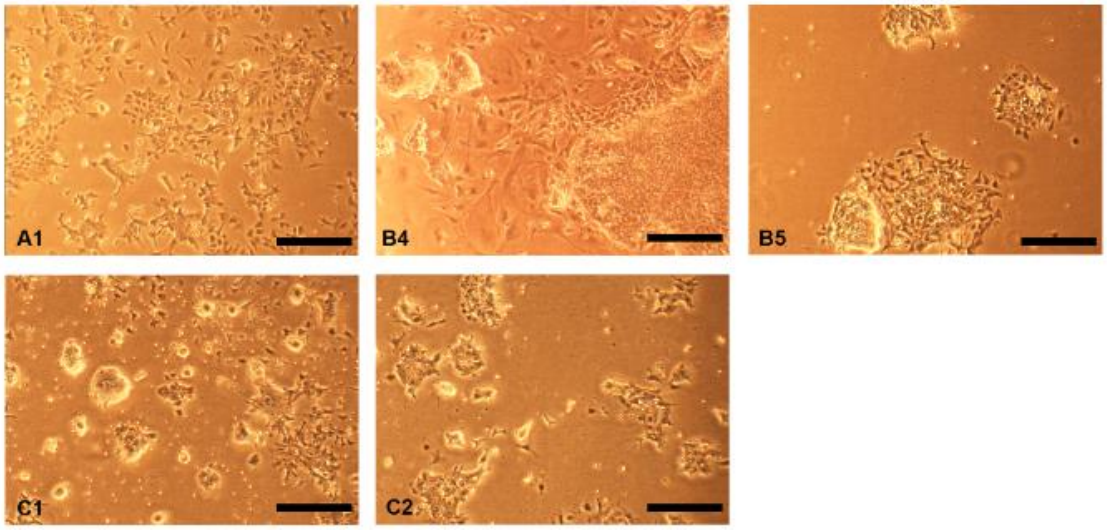


Figure 3-16. Knockout mESCs exhibit a decrease in raised, dome-like morphology. Images show mutant colonies upon expansion. Their morphologies were different to wild-types and excessive cell debris can be seen in C1. Scale bars = 300 µm.

3.5.6 Characterisation of the mutation in cell line B5

The colony B5 was chosen for further analysis and characterisation due to it containing the largest deletion of those investigated. From the alignment in Figure 3-15 it can be seen that there is a 221-base pair deletion in colony B5. Two more pairs of primers were designed, going further out from the target site in either direction, namely *Hdac4*_1000_F, *Hdac4*_1000_R, *Hdac4*_1600_F and *Hdac4*_1600_R. These products were run on a 1.5% agarose gel shown in Figure 3-17 and subject to Sanger sequencing, an illustration of the primers relative to the target site is shown in Figure 3-18. Two bands would be expected to show on the gel in the case of a heterozygous mutation. However, only one allele is apparent. The size of the second allele, therefore, warrants further analysis as an identical homozygous deletion of this size is unlikely. These products were also aligned with wild-type controls and those results are shown in Figure 3-19. Sanger sequencing of DNA extracted from cells and subsequent alignment showed a consistent deletion size of 221 base pairs with all primers used. The results therefore indicate that this deletion took place in at least one allele of the *Hdac4* gene.

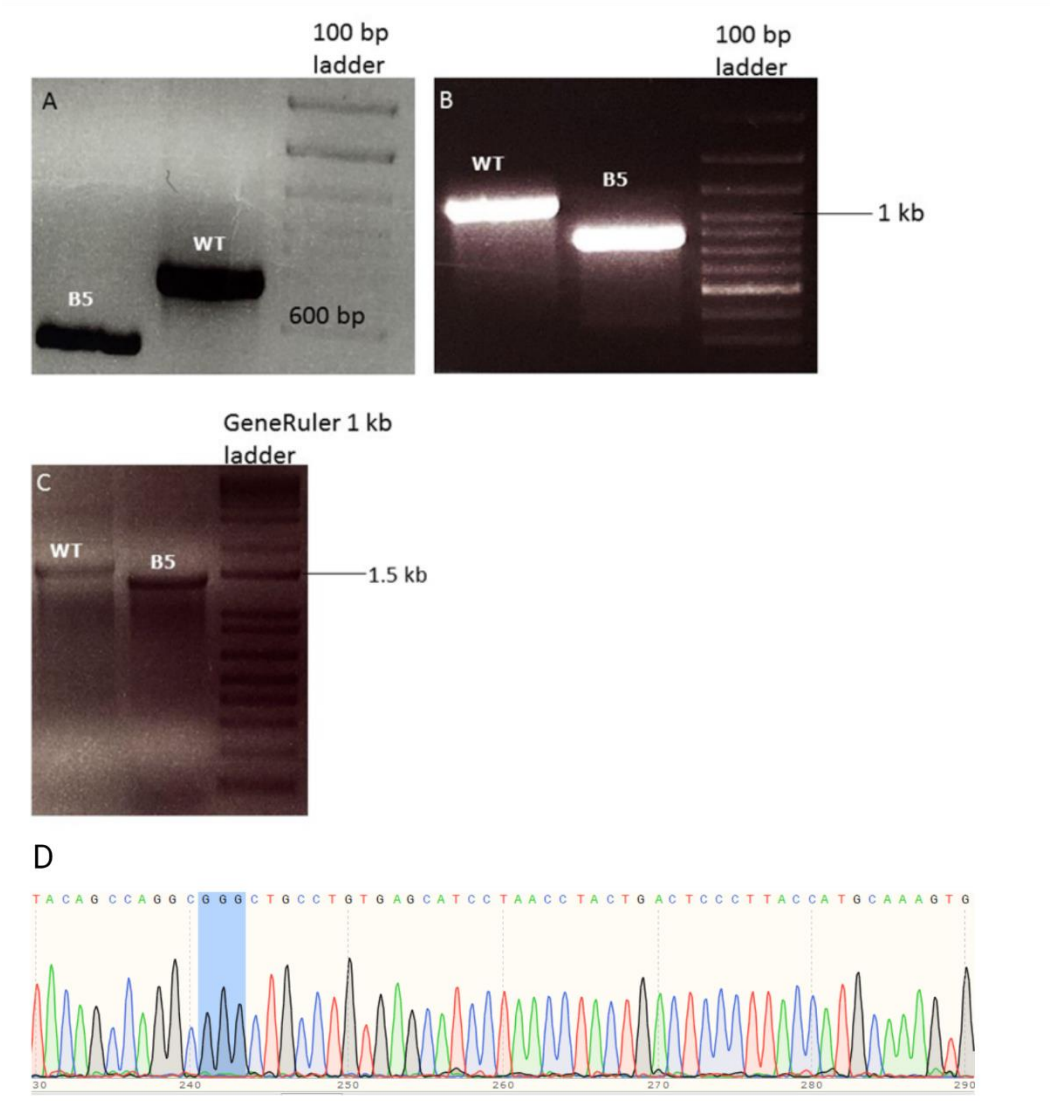


Figure 3-17. DNA extracted from colony B5 shows a ~220-bp deletion when compared to wild-type. Panel A shows products using primers *Hdac4*_SG10_700_F and *Hdac4*_SG10_700_R. Panels B shows products using primers *Hdac4*_1000_F and *Hdac4*_1000_R. Panel C show products obtained when using primers *Hdac4*_1000_F and *Hdac4*_1600_R. In all cases, a ~220-bp difference in size can be clearly seen. Panel D shows the sequence trace obtained when sequencing using *Hdac4*_SG10_700_F and *Hdac4*_SG10_700_R with the PAM sequence highlighted. In all gel images, the type of ladder used is indicated, as well as the size of the band closest to the product. WT: wild-type.

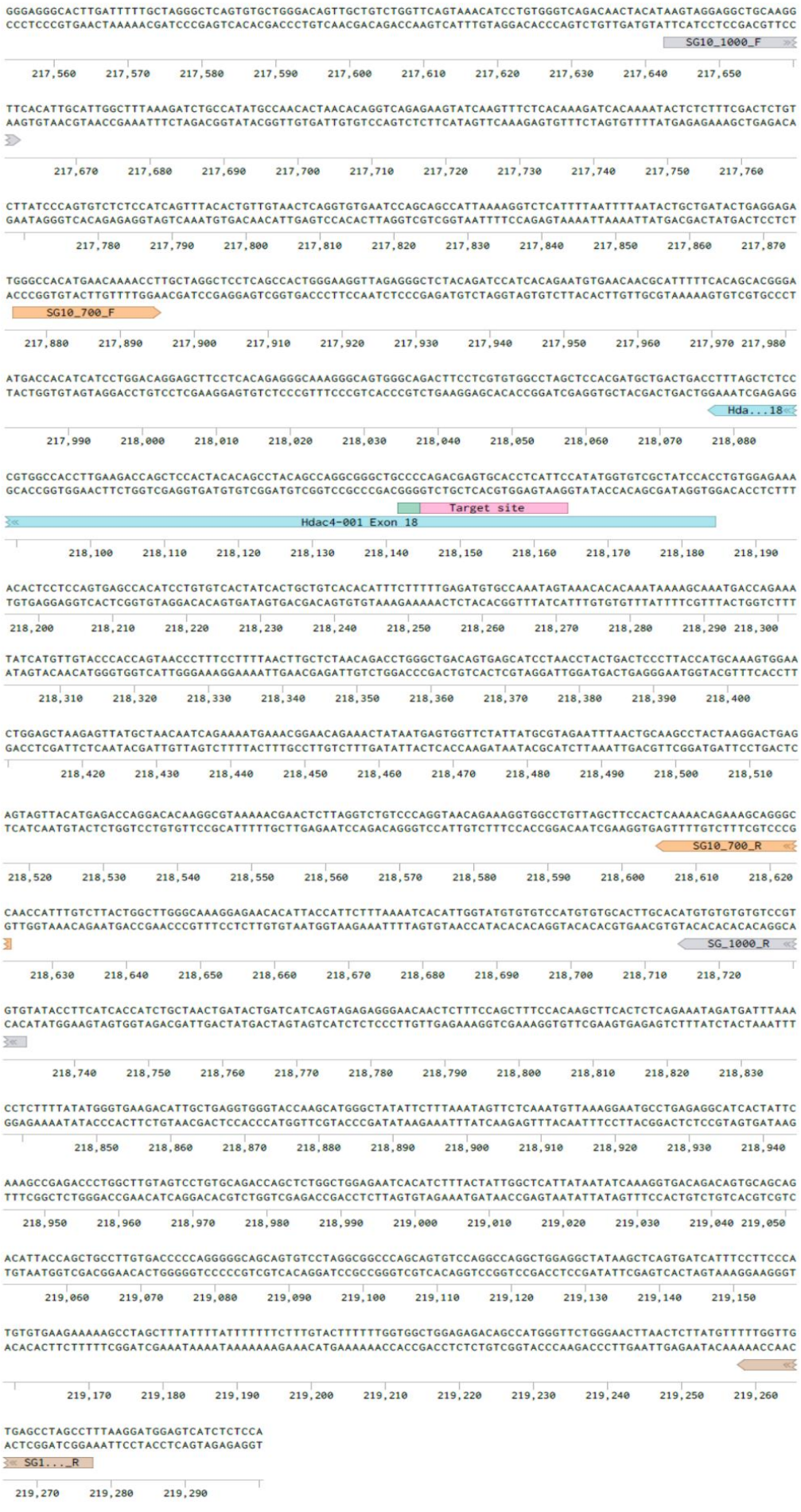

SG10_1000_F
SG10_700_F
Hda...18
Target site
Hdac4-001 Exon 18
SG10_700_R
SG_1000_R
SG1..._R

Figure 3-18 An illustration of the relative locations of the primer pairs used relative to the genomic target site and their orientations. *Hdac4* exons are located on the complement strand and exon 18 is marked with a sky blue arrow. The target site is marked with a pink rectangle and the PAM sequence is marked with a green box. Grey arrows indicate *Hdac4*_1000_F and *Hdac4*_1000_R. *Hdac4*_SG10_700_F and *Hdac4*_SG10_700_R are marked by orange arrows. Brown arrow indicates *Hdac4*_1600_R.


A
WT AACAACGCATTTTTCACAGCACGGGAATGACCACATCATCCTGGACAGGAGCTTCCTCAC
B5 AACAACGCATTTTTCACAGCACGGGAATGACCACATCATCCTGGACAGGAGCTTCCTCAC
WT AGAGGGCAAAGGGCAGTGGGCAGACTTCCTCGTGTGGCCTAGCTCCACGATGCTGACTGA
B5 AGAGGGCAAAGGGCAGTGGGCAGACTTCCTCGTGTGGCCTAGCTCCACGATGCTGACTGA
WT CCTTTAGCTCTCCCGTGGCCACCTTGAAGACCAGCTCCACTACACAGCCTACAGCCAGGC
B5 CCTTTAGCTCTCCCGTGGCCACCTTGAAGACCAGCTCCACTACACAGCCTAC--------
WT GGGCTGCCCCAGACGAGTGCACCTCATTCCATATGGTGTCGCTATCCACCTGTGGAGAAA
B5 --
WT ACACTCCTCCAGTGAGCCACATCCTGTGTCACTATCACTGCTGTCACACATTTCTTTTTG
B5 --
WT AGATGTGCCAAATAGTAAACACACAAATAAAAGCAAATGACCAGAAATATCATGTTGTAC
B5 --
WT CCACCAGTAACCCTTTCCTTTTAACTTGCTCTAACAGACCTGGGCTGACAGTGAGCATCC
B5 ---------------------------------AGCCAGGCGGGCTGCCTGTGAGCATCC
WT TAACCTACTGACTCCCTTACCATGCAAAGTGGAACTGGAGCTAAGAGTTATGCTAACAAT
B5 TAACCTACTGACTCCCTTACCATGCAAAGTGGAACTGGAGCTAAGAGTTATGCTAACAAT
WT CAGAAAATGAAACGGAACAGAAACTATAATGAGTGGTTCTATTATGCGTAGAATTTAACT
B5 CAGAAAATGAAACGGAACAGAAACTATAATGAGTGGTTCTATTATGCGTAGAATTTAACT
B
WT_F GGGAATGACCACATCATCCTGGACAGGAGCTTCCTCACAGAGGGCAAAGGGCAGTGGGCA
B5_F GGGAATGACCACATCATCCTGGACAGGAGCTTCCTCACAGAGGGCAAAGGGCAGTGGGCA
WT_F GACTTCCTCGTGTGGCCTAGCTCCACGATGCTGACTGACCTTTAGCTCTCCCGTGGCCAC
B5_F GACTTCCTCGTGTGGCCTAGCTCCACGATGCTGACTGACCTTTAGCTCTCCCGTGGCCAC
WT_F CTTGAAGACCAGCTCCACTACACAGCCTACAGCCAGGCGGGCTGCCCCAGACGAGTGCAC
B5_F CTTGAAGACCAGCTCCACTACACAGCCTACAGCCAGGCGGGCTGCCTGTGAGCATCCTAA
WT_F CTCATTCCATATGGTGTCGCTATCCACCTGTGGAGAAAACACTCCTCCAGTGAGCCACAT
B5_F CCTACT--
WT_F CCTGTGTCACTATCACTGCTGTCACACATTTCTTTTTGAGATGTGCCAAATAGTAAACAC
B5_F --
WT_F ACAAATAAAAGCAAATGACCAGAAATATCATGTTGTACCCACCAGTAACCCTTTCCTTTT
B5_F --
WT_F AACTTGCTCTAACAGACCTGGGCTGACAGTGAGCATCCTAACCTACTGACTCCCTTACCA
B5_F --GACTCCCTTACCA
WT_F TGCAAAGTGGAACTGGAGCTAAGAGTTATGCTAACAATCAGAAAATGAAACGGAACAGAA
B5_F TGCAAAGTGGAACTGGAGCTAAGAGTTATGCTAACAATCAGAAAATGAAACGGAACAGAA
WT_F ACTATAATGAGTGGTTCTATTATGCGTAGAATTTAACTGCAAGCCTACTAAAGGACTGAG
B5_F ACTATAATGAGTGGTTCTATTATGCGTAGAATTTAACTGCAAGCCTACTA-AGGACTGAG
WT_F AGTAGTTACATGAGACCAGGACACAAGGCGTAAAAACGAACTCTTAGGTCTGTCCCAGT-
B5_F AGTAGTTACATGAGACCAGGACACAAGGCGTAAAAACGAACTCTTAGGTCTGTCCCAGGT
C
WT_F TGGGCAGACTTCCTCGTGTGGCCTAGCTCCACGATGCTGACTGACCTTTAGCTCTCCCGT
B5_F TGGGCAGACTTCCTCGTGTGGCCTAGCTCCACGATGCTGACTGACCTTTAGCTCTCCCGT
WT_F GGCCACCTTGAAGACCAGCTCCACTACACAGCCTACAGCCAGGCGGGCTGCCCCAGACGA
B5_F GGCCACCTTGAAGACCAGCTCCACTACACAGCCTACAGCCAGGCGGGCTGCCTGTGAGCA
WT_F GTGCACCTCATTCCATATGGTGTCGCTATCCACCTGTGGAGAAAACACTCCTCCAGTGAG
B5_F TCCTAACC--
WT_F CCACATCCTGTGTCACTATCACTGCTGTCACACATTTCTTTTTGAGATGTGCCAAATAGT
B5_F --
WT_F AAACACACAAATAAAAGCAAATGACCAGAAATATCATGTTGTACCCACCAGTAACCCTTT
B5_F --
WT_F CCTTTTAACTTGCTCTAACAGACCTGGGCTGACAGTGAGCATCCTAACCTACTGACTCCC
B5_F --TACTGACTCCC
WT_F TTACCATGCAAAGTGGAACTGGAGCTAAGAGTTATGCTAACAATCAGAAAATGAAACGGA
B5_F TTACCATGCAAAGTGGAACTGGAGCTAAGAGTTATGCTAACAATCAGAAAATGAAACGGA
WT_F ACAGAAACTATAATGAGTGGTTCTATTATGCGTAGAATTTAACTGCAAGCCTACTAAGGA
B5_F ACAGAAACTATAATGAGTGGTTCTATTATGCGTAGAATTTAACTGCAAGCCTACTAAGGA

Figure 3-19. Sequence alignments of DNA extracted from wild-type and mutant cells using different primers pairs consistently shows 221-bp deletion. Panel A shows products using primer *Hdac4*_SG10_700_F for sequencing. Panels B shows products using primer *Hdac4*_1000_F for sequencing. Panel C shows products using primer *Hdac4*_1600_F for sequencing. In all 3 alignments, a 221-bp deletion can be seen.

Upon closer inspection, it was found that the deleted segment was located in intronic DNA. The sequence below is the deleted portion as deduced from sequence alignment with wild-type; intronic sequence is in lowercase and exonic sequence is in uppercase letters:

ggttaggatgctcactgtcagcccaggtctgttagagcaagttaaaaggaaagggttactggtgggtacaacatgatatttc
tggtcatttgcttttatttgtgtgtttactatttggcacatctcaaaaagaaatgtgtgacagcagtgatagtgacacaggatgtg
gctcactggaggagtgttttctccacagGTGGATAGCGACACCATATGGAATG

25 bases were deleted from exon 18. The deletion led to an out of frame mutation resulting in a smaller protein as predicted by SnapGene software. It is in the HDAC catalytic domain. The 25 nucleotides removed from the exon lead to a frameshift mutation and the introduction of a premature stop codon (TAG) in the sequence 33 bases after the deletion.

The original gene size is 8100 bp, produces a predicted protein of 1076 amino acids with a molecular weight of ~130 kDa. Prior to translation, introns are spliced out. Panel A of Figure 3-20 shows normal splicing and translation around exon 18, the location of the target site, which translates to amino acids in the catalytic domain of Hdac4. The target site in exon 18 was located at a splice site and the resultant protein would likely have been truncated (panel B of Figure 3-20). The predicted protein is 858 amino acids with a molecular weight of 94.8 kDa. Figure 3-20 below shows a diagram of the mouse Hdac4 protein, indicating the predicted mutation site and the possible consequent truncated protein.

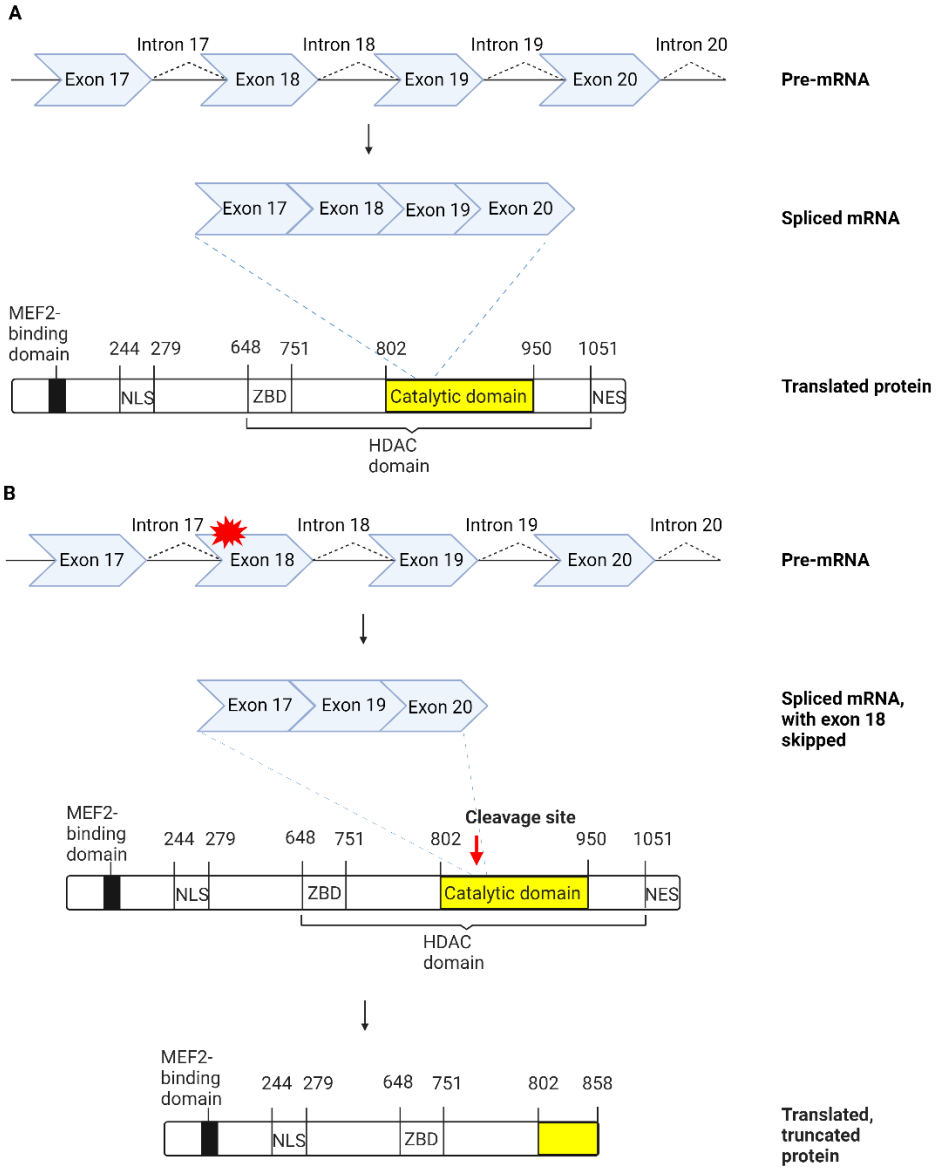


Figure 3-20. Cleavage at the target site is predicted to result in a truncated protein. (A) Shows the structure of pre-mRNA including introns. These are spliced out and exons are joined to produce mRNA which is then translated into the protein. Exon 18 translates to amino acids within Hdac4's catalytic domain. Other protein domains are shown. (B) Depicts the potential consequence of introducing a premature stop codon in exon 18 (red spark). Being near a splite site, the translated protein would be expected to be tuncated. The cleavage site is shown relevant to the protein domains. Numbers indicate amino acid number. NLS, nuclear localisation site ; ZBD, zinc-binding domain; NES, nuclear export signal. This schematic is intended to be illustrative and is not to-scale. Created with Biorender.com.

3.5.7 Western Blot to confirm the presence of a truncated protein.

A Western blot was performed to confirm that the *Hdac4* mutation at the gene level had any consequences on the protein product, Figure 3-21 (A). 50 μg of protein lysate were loaded onto a SDS-PAGE gel and transferred to a PVC membrane which was then probed with an anti-HDAC4 antibody. Attempts to optimise the protocol did not succeed and the image below is the clearest result obtained. In the wild-type lane, a faint band near the 130 kDa mark was seen, indicated with a white oval in Figure 3-21 A. Expected HDAC4 size is 140 kDa. It cannot be concluded with absolute certainty that this is HDAC4. In the B5 lane, a faint smaller band near the 100 kDa was seen, however the lane contained several non-specific bands as well. GAPDH was used as a loading control. The result from the Western therefore is not conclusive.

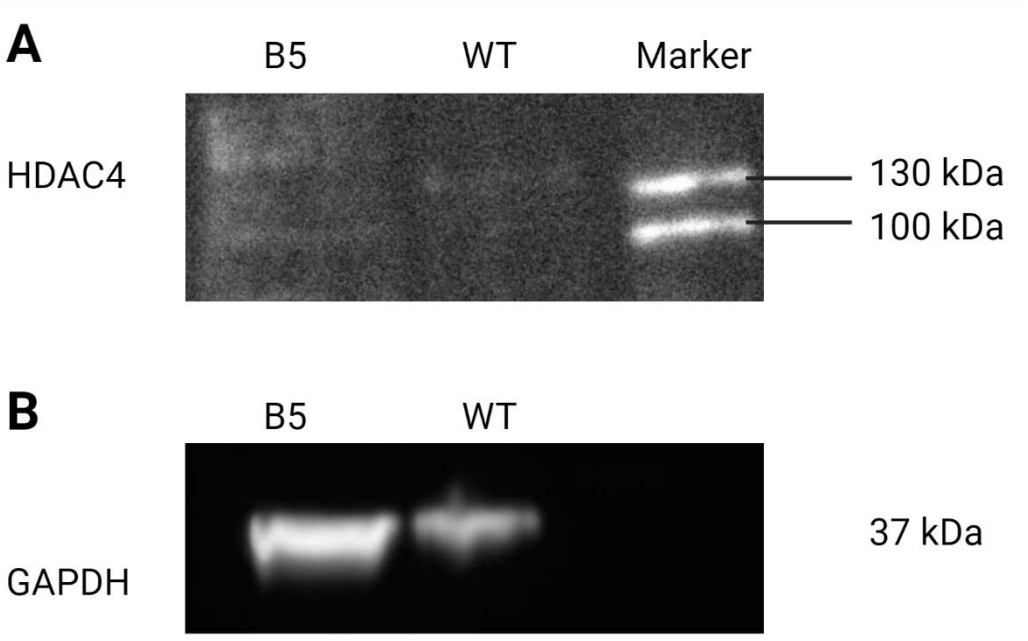


Figure 3-21 . Western Blot result using anti-HDAC4 antibody was not conclusive. Panel (A) shows results from running whole cell lysates from B5 undifferentiated cells as well as wild-type undifferentiated cells and probing the membrane using an anti-HDAC4 antibody. Faint bands can be seen in the B5 lane but not in the wild-type. (B) shows results obtained from probing the membrane using an anti-GAPDH antibody as control.

3.5.8 Differentiation of the B5 mutant line.

To investigate if *Hdac4* played a role in cardiogenesis, B5 mutant cells were differentiated as previously. After expansion of the colony, cells were cultured in hanging drops for 3 days followed by plating. In their undifferentiated state, there was a decrease in the number of dome-shaped, raised colonies usually seen shown in Figure 3-16. Flatter colonies were seen and suggested that the cells may be differentiating. Interestingly, upon hanging drop differentiation, the cells appeared to resemble TSA-treated cells in their morphology, as indicated by visual inspection. Cells appeared thinner, flatter and more elongated with a less dense centre. Photographs of differentiating B5 cells were taken and are shown in Figure 3-22.

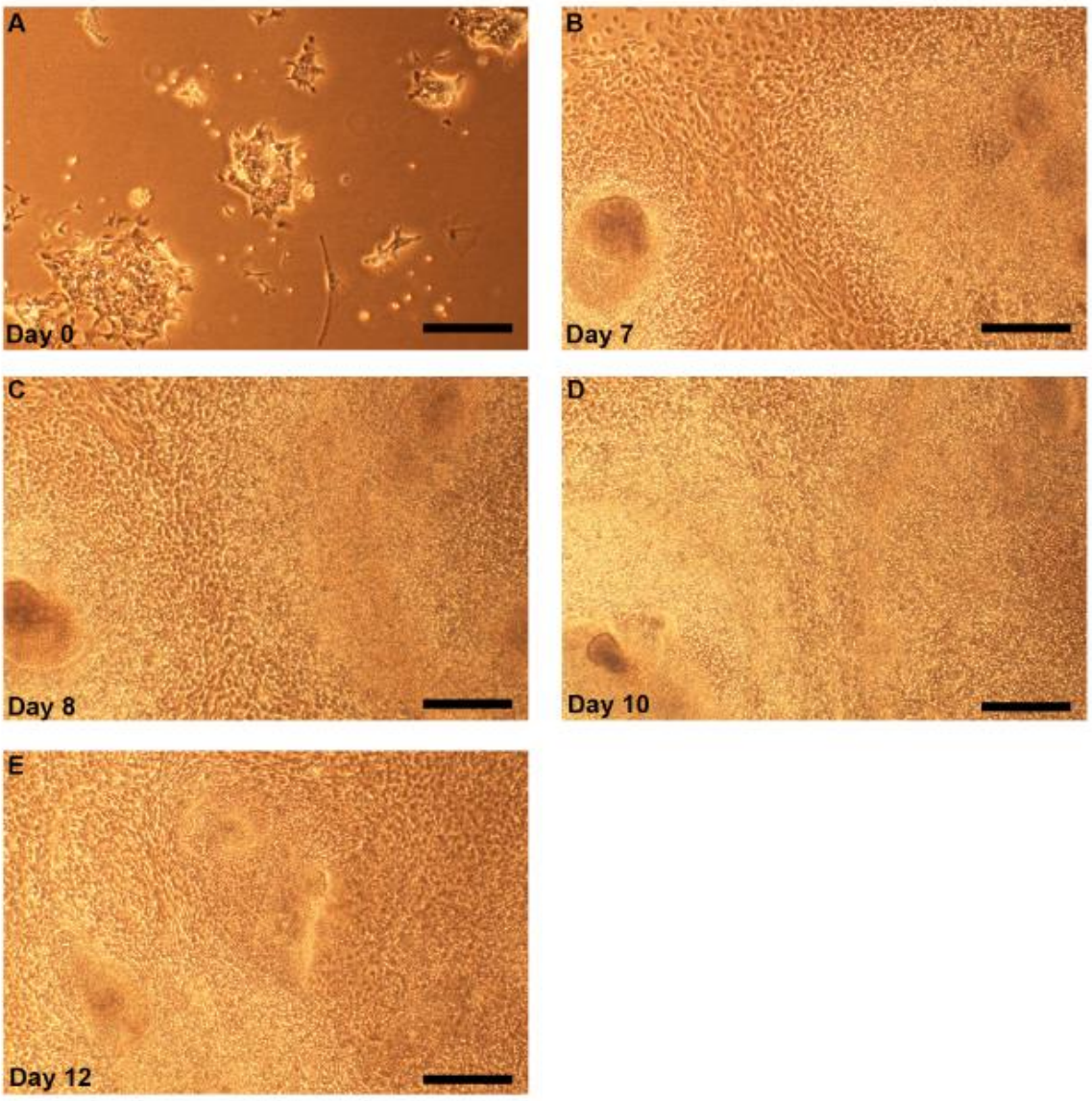


Figure 3-22. Colony B5 mESCs are able to differentiate via EBs. The cells were taken through the same differentiation procedure as previously described and EBs were monitored and photographed at the days indicated on the bottom left of each panel. Scale bars = 300 µm. Images taken at 100X magnification.

Beating foci were smaller than wild-types and shared a similar beating pattern to those treated with TSA. Day of beating onset was noted and plotted for all experimental replicates (n=32), shown in Figure 3-23. Comparison to beating onset in wild-types did not show a significant difference, though beating occurred later on average (day 12.13 compared to day 11.11 in wild-types) as indicated by an unpaired t-test. Beating time-lapse images of *Hdac4* KOs were taken and are shown in Movies 7-9.

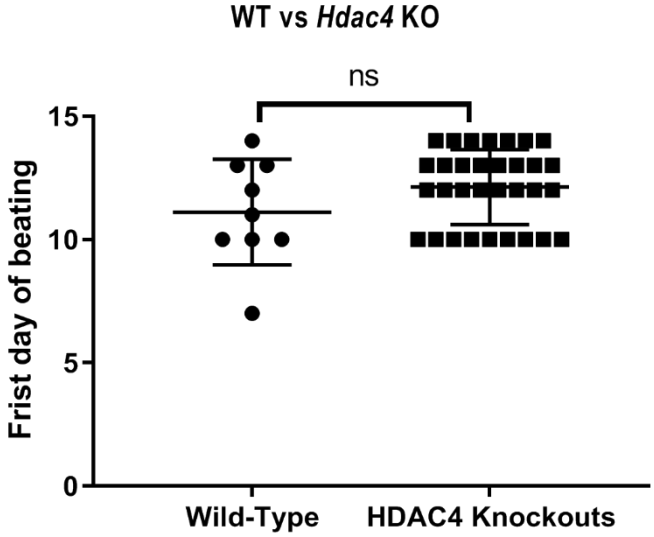


Figure 3-23. *Hdac4* knockout did not significantly affect beating onset. The graph shows a scatter plot of earliest beating detected for wild-type controls and B5 colony knockout. The horizontal line shows the mean. N= 32 for each group.

3.5.9 Beating analysis and comparison of differentiated wild-types, TSA-treated and *Hdac4* knockout cells

To better quantify the beating seen in the cardiomyocytes generated. A Macro named "MYOCYTER" written in ImageJ macro language was used (Grune *et al.,* 2019) The macro is able to detect moving regions in videos containing beating cells. The analysis produces a host of parameters as a means to quantify beating. For this project, 'speed' and 'amplitude' were recorded. 3 videos showing beating from each

category were analysed using the macro code. Screenshots from the program indicating the recognised beating regions are shown in Figure 3-24 and the results were plotted as seen in Figure 3-25. The amplitude is a measure of difference in pixel intensity between every frame and an assigned reference image. The macro is able to automatically assign a reference image, which was utilised in this analysis. The reference image represents the resting phase, thus a higher amplitude represents a larger deviation from the resting phase. Beating cardiomyocytes derived from wild-type mESCs showed the highest beating amplitude as is evident from the graph. Compared to a visual inspection of the beating cells, the macro was able to robustly recognise beating regions. However, it counted a far lower number of beats for wild-type cells (mean= 2.67±1.2, n=9) than for TSA-treated (mean= 69.33±30.27, n=3) or knockouts (mean= 55.57±14.10, n=7) groups. This could be due to the frame rate that the images were acquired as the macro was used long after image acquisition and could not be modified to precisely analyse these cells. There was also a large variability in the data for the wild-type cells. Despite that, it is able to provide insight into the difference these treatments had on beating.

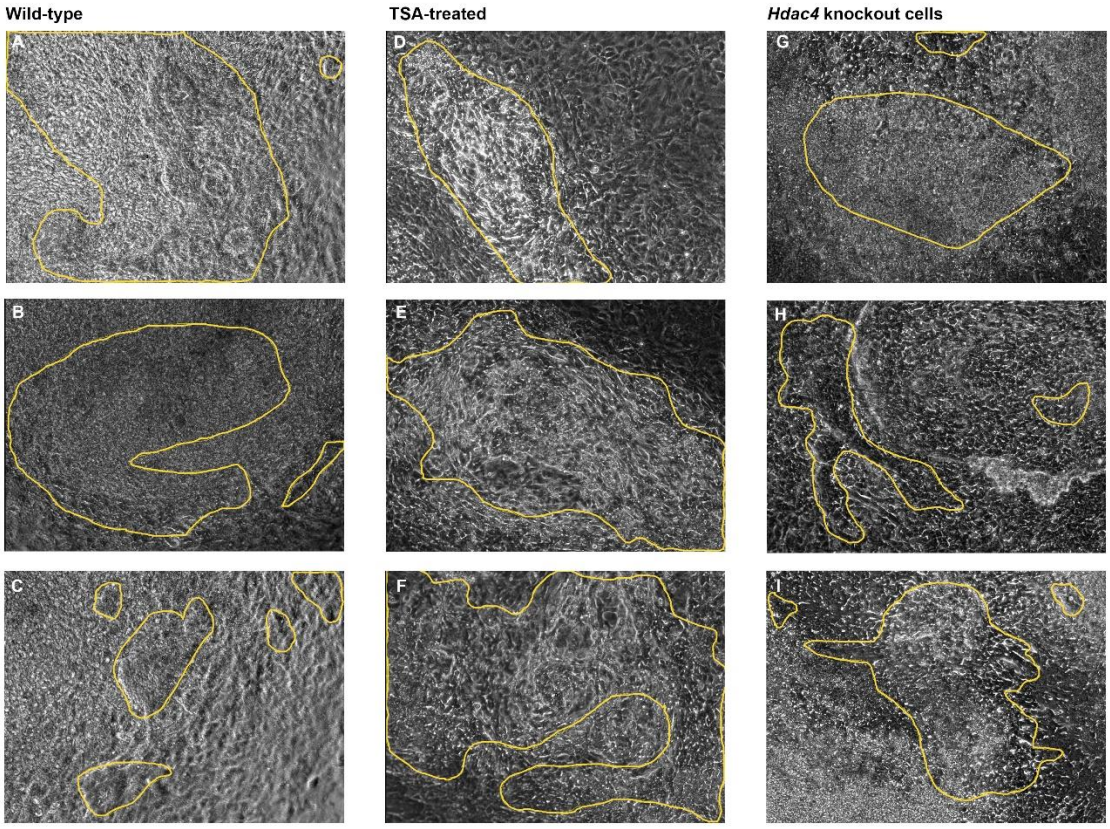


Figure 3-24. Screenshots from MYOCYTER output show what the programme recognises as beating regions. This was accurate when visually inspected.

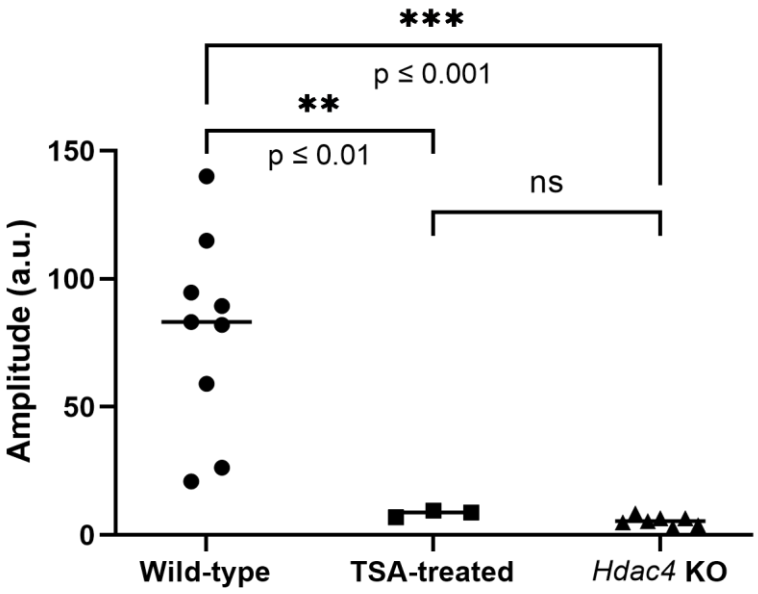


Figure 3-25. Wild-type beating cells were compared to TSA-treated and knockouts using MYOCYTER. Wild-type (n=9), TSA (n=3) and knockouts (n=7). One-way ANOVA with Tukey's multiple comparisons test was used to assess statistical significance, an asterisk indicates significance, p<0.05 was used as a threshold, p-values are indicated for each comparison. Ns, not significant.

Overall, results obtained in this chapter demonstrated the suitability of utilising mESCs as models of cardiac differentiation, the effects of TSA-treatment on cell morphology and beating and showed evidence of the occurrence of CRISPR/Cas9-mediated genetic editing of *Hdac4*. DNA evidence from the knockout experiment suggested a 221-bp deletion in at least one allele of *Hdac4*. However, the Western blot data was not sufficient to make solid conclusions about what happened at the protein level.

3.6 Discussion

The preliminary study reported in this chapter served as a primary step to inform the decision of model selection for further studies. It was conducted to establish a baseline for the two cell lines' differentiation abilities.

3.6.1 Comparing P19CL6 cells to embryonic stem cells as *in vitro* models of cardiac differentiation

3.6.1.1 P19CL6 embryonic carcinoma cells

As previously mentioned, P19CL6 is a subclone of the P19 cell line that is capable of differentiating into mesoderm lineages with more efficiency than original P19 cell lines. This subline, therefore, is not committed to a mesodermal lineage but is a step closer to differentiated cardiomyocytes that the original P19 line (Habara-Ohkubo, 1996).

The P19CL6 cell line has also been instrumental in finding signalling pathways that function in cardiac development, such as FGF and BMP signalling. For example, a sub-line expressing noggin, a BMP antagonist, was made and the cells did not differentiate into cardiomyocytes, consequently demonstrating that BMP is necessary for cardiac differentiation (Sharma *et al.*, 2017). They were also used to demonstrate that oxytocin is able to induce cardiac differentiation and that DMSO likely functions through the oxytocin/oxytocin receptor pathway (Paquin *et al.*, 2002; Fathi *et al.*, 2009).

Interestingly, P19CL6 cells were found to function *in vivo* as well. P19CL6-derived cardiomyocytes were transplanted into the retroperitoneal area, on the omentum and around the femoral artery of mice. The cells adhered to the surfaces and grew to form masses in the transplanted area. These masses then began to pulsate albeit irregularly and slower than the host heart (Ohtsu *et al.*, 2005). Taken together, these properties show the P19CL6 cell line's suitability to be used as a model system to investigate the effect certain genetic manipulations can have on cardiomyocyte differentiation.

However, in this study, the prime factors used to assess differentiation were beating frequency and beating onset as readouts of cardiomyocyte formation. The P19CL6 cell line displayed various inconsistencies, even from one experiment to another. Despite the ease of the differentiation procedure, beating was seen in 54% of attempts made. Beating foci were also small and hard to find using a standard inverted microscope and the naked eye.

Study-to-study variations were also present in the literature. Beating was reported to have started as early as day 5.5 (Anisimov *et al.*, 2002) or days 7-8 (Grépin *et al.*, 1995). A study by Peng et al demonstrated that the earliest beating occurred at day

10 (Peng *et al.*, 2002). Studies where P19 cells overexpressed *Tbx5* demonstrated its ability to induce beating earlier, at day 7 instead of day 9 in a study conducted by Hiroi et al and at 12 instead of day 15 in a study by Fijnvandraat et al (Hiroi *et al.*, 2001; Fijnvandraat *et al.*, 2003). Even during the course of this project, beating onset, as a definite readout of differentiation, displayed a lack of consistency that made data reproducibility challenging.

P19 cells provide clear advantages justifying their use in a study of this type. Their ability to differentiate into cardiomyocytes has been instrumental in investigating the role of various factors in this process, including *Nkx2.5*, *Tbx5* and *Nppa* (reviewed in (van der Heyden and Defize, 2003)). While they were an invaluable resource in the field, caveats must be taken into account when interpreting results. P19 is a cancer cell line and while it mirrors some aspects of development, it is not always the best model. Moreover, P19-differentiated cardiomyocytes were reported to be contaminated with cells of endodermal origin, since DMSO is also shown to induce endoderm differentiation (Smith *et al.*, 1987; Schultheiss, Xydas and Lassar, 1995).

3.6.1.2 Mouse embryonic stem cells

mESCs on the other hand displayed much more robust differentiation. Upon differentiation, cells consistently formed beating cardiomyocytes. Moreover, the experimental procedures involved are not much more challenging than P19 DMSO-mediated differentiation and the hanging drop procedure was almost identical. Therefore their use was more suitable for the purposes of this study. To gain a better understanding of developmental events involved in embryonic heart formation, the use of embryonic stem cells would recapitulate these events better than an embryonic carcinoma cell line.

Studies investigating stem cell-derived cells often report that terminally differentiated cells displayed features typical of specialised cells: mESC-derived cardiomyocytes shared properties with atrial, ventricular, 125 urkinje- and pacemaker-like . mESC derived neuronal cells also displayed inhibitory and excitatory synapses. Other features displayed by *in vitro* differentiation of mESCs include cell type-specific ion channels and membrane receptors (Wobus, Wallukat and Hescheler, 1991; Strübing *et al.*, 1995; Drab *et al.*, 1997; Wobus *et al.*, 1997;

Guan, Rohwedel and Wobus, 1999). Consequently, a wide catalogue of protocols is available for differentiating mESCs became available.

Both cell lines showed the ability to form Ebs. Ebs are a valuable model of *in vitro* differentiation. They were initially derived from embryonic carcinoma cell lines before ES cell lines became available. They feature as a first step in a wide plethora of differentiation protocols. Ebs are especially insightful because they closely model early events of embryonic development. Cells in Ebs mimic interactions that occur in embryos (Spangler *et al.*, 2018).

There are several methods to form Ebs. The most common one is to culture cells in non-adherent conditions in bacterial petri dishes. They can be cultured in suspension in liquid media or with methylceullolse supplements. The clear disadvantage of this method is the generation of Ebs of varying shapes and sizes. This can have a significant effect on differentiation potential as evidenced by the fact that small Ebs cultured with activin will form endoderm while larger Ebs tend to form mesoderm (Livigni *et al.*, 2009). The method used to form Ebs was the hanging drop method, chosen for the control of and homogeneity in EB sizes. The size can be varied by varying the number of cells per drop. A third method is to culture cells in suspension in non-adherent micro-well plates, also allowing control of EB size (Hwang *et al.*, 2009; Spelke *et al.*, 2011).

Interestingly, Ebs demonstrate non-uniform gene expression indicating axis formation and a degree of self-organisation. Ebs from mESCs demonstrate asymmetric Wnt pathway activation. Nusse et al showed that there was a localised source of Wnt signals that led to anterior-posterior patterning similar to that seen in a mouse embryo (Berge *et al.*, 2008). Germ layer formation, axis formation and elongation are other examples of collective behaviour demonstrated by cells in Ebs (Brink *et al.*, 2014).

3.6.1.3 Cellular model system for further analysis

Taken together, while the embryonic carcinoma cell line P19CL6 did show a propensity to form Ebs and beating cardiomyocytes, its malignancy and inefficiency were reasons to not favour using them for differentiation studies. Lab-to-lab and even experiment-to-experiment variations greatly reduced reproducibility and would cast doubt on future transcriptomic data. Embryonic stem cells on the other hand, are

karyotypically normal and have been shown in the literature to be able to closely mimic developing embryos in self-organisation and gene expression.

3.6.1.4 Investigating the role of histone deacetylation in cardiomyocyte differentiation by gene editing of *Hdac4* and and chemical inhibition

In the second part of this chapter, an attempt was made to elucidate the role of histone deacetylation in general and the role of *Hdac4* in particular in cardiac differentiation of stem cells. The study conducted in this chapter was to inform and aid in hypothesis generation for subsequent RNA-Sequencing analysis. Baseline HDAC4 expression in differentiating mESCs was first established, followed by TSA treatment of differentiating mESCs and finally CRISPR/Cas9-mediated knockout of *Hdac4* and assessing the consequences of that on cardiac differentiation.

3.6.1.5 Chemical inhibition of Class I and II histone deacetylases

Trichostatin A is a Class I and II inhibitor that has been gaining traction for its potential use as a cancer therapeutic (Kim and Bae, 2011). In this instance, treatment with TSA showed a level of toxicity evident in cell death and detachment from the plate. TSA also slowed down growth and prevented cells from forming dense colonies.

TSA treatments of stem cells have been reported in the literature. A study by Chen et al reported treating Ebs with 50 nM TSA from day 8 to 15. Treatment increased cell resistance to oxidative stress and led to bigger EB diameters in suspension in addition to increasing upregulation of *Gata4*, *Mef2c*, *Nkx2.5*, cardiac actin, and *α-SMA* mRNA and protein levels. The authors propose that both TSA and sodium butyrate treatments led to a significant increase in cardiac lineage commitments (Chen *et al.*, 2011). An epigenetic study conducted by Karantzali et al reported findings that agreed with those of Chen et al. TSA treatment for 6-12 hours induced global transcriptomic changes in addition to morphological changes indicative of differentiation. The authors described a decrease in expression of pluripotency-associated transcription factors. They also observed an increase in epigenetic marks associated with active genes such as histone H3 acetylation and K4 trimethylation and a decrease in repressive marks such as K27 trimethylation. They hypothesise that TSA aids in facilitating the epigenetic transition between the undifferentiated and differentiated states by facilitating the increase in activation marks (Karantzali *et al.*,

2008). It has also been reported that TSA induces apoptosis (Kijima *et al.*, 1993) which could be a possible explanation behind the cell death seen in the experiments reported in this thesis.

Kawamura et al described results that agreed with those obtained by Chen et al and Karantzali et al. They treated ES cells with 10 ng/ml TSA for 24 hours on day 7 post-differentiation. They report an increase in ES cell commitment towards cardiac lineage and state that it is due to an increase in GATA4 acetylation. TSA treatment increased the expression of GFP driven by an *Nkx2.5* promoter in addition to *Myh7*. Interestingly, they correlate their findings to *P300* expression levels and find that TSA treatment increases P300 protein expression, which in turn acetylates GATA4 (Kawamura *et al.*, 2005).

Furthermore, in adult animal models, HDAC inhibitors have been shown to play a positive role in various cardiac pathological models. For example, TSA was able to reverse cardiac hypertrophy due to pressure overload when administered for 2 weeks after pressure induction (Kee *et al.*, 2006). Moreover, treatment with another HDAC inhibitor suberoylanilide hydroxamic acid (SAHA) was effective in reducing infarct size in addition to enhancing cardiac function in a rabbit model of ischaemia-reperfusion injury (Xie *et al.*, 2014). Intriguingly, the role played by class Iia HDACs in cardiac hypertrophy is not reliant on their catalytic activity (Zhang *et al.*, 2002). Therefore it is thought that the effectiveness of HDAC inhibitors in ameliorating pathological cardiac modelling may be through their inhibition of Class I HDAC isoforms (Kate L Weeks and Avkiran, 2015). In the context of heart failure, treatment with another HDAC inhibitor valproic acid (VPA) treatment was shown to be associated with a reduced risk of myocardial infarctions in epileptic patients (Olesen *et al.*, 2011).

It has been reported that TSA treatment reduced embryonic stem cell differentiation. The authors treated differentiating mouse embryonic stem cells with 10 nM TSA for 6 days after placing cells in LIF- media. They state that TSA treatment blocked the initial wave of widespread histone deacetylation usually seen in ESCs differentiation. TSA-treated cells also retained alkaline phosphatase activity, which is associated with pluripotent stem cells (Lee, Hart and Skalnik, 2004). This is not in agreement with the aforementioned studies where TSA treatment increased stem cell differentiation. It is clear that global HDAC inhibition leads to widespread profound

epigenetic changes. Treating cells with VPA greatly improved the efficiency of reprogramming human fibroblasts into induced pluripotent stem cells (Huangfu *et al.*, 2008). Exposing embryos that have undergone somatic cell nuclear transfer to TSA improves heterochromatin organisation and remodelling, improving their viability (Maalouf *et al.*, 2009).

The wide-scale genomic consequences of HDAC inhibitor treatment will be investigated using RNA-Seq in the next chapter. The effect it had on cell viability was clear to see and plates containing TSA-treated cells contained far more cell debris from cell death. TSA performs its inhibitory function by chelating the zinc ion in the catalytic active site (Porter and Christianson, 2019). However, other than HDACs, there are more than 300 zinc-dependent enzymes with members of all six enzyme families. These enzymes share a common tetrahedral structure containing a zinc ion coordinated by three amino acids. HDAC inhibitors can interfere with zinc-dependent enzymes or other metalloproteins (Gryder, Sodji and Oyelere, 2012). It is therefore likely, that these can be responsible for the pleiotropic or therapeutic effects observed upon treating cells with inhibitors.

Results obtained in this chapter, do not lead to a solid conclusion leaning towards agreeing with one or another of the studies mentioned above. The average first day of beating did decrease but that was not statistically significant and so no firm conclusions can be drawn. Global histone deacetylase inhibition is predicted to cause widespread effects. The consequences of which were clear in its effect on cell health. TSA effect on beating can be seen in the accompanying videos. Beating foci showed a beating pattern different and slower than wild-types. Beating was also weaker and some foci displayed an elongated ‘fibrous-like’ morphology that was not seen in the untreated group. Attempts at quantifying the difference in beating were made. Results from the MYOCYTER macro analysis indicated that TSA-treated cells showed a lower speed and amplitude than untreated wild-type controls.

3.6.1.6 CRISPR/Cas9-mediacted knockout of *Hdac4*

To knock out *Hdac4*, a plasmid vector containing Cas9, the guide RNA and selectable markers was electroporated into cells. Cells were left to recover for 48 hours post electroporation prior to antibiotic selection. Treating with 100 μg/ml Hygromycin B was sufficient to kill any non-resistant cells in 14 days. Colonies were

picked and expanded 15 days after antibiotic selection. Mutations near the target site were evident upon DNA sequencing and subsequent alignments with DNA from wild-type cells. Mutations included indels as well as substitutions that would have arisen due to error-prone non-homologous end joining (NHEJ). Since the purpose of this study was to knockout *Hdac4*, the main objective was to introduce an inactivating mutation of any kind into the gene, preferably in a region close to the catalytic domain of the protein to prevent any histone deacetylase activity.

The colony that was chosen for fur”her ’haracterisation was one with a large deletion as evident from sequencing analysis. The deletion, despite being mainly intronic did lead to a frameshift and thus a predicted premature stop codon. DNA evidence was not sufficient to discern whether the deletion was homozygous or heterozygous. While gel electrophoresis analysis showed a single band, it is a possibility that the other allele contains a mutation of a different kind, like a larger deletion that took out all primer binding sites. Large scale deletions of this kind have been reported in previous CRISPR/Cas9 gene editing experiments (Adikusuma *et al.*, 2018; Kosicki, Tomberg and Bradley, 2018).

It has also been reported that premature termination codons (PTCs) introduced by CRISPR/Cas9 gene modifications can lead to exon skipping events (Lalonde *et al.*, 2017). If these exons were of a length that was a multiple of 3, skipping it would still maintain the reading frame and a protein may be translated. In this project, it is a possibility that this has taken place, and is illustrated in Figure 3-26. The targeted exon was a multiple of 3, 108 bp long. The data from the Western blot was also inconclusive and it cannot be stated with certainty whether a PTC-caused truncated protein was produced or one with an exon skipping event.

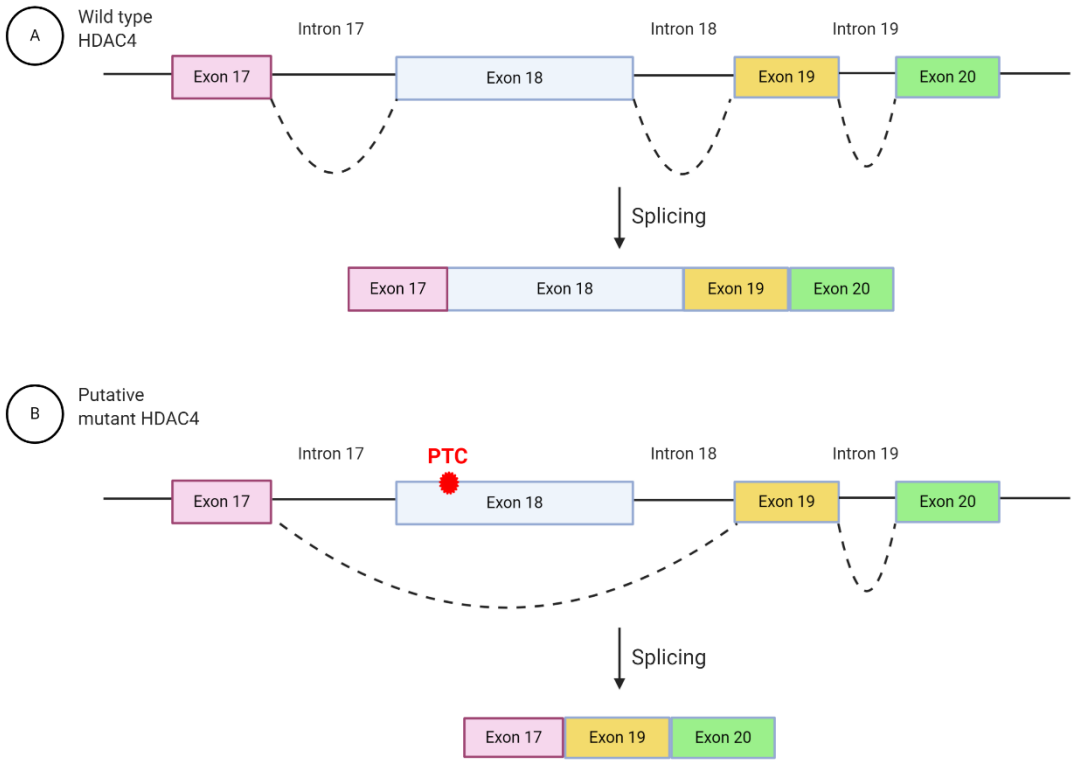


Figure 3-26. Possible exon skipping event could have taken place due to CRISPR/Cas9 editing of *Hdac4*. (A) shows splicing of wild-type *Hdac4*. (B) shows splicing in the putative *Hdac4* mutant. Exon 18 is skipped due to containing a premature termination codon (PTC), indicated in red. Figure created using Biorender.com

Knocking out both alleles of *Hdac4* in mice is lethal within two weeks of birth. Knockout mice show cerebellar degeneration. However, conditional deletion of *Hdac4* in the central nervous system did not affect neuron viability or brain architecture (Price, Wang and D'Mello, 2013). Conditional knockouts in peripheral sensory neurons led to a reduction in the progression of chronic inflammatory pain in mice (Crow *et al.*, 2015).

In a study by Luo et al., inducible skeletal *Hdac4* knockout mice were generated. *Hdac4* knockout was induced at 3 months of age. They predicted to see a decrease in the expression of *Mef2c* and *Mef2* target genes. Surprisingly, the knockout did not affect expression levels of those in muscles. However, the study was able to identify a role for *Hdac4* in protecting denervated leg muscles from atrophy. In denervated legs from knockouts, expression of *Mef2a* and *Mef2c* was reduced. They also

identified previously unknown *Hdac4* targets which include myosin heavy chain, peroxisome proliferator-activated receptor gamma co-activator 1alpha (PGC-1α), and heat shock cognate 71 kDa protein (Hsc70). The authors speculate that HDAC4's muscular protective properties are conferred through its interaction with myosin heavy chain isoforms (Luo *et al.*, 2019).

In this study, the effects of *Hdac4* knockout on cardiac differentiation were assessed using beating onset and image analysis using the MYOCYTER macro. Beating was delayed in the differentiated knockouts though that was not significant. MYOCYTER analysis served as a preliminary means of quantifying beating and showed a reduction in both speed and amplitude of beating, as was the case with TSA treatment.

In a study utilising P19 cells as a model of cardiac development, Karamboulas et al aggregated the cells in the presence of TSA and compared it to DMSO-induced cardiac differentiation. They reported an increase in the expression of cardiac markers *Nkx2.5*, *Mef2c*, *Gata4* and α-actin. Moreover, in a P19 cell line constitutively expressing a dominant negative form of MEF2C that binds Class II HDACs, cells differentiated into cardiomyocytes more efficiently than controls. In the same paper they also report that overexpression of HDAC4 partially inhibited cardiomyogenesis evidenced by a decrease in cardiac gene expression. These results strongly suggest the involvement of Class II HDACs, and HDAC4 in cardiomyogenesis. The discordance seen in phenotypes between inhibiting all HDACs and overexpressing HDAC4 on its own points to the redundancy between Class II HDACs. Class II HDACs are phosphorylated by Ca2+/calmodulin-dependent kinase (CaMK), leading to their inhibition (Backs *et al.*, 2006). The authors expressed an activated CamKIV in P19 cells and noted an increase in the expression of *Nkx2.5*, *Gata4* and *Mef2c*, in addition to an increase in cardiac muscle development. This study strongly suggests the involvement of Class II HDACs, and HDAC4 in particular, in the differentiation of mesoderm cells into cardiomyocytes. Their results show that HDAC4 regulates GATA4, as activated CaMKIV led to an upregulation of *Gata4* while inhibition of CaMK signalling reduced *Gata4* expression. Also, HDAC4 overexpression led to *Gata4* and *Nkx2.5* reduction (Christina Karamboulas *et al.*, 2006). This links with results obtained by our group in zebrafish knockdown models of *kat2a* and *kat2b*. *kat2a* and *kat2b* knockdown

phenotypes mirror those in *Tbx5* knockdowns. Interestingly, injecting *camk2d1* mRNA, a target of *Tbx5*, rescues the phenotype (Tushar K Ghosh *et al.*, 2018). Moreover, further work conducted by our group showed that PRKD1, a kinase, is able to alleviate HDAC4/HDAC5-mediated repression of TBX5, by phosphorylation (Ghosh *et al.*, 2019). Phosphorylation takes place on specific serine residues and results in nuclear export, an illustration of the effects of phosphorylation on HDAC4/5 and the effect on *Tbx5* is shown in Figure 3-27. This suggests the presence of functional links between HDAC regulation by phosphorylation, acetylation and deacetylation in cardiac differentiation. It is even suggested that DMSO is able to drive cardiac differentiation in P19 cells by increasing intracellular calcium concentration, leading to the activation of CamKs and HDACs inhibition.

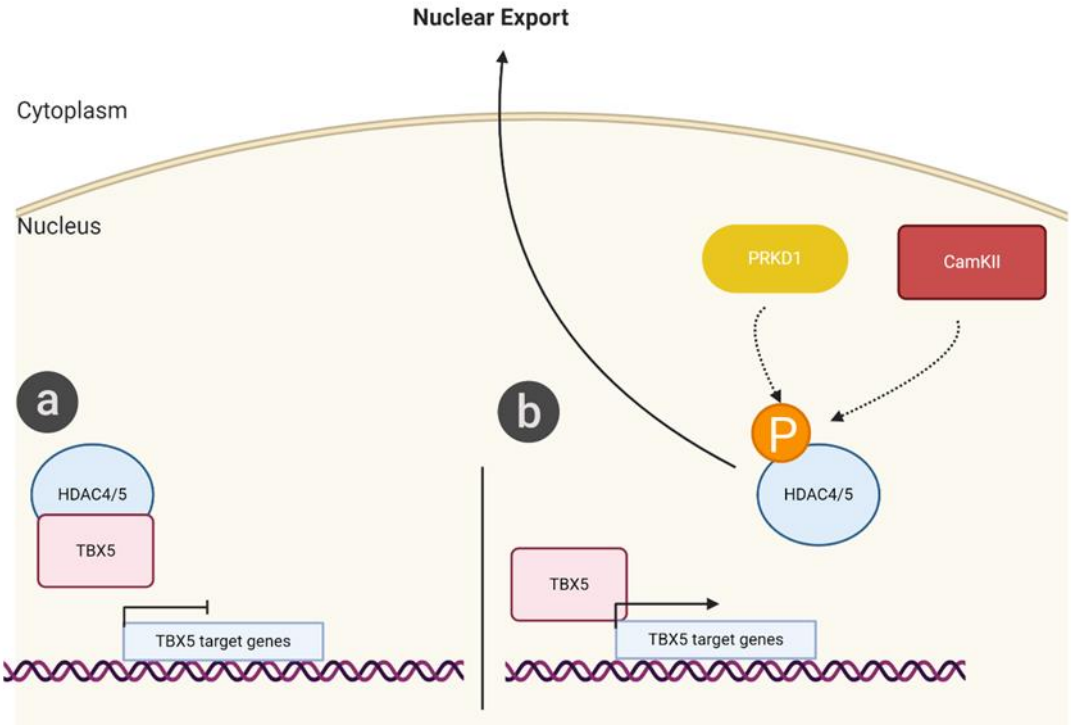


Figure 3-27. Phosphorylation of HDAC4/5 leads to their nuclear export and activation of *Tbx5* targets. In (a) HDAC4 or HDAC5, is bound to *Tbx5*, preventing it from activating transcription of its target genes. In (b) a phosphorylation mark laid on HDAC4 or 5, marked by an orange P, laid by PRKD1 or CamKII leads to its nuclear export. *Tbx5* is then able to activate transcription of its target genes. Figure created using Biorender.com

Results obtained in this chapter suggest that *Hdac4* was knocked down in these cells as evidenced from DNA sequences. Further validation would still need to be carried out to confirm this. However, visual observations indicate a similarity in morphology and beating pattern between differentiated mutants and TSA-treated cells. Whether they have similar transcriptional profiles would be determined among closer examination of their RNA expression profiles, which will be presented and discussed in the next chapter.

4 CHAPTER 4: RNA-SEQ ANALYSIS OF CARDIAC DIFFERENTIATION

4.1 Introduction

The advent of high-throughput sequencing has revolutionised the field of genetics. It has enabled scientists to conduct much deeper investigations and infer a large volume of information on genes and genomes than was otherwise possible. High-throughput sequencing ushered in the era of RNA-Sequencing (RNA-Seq) which enables investigators to take detailed snapshots of gene expression events taking place in as little as a single cell. Unlike older wide-scale methods of transcriptomic analysis like microarrays or RT-PCR, RNA-Seq does not require any *a priori* knowledge of the genes being investigated (Chatterjee *et al.*, 2018). In the present study 3' Quant-Seq was used because of its economic feasibility while being able to answer biological questions relevant to this thesis (Moll *et al.*, 2014).

4.2 Chapter Aims

This chapter aims to analyse data from RNA-Seq on mouse ES cells to elucidate the regulatory role of *Hdac4* during cardiomyocyte differentiation. Two parallel approaches have been adopted. In one, Trichostatin A (TSA), a well characterised inhibitor of Class I and Class II histoine deacetylases was used and in the other, I performed CRISPR/Cas9 knockout of *Hdac4*. I report the transcriptional consequences on mouse ESCs differentiation of TSA treatment and as a consequence of *Hdac4* knockout. The goal is to explore the transcriptomic changes during differentiation and how those are affected by TSA treatment and *Hdac4* knockout.

The chapter sets out to study genes differentially expressed during differentiation and to take a closer look at genes involved in beating. This was done by comparing gene expression between cells in the differentiated and undifferentiated states. Differentiation led to the generation of beating foci. RNA was extracted from those beating cells and from non-beating differentiated cells. A schematic of the

experiment showing the different groups is shown in Figure 3-27

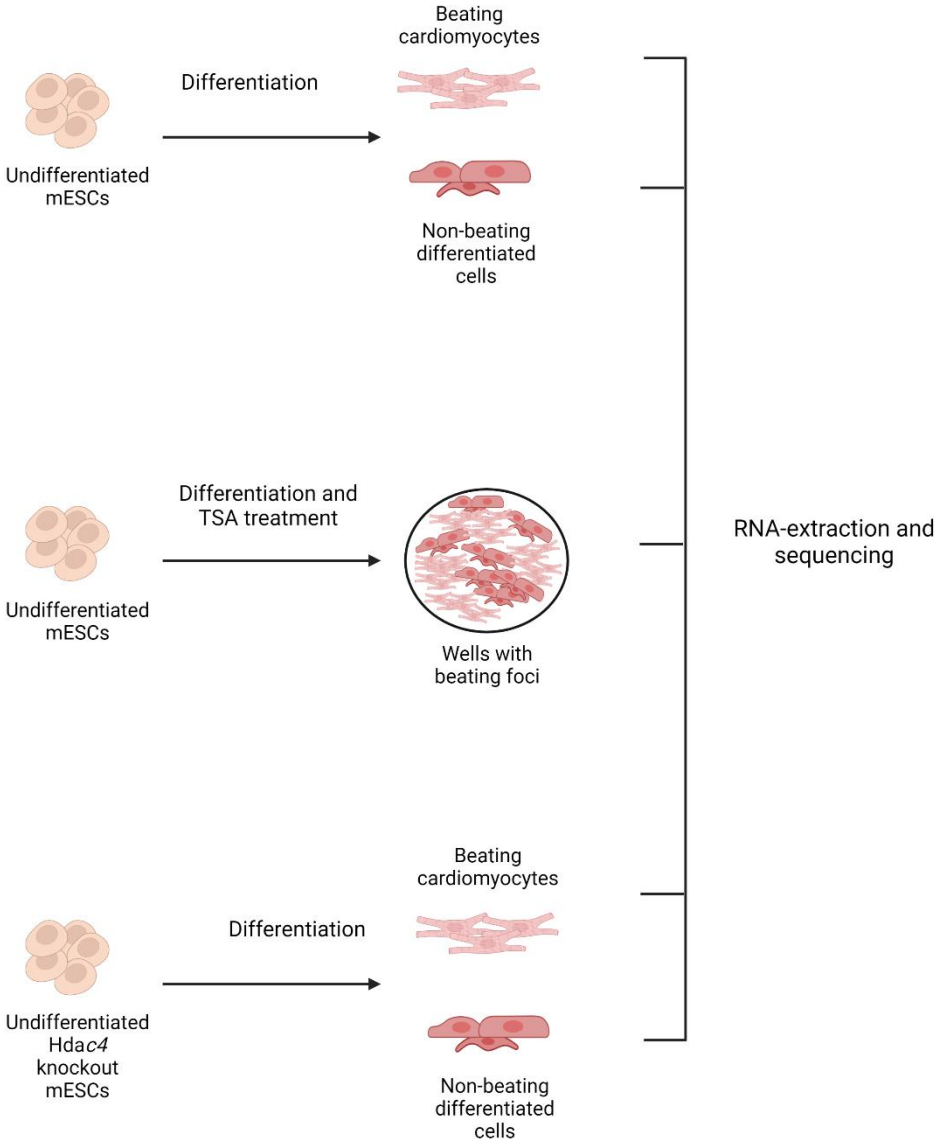


Figure 4-1 RNA was extracted from undifferentiated and differentiated cells for RNA-Seq analysis.

Moreover, to gain further understanding of the affected biological pathways, results of the RNA-Seq analysis were used to conduct Ingenuity Pathway Analysis. Figure 4-2 illustrates the steps involved in the RNA-Seq analysis reported herein.

The concept being tested in this chapter is that TSA treatment and *Hdac4* knockout would lead to significant changes in gene expression in the context of cardiac differentiation. Global transcriptomic changes are to be expected during such a complex process, but they can also arise as a result of multiple passages . Cells in culture have been shown to undergo genetic drift as they are propagated. Therefore,

while a change in cardiac gene transcription is expected, *exact* gene expression alterations cannot be predicted. Some of the genes expressed may be as a consequence of unforeseen complexities of genetic drift, gene pathway perturbation and differentiation along a cardiomyocyte pathway.

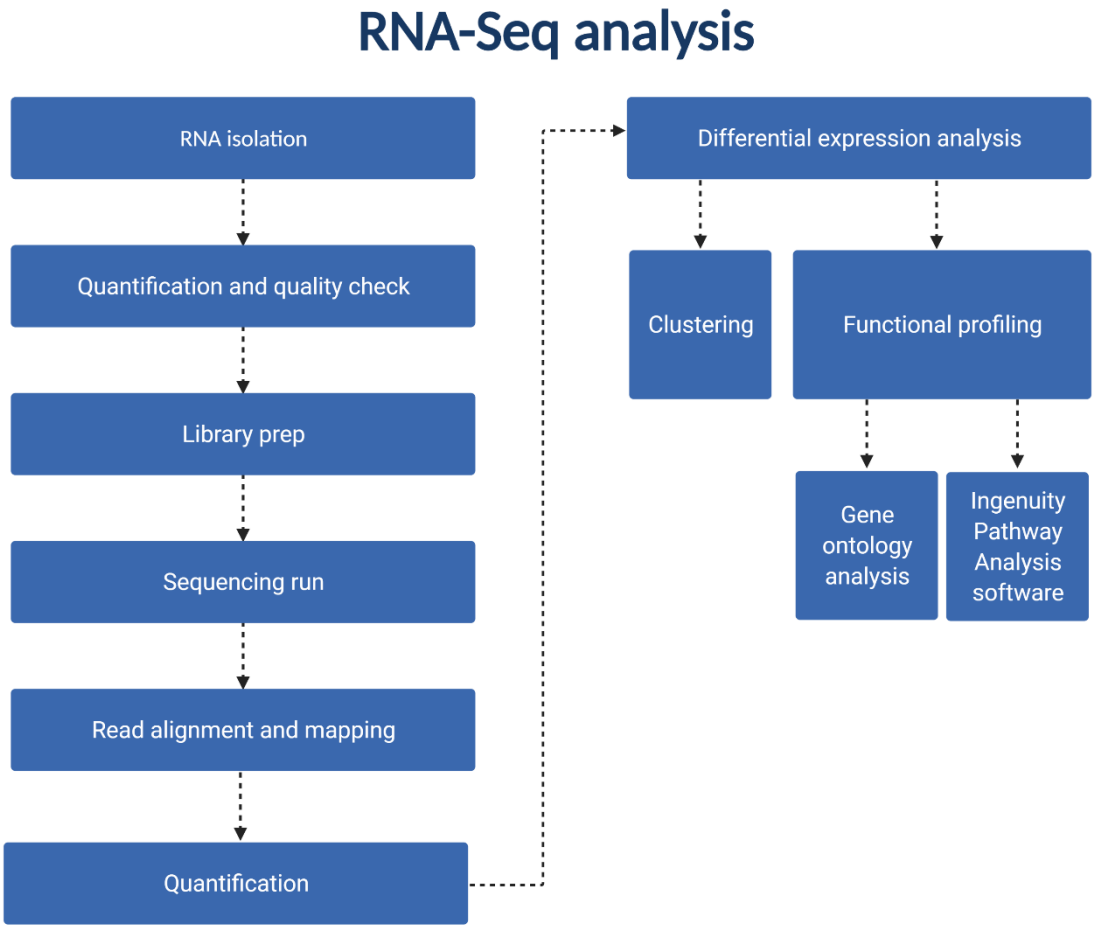


Figure 4-2. A schematic explaining the steps taken to analyse RNA samples.

4.3 4.3 Results:

4.3.1 RNA extraction and quality control

In order to assess the effect of the differentiation procedure, whole RNA was extracted from undifferentiated and differentiated cells, including wild-type and those subject to TSA treatment and *Hdac4* knockout. A distinction between beating and non-beating cells was made in the wild-type and *Hdac4* knockout samples. The first step in the RNA-Seq analysis pipeline was to assess the quality of RNA.

As outlined in the methods section, cloning rings were used to isolate beating regions. However, in the case of TSA-treated cells, the beating regions were small and not enough RNA could be isolated this way. For TSA-treated cells, RNA was extracted from entire wells with beating regions so this would contain RNA from some beaters but mostly non-beaters. Every effort was taken to ensure a comparable number of beating foci between wells.

RNA of sufficient integrity and purity as determined by NanoDrop and Qubit was used. All samples except one had RIN>8, wt_diffNB_2 had a lower RIN number of 7.4 but it produced an intact trace and so was used for library generation. Sample IDs and their descriptions are summarised in Table 4-1. 5 biological replicates were used for each group. Attempts were made to extract RNA from TSA-treated non-beating cells but those failed QC checks and so were not taken further in the analysis. Time constraints prevented the repetition of those experiments.

Table 4-1 Samples used for RNA-Sequencing and analysis

Sample ID	Description	Number of replicates
wt_undiff	Undifferentiated mESCs	5
wt_diffB	Differentiated beating wild-type mESCs	5
wt_diffNB	Differentiated non-beating wild-type mESCs	5
wt_tsaB	Differentiated TSA-treated mESCs	5
hdac4_koB	Differentiated beating Hdac4 knockout mESCs	5

hdac4_koNB	Differentiated non-beating Hdac4 knockout mESCs	5

4.3.2 Sequencing reads and mapping

From each sample, libraries were generated and sequenced on an Illumina NextSeq 500, generating 5 million 75-bp single end reads per library. To generate these libraries, cDNA fragments were generated from total RNA. These cDNA fragments were then sequenced and trimmed to remove sequences with low quality scores as well as adapter sequences. Those were then mapped to the reference genome (Ensembl mM 10) using STAR mapping tool (Dobin *et al.*, 2013). The results from this initial step are shown in panel A of Figure 4-3. For each read generated per sample, the number of reads that map to the reference genome is indicated. As a read can map to more than one location, the 'Uniquely Mapped Reads' is the most important metric. It is a measure of how many reads specifically and uniquely map to a single location in the genome. They are also presented in terms of percentage proportions of all reads. A good sequencing library is expected to generate at least 75% uniquely mapped reads. Percentages below 50% are indicative of problems in library production (Dobin and Gingeras, 2015). For this project, uniquely mapped percentages were above 75% except for the wt_undiff sample group.

The BAM (binary alignment map) files generated by the mapping and alignment steps were subject to further quality checks, using SeqMonk software. Results of this step are shown in panel B of Figure 4-3. Overall, the RNA was of sufficient quality to undergo further analysis. The percentage of RNA in genes and in exons was lower than usual because the library preparation method used focuses on sequencing from the 3' end. The results also show that nearly 100% of the sequence is in the sense strand, which is expected given the initial priming step takes place at the 3' end of the transcript.

A

Sample name and number	Trimmed Reads	Mapped Reads		Uniquely Mapped Reads	
		Counts	Percentage	Counts	Percentage
Hdac4 KO B 1	9182187	8975170	97.75%	6947377	75.66%
Hdac4 KO B 2	9425533	9213103	97.75%	7228721	76.69%
Hdac4 KO B 3	8650953	8431640	97.46%	6586805	76.14%
Hdac4 KO B 4	9152268	8914405	97.40%	7047462	77.00%
Hdac4 KO B 5	10688835	10449330	97.76%	7978038	74.64%
Hdac4 KO NB 1	10294513	10054688	97.67%	7691802	74.72%
Hdac4 KO NB 2	9195235	8991171	97.78%	6968055	75.78%
Hdac4 KO NB 3	8930590	8706972	97.50%	6797112	76.11%
Hdac4 KO NB 4	10037371	9787652	97.51%	7630033	76.02%
Hdac4 KO NB 5	9249464	9035850	97.69%	7076420	76.51%
WT diff B 1	8569078	8417480	98.23%	6502233	75.88%
WT diff B 2	9284847	9005710	96.99%	6935506	74.70%
WT diff B 3	10176186	9941480	97.69%	7735870	76.02%
WT diff B 4	10332579	10088466	97.64%	7811481	75.60%
WT diff B 5	9659873	9445516	97.78%	7475464	77.39%
WT diff NB 1	9936733	9724663	97.87%	7546809	75.95%
WT diff NB 2	10103993	9788865	96.88%	7585702	75.08%
WT diff NB 3	10377506	10160999	97.91%	7878913	75.92%
WT diff NB 4	9411579	9162932	97.36%	7067183	75.09%
WT diff NB 5	8882040	8665309	97.56%	6809847	76.67%
WT TSA B 1	9447087	9162900	96.99%	7267294	76.93%
WT TSA B 2	10507300	10282960	97.86%	8141687	77.49%
WT TSA B 3	8354475	8190802	98.04%	6478287	77.54%
WT TSA B 4	9087361	8898719	97.92%	7012873	77.17%
WT TSA B 5	9270610	9085000	98.00%	7175898	77.40%
WT undiff 1	10866543	10580514	97.37%	7535366	69.34%
WT undiff 2	9828639	9518866	96.85%	6824861	69.44%
WT undiff 3	10103288	9758164	96.58%	6925385	68.55%
WT undiff 4	9411393	9147176	97.19%	6487261	68.93%
WT undiff 5	9265970	8950487	96.60%	6413798	69.22%

B

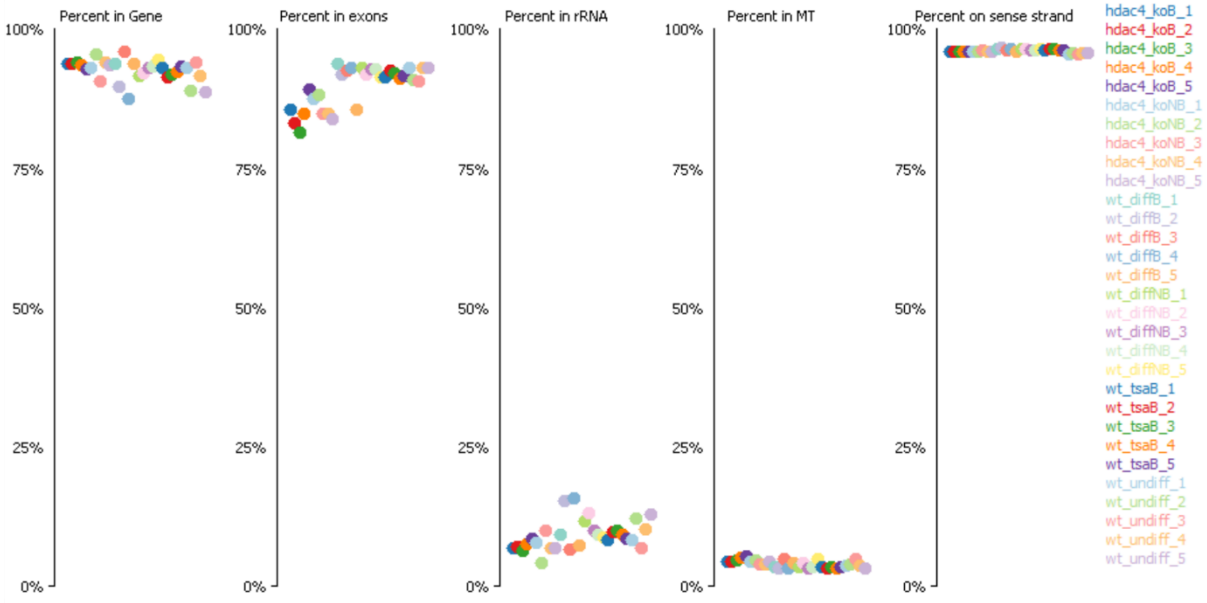


Figure 4-3. Initial quality control checks on data from RNA-Seq shows that DNA was of sufficient mapping quality for downstream analyses. Panel A shows alignment and mapping results. Panel B shows quality check plots generated on SeqMonk.

4.3.3 Stem cells undergo significant transcriptomic changes during differentiation

First, in order to assess if samples from the same group cluster together, a heat map was generated, depicting hierarchical clustering of samples. Each row represents an individual gene and each column represents a sample. The log of normalised counts is used to plot the gene's intensity of expression. The resultant heatmap (Figure 4-4) showed that according to differential gene expression values, samples from the same replicate did cluster together. This indicates that replicates had similar gene expression profiles. SeqMonk software was used to conduct a DeSEq2 analysis. The genes identified as differentially expressed and having a $\log_2$ fold-change of >1 or <-1 were used to plot the heat map. 14,598 genes were identified by the analysis to be differentially expressed at $p<0.05$ significance.

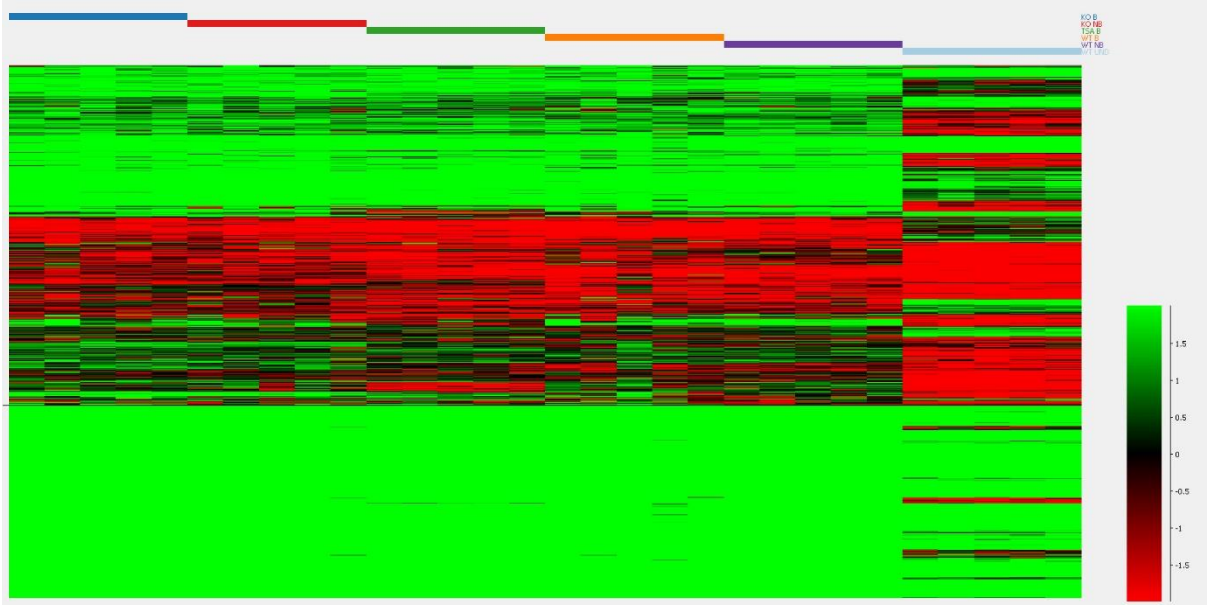


Figure 4-4. Heat map of differentially expressed genes shows that replicate samples cluster together. Each row represents a gene and every column represents a replicate sample. Horizontal lines at the top indicate sample groups. From left to right: blue – *Hdac4* KO beating cells, red – *Hdac4* KO non-beating cells, green – TSA-treated cells, orange – wild-type beating cells, purple – wild-type differentiated non-beating cells and sky blue – wild-type undifferentiated cells. The colour indicates log fold-change of gene expression where green shows an upregulation and red shows a downregulation.

To study the changes in gene expression that occur during differentiation, pair-wise comparisons were conducted between undifferentiated wild-types and each of the differentiated groups. The DESEq2 tool on the Galaxy platform was used to study the number of differentially expressed genes. The results of the analysis is shown in Table 4-2. A $\log_2$ fold change of 1 would indicate a gene has doubled in expression and a $\log_2$ fold change of -1 would indicate its expression has halved.

Table 4-2 Differential gene expression analysis comparing wild-type undifferentiated cells to each group of differentiated cells, irrespective of beating. The threshold for statistical significance was p<0.05

Comparison	Number of DEGs	Number of upregulated genes (log2 fold change >1)	Number of downregulated genes (log2 fold change <-1)
WT undifferentiated vs WT differentiated beating cells	10,215	4,406	2,578
WT undifferentiated vs WT differentiated non-beating cells	11,666	4,639	2,806
WT undifferentiated vs Hdac4 KO differentiated beating cells	11,045	4,471	2,417
WT undifferentiated vs Hdac4 KO differentiated non-beating cells	10,617	4,164	2,257
WT undifferentiated vs TSA-treated differentiated cells	11,788	4,258	3,149

Furthermore, a principal component analysis (PCA) was conducted on these sample groups (Figure 4-5). Principal Component Analysis (PCA) is a clustering method that enables the investigator to assess variance among experimental groups. On a PCA plot, closely-related samples cluster together. PCA allows one to reduce the dimensionality of the data, visualising it in 2 dimensions while still maintaining variability (Ringnér, 2008). Variables are reduced into principal components, where most variance in the data is explained by the first principal component, most of the rest of the variance would then be explained by the second principal component, and

so on. There was distinct separation between undifferentiated and differentiated samples in all comparisons with PC1 accounting for the most variance

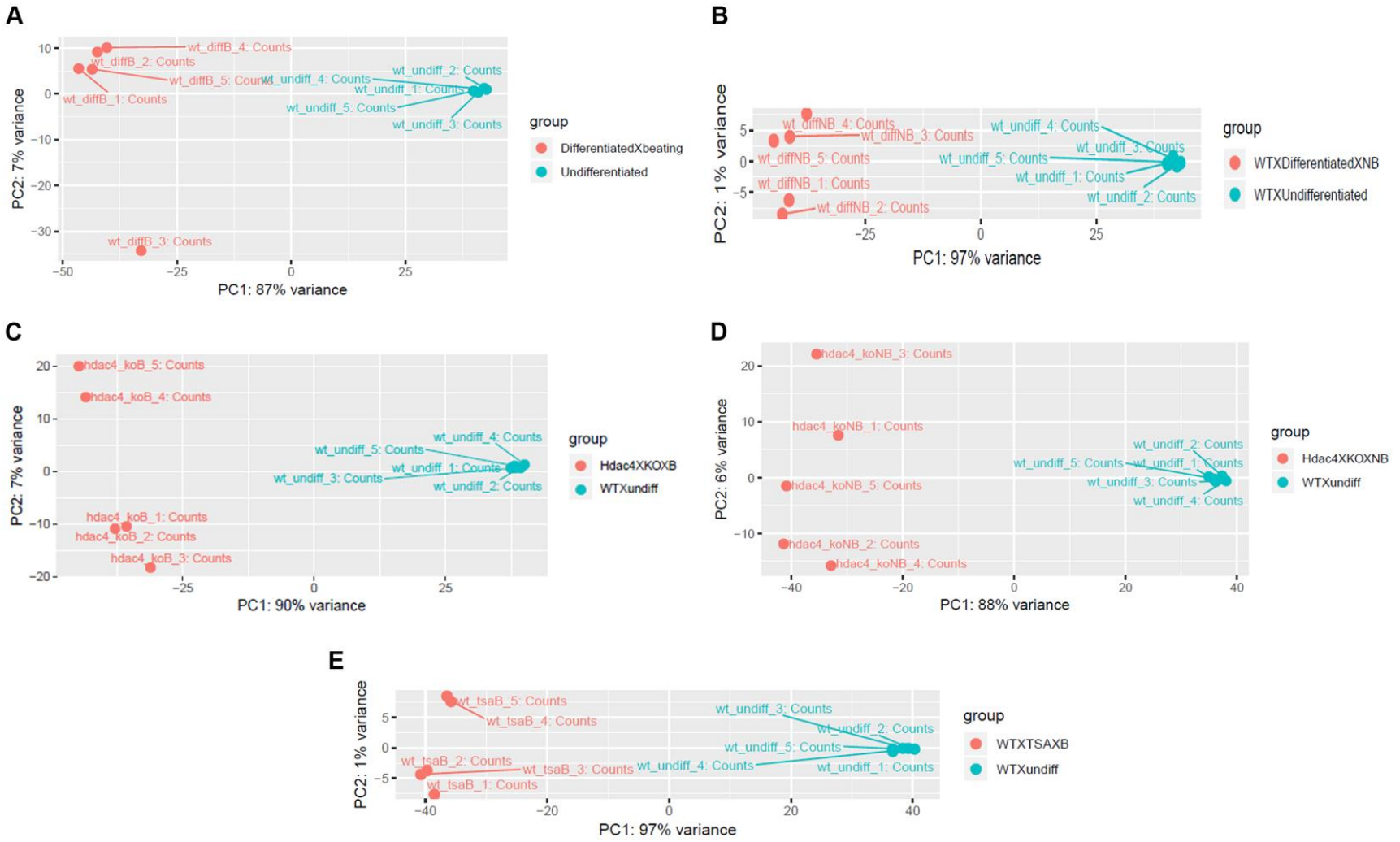

A
wt_diffB_4: Counts
wt_diffB_2: Counts
wt_diffB_5: Counts
wt_undiff_4: Counts
wt_undiff_2: Counts
wt_undiff_1: Counts
wt_diffB_1: Counts
wt_undiff_5: Counts
wt_undiff_3: Counts
wt_diffB_3: Counts
PC2: 7% variance
PC1: 87% variance
group
DifferentiatedXbeating
Undifferentiated
B
wt_diffNB_4: Counts
wt_diffNB_3: Counts
wt_undiff_4: Counts
wt_undiff_3: Counts
wt_diffNB_5: Counts
wt_undiff_5: Counts
wt_undiff_1: Counts
wt_diffNB_1: Counts
wt_undiff_2: Counts
wt_diffNB_2: Counts
PC2: 1% variance
PC1: 97% variance
group
WTXDifferentiatedXNB
WTXUndifferentiated
C
hdac4_koB_5: Counts
hdac4_koB_4: Counts
wt_undiff_4: Counts
wt_undiff_5: Counts
wt_undiff_1: Counts
wt_undiff_3: Counts
wt_undiff_2: Counts
hdac4_koB_1: Counts
hdac4_koB_2: Counts
hdac4_koB_3: Counts
PC2: 7% variance
PC1: 90% variance
group
Hdac4XKOXB
WTXundiff
D
hdac4_koNB_3: Counts
hdac4_koNB_1: Counts
wt_undiff_2: Counts
wt_undiff_5: Counts
wt_undiff_1: Counts
wt_undiff_3: Counts
hdac4_koNB_5: Counts
wt_undiff_4: Counts
hdac4_koNB_2: Counts
hdac4_koNB_4: Counts
PC2: 6% variance
PC1: 88% variance
group
Hdac4XKOXNB
WTXundiff
E
wt_tsaB_5: Counts
wt_tsaB_4: Counts
wt_undiff_3: Counts
wt_undiff_2: Counts
wt_undiff_5: Counts
wt_tsaB_2: Counts
wt_tsaB_3: Counts
wt_undiff_4: Counts
wt_undiff_1: Counts
wt_tsaB_1: Counts
PC2: 1% variance
PC1: 97% variance
group
WTXTSAXB
WTXundiff

Figure 4-5 Principal component analysis of comparisons between undifferentiated cells and each of the differentiated groups shows that control replicates cluster together. A. WT undifferentiated vs WT differentiated beating. B. WT undifferentiated vs WT differentiated non-beating. C. WT undifferentiated vs Hdac4 KO differentiated beating. D. WT undifferentiated vs Hdac4 KO differentiated non-beating. E. WT undifferentiated vs WT TSA-treated differentiated. The plots show that in all comparisons, PC1 accounted for most of the variance. Various differentiated groups showed variance along PC2. In all plots, blue dots represent the undifferentiated controls while pink dots represent the differentiated samples.

These initial findings suggest that a global change in gene expression has taken place during the differentiation process. Following on, I sought to investigate genes and associated pathways that were up or downregulated in the different groups. I also aimed to shed some light on the genetic basis of contractility.

4.3.4 Unsupervised Multiple pair-wise comparisons show that differentiation-related genes are upregulated

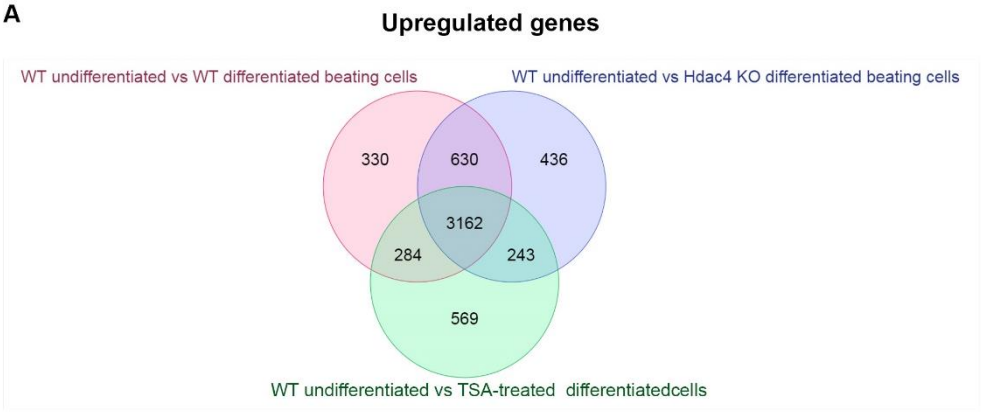
To investigate genes differentially expressed in beating cells, pair-wise comparisons with the undifferentiated state were conducted. These individual comparisons were then grouped together to examine any changes in gene expression during differentiation that can be attributed to TSA treatment or *Hdac4* knockout (Figure 4-6A and B). The genes at the intersection of all of them were used for gene ontology analysis.

At first glance, the top 20 enriched biological pathways (Figure 4-6 panel C) are generally related to anatomical development and organogenesis. Most terms relate to generic biological functions one would expect to find during stem cell differentiation, such as anatomical structure morphogenesis, cell adhesion, tissue development and cell differentiation. It is therefore noteworthy that the only specific organ system-related term is circulatory system development. Notably, genes in this subset contained those that are targeted by the mesodermal regulator *Brachyury*. These include, *Meis1* (known to be expressed in the primitive streak during gastrulation) (Evans *et al.*, 2012), *Erg*, *Snai2*, and *Ebf2*. Genes involved in morphogenesis included *Gabra1*, *Gfra3*, *Cbln3*, which play roles in anchoring plasma membrane to cytoskeletal proteins (Evans *et al.*, 2012).

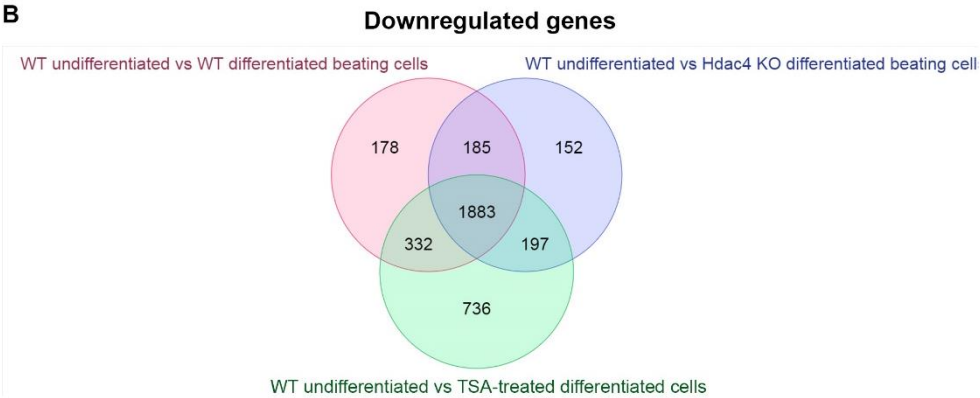
Genes encoding for members of signalling pathways known to be involved in cellular differentiation were also upregulated. These included genes for TGFβ signalling pathway ligands *Gdf6*, *Gdf10* and *Gdf11*. Members of the Wnt signalling pathway, involved in lineage commitment, cell migration, cell polarity and anterior-posterior elongation were also upregulated in this subset (Jang *et al.*, 2017). These include *Wnt11*, *Wnt2*, *Wnt4*, *Wnt5a*, and *Wnt6*. Members of the cadherin family, key mediators of cell-cell adhesion, such as *Cdh2*, *Cdh5* and *Cdh6* were also present.

As for the downregulated genes, these were related to biological processes related to general metabolism and RNA biogenesis. Downregulated genes included known pluripotency-associated genes such as *Nanog*, *Sox2*, *Klf5*, *Sall1*, *Etv5*, *Jarid2* and *Esrrb*. Interestingly, the list also contained *Cbx1*, *Daxx* and *Smarcad1*. *Cbx1* encodes for a subunit of heterochromatin protein 1 that functions in gene repression, mutations in which lead to global changes in transcription (Iwata-Otsubo *et al.*, 2020). *Daxx* and *Smarcad1* also encode for proteins involved in heterochromatin formation (Navarro *et al.*, 2020). Notably, *Sarcad1* was shown to be essential for maintaining pluripotency in naïve stem cells and was previously shown to exhibit a sharp decrease in expression levels as cells exit pluripotency (Navarro *et al.*, 2020). These results show the epigenetic factors at play in controlling differentiation-associated gene expression.

A



B



C **Upregulated genes at intersection of all 3 sets**

Biological pathway	Term ID	Adjusted p-value
system development	GO:0048731	3.63E-115
anatomical structure morphogenesis	GO:0009653	1.27E-111
multicellular organism development	GO:0007275	4.53E-108
anatomical structure development	GO:0048856	4.37E-98
developmental process	GO:0032502	1.75E-93
tissue development	GO:0009888	9.78E-83
animal organ development	GO:0048513	1.33E-82
animal organ morphogenesis	GO:0009887	1.50E-76
regulation of multicellular organismal process	GO:0051239	1.37E-73
circulatory system development	GO:0072359	1.98E-71
cell differentiation	GO:0030154	4.43E-67
regulation of developmental process	GO:0050793	8.27E-67
tube development	GO:0035295	6.32E-66
cellular developmental process	GO:0048869	1.41E-65
regulation of localization	GO:0032879	1.56E-61
tube morphogenesis	GO:0035239	8.18E-61
positive regulation of cellular process	GO:0048522	9.71E-61
regulation of signaling	GO:0023051	3.50E-60
regulation of cell communication	GO:0010646	1.07E-58
anatomical structure formation involved in morphogenesis	GO:0048646	1.68E-58

D **Downregulated genes at intersection of all 3 sets**

Biological pathway	Term ID	Adjusted p-value
heterocycle metabolic process	GO:0046483	3.50E-78
cellular nitrogen compound metabolic process	GO:0034641	1.52E-77
nucleobase-containing compound metabolic process	GO:0006139	4.39E-76
cellular aromatic compound metabolic process	GO:0006725	5.99E-74
organic cyclic compound metabolic process	GO:1901360	2.38E-70
nucleic acid metabolic process	GO:0090304	9.43E-70
ribonucleoprotein complex biogenesis	GO:0022613	1.96E-66
ribosome biogenesis	GO:0042254	6.39E-65
ncRNA metabolic process	GO:0034660	8.76E-64
ncRNA processing	GO:0034470	2.26E-57
rRNA processing	GO:0006364	3.34E-55
rRNA metabolic process	GO:0016072	6.06E-54
DNA metabolic process	GO:0006259	5.71E-52
nitrogen compound metabolic process	GO:0006807	8.32E-52
cellular metabolic process	GO:0044237	3.78E-51
RNA processing	GO:0006396	4.36E-46
primary metabolic process	GO:0044238	2.12E-45
organic substance metabolic process	GO:0071704	9.32E-43
metabolic process	GO:0008152	4.08E-41
cellular response to leukemia inhibitory factor	GO:1990830	2.06E-40

Figure 4-6 Comparing undifferentiated "ground-state" stem cells to beating cells in all treatments reveals a dynamic change in transcription. A. 3,162 genes are upregulated in all differentiated beating states. B. 1,883 genes are

downregulated in all differentiated beating states. C. Top 20 upregulated biological pathways as shown by GO analysis indicates an activation of developmental-related genes, including the circulatory system. D. Top 20 downregulated biological pathways show a deactivation in ribosomal biogenesis-related processes.

Next, the genes that were uniquely upregulated in the wild-type beating vs undifferentiated (330 genes in the red circle in panel A of Figure 4-6), TSA-treated vs undifferentiated (569 genes in the green circle in panel A of figure) and *Hdac4* knockout beating cells vs wild-type undifferentiated (436 genes in the blue circle in panel A of Figure 4-6) were also subject to gene ontology analysis to look at possible uniquely affected biological pathways (Figure 4-7A-C). Interestingly, the 330 genes upregulated in the wild-type beaters compared to undifferentiated resulted in biological pathways related to the immune function in general and interleukin-8 (IL-8) regulation in particular. As for the *Hdac4* knockouts and TSA-treated cells vs wild-type undifferentiated, the upregulated biological pathways were generally similar and mostly comprised of differentiation-related pathways. The same was done for downregulated gene lists (Figure 4-8). In the wild-types and TSA-treated cells, the downregulated genes were mostly related to metabolism. Looking at downregulated pathways in *Hdac4* knockouts only did not yield any significant biological pathways.

Regarding the TSA-treated samples, it must be noted that the RNA was collected from a mixed population of beaters and non-beaters. While effort was made to control for variability using biological replicates and randomising sample collection to minimise batch effects, this difference must be noted when considering the results. Future studies should include a chemical vehicle control for increased robustness. As the treated ESCs were differentiated using the same methods as the wild-type and knockouts, this analysis can still provide some insights on the global transcriptomic changes that take place as a result of pan-HDAC inhibition. This population is therefore, theoretically expected to still express cardiac differentiation-associated genes. The experiment aimed to gain a basic understanding of the potential consequences of TSA treatment, in the context of results generated from the non-

treated and knockout cells. The analysis therefore reports on global gene expression changes in that population as a whole rather than selected beating cells. Optimisation of TSA-directed differentiation to generate more robust beating colonies should be performed to enable direct comparisons between sub-populations. Using the RNA-Seq data generated in this project as a starting point, it would be interesting to hone in on the genes and biological pathways that control cell-fat decisions and whether they are affected by HDAC inhibition.

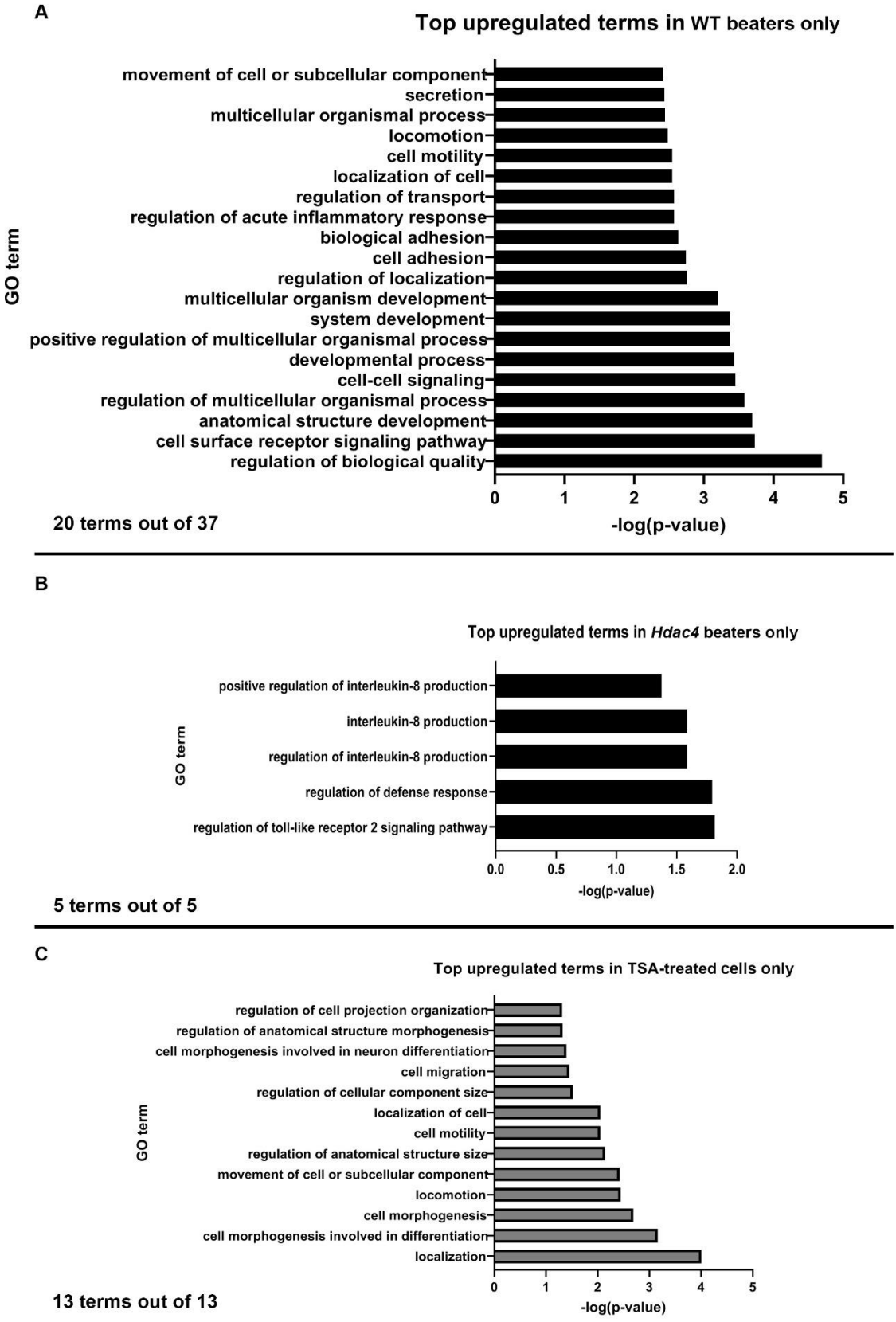

A
Top upregulated terms in WT beaters only
movement of cell or subcellular component
secretion
multicellular organismal process
locomotion
cell motility
localization of cell
regulation of transport
regulation of acute inflammatory response
biological adhesion
cell adhesion
regulation of localization
multicellular organism development
system development
positive regulation of multicellular organismal process
developmental process
cell-cell signaling
regulation of multicellular organismal process
anatomical structure development
cell surface receptor signaling pathway
regulation of biological quality
GO term
0 1 2 3 4 5
-log(p-value)
20 terms out of 37
B
Top upregulated terms in Hdac4 beaters only
positive regulation of interleukin-8 production
interleukin-8 production
regulation of interleukin-8 production
regulation of defense response
regulation of toll-like receptor 2 signaling pathway
GO term
0.0 0.5 1.0 1.5 2.0
-log(p-value)
5 terms out of 5
C
Top upregulated terms in TSA-treated cells only
regulation of cell projection organization
regulation of anatomical structure morphogenesis
cell morphogenesis involved in neuron differentiation
cell migration
regulation of cellular component size
localization of cell
cell motility
regulation of anatomical structure size
movement of cell or subcellular component
locomotion
cell morphogenesis
cell morphogenesis involved in differentiation
localization
GO term
0 1 2 3 4 5
-log(p-value)
13 terms out of 13

Figure 4-7 Upregulated terms in wild-type beaters only differ from those found in the *Hdac4* KOs or TSA-treated beaters.

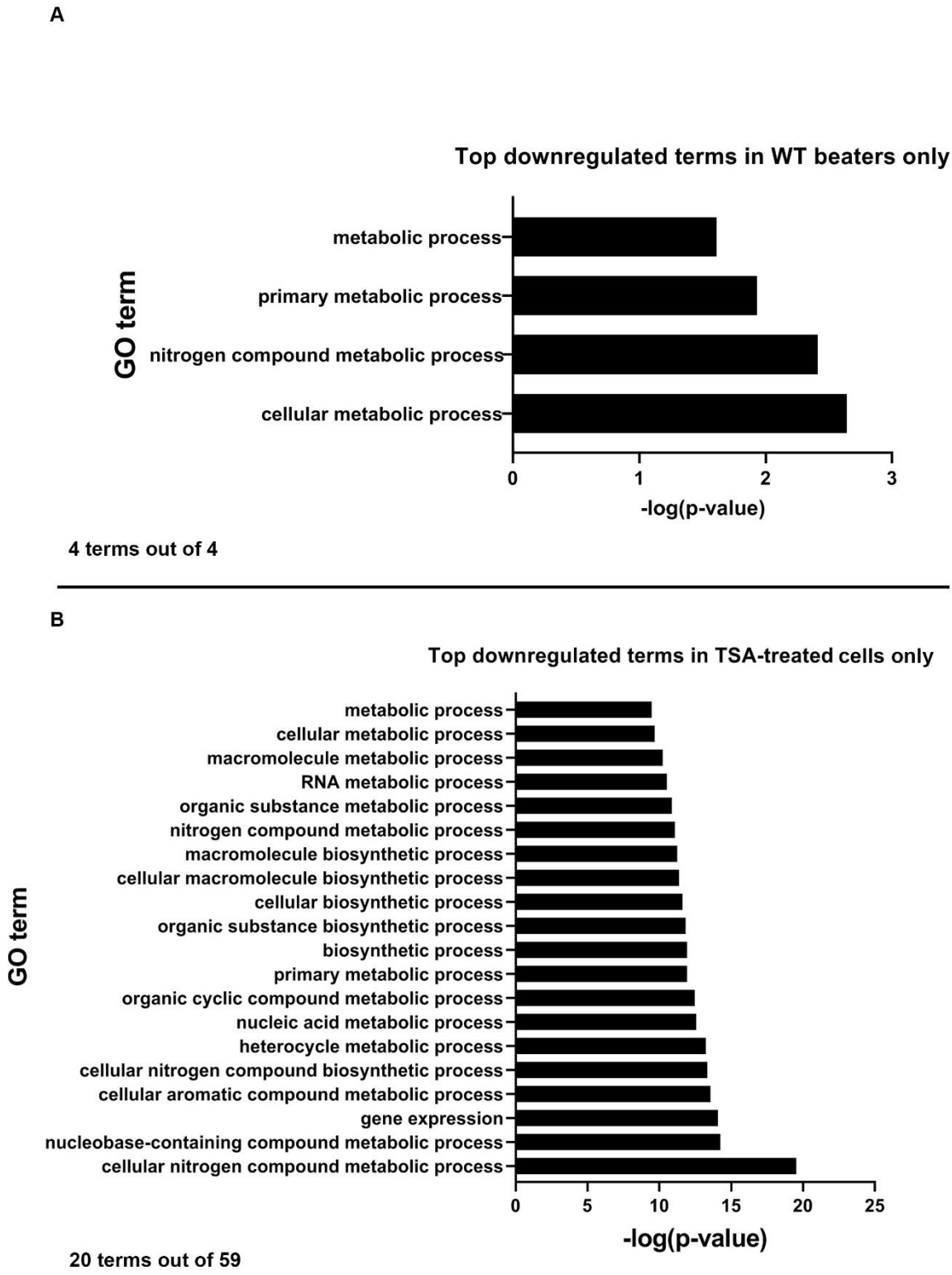


Figure 4-8. Downregulated genes in wild-type and TSA-treated beaters belonged to similar biological pathways mostly related to metabolism.

The gene ontology analysis provided a good overview of the genes enriched in affected biological pathways. To gain more insights into individual genes, MA plots were generated for each of the comparisons (

Figure 4-9). MA plots are a variation of the Bland-Altman plot to show differences between two samples or assays. In this context, they show $\log_2$ of fold change (M) versus the $\log_2$ of the mean of normalised counts (A). Each point on the plot represents a gene. Genes falling above or below 0 indicate up- or downregulation, respectively. Along with these plots, Figure shows the top 25 up and down regulated genes for each comparison, ordered in decreasing fold change. Panels A and B show that there are similarly affected genes. For example, *Pgm5 Fgb* and *Dnm3os* were upregulated in all three groups. *Platr10*, *Dpys*, *Cpsf4l* were downregulated in three groups. It was noteworthy to find *Mylk* upregulated in the knockout group.

The top upregulated genes in panel A include *F13a1*, which encodes for a transglutaminase enzyme, expressed in bone marrow and mesenchymal lineages and plays roles in phagocytosis, wound healing and bone and matrix remodelling (Mitchell and Mutch, 2019). *Pgm5* encodes for a member of the α-D-phosphohexomutase superfamily. This protein binds to dytrophin and is known to have roles in myofibril assembly and maintenance (Muenks, Stiers and Beamer, 2017). Pgm5 protein was also found to localise to intercalated discs and Z-discs in cardiac muscle (Molt *et al.*, 2014). *Fmod* and *Lum* encode for proteoglycan components of the ECM, known as fibromodulin and lumican, respectively. Fibromodulin was found to play a role myoblast differentiation by regulating calcium channel gene expression (Lee, Nam and Choi, 2018; Chen *et al.*, 2020). Notably, treating human fibroblasts with recombinant fibromodulin was sufficient to reprogramme them into iPSCs, capable of differentiating into multiple lineages, including cardiomyocytes (Zheng *et al.*, 2012). *Igfbp1* encode for an insulin-like growth factor binding protein and plays a role in cellular processes such as angiogenesis, growth, mitogenesis and proliferation (Piecewicz *et al.*, 2012).

Downregulated genes include *Fgf17*, which is involved in the development of the midbrain, inferior colliculus and vermis cerebellum (Liu Zhonghao and Ornitz, 2000). *Acsbg3* encodes for a member of the acyl-coA synthase bubblegum family, known to function in lipid metabolism and brain development (Lopes-Marques *et al.*, 2018). *Nr0b1* is involved in regulating the multipotency of trophoblast stem cells in mouse embryos (Kuales *et al.*, 2015). Collectively, the differentially expressed genes show a pattern expected of mESCs losing their stemness and differentiating into mesodermal cardiomyocytes.

In panel B, upregulated genes in *Hdac4* KO cells contain *Mgp*, known to regulate endothelial cell differentiation by inhibiting BMP4 (Yao *et al.*, 2016). *Tcf21* encodes for a transcription factor of the helix-loop-helix family (Ao *et al.*, 2020). *Tcf21* is mesoderm-specific and plays a key role in proliferation, differentiation, autophagy and EMT (Hu *et al.*, 2020). *Fgb* encodes fibrinogen β chain, which functions in blood clotting and mesodermal-derived non-haematopoietic cells, including hepatobiliary lineages (Wang *et al.*, 2020). *Ccl3* and *Ccl4* were also upregulated in this subset. These code for chemotactic cytokines (also known as chemokines) that have roles in embryonic development and cell differentiation. Interestingly, these have been shown to be regulated by histone deacetylation by studying the effects of HDAC inhibition (Gatla *et al.*, 2019).

Downregulated genes in panel B include *Nkx6.3*, which codes for a homeodomain protein that regulates the development of the pancreas, central nervous system and gastrointestinal tract . *Krt4* encodes a member of the keratin family that is involved in the differentiation of simple and stratified epithelium and was shown to be increased by *Meis1* knockdown (Mahmoudian *et al.*, 2019). Additionally, *Gbx2* is also downregulated, which encodes for a homeobox protein that acts downstream of the LIF/Stat3 signalling pathway to maintain stem cell pluripotency. Overexpressing *Gbx2* was shown to enhance reprogramming of epiblast stem cells to naïve stem cells (Tai and Ying, 2013).

Looking at panel C, top upregulated genes in TSA-treated cells include *Afp*. *Afp* encodes for a foetal glycoprotein and is part of a gene family that codes for albumin, alpha-albumin and vitamin D binding protein (Gabant *et al.*, 2002; Goldman *et al.*,

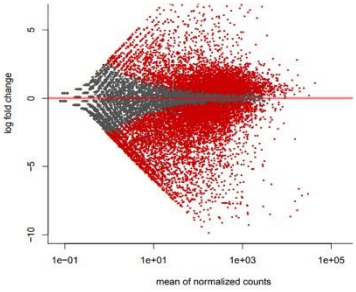
2016). Afp protein is highly expressed in embryonic development and is involved in endothelial differentiation of hepatoblasts and EMT. Another upregulated gene is *Ifi27*, which encodes for a mitochondrial-targeting protein with potential roles in apoptosis and EMT (Villamayor *et al.*, 2023). *Hapln1* is also upregulated, it encodes for a protein that contributes to the formation of cardiac jelly ECM, which is important for cardiac development (Palpant *et al.*, 2013). Furthermore, the zebrafish homologue *hapln1a* was found to specify left-right orientation of the ECM in the developing heart tube (Derrick *et al.*, 2022).

Moreover, interestingly in the TSA-treated group, *Tbx5*, *Hand2* and *Hand2os1* were among the top upregulated genes, a result not seen in other groups. This suggests that global class II HDACs relieved repression of these genes, even in a mixed cell population. It would be of interest to investigate the role HDACs play in lineage commitment and how TSA affects global transcription. Previous studies have shown that chemical HDAC inhibition results in increased methylation of H3K4Me2 and H3K4Me3 leading to transcriptional activation (Lillico *et al.*, 2016). H3K4Me3 is one of the markers of bivalent promoters in ESCs, regulating transcriptional switching in the differentiated state (Jeon and Tucker-Kellogg, 2020). It would thus be interesting to explore this mechanism further.

Downregulated genes include pluripotency-associated genes such as *Nr0b1* and *Nanog*. Genes involved in exiting the pluripotent state like *Errb* (Festuccia *et al.*, 2018) and *Lefty2* (Kim *et al.*, 2014) were also decreased in the TSA-treated population. *Fgf4*, a member of the FGF family was downregulated, consistent with the finding that *Fgf4* is essential for maintaining pluripotency, which it does via the activation of the ERK1/2 signalling cascade (Mossahebi-Mohammadi *et al.*, 2020). These results point to the significant transcriptional changes that take place in differentiation, and the factors responsible for its tight regulation.

A

WT undifferentiated vs WT differentiated beating cells



Top 25 upregulated genes

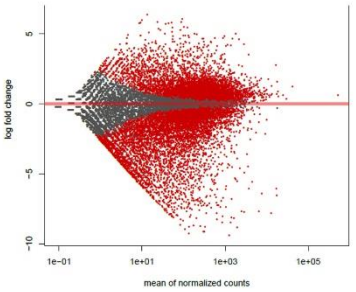
Gene ID	log2(FC)	P-adjusted
F13a1	9.881379	2.43E-27
Pgm5	9.407289	3.15E-25
Lum	9.271668	1.39E-81
Igfbp1	9.114122	5.58E-18
Fmod	9.0453	8.16E-24
Ctss	8.931663	1.57E-16
Gria1	8.922324	4.42E-23
Fgb	8.887206	5.98E-16
Cx3cr1	8.789754	2.89E-41
Col6a3	8.770739	2.46E-56
C1qc	8.739672	3.47E-19
Dnm3os	8.718427	8.58E-42
Csf1r	8.670527	9.48E-22
Col3a1	8.657801	4.93E-178
Mgp	8.626197	9.80E-26
Tcf21	8.524703	2.79E-30
Dcn	8.520318	4.59E-87
Sparcl1	8.516583	1.03E-39
Msr1	8.443851	1.18E-18
Tyrobp	8.406163	3.21E-20
Lilrb4a	8.365888	2.50E-19
Afp	8.357729	1.02E-28
Apoa1	8.337135	1.05E-14
Lyz2	8.304713	7.92E-17
C1qa	8.302573	1.75E-16

Top 25 downregulated genes

Gene ID	log2(FC)	P-adjusted
Dpys	-9.12447	1.09E-25
2310043M15Rik	-8.94382	1.59E-23
Fgf17	-8.24818	4.44E-20
Acsbg3	-8.16373	9.47E-24
Nr0b1	-7.66745	1.83E-108
Platr10	-7.49151	2.44E-63
Krt42	-7.34814	2.34E-33
Tdh	-7.19983	1.23E-161
Tcl1	-7.09515	1.62E-66
Esrrb	-6.9893	9.43E-102
Chrna9	-6.91701	1.64E-14
Cpsf4l	-6.90326	4.98E-42
T	-6.84233	5.19E-11
Epp13	-6.83737	1.55E-19
Utf1	-6.83288	1.39E-251
Gdf3	-6.76271	1.24E-143
Smim40	-6.73687	4.38E-70
Tdgf1	-6.71035	1.36E-90
Slc28a1	-6.68916	2.39E-42
Triml1	-6.65953	1.65E-47
EU599041	-6.63426	1.97E-12
Nkx6-3	-6.61034	8.76E-12
Lncenc1	-6.57625	5.40E-108
4930526L06Rik	-6.47543	1.34E-11
Ifitm7	-6.46532	1.85E-14

B

WT undifferentiated vs *Hdac4* KO differentiated beating cells



Top 25 upregulated genes

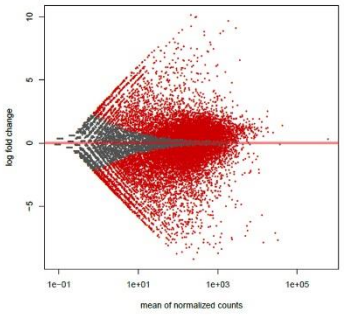
Gene ID	log2(FC)	P-adjusted
Mgp	9.410841	9.71E-44
Pgm5	9.274415	4.83E-26
Tcf21	9.143624	4.61E-42
Fgb	9.117958	3.89E-20
Ccl3	8.959591	1.00E-23
Afp	8.835217	4.53E-39
Cd93	8.791877	1.83E-25
Dnm3os	8.789753	7.07E-49
Pf4	8.722646	6.46E-23
Apoa1	8.709329	9.45E-21
F13a1	8.632979	4.91E-22
Ttr	8.488118	2.43E-31
Sparcl1	8.476496	3.96E-43
Agtr2	8.35185	1.67E-22
Col6a3	8.260189	1.77E-44
Hspb7	8.258977	2.07E-23
Nr2f2	8.185972	1.45E-215
Cx3cr1	8.173037	1.55E-44
C1qc	8.1298	1.94E-19
Alb	8.124663	1.75E-16
Igfbp1	8.091735	1.97E-20
Gria1	8.047328	6.21E-19
Mylk	8.034003	7.82E-24
Lilrb4a	8.016527	3.99E-19
Ccl4	8.012069	1.07E-18

Top 25 downregulated genes

Gene ID	log2(FC)	P-adjusted
2310043M15Rik	-8.64709	1.08E-23
Nkx6-3	-6.36312	5.02E-12
Krt42	-6.05947	2.17E-47
Cyp2j13	-5.98885	7.30E-11
Acsbg3	-5.85637	1.02E-39
Chrna9	-5.84347	2.22E-16
Gbx2	-5.80885	1.79E-28
Ube2dnl1	-5.79833	1.67E-09
Kirrel2	-5.77281	8.41E-10
Fgf17	-5.74152	4.73E-25
Serpinb6c	-5.71638	3.87E-24
Cpsf4l	-5.47664	1.05E-57
Dpys	-5.4746	1.71E-68
Rinl	-5.47344	2.69E-32
Ifitm7	-5.34851	5.06E-18
Hpdl	-5.29438	3.81E-20
Patl2	-5.29289	8.88E-40
Napsa	-5.1308	8.10E-34
Gm32885	-5.10825	2.74E-11
Tdh	-5.02192	8.02E-192
Smim40	-5.01704	1.94E-85
Psma8	-5.00511	1.62E-25
Platr10	-4.98009	2.05E-76
9430069I07Rik	-4.93064	4.34E-07
Slc28a1	-4.89024	1.36E-54

C

WT undifferentiated vs TSA-treated differentiated cells



Top 25 upregulated genes

Gene ID	log2(FC)	P-adjusted
Fgb	9.214887	2.20E-25
Pgm5	8.801355	2.03E-25
Hand2	8.729614	7.75E-162
Dnm3os	8.687279	4.85E-56
Fmod	8.653431	1.61E-25
Afp	8.404693	8.56E-61
Ifi27	8.36694	2.72E-56
Hand2os1	8.305572	4.85E-37
Hapln1	8.271928	1.04E-43
Alb	8.265816	4.30E-41
Rtl1	8.143965	2.11E-21
Col14a1	8.023745	1.10E-52
Lum	8.023223	8.21E-62
Tmem132c	8.015867	1.89E-41
Dkk2	7.999405	6.99E-175
Tbx5	7.967797	2.40E-20
Ccl17	7.903389	8.78E-18
Postn	7.891951	4.17E-238
Dlk1	7.886104	0
Pitx1	7.880952	9.25E-122
Mgp	7.872727	1.46E-29
Ttr	7.870535	5.51E-54
Hspb7	7.864939	3.89E-21
Csf1r	7.687563	4.24E-20
H19	7.673179	0

Top 25 downregulated genes

Gene ID	log2(FC)	P-adjusted
Platr10	-10.1352	1.10E-33
Tcl1	-10.0063	7.64E-37
Fgf4	-9.96195	2.94E-37
Tdh	-9.66604	1.68E-227
Fam25c	-9.24138	5.15E-39
Tdgf1	-9.10668	0
Dpys	-8.96846	5.50E-29
Trh	-8.89046	3.86E-213
Nr0b1	-8.85337	4.41E-87
Cpsf4l	-8.71783	3.61E-27
Lefty2	-8.69272	4.26E-62
Gdf3	-8.53422	4.38E-101
2310043M15Rik	-8.27667	1.13E-23
Mup6	-8.0023	2.85E-22
Mymx	-7.97066	2.32E-27
Esrrb	-7.97006	1.96E-129
Slc28a1	-7.90594	1.78E-33
Nanog	-7.81095	5.85E-180
Nphs1	-7.7244	3.97E-20
Dppa3	-7.67115	2.78E-48
Ooep	-7.67016	4.82E-48
1700029P11Rik	-7.59943	4.02E-18
Septin1	-7.58332	3.04E-33
Morc1	-7.53305	7.35E-73
Tcf15	-7.48539	1.04E-104

Figure 4-9. Differential gene expression analysis of WT undifferentiated and differentiated beating cells shows a significant change in gene expression. For each comparison, top 25 up an downregulated genes are shown.

4.3.5 Effect of TSA treatment and *Hdac4* knockout on beating cells

To investigate any similarities or differences on beating between pan-class IIa chemical ablation and genetic knockout of *Hdac4*, the gene expression profiles of treated beating cells were analysed.

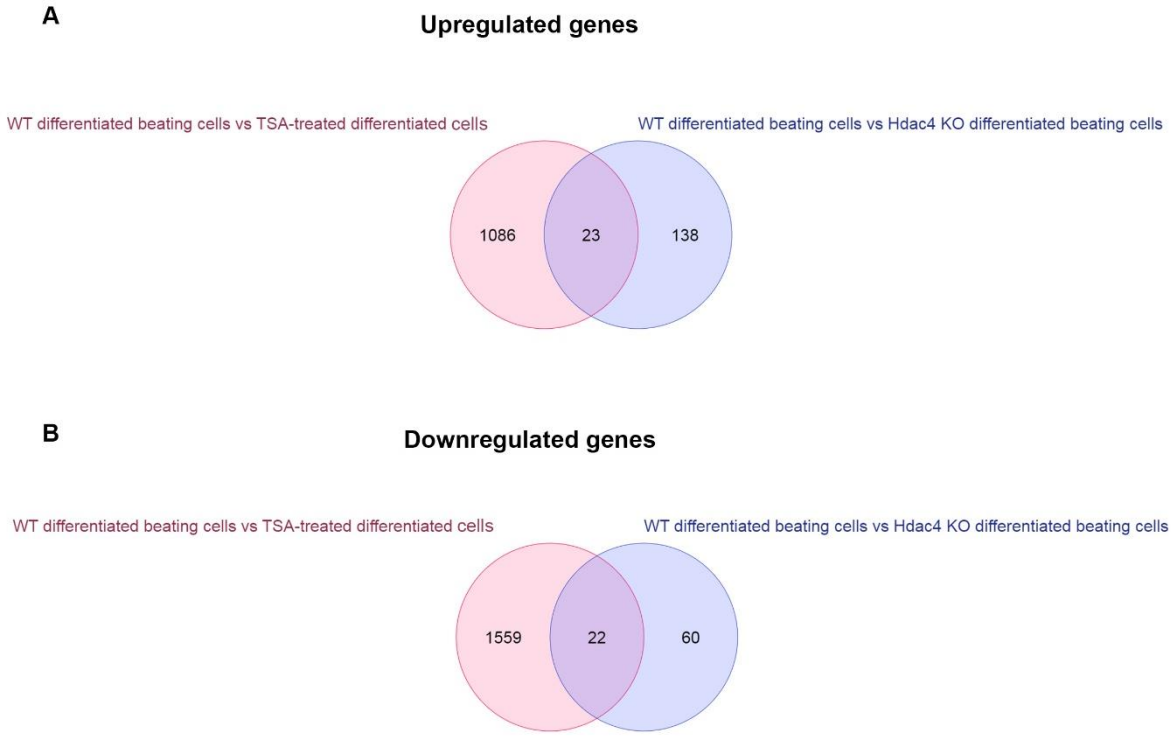


Figure 4-10. Comparing differentially expressed genes in WT beating vs TSA treated or Hdac4 KO showed a small number of similarly regulated genes.

The 23 genes at the intersection of upregulated genes only generated two pathways, namely “cellular response to UV-c” and “regulation of apoptotic signalling pathway”. The 22 genes at the intersection of downregulated genes did not result in any significantly enriched pathways. Genes that were up- or down-regulated in wild-type differentiated beating vs TSA-treated cells (1086 genes in the red circle in panel A and 1559 genes in red circle in panel B in Figure 4-10 above) and wild-type differentiated beating vs *Hdac4* KO differentiated beating cells (138 genes in the

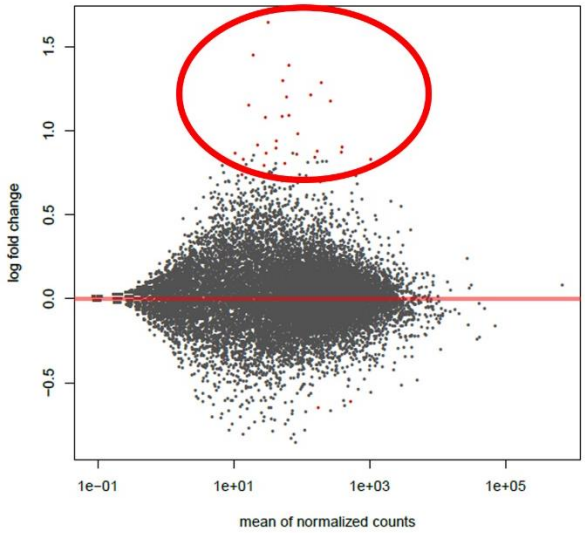
blue circle and 60 genes in blue circle in panel B of Figure 4-10 above) were then queried for enriched biological pathways. The genes upregulated in the TSA treatment only were enriched for pathways involved in general development such as "developmental process" (GO:0015081), "regulation of molecular function" (GO:0065009) and "multicellular organism development" (GO:0007275). While genes upregulated in the knockouts only were enriched for metabolic pathways such as "nucleic acid metabolic process" (GO:0090304), "cellular aromatic compound metabolic process" (GO:0006725) and "cellular nitrogen compound metabolic process" (GO:0034641).

In both treatment groups, downregulated genes were enriched for pathways that involve the immune system such as "immune system response" (GO:0002376) and "response to cytokine" (GO:0034097). The knockout beating cells in particular, showed an enrichment for "cellular response to interferon-beta" (GO:0035456, GO:0035458) and "cellular response to interferon-alpha" (GO:0035457)

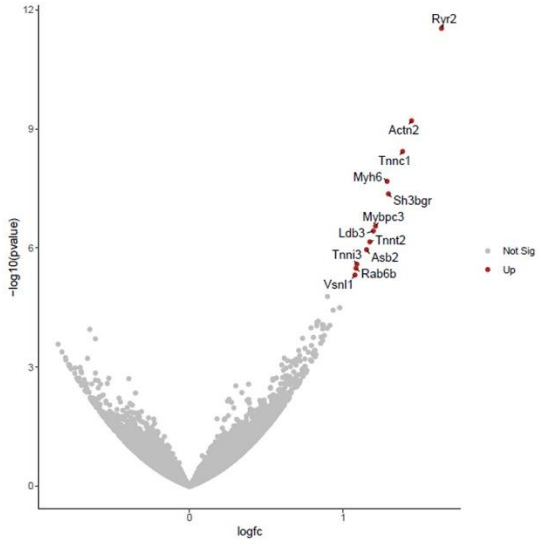
4.3.6 Contractility protein-coding genes are differentially expressed in the beating state

Despite cells always being differentiated and treated the same way, not all went through to show beating. A comparison was made between differentiated cells in the beating and non-beating states to study the genetic basis of differentiation. This aimed to elucidate which genes were being differentially expressed in the beating phenotype. There were no significantly downregulated genes. Panel A of Figure 4-11 shows an MA plot of the comparison with the upregulated genes circled. A volcano plot where statistical significance (-log (p-value)) was plotted against log fold change (panel B). The genes with the highest fold change at the highest significance are indicated. These genes are also outlined in the table in panel C. Table 4-3 provides an overview of the proteins encoded by their genes and their function in the heart, if any. *Sh3bgr* was of particular interest. While its expression has been mapped to the heart, it is yet to be implicated in CHDs.

A



B



C

Gene ID	log2(FC)	Adjusted p-value
Ryr2	1.641874	4.53E-08
Actn2	1.447021	4.81E-06
Tnnc1	1.388491	1.90E-05
Sh3bgr	1.296203	0.000133
Myh6	1.287061	8.04E-05
Mybpc3	1.212197	0.000721
Ldb3	1.197479	0.000819
Tnnt2	1.174712	0.001344
Asb2	1.153627	0.001883
Tnni3	1.090443	0.003919
Rab6b	1.084919	0.004527
Vsnl1	1.078337	0.006129
Rbm24	0.979022	0.035128
Add2	0.935877	0.037752
Chd7	0.899155	0.01971

Figure 4-11. Comparison of wild-type differentiated beating and non-beating cells showed an upregulation of contractility protein-coding genes.

Table 4-3. A summary of the functions of the upregulated genes in the beating cells.

Gene	Protein	Function	Reference
Ryr2	Cardiac ryanodine receptor 2	Binds to calmodulin, involved in regulation of cardiac contraction,	(Nadadur *et al.*, 2017; Sun *et al.*, 2021)

		cytosolic Ca2+ release and ion transport and development of the left ventricle. Loss-of-function mutation has recently been associated with a new disorder, Ryr2 calcium release deficiency syndrome. Gene expression is repressed by PITX2, which is directly activated by TBX5	
Actn2	α-actinin 2	Located in the Z-disc of sarcomeres anf functions in muscle contraction. Mutations in this gene were linked to dialated cardiomyopathy and arrhythmogenic right ventricular cardiomyopathy	(Guo *et al.*, 2021)
Tnnc1	Troponin C1	Key regulatory protein of muscle contractions, mutations in Tnnc1 are linked to dialated cardiomyopathy	(Mahmud *et al.*, 2021)
Sh3bgr	SH3-binding domain glutamic acid-rich protein	Not well-characterised, mutations have been mapped to chromosome 21in the Down syndrome CHD region	(Egeo *et al.*, 2000)
Myh6	Myosin heavy chain 6	Involved in cardiac differentiation, encodes fir the α heavy chain subunit of cardiac myosin which functions in muscle contractions. Mutations are associated with familial hypertrophic cardiomyopathy and ASD	(Zuo *et al.*, 2022)
Mybpc3	Myosin binding protein C3	Expressed exclusively in the heart muscle and regulates cardiac contraction by binding myosin. Mutations in Mybpc3 can lead to hypertrophic cardiomyopathy	(Fernández Suárez *et al.*, 2023)
Ldb3	LIM domain binding protein 3	Interacts with α-actinin 2 and is involved in cytoskeletal assembly.	(Koopmann *et al.*, 2023)

		Mutations have been linked with myofibrillar myopathy and dialated cardiomyopathy	
Tnnt2	Troponin T2	Encodes a subunit of the troponin complex that regulates calcium concentration-dependent contractions. Mutations can lead to familial hypertrophic cardiomyopathy and dilated cardiomyopathy	(Tsaturyan *et al.*, 2023)
Asb2	Ankyrin repeat and SOCS box containing protein 2	Encodes a subunit of the ubiquitin E3 ligase complex which regulates the degradation of actin-binding proteins. Knockouts, FHF and SHF mutations are all embryonic lethal due to heart defects. Mutations in the anterior heart field result in DORV. It is involved in cardiac morphogenesis	(Yamak *et al.*, 2020)
Tnni3	Troponin I3	Encodes the inhibitory subunit of the troponin complex, mediating muscle relacation by blocking actin-mypsin interactions. Mutations lead to familial hypertrophic cardiomyopathy and familial restrictive cardiomyopathy	(Tian *et al.*, 2022)
Rab6b	Ras-related protein Rab-6B	Not thoroughly characterised. Involved in Golgi apparatus vesicular transport	(Seifert *et al.*, 2015)
Vsnl1	Visin like protein 1	Encodes a neuronal calcium sensor protein that modulates intracellular pathways	(Halbgebauer *et al.*, 2022)
Rbm24	RNA binding motif protein Y-linked family 1 member A1	Contains an RNA-binding motef and is predicted to regulate splicing in spermatogenesis	(Yan *et al.*, 2017)

Add2	Adducin 2	Encodes a subunit of the adducin membrane skeletal proteins. They have been linked with regulating blood pressure in hypertension animal models	(Kardia *et al.,* 2007)
Chd7	Chromodomain helicase DNA binding protein 7	Chromatin remodeller where mutations cause CHARGE syndrome	(Sanosaka *et al.,* 2022)

Abbreviations: ASD, atrial septal defect; CHARGE, coloboma, heart disease, atresia of the choanae, retarded growth and mental development, genital anomalies, and ear malformations and hearing loss; CHD, congenital heart disease; DORV, double outlet right ventricle; FHF, first heart field; SHF, second heart field.

4.3.7 Ingenuity Pathway Analysis

To query the RNA-Seq data and put it in biological context, Ingenuity Pathway Analysis (IPA, Qiagen, Heidelberg, Germany) was used to analyse expression data. IPA is an advanced bioinformatic tool with a built-in knowledge base. The knowledge base is a curated collection of experimentally validated data. Using algorithms, IPA is able to delineate the molecules, genes, proteins, chemicals and drugs responsible for the gene expression pattern seen in the data (Krämer *et al.*, 2014). IPA can also show the relationships between these molecules and generate molecular networks based on published experimental data or infer these relationships using machine learning if experimental evidence is unavailable. IPA is able to generate graphical summaries of the data, identity enriched canonical pathways, functions, regulators, causal networks and clinically-relevant phenotypes.

Due to licensing restrictions and download limits, "Canonical pathways", "Tox functions and Graphical summary" were chosen to include in this thesis. The aim of this analysis was to observe if cardiac-related pathways were enriched in the different cell groups and to investigate the effect of *Hdac4* knockout.

In this study, lists of differentially expressed genes in pairwise comparisons were input into IPA to as follows:

- Wild-type undifferentiated vs wild-type differentiated beating
- Wild-type undifferentiated vs wild-type differentiated non-beating
- Wild-type undifferentiated vs *Hdac4* KO beating
- Wild-type undifferentiated vs *Hdac4* KO non-beating
- Wild-type undifferentiated vs TSA-treated
- Wild-type differentiated beating vs wild-type differentiated non-beating
- Wild-type differentiated beating vs *Hdac4* KO beating
- Wild-type differentiated beating vs TSA-treated
- Wild-type differentiated non-beating vs *Hdac4* KO non-beating
- TSA-treated vs *Hdac4* KO beating

Lists of genes and their corresponding fold-change, p-value and false discovery rate were input into IPA for each of the comparisons above.

4.3.7.1 Canonical pathways involved in cardiac hypertrophy are activated

The first analysis conducted comprised of entering all comparisons into IPA at once and looking at enriched biological pathways. The 'Canonical Pathways' feature was used. In this analysis, IPA identifies established signalling or metabolic pathways that were either activated or inhibited based on differential gene expression. IPA also generates z-scores (Table 4-4) . These are based on statistical tests and z-scores with an absolute value greater than or equal 2 is considered statistically significant. The z-score is a representation of the ratio of identified DEGs compared to all the genes in that pathway. A positive value indicates that the canonical pathways was activated. A negative z-score indicates that the pathway was inhibited. A z-score of 0 means that the values for activation and inhibition were equal so no prediction about the pathway can be made. Out of a total of 414 pathways, 335 were either activated or inhibited in at least one of the comparisons. The full list can be found in the appendix.

Of the 335, 5 were related to cardiac signalling (ranked 3, 12, and 15, 206, 283 out of 335, respectively). The names and z-scores are detailed in the Table 4-4 below. The comparisons (WT diff B vs WT diff NB) and (WT diff B vs *Hdac4* KO B) resulted in z-score values of 0.

The results showed an increase in cardiac signalling activation in the differentiated cells, specifically signalling related to cardiac hypertrophy. Cardia hypertrophy-associated pathways also included "Role of NFAT in cardiac hypertrophy" though that did not reach statistical significance in all comparisons. Cardiac β-adrenergic signalling was only significantly inhibited in the WT vs *Hdac4* KO differentiated non-beating cells. Apelin cardiac fibroblast signalling pathway was found to be inhibited only in the WT TSA B vs *Hdac4* KO B comparison, at an exact value of -2.

Table 4-4. Canonical pathway analysis indicates that cardiac hypertrophy signalling is enhanced in the differentiated state.

Canonical Pathways	WT undiff vs WT diff B	WT undiff vs WT diff NB	WT undiff vs *Hdac4* KO B	WT undiff vs *Hdac4* KO NB	WT undiff vs TSA B	WT diff NB vs *Hdac4* KO diff NB	WT diff B vs TSA B	WT TSA B vs *Hdac4* KO B
CREB Signaling in Neurons	9.935	9.815	10.839	10.604	8.066	-1.342[ns]	-3.101	4.006
Phagosome Formation	9.035	8.832	9.767	9.549	6.971	-1.606	-5.039	5.41
Cardiac Hypertrophy Signaling (Enhanced)	7.869	7.519	8.493	8.951	7.391	-0.229[ns]	-3.677	2.324
Pulmonary Fibrosis Idiopathic Signaling Pathway	7.385	7.606	8.795	8.327	6.976	0.728[ns]	-3.464	3.101
Wound Healing Signaling Pathway	8.024	8.091	7.937	7.981	7.136	0.894[ns]	-2.92	3.286
Hepatic Fibrosis Signaling Pathway	7.3	7.561	7.956	7.675	7.034	-0.447[ns]	-3.753	2.832
GP6 Signaling Pathway	6.671	6.952	6.671	6.765	5.986	2.309	-4.243	4.352
G-Protein Coupled Receptor Signaling	7.276	7.338	8.397	7.595	5.986	-1.279[ns]	-2.683	3.085
Breast Cancer Regulation by Stathmin1	7.366	7.35	8.772	7.829	6.23	-0.5[ns]	-2.54	2.929

Colorectal Cancer Metastasis Signaling	7.319	7.758	7.677	7.695	6.807	1 ns	-3.53	1.4 ns
Synaptogenesis Signaling Pathway	6.592	6.187	6.091	6.519	5.768	-0.577 ns	-3.286	2.596
Cardiac Hypertrophy Signaling	6.328	6.601	6.395	6.881	6.466	1.342 ns	-2.065	1.147 ns
IL-8 Signaling	6.51	6.184	6.671	6.6	6.647	-0.378 ns	-2.132	1.279 ns
Calcium Signaling	6.455	5.612	6.119	6.35	4.636	-1.633 ns	-1.667	2.668
Role of NFAT in Cardiac Hypertrophy	6.54	6.466	6.183	6.54	6.037	0.378 ns	-1.5 ns	1.147 ns
Production of Nitric Oxide and Reactive Oxygen Species in Macrophages	5.367	5.823	5.063	5.498	5.185	0.632 ns	-3.545	3.266
Neuroinflammation Signaling Pathway	6.582	6.237	5.635	5.942	4.87	0 ns	-2.534	2.16
ILK Signaling	5.421	5.58	5.969	6.053	5.185	-0.378 ns	-2.236	3
Integrin Signaling	5.009	5.356	5.085	5.662	5.341	-1 ns	-2.683	2.4
Tumor Microenvironment Pathway	4.472	3.882	5.742	5.735	4.359	-0.775 ns	-3	3.773
eNOS Signaling	5.88	5.798	5.252	6.021	5.374	N/A	-2.138	1.265 ns
Oxytocin Signaling Pathway	5.364	4.666	5.613	5.757	4.9	-0.905 ns	-1.3 ns	2.828
STAT3 Pathway	4.907	4.901	5.485	5.555	5.217	0.447 ns	-2.673	2.138

Adrenomedullin signaling pathway	5.444	5.607	5.208	5.208	4.391	0.378 [ns]	-2.6	2.449
Signaling by Rho Family GTPases	5.814	5.59	4.95	5.277	5.812	0.447 [ns]	-1.633 [ns]	1.4 [ns]

[Ns]: not significant

4.3.7.2 Tox functions associated with cardiac disease are inhibited

In addition to enriched metabolic pathways, IPA is able to generate lists of "Tox Functions". These show the relationship between experimental data and known pathologies. Tox Lists are composed of molecules known to play a role in a particular type of toxicity or clinical phenotype. These are genes involved in biological processes and key toxicological responses (Qiagen, Heidelberg, Germany). IPA uses the name tox functions as a proxy for clinical pathology endpoints. This feature is able to link changes in gene expression to known clinical phenotypes and predict responses to drugs.

The same comparisons as in the previous section were input into the software to look for Tox functions that are a result of differential gene expression. As with the Canonical Pathways function, IPA generates a z-score for each Tox Function. A z-score with an absolute value of greater than or equal to 2 is statistically significant. Out of a possible 743 pathways, 105 were identified to be activated or inhibited in the dataset. Table 4-5 below shows the top 20 Tox functions. The full list can found in the appendix. The comparisons (WT diff B vs WT diff NB) and (WT diff B vs *Hdac4* KO B) resulted in z-score values of 0.

Table 4-5. Tox function analysis showed an enrichment for congenital heart disease related pathway inhibition.

Tox Functions	**WT undiff vs WT diff B**	**WT undiff vs WT diff NB**	**WT undiff vs *Hdac4* KO B**	**WT undiff vs *Hdac4* KO NB**	**WT undiff vs TSA B**	**WT diff NB vs *Hdac4* KO diff NB**	**WT diff B vs TSA B**	**WT TSA B vs *Hdac4* KO B**
Tox functions								

Congenital heart disease	-6.216	-5.694	-6.779	-6.919	-4.823	2.321	1.834^{ns}	-2.997
Atrial or ventricular septal defect	-4.439	-3.945	-5.319	-5.35	-3.789	1.891^{ns}	1.643^{ns}	-3.398
Ventricular septal defect	-4.315	-3.893	-5.055	-5.173	-3.692	1.729^{ns}	2.138	-3.432
Hydronephrosis	-5.07	-5.349	-4.66	-5.07	-4.442	0	1.652^{ns}	-3.098
Increased Levels of Alkaline Phosphatase	4.53	4.767	5.654	4.83	3.906	-0.359^{ns}	-1.309^{ns}	2.633
Increased activation of alkaline phosphatase	4.501	4.821	5.503	4.65	3.931	-0.079^{ns}	-1.132^{ns}	2.494
Familial congenital heart disease	-4.775	-4.111	-4.422	-4.794	-3.606	0	0	-2.132
Conotruncal heart malformations	-4.562	-3.874	-4.199	-4.584	-3.349	0	0	-1.913^{ns}
Activation of hepatic stellate cells	3.936	3.862	4.172	4.163	4.188	0.555^{ns}	-0.415^{ns}	0.696^{ns}
Persistent truncus arteriosus	-4.36	-4.002	-3.964	-4.367	-3.361	0	0	-1.89^{ns}
Congestive heart failure	-3.557	-3.44	-3.911	-3.5	-3.96	0	1.432^{ns}	-1.764^{ns}
Increased Levels of ALT	2.967	3.338	3.354	2.807	2.809	0	-2.8	2.941

Increased Levels of LDH	3.498	3.874	3.874	3.62	3.064	0	-1.294 ns	1.777 ns
Failure of heart looping	-3.761	-3.761	-3.889	-4.208	-3.499	0	0	0
Proliferation of kidney cells	3.06	3.183	3.275	2.944	3.448	-1.04 ns	-0.666 ns	1.459 ns
Increased Levels of Red Blood Cells	2.865	2.878	3.661	4.36	2.706	-1 ns	-0.647 ns	0.594 ns
Atrial septal defect	-2.781	-2.504	-3.502	-3.421	-2.424	0.896	0.816	-2.138
Nephritis	-3.268	-3.125	-3.381	-2.428	-3.206	-2.043	-0.165	-0.614
Hypoplasia of heart ventricle	-3.853	-3.249	-3.853	-3.379	-3.842	N/A	N/A	N/A
Increased release of LDH	3.064	3.356	3.066	3.066	3.066	N/A	-1.172	1.292

ns: not significant

The top 20 results showed that differential gene expression in the comparisons correlated with an activation/inhibition of 10 cardiac-related diseases. Some cardiac tox functions were activated though not significantly, except “ventricular septal defect” in the WT diff B vs TSA treated comparison. This indicates an increase in expression of genes associated with that as a result of TSA treatment in the differentiated state.

4.3.8 IPA graphical summary suggests DNA methylation plays a role in cardiomyocyte beating

In addition to functional enrichment, IPA can be used to infer relationships between these enriched pathways or biological functions, revealing interaction networks that may drive changes in gene expression. The Graphical Summary feature provides an overview of the major biological themes in the data and how they are related to one

another. To generate these summaries, IPA uses the most significant entities. The software uses the IPA Knowledge Base to plot relationships based on experimentally validated data and machine learnings to infer these relationships if they did not exist in the Knowledge Base. All entities in the graphical summary are statistically significant ($p<0.05$ Fisher's test and $|z\text{-score}|\geq 2$).

This feature was used to query the molecular basis of beating, to uncover possible novel regulators. The DGE coparison of wild-type differentiated beating cells vs wild-type differentiated non-beating was input into the software. The network generated is shown in Figure 4-12. The network revealed a positive feedback loop between the transcription factors Tbx5, Gata4 and Mef2c, where they were all activated. These are known cardiac regulators and are sufficient to induce transdifferentiation from fibroblasts to cardiomyocytes (Efe *et al.*, 2011; Wang *et al.*, 2015; Isomi *et al.*, 2021). Moreover, the shoftware predicted a role for DNA methyltransferases Dnmt3a and Dnmt3b, in addition to lysine specific demethylase 5 Kdm5a. They were all significantly downregulated. Dotted lines on the network signify a relationship that was inferred using machine learning. The direction of that relationship between Gata4 and Dnmt3b and between Dnmt3b and Kdm5 could not be determined. This result suggests that DNA methylation, or the absence of it, plays a role in regulating master cardiac regulators.

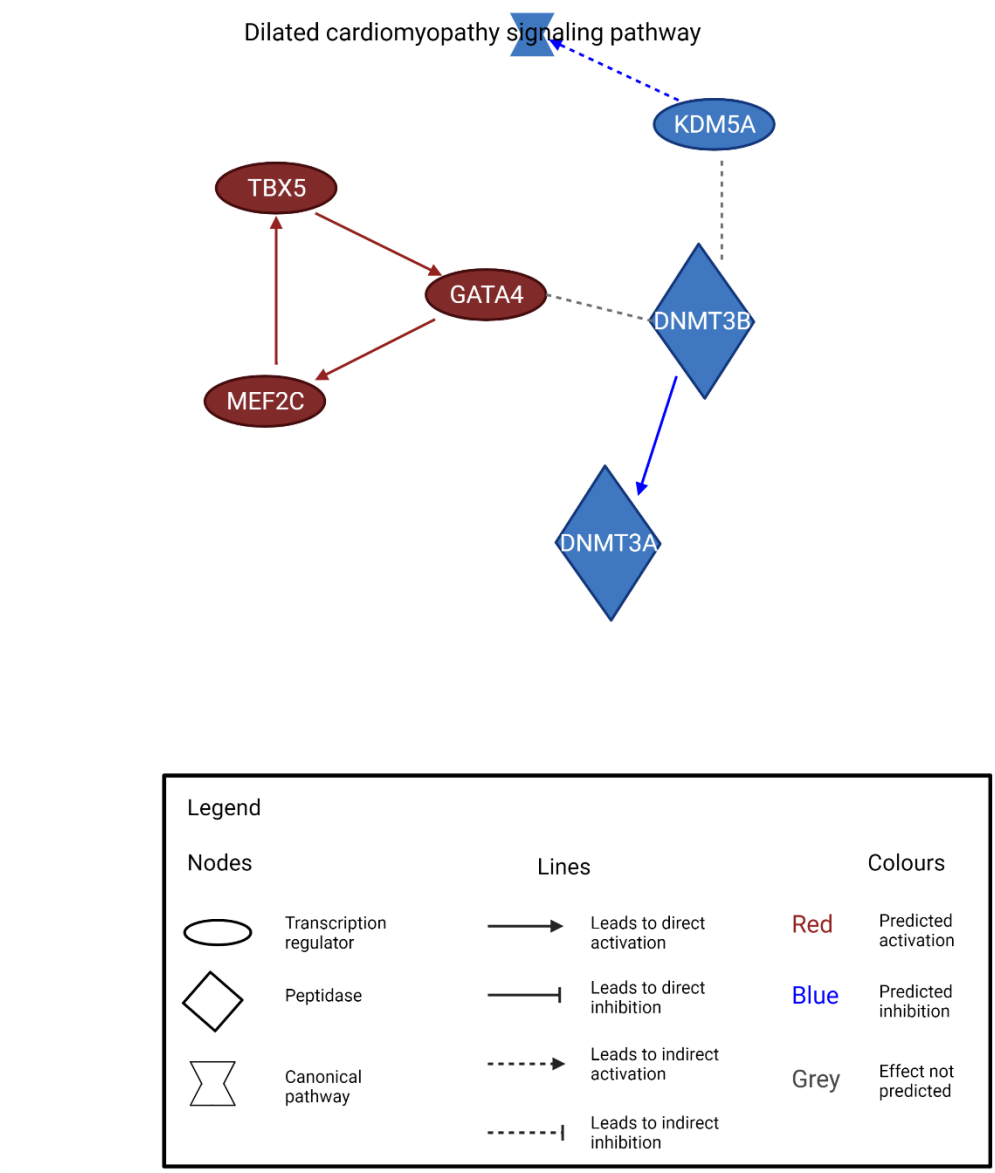


Figure 4-12 Graphical summary of DGE results between wild-type beating and differentiated non-beating cells reveal a possible role for DNA methylation in cardiomyocyte biology

4.3.9 Graphical summary of wild-type and *Hdac4* KO stem cell-induced cardiomyocytes

The Graphical summary feature was also used to compare wild-type beating cells to *Hdac4* KOs (Figure 4-13). This was done to explore the biological systems that were affected due to the knockout.

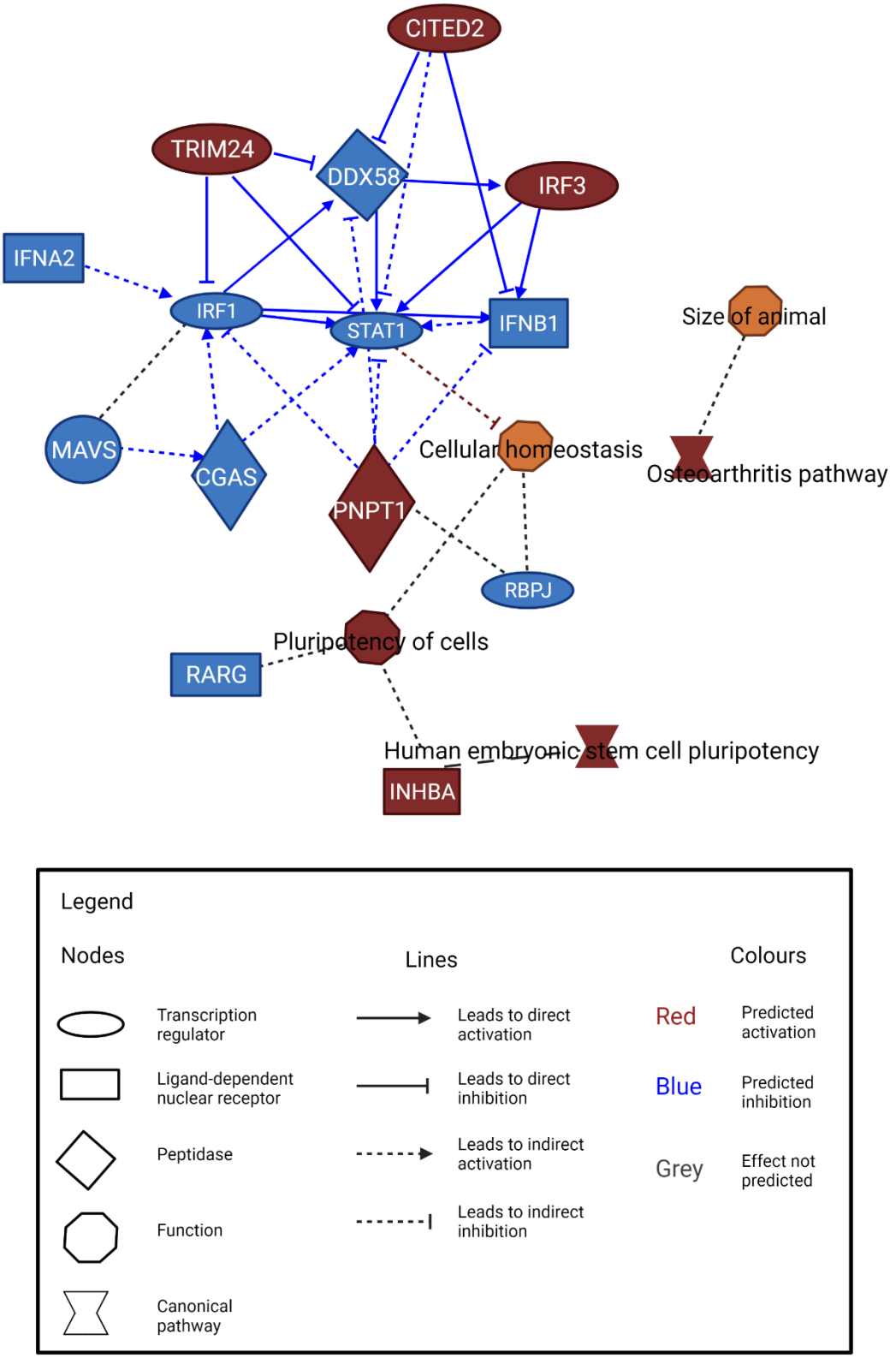


Figure 4-13. Graphical summary of wild-type and *Hdac4* KO beaters hints at implicating *Hdac4* in interferon signalling in cardiomyocytes

The network showed an upregulation of Cited2 (Cbp/P300-Interacting Transactivator 2), a transcriptional coactivator with a role in embryonic stem cell differentiation (Li *et al.*, 2012). Trim24 was also activated. It is transcriptional coactivator that can recognise the acetylation mark H3K27ac (Tsai *et al.*, 2010). From the data, Cited2 and Trim24 are predicted to inhibit Ddx58, an RNA helicase. Ddx58 was in turn predicted to activate interferon regulatory factor 3 (Irf3). It belongs to a family of homologous proteins that regulate the transcription of interferons and interferon-induced genes. All interferons signal through the JAK-STAT pathway (Antonczyk *et al.*, 2019). Moreover, Mavs and Cgas are both involved in the type 1 interferon signaling pathway.

The network predicted an activation of Pnpt1 and an inhibition of Rbpj which in turn was inferred to be associated with cellular homestasis. The direction of that association (whether Rbpj had an activatory or inhibitory effect on genes in cellular homestasis function) could not be determined. Pnpt1 plays a role in RNA import and its disruption can trigger an altered immune response (Dhir *et al.*, 2018; Pajak *et al.*, 2019).

In association with pluripotency of cells, Rarg and Inhba were inhibited and activated, respectively. Rarg encodes for a retinoic acid receptor (RAR). RARs cooperate with HATs and HDACs to regulate gene expression in determining cell fate (Stefanovic and Zaffran, 2017). Inhba is a member of the TGF-β superfamily of proteins. It has been implicated in cardiac regneration in zebrafish by functioning as a mitogen in cardiomyocytes (Dogra *et al.*, 2017). Overall, the network shows differential expression of factors regulated by acetylation and points to the potential involvement of *Hdac4* in interferon signalling. *Hdac4* was shown to have a role in type 1 interferon signalling and viral replication was enhanced cells lacking *Hdac4*. It was also shown to be a target for degradation during vaccinia virus infection by an interferon agonist (Lu *et al.*, 2019). Additionally *Hdac4* was found to repress the nuclear translocation of Irf3, thus decreasing downstream IFN-β expression by blocking the phosphorylation of Irf3 (Yang *et al.*, 2019).

4.4 Discussion

Embryonic stem cells are an invaluable resource to study embryonic development and possible perturbations. Understanding the complex genetic processes that take place during their differentiation can also get us closer to improving differentiation protocols that may be useful in the context of organ repair. In this study, embryonic stem cells were differentiated into beating cardiomyocytes in their wild-type form, in addition to being treated with a pan-HDAC inhibitor TSA and after CRISPR-Cas9 mediated knockout of *Hdac4*. This was done to investigate a possible role of HDAC proteins and *Hdac4* in cardiac differentiation and if they have a function in the pathogenesis of CHDs.

Attempts to derive pure beating cardiomyocyte populations were not successful. Consequently, the decision was made to use cloning rings to surround the beating clusters and extract RNA from those. For the TSA-treated cells, beating clusters were small, thin and far more spread out. Therefore, RNA in these cases was extracted from whole wells. The heterogeneity in RNA sources may be a confounding factor when interpreting RNA-Seq results. It should also be kept in mind when considering results of this study in the context of the literature, that published work often refers to cardiomyocytes that have been genetically purified from the wider differentiating cell pool.

RNA-Sequencing makes transcriptomic profiling in exquisite detail possible. It has the advantage of not needing prior knowledge of genes involved in the process or cell type being investigated compared to microarrays. It allows for quantitative and comparative measurements of gene expression. It was selected for the wealth of data it provides at an economical cost.

For this study, the 3’ Quant-Seq library generation method followed by sequencing on the Illumina NextSeq sequencer were performed. It offers the advantage of providing detailed information about differentially expressed genes. Since alternative splicing was not an objective of this project, 3’ Quant-Seq was chosen over traditional whole RNA sequencing due to its ease and affordability.

Extracted RNA was subject to strict QC measures and only intact RNA with the highest purity was subject to library preparation and subsequent sequencing. 5

biological replicates per condition were obtained and analysed to increase statistical power. Independent wells in differentiation plates were treated as independent biological replicates.

Exploratory, unsupervised analyses were conducted on the data to study global changes in gene expression. Initial clustering using the top most differentially expressed genes showed that samples clustered well together by group. This suggests that the degree of variance between groups is higher than that among samples within a group. PCA analyses indicated that PC1 was responsible for the highest variance, demonstrating that differentiation itself is the most contributing factor to the change seen in global gene expression change.

It was evident from comparing differentiated beating cells to the undifferentiated wild-types that a global wave of change in gene expression has taken place. Differentiation is a complex, highly dynamic process (Boheler *et al.*, 2002). Conducting enrichment analysis of differentially expressed genes showed the upregulation of biological pathways associated with animal development, organogenesis and anatomical development, consistent with differentiation. It was of note that among the top 20 upregulated pathways, “cardiovascular development” was the only one on the list associated with a particular organ system.

Enrichment analysis also showed the downregulation of pathways associated with ribosomal biogenesis and rRNA processing. The downregulation latter processes were proposed to trigger cell differentiation in a study by Hayashi and colleagues (Hayashi *et al.*, 2014), in line with GO analysis showed in this study. Global translation has been shown to be inhibited in adult and embryonic stem cells. in stem cells, global translation increases in the EBs (Ingolia, Lareau and Weissman, 2011; Tahmasebi, Amiri and Sonenberg, 2019).

In an attempt to query the effect of *Hdac4* KO or TSA treatment, a three-way comparison of differentially expressed genes between each treatment and the undifferentiated “ground state” cells. This comparison was used as a basis to carry out enrichment analysis on genes up- or down-regulated exclusively in each group. These resulted in a similar upregulation pattern in the TSA-treated and *Hdac4* KOs where most terms belonged to developmental cellular processes. It was notable that

in the wild-type beating cells, an upregulation of interleukin-8 and toll-like receptor 2 signalling pathways was seen. IL-8 is known for regulating stemness in small cell lung cancer cells (Jin *et al.*, 2018), inducing angiogenesis and promoting the homing of vascular endothelial cells (L. Wang *et al.*, 2021).

To take a deeper look into the possible biological systems that may underlie the changes in gene expression, IPA software was used. Using its "Canonical pathways" feature, 3 of the top 20 most significant pathways were related to cardiac hypertrophy or signalling pathways, such as NFAT, in hypertrophy. NFAT mediates calcineurin-regulated hypertrophy in the heart (Molkentin, 2004). Looking at those specific genes, it was interesting to see *Hand2* and *Tbx5* among the top most upregulated genes in the TSA-treated cells. This result was particularly interesting considering the cell population the RNA was extracted from. It is normal for non-beating cells to be present in differentiating cardiac populations (Dubois *et al.*, 2011; Friedman *et al.*, 2018). Despite the fact that they were not all beaters, a significant increase in *Tbx5* and *Hand2* expressions was seen. This suggests the possibility of derepression of these genes via acetylation. *Hand1* and *Hand2* are essential for cardiac development and heart morphogenesis (Vincentz, Barnes and Firulli, 2011).

Using IPA's "Tox functions" feature revealed a bias towards cardiac pathologies. The list showed that 10 out of the top 20 clinical phenotypes were driven by the observed change in gene expression in the data. It was of particular interest that with the exception of "congestive heart failure", all of the terms were related to CHDs. These pathologies were consistently inhibited in all comparisons except (WT diff NB vs *Hdac4* KO NB) and (WT diff B vs TSA B) where results were inconclusive. The z-scores did not reach statistical significance in these. However, this particular disparity points towards the regulatory role for HDACs in CHD development. Knockout models for *Hdac2*, *Hdac5* and *Hdac9* have cardiac defects while some heart diseases have been linked to aberrant HDAC activity (Seto and Yoshida, 2014). *Hdac4* expression was shown to inhibit cardiomyogenesis (Kawamura *et al.*, 2005; Hosseinkhani *et al.*, 2007; Mathias, Guise and Cristea, 2015). Class IIa HDACs in particular, have an established role in cardiac hypertrophy. Cardiac remodelling in hypertrophy occurs in response to pressure or injury (Mathias, Guise and Cristea, 2015). Hypertrophy is driven by a "foetal gene programme" which results in the

expression of proteins involved in contractility and calcium absorption (Frey and Olson, 2003). In the absence of hypertrophic stimuli, this gene programme is repressed by nuclear HDACs (McKinsey, Zhang and Olson, 2002; Zhang *et al.*, 2002; Mathias, Guise and Cristea, 2015). Moreover, a significant increase in class I, IIa and IIb HDAC catalytic activity was observed in right ventricles of single ventricle patients relative to non-failing controls (Blakeslee *et al.*, 2017). TSA is also capable of inducing cardiac differentiation of mesodermal cells (C. Karamboulas *et al.*, 2006). Taken in context of what is known about HDAC activity in cardiac development and disease, these results warrant further investigation to find more about HDACs mode of action.

Using IPA's "Graphical summary" feature, an attempt was made to elucidate the genetic basis of beating. As non-beating cells are often found in population of stem-cell-derived cardiomyocytes (Dubois *et al.*, 2011), it would be interesting to see what genes are behind exhibiting a beating phenotype. The schematic that was generated by IPA revealed that a positive feedback loop of TFs Tbx5, Mef2c and Gata4 was driving the upregulation of contractility proteins.

It was notable to see an inhibition of demethylases as a possible explanation for the observed change in gene expression. While the role of histone acetylation has been extensively studied in cardiac development and disease, the role of methylation remains to be determined (Madsen *et al.*, 2020). Histone demethylases Kdm5a, Dnmt3b and Dnmt3a were identified by IPA. The software predicted a relationship between Dnmt3b and Gata4 but could not determine the direction. *Kdm5* encodes for a H3K4me3/me2 histone demethylase and is activated in many cancers as it modulates *p53* function. It also plays a role in tumour angiogenesis (Hu *et al.*, 2018; Yang *et al.*, 2021). Whole-exome sequencing has also implicated *KDM5A* in CHDs (Zaidi *et al.*, 2013; Szot *et al.*, 2018). Studies have shown its involvement in cardiomyopathies by virtue of being activated by lamin protein (Pradas *et al.*, 2020) and suppressing mitochondrial activity (Váraljai *et al.*, 2015). It has been shown to be activated in the development of heart failure (Chen *et al.*, 2017). The network depicted an indirect inhibitory relationship between Kdm5a and dilated cardiomyopathy signalling. These results suggest the possible involvement of *Kdm5a* in regulating the cardiac gene programme.

Controlling dynamic methylation levels in cardiomyocytes requires the cooperation of histone methyltransferases and demethylases. Dnmt3a and Dnmt3b proteins are responsible for de novo methylation at CpG sites (W. Wang *et al.,* 2021). *Dnmt3a* knockout in mice results in stunted development and death at 3 weeks and *Dnmt3b* knockout is embryonically lethal with heart abnormalities (Kaneda *et al.*, 2004; Nührenberg *et al.*, 2015). *Dnmt3b* inducible knockout in adult mice led to spontaneous cardiomyopathy (Vujic *et al.*, 2015). However, a study generating cardiomyocyte-specific knockouts of *Dntm3a* and *Dnmt3b* found them to be dispensable for cardiac remodelling under overload (Nührenberg *et al.*, 2015). In human smooth muscle cells, decreased DNMT3A protein levels resulted in hypomethylation at contractile gene promoters, leading to increased expression (Jeong *et al.*, 2021). *DNTM3A* is also downregulated in patients with tetralogy of Fallot (Sheng *et al.*, 2013). SiRNA knockdown of *Dnmt3a* in cardiomyocytes showed a decreased level of methylation at promoters of *Myh7*, *Myh7b*, *Tnni3* and *Tnnt2*, all crucial for contraction. IPA analysis of *Dnmt3a* siRNA knockdowns indicated an activation of cardiac factors *Gata2*, *Gata4*, *Mef2a*, *Mef2c*, *Mef2d*, *Hand2* and *Nkx2.5* (Fang *et al.*, 2016). In light of these findings, the precise role of methylation in cardiomyocytes warrants further investigation.

Also within the genes upregulated genes in contractility was *Sh3bgr*. *Sh3bgr* was discovered in an effort to map the genes on human chromosome 21, within the CHD region (Mazzocco *et al.*, 2002). Overexpression of *Sh3bgr* was intriguingly found not to affect heart morphogenesis in mice (Sandri *et al.*, 2004). However, studies in *Xenopus* showed that knockdown leads to severe defects in heart development and is necessary for sarcomere function. Overexpression of *Sh3bgr* altered heart and sarcomere morphology (Jang *et al.*, 2015). Its upregulation in the beating cells supports the notion that it is indeed in cardiomyocyte biology and can be a potential candidate causative gene for CHDs.

Using the “Graphical summary” feature to investigate the network that may be driving the changes in gene expression seen when comparing the wild-type beating cells to *Hdac4* knockout beaters revealed the possible inhibitory effect of Cited2. Cited2, in addition to Trim24 and Irf3 were activated. The network showed they were activated and inhibited a host of proteins with roles in interferon signalling.

Cited2 is a transcriptional co-activator that interacts with the histone acetylase p300. It was found to regulate pluripotency and cardiomyocyte differentiation of ESCs. *Cited2* knockout cells showed delayed and disturbed cardiomyocyte differentiation (Li *et al.*, 2012). Moreover, *Trim24* was found to promote cardiomyocyte hypertrophy and was upregulated in hypertrophic or dilated mouse and human hearts (Borlepawar *et al.*, 2017). *Irf3* regulates cardiac fibrosis in induced hypertension and controls cardiac inflammatory cytokine expression in response to myocardial infarction (Tsushima *et al.*, 2011; King *et al.*, 2017). Transcription factor Irf3 controls *Ifnb1* expression post-myocardial infarction (King *et al.*, 2017). Interestingly, it was shown that Hdac4 has an inhibitory effect on *Irf3* in regulating host viral response (Yang *et al.*, 2019).

The network also showed a possible activation of Pnpt1 which may inhibit Stat1. Pnpt1 encodes for a protein with a role in RNA import. Mutations in *Pnpt1* lead to a wide array of phenotypes, including cardiovascular abnormalities. The exact relationship between particular genotypes and phenotypes is yet to be determined (Rius *et al.*, 2019). Stat1 is a transcription factor involved in cardiomyocytes response to ischaemia/reperfusion injury and its deficiency is thought to be protective against myocardial infarction (Mccormick *et al.*, 2012). Downregulated *Rbpj* was depicted to be linked to *Pnpt1* activation. *Rbpj* encodes for the DNA-binding component of the Notch signalling pathway and is ubiquitously expressed as a transcriptional silencer in the absence of Notch (Kulic *et al.*, 2015). In the absence of Notch signal, it assembles a corepressor complex containing NCoR/HDACs (Oswald *et al.*, 2016) and histone demtylases (Xu *et al.*, 2017).

Additionally, an activation of the “pluripotency of cells” function was seen, linked with an inhibition of Rarg. *Rarg* encodes for a retinoic acid receotor. Retinoic acid receptors interact with HATs and HDACs to regulate gene activity and determine cell fate (Stefanovic and Zaffran, 2017).

These results points to a possible activation of *Cited2* due to *Hdac4* knockout. Due to Cited’2 association with p300, a HAT with a known function in cardiac development, and itself being a regulator of cardiac differentiation, this calls for

further validation and study. They also predict a possible role for *Hdac4* in regulating inflammatory signalling via *Irf3*.

Overall the analysis conducted in this chapter showed the global changes in gene expression that took place during cardiac differentiation. The results showed the activation of cardiac-related genes and pathways and suggested that cardiomyocyte contractility may be regulated by methylation. They also pointed towards the involvement of *Hdac4* in regulating Irf3.

5 CHAPTER 5: GENERAL DISCUSSION

The aim of this study was to first establish a cellular model of cardiac differentiation. This was first done by comparing cardiac differentiation ability of P19CL6 embryonic carcinoma cell line and CGR8 embryonic stem cell line. The stem cell line was found to have a higher differentiation efficiency. Next, to address the aim of studying the effect of HDAC inhibition, differentiating cells were treated with Trichostatin A. Moreover, to study the role of *Hdac4* in cardiac differentiation, CRISPR/Cas9 was used to knock out the gene before differentiating the knockout cells. RNA-Seq was then used to analyse gene expression profiles.

Mammalian heart development is a complex feat and cardiomyocyte differentiation is a key process (Bruneau, 2013). Understanding how that takes place can lead us closer to understanding what may go wrong resulting in congenital heart disease (Xin, Olson and Bassel-Duby, 2013). Concurrently, refining differentiation protocols will be key for clinical usage of stem cells for repair .

In this study, two murine cell line models of cardiac differentiation were used, namely the embryonic carcinoma cell line P19CL6 and the embryonic stem cell (mESC) cell line CGR8. They were both differentiated into cardiomyocytes using the established method of hanging drops (Moore *et al.*, 2004; Behringer *et al.*, 2016). This method forms three-dimensional cellular aggregates named embryoid bodies (EBs). These were then plated and observed for the presence of beating clusters. The beating was used as an initial mark of cardiac differentiation. It was apparent that while the two cell lines were both capable of forming EBs, a mark of pluripotency, their ability to differentiate into cardiomyocytes was different. P19 cells were less efficient and produced beating clusters with lower frequency and consistency than mESCs. The latter were therefore the model of choice for this project.

Embryonic stem cells provide a valuable resource to study embryonic cardiac development and the effect of chemical or genetic perturbations on that process (Musunuru, Domian and Chien, 2010). To further understand the genetic events

controlling cardiac differentiation, wild-type mESCs were taken through cardiomyocyte differentiation for 15 days and RNA was extracted for gene expression profiling. Moreover during differentiation, the cells were treated with a pan-Class IIa HDAC inhibitor, Trichostatin A (TSA) to assess its effects on cardiac gene expression. The cells were monitored throughout the treatment and were seen to grow thinner on the plate and beat slower than untreated controls. RNA was also collected at the end of the treatment for transcriptomic profiling.

To take a closer look at the role of a particular Class IIa HDAC, namely HDAC4, a CRISPR/Cas9 experiment was designed to knock out the encoding gene. Guide RNAs were designed using online tools and they were tested *in vitro* for their cleavage efficiency. The guide RNA with the highest efficiency was chosen. Cells were electroporated with a vector containing the guide sequence, *Cas9* mRNA and a selectable marker. Colonies were obtained, expanded and subject to Sanger sequencing to look for any mutations around the target site. 11 mutant colonies were identified and the colony with the largest deletion was selected for further investigation.

The chosen colony, referred to as B5, had a 221-bp deletion within the *Hdac4* gene. The last 25bp of the deleted interval are located in exon 18 of *Hdac4*. Cells from this colony were differentiated as before and observed. Beating onset was not significantly different to that observed in wild-type controls. Visual inspection however, did show that beating was slower and more similar to TSA-treated cells (Movies 4-6 for TSA and 7-9 for B5). At day 15 of differentiation, RNA was also collected for sequencing.

3’ Quant-Seq was chosen for its efficiency in detecting differentially expressed genes while maintaining relative affordability (Moll et al., 2014). All library preps, sequencing and bioinformatics analyses were conducted at Deep Seq at the University of Nottingham. RNA from undifferentiated wild-type mESCs was compared to day 15 differentiated wild-types (beating and non-beating), TSA-treated and *Hdac4* KO (beating and non-beating). RNA-Seq data were further analysed using Ingenuity Pathway Analysis software to understand their biological context.

5.1.1 Embryonic stem cells are better models of heart development

The first objective of the study was to find a cellular model of cardiac differentiation. Attempts at differentiating P19CL6 cells to cardiomyocytes were made, and compared with mESCs. The efficiency and consistency with which mESCs were converted to beating cardiomyocytes were the reasons why they were chosen to be carried forward in experiments. P19CL6 cells do have an intrinsic ability to form beating cardiomyocytes, albeit with DMSO induction. However, the cell line is of a teratoma origin with a euploid karyotype (McBurney, 1993). This makes them unpredictable to apply in clinical settings, despite studies reporting their functionality upon transplantation into infarcted mouse hearts (Ohtsu *et al.*, 2005). P19CL6 cells were found to differentiate to cells deriving from all three embryonic layers but their contribution to the germline is not well characterised (Jasmin et al., 2010).

Notably, they beat slower and more irregularly than host cells. The mechanism with which these cells more readily form cardiomyocytes is also not fully understood. The most accepted explanation is that DMSO frees up intracellular calcium storage, activating a cascade of signalling pathways (Morley and Whitfield, 1993). Moreover, in the context of genome engineering studies, P19s present another challenge, which is their DNA repair mechanisms. Being a cancer cell line, genomic instability caused by gene editing can lead to more unexpected or larger genomic lesions (Kosicki, Tomberg and Bradley, 2018; Thomas *et al.*, 2019). Unpredictable DNA repair events will make comparisons to normal tissue and clinical applications challenging.

On the other hand, mESCs are originally derived from embryonic blastocysts and are pluripotent (Behringer *et al.*, 2016). They do not require chemical induction and can form beating cardiomyocytes spontaneously. They are also karyotypically normal and can be expected to behave more stably upon injection. They can also provide an immense resource for cardiac repair in the clinic. They do not present the problem of tumorigenesis. Therefore, parallels can be drawn from the genetic processes involved during their differentiation to what takes place in a developing embryo. It is hence worthwhile to use them in the context of studying congenital heart diseases.

5.1.2 Effect of chemical HDAC inhibition on cardiac differentiation

Trichostatin A is a known pan-Class I and IIa HDACs inhibitor. TSA and other HDAC inhibitors have been shown to block pathological cardiac changes (reviewed in (Kate L. Weeks and Avkiran, 2015)). The study described in this thesis set out to investigate whether global Class IIa HDAC inhibition would have any effect on cardiogenesis. The results showed that there was no significant difference in beating onset. However, visual inspection of beating videos indicated a difference in speed and beating pattern. Moreover, RNA-Seq data showed a significant upregulation of *Tbx5* and *Hand2* in treated cells. TSA has been shown to increase cardiac gene expression in other studies ((Christina Karamboulas *et al.*, 2006; Hosseinkhani *et al.*, 2007; Chen *et al.*, 2011; Yang *et al.*, 2012; Lim *et al.*, 2013). This suggests that the chemical inhibition of Class IIa HDACs led to the derepression of these genes.

5.1.3 CRISPR/Cas9-mediated knock out of *Hdac4*

TBX5 has been shown to be acetylated by KAT2A and KAT2B (T.K. Ghosh *et al.*, 2018) and deacetylated by HDAC4 and HDAC5 (Ghosh *et al.*, 2019). It was therefore of interest to study the consequences of *Hdac4* knockouts and also compare the consequences to what happens upon widescale chemical inhibition of HDACs. It was interesting to find that RNA-Seq generated profiles of *Hdac4* KO beating cells and TSA treated cells showed a high degree of similarity when performing a differential gene expression (DGE) analysis. This suggests the presence of a common mechanism. It was interesting to see an upregulation of *Tbx5* expression in TSA-treated cells and *Hdac4* KOs, at a level higher than the wild-type beating cells.

CRISPR/Cas9 enables targeted, precise gene editing. However, unexpected genetic events have been commonly reported as results of CRISPR/Cas9-mediated editing, especially in the absence of a repair template (Thomas *et al.*, 2019). The majority of deletions caused by Cas9 cleavage are indels of less than 20 bases in size. Nevertheless, much larger deletions have been described, despite their rarity (Kosicki, Tomberg and Bradley, 2018). Deletions up to 600 bp (Shin *et al.*, 2017), greater than 600 (Ottaviani, LeCain and Sheer, 2014) ,6 kb (Kosicki, Tomberg and Bradley, 2018), 100-800 bp, 2.3 kb (Adikusuma *et al.*, 2018), and an intriguing 42.6 kb (B. A. Parikh *et al.*, 2015) using single sgRNAs were reported. Adikusuma and colleagues described a range of different deletions suggesting that the mechanism

underpinning those is stochastic (Adikusuma *et al.*, 2018). These deletions also appear to be independent of sgRNA CG content (Shin *et al.*, 2017). Moreover, deletions events favour nucleotides upstream rather than downstream of the PAM site (Ottaviani, LeCain and Sheer, 2014). These studies therefore confirm the possibility of deletions larger than expected.

Due to the PCR analysis often used, amplifying small regions containing the target site, these large deletions can be missed (B. A. Parikh *et al.*, 2015). Evidence from DNA extraction and subsequent sequencing of B5 colonies strongly indicated a large deletion. A second band was still not seen on the gel when primers further away from the target site were used. While the absence of a wild-type size band on the gel can suggest a homozygous identical deletion on both alleles, it is unlikely. A possible explanation for that can be the presence of a much larger deletion in the second allele where even the primer sites for the largest product size were removed.

Moreover, the Western blot evidence was not sufficient to make definite conclusions about what took place at protein level. A slightly smaller band than the wild-type was seen but despite optimisation attempts already made, more must be done to ascertain the size of the resultant protein. A possible explanation is that of exon skipping. CRISPR/Cas9-induced exon skipping events have been reported. A study by Chen et al showed that a 55-bp deletion at an intron-exon boundary with 22 of the 55-bp deleted from the exon, was sufficient to lead to skipping of that exon in the migratory locust (Chen *et al.*, 2018). Changes to RNA splicing as consequences of CRISPR/Cas9 have also been described (Mou *et al.*, 2017). A single base mutation in an exon of *FLOT-1* in HeLa cells led to random splicing events (Kapahnke, Banning and Tikkanen, 2016). Frameshift indels have been shown to lead to in-frame skipping of exons that are in multiples of 3 (Lalonde *et al.*, 2017). *Hdac4* exon 18 targeted in this study was 108-bp long. Thus an exon skipping event for this exon would maintain the reading frame of the protein, if translated. A study conducted by Sui et al showed that various lengths of deletions that led to premature termination codons (PTC) can lead to exon skipping in rabbits (Sui *et al.*, 2018). PTCs can trigger nonsense-associated alternative splicing (NAS) that consequently leads to exon skipping to avoid the PTC altogether (Hentze and Kulozik, 1999; Liu *et al.*,

2001). Exon skipping events can lead to the generation of proteins with partial activity (Lalonde *et al.*, 2017).

The concept of in-frame exon skipping may also explain why a significant decrease in *Hdac4* was not reflected in the RNA-Seq data. Had time allowed this aspect could have been investigated further. The RNA-Seq method of choice would read transcripts from the 3' end and produce short reads of 50-100 bp. This would consequently make it challenging to detect a significant decrease in *Hdac4* counts from the RNA-Seq data if an in-frame mutation led to exon 18 skipping.

Results from knock out experiments suggested that *Hdac4* was still expressed. Whether it resulted in a truncated protein with a missing exon remains to be confirmed. Rajan et al produced a HDAC4 truncation homozygous mutation phenotype mouse model. The protein was missing the putative catalytic domain and the C-terminal domain. The mice were viable and survived for over a year with no gross development abnormalities (Rajan et al., 2009). It has been shown that amino acids 118-208 of HDAC4 were sufficient for MEF2C interaction and repression (Wang et al., 1999). Moreover, phosphorylation sites needed for HDAC4 nuclear transport, Ser246, Ser467 and Ser632, in addition to the 14-3-3 interaction position are also located in the N-terminal region. This indicates that amino acids 1-600 are sufficient for HDAC4 nucleo-cytoplasmic shuttling (Grozinger and Schreiber, 2000; McKinsey, Zhang and Olson, 2000; Wang *et al.*, 2000; Backs *et al.*, 2006). Exon 18 of *Hdac4* encodes for amino acids 748-783.

Illustrative analysis of the possible biological themes underlying the differences between *Hdac4* KO differentiated cells and their wild-type counterparts suggests an activation of Cited2. The predicted activation of Cited2 was particularly interesting as it associates with p300, an acetylase. *Cited2* plays a role in cardiomyocyte differentiation (Li *et al.*, 2012). Mutations in this gene have been implicated in congenital heart disease (Sperling *et al.*, 2005; Liu *et al.*, 2014; Dianatpour *et al.*, 2020). Aberrant methylation of the *CITED2* promoter was also implicated in CHDs (Xu *et al.*, 2014). The possible involvement of *Hdac4* in the regulation of *Cited2* in cardiomyocytes would be an interesting avenue of further research.

5.1.4 Contractility proteins may be regulated by methylation

Analysis of differential gene expression of differentiated beating and non-beating cells revealed that contractility proteins may be regulated by methylation. Various studies using mESCs, human iPSCs and human ESCs have reported phenotypic heterogeneity post-differentiation (Paige *et al.*, 2012; Wamstad *et al.*, 2012; Parmacek and Epstein, 2013; Tompkins *et al.*, 2016; Selewa *et al.*, 2020). Results from a study by Friedman and colleagues are in agreement with those seen in this study where non-beating cells showed a lower expression of cardiac factors (Friedman *et al.*, 2018).

IPA software predicted the difference in gene expression to be driven by a positive feedback loop of Tbx5, Mef2c and Gata4. It also predicted these factors to be regulated by demethylase Kdm5a and methyltransferases Dnmt3a and Dnmt3b. DNA methylation is crucial for cardiomyocyte development and disease progression. For instance, *Myh6* and *Myh7* show progressive demethylation in cardiomyocytes purified from new-born compared to adult and failing hearts. *Dnmt3a* and *Dnmt3b* are also thought to be responsible for de novo methylation in cardiomyocytes. Dynamic methylation of the foetal troponin *Tnni1* and adult troponin *Tnni3* genes is mediated by *Dnmt3a/b*. *Tnni1* was demethylated at birth and de novo methylated in adult cardiomyocytes. On the other hand, *Tnni3* was demethylated and methylation marks were laid on after birth (Gilsbach *et al.*, 2014).

In adult cardiomyocytes, demethylated regions were enriched for motifs of cardiac factors such as *Mef2c* and *Gata1*. These TF-binding regions were enriched for histone marks of active chromatin such as H3k4me1 or H3K27ac. Methylation patterns also change in response to chronic pressure overload (Gilsbach *et al.*, 2014).These observations are in line with the software's prediction and emphasise the role of methylation in cardiomyocyte biology. Further insight into the regulatory programme of cardiomyocyte function can aid in developing better differentiation protocols leading to more accurate disease models and therapeutic insights.

5.1.5 Concluding remarks

This study provided a window into the transcriptomic events that take place during cardiac differentiation of stem cells which can be translated into embryonic

cardiogenesis. It also contributed to understanding the role HDACs may play in this process. This can lead to better understanding of the regulatory mechanisms of the cardiac genome and thus, the development of CHDs.

It is evident that HDACs function in transcriptional regulation of cardiac genes. These may be studied further and provide possible treatment targets. HDACs and HDAC inhibitors are already being used as therapeutic targets and treatments. HDAC inhibitors have been shown to block pathological cardiac hypertrophy, improve muscle contractility and reverse malignant cardiac remodelling that happens as a result of ischaemic injury (reviewed in (Habibian and Ferguson, 2018)) . This study has shown that chemical inhibition of HDACs and knocking out *Hdac4* can activate cardiac gene transcription and thus provide a new venue to pursue in treatments for CHDs.

5.1.6 Study Limitations

While the results reported herein offer a better understanding of the role HDACs play in cardiogenesis, we are nowhere near getting the full picture. The complexities of transcriptional and epigenetic regulations of such a complex process are far from being fully deciphered. Further characterisations of the second allele to determine whether an unlikely equal deletion took place on both alleles or if the second allele harbours a larger deletion need to be conducted.

This study has made the following contributions to the field:

- An efficient mESCs cardiomyocyte differentiation model
- Generated transcriptional profiles of cardiac differentiation
- In regards to CRISPR/Cas9, a viable target site in the Hdac4 catalytic domain was found, and reported on gene expression changes in mutated mESCs
- Produced 6 mESC cell lines harbouring mutations in *Hdac4*
- Presented differential gene expression results as a consequence of pan-Class IIa chemical inhibition
- Identified a potential candidate gene for CHDs, *Sh3bgr,* involved in cardiomyocyte contractility

- Showed a link between *Ryr2* and differentiated cardiomyocyte contractility, supporting its involvement in a recently-identified CHD, Ryr2 calcium release deficiency syndrome

The differentiation process described would have benefited from a more detailed analysis of cellular morphology, with the use of morphometric software. Attempts were made at quantifying beating using MYOCYTER but a more detailed analysis and modifying the macro code can be beneficial. Moreover, the study can be improved by optimising TSA-treated differentiated cells, introducing a chemical negative control and mapping out the consequences of TSA treatment at different time points. A time series where RNA is extracted and analysed at regular intervals between D0 and D15 would increase the robustness of the data by elucidating the transcriptional networks that govern lineage commitment. This study can identify time-critical points where TSA or *Hdac4* may affect epigenetic gene control. Additionally, challenges with cell population purity can be circumvented with the use of a selectable marker, such as GFP-tagged Nkx2.5 or α-actinin, which can be used for fluorescence-activated cell sorting. Furthermore, functional analysis of the electrophysiological properties of the different cell groups may have shed light on the effects of the different treatments on beating.

HDAC activity in the cells can also be measured using fluorometric assays for better functional analysis. Time constraints, budget limitations and optimisation difficulties made for barriers that prevented these more detailed analyses.

5.1.7 Future Work

The data obtained from RNA-Seq remain to be validated. This can be done using RT-PCR and qPCR. Moreover, sequencing entire transcriptomes rather than 3’ ends can provide a more detailed gene expression analysis. The cell colonies produced harbouring different mutations and the consequences of those on *Hdac4* gene and the protein remain to be fully characterised. It would also be interesting to investigate the effect of those mutations on HDAC4 interaction with TBX5. This would require further optimisation of the Western blot protocol. Further, the mutant cell lines require characterisation, particularly in their ability to differentiate. CHIP-Seq of the

various colonies and studying acetylation events at individual cardiac genes will also aid the aims of understanding how these genes are regulated.

Thus although some of the aims of the study have been completed successfully much work remains to understand fully the relevance of *Hdac4* to cardiac development and to congenital heart disease.

6 BIBLIOGRAPHY

Abdelwahid, E. *et al.* (2016) 'Stem cell death and survival in heart regeneration and repair.', *Apoptosis : an international journal on programmed cell death*, 21(3), pp. 252–68. Available at: https://doi.org/10.1007/s10495-015-1203-4.

Adiconis, X. *et al.* (2013) 'Comparative analysis of RNA sequencing methods for degraded or low-input samples', *Nature Methods*, 10(7), pp. 623–629. Available at: https://doi.org/10.1038/nmeth.2483.

Adikusuma, F. *et al.* (2018) 'Large deletions induced by Cas9 cleavage', *Nature*, 560(7717), pp. E8–E9. Available at: https://doi.org/10.1038/s41586-018-0380-z.

Adrián Ruiz-Villalba and José M Pérez-Pomares (2012) 'The expanding role of the epicardium and epicardial-derived cells in cardiac development and disease', *Current Opinion in Pediatrics*, 24(5), pp. 569–576. Available at: https://pubmed.ncbi.nlm.nih.gov/22890066/ (Accessed: 13 November 2023).

Afgan, E. *et al.* (2016) 'The Galaxy platform for accessible, reproducible and collaborative biomedical analyses: 2016 update', *Nucleic acids research*, 44(W1), pp. W3–W10. Available at: https://doi.org/10.1093/NAR/GKW343.

Akerberg, B.N. *et al.* (2019) 'A reference map of murine cardiac transcription factor chromatin occupancy identifies dynamic and conserved enhancers', *Nature Communications*, 10(1), p. 4907. Available at: https://doi.org/10.1038/s41467-019-12812-3.

Allfrey, V.G., Faulkner, R. and Mirsky, A.E. (1964) 'ACETYLATION AND METHYLATION OF HISTONES AND THEIR POSSIBLE ROLE IN THE REGULATION OF RNA SYNTHESIS', *Proceedings of the National Academy of Sciences*, 51(5), pp. 786–794. Available at: https://doi.org/10.1073/pnas.51.5.786.

Anderson, R.H. *et al.* (2014) 'The development of septation in the four-chambered heart.', *Anatomical record (Hoboken, N.J. : 2007)*, 297(8), pp. 1414–29. Available at: https://doi.org/10.1002/ar.22949.

Anisimov, S. V. *et al.* (2002) 'SAGE identification of differentiation responsive genes in P19 embryonic cells induced to form cardiomyocytes in vitro', *Mechanisms of Development*, 117(1–2), pp. 25–74. Available at: https://doi.org/10.1016/S0925-4773(02)00177-6.

Antonczyk, A. *et al.* (2019) 'Direct inhibition of IRF-dependent transcriptional regulatory mechanisms associated with disease', *Frontiers in Immunology*, 10(MAY), p. 1176. Available at: https://doi.org/10.3389/FIMMU.2019.01176/BIBTEX.

Ao, X. *et al.* (2020) 'TCF21: a critical transcription factor in health and cancer', *Journal of Molecular Medicine*, 98(8), pp. 1055–1068. Available at: https://doi.org/10.1007/S00109-020-01934-7/METRICS.

Ayer, D.E. (1999) 'Histone deacetylases: transcriptional repression with SINers and NuRDs.', *Trends in cell biology*, 9(5), pp. 193–8.

Backs, J. *et al.* (2006) 'CaM kinase II selectively signals to histone deacetylase 4 during cardiomyocyte hypertrophy', *Journal of Clinical Investigation*, 116(7), p. 1853. Available at: https://doi.org/10.1172/JCI27438.

Backs, J. and Olson, E.N. (2005) 'Control of Cardiac Growth by Histone Acetylation/Deacetylation', *Circulation Research*, 98(1), pp. 15–24. Available at: https://doi.org/10.1161/01.RES.0000197782.21444.8f.

Bannister, A.J. and Kouzarides, T. (2011) 'Regulation of chromatin by histone modifications', *Cell Research*. Nature Publishing Group, pp. 381–395. Available at: https://doi.org/10.1038/cr.2011.22.

Barbash, S. *et al.* (2017) 'Neuronal-expressed microRNA-targeted pseudogenes compete with coding genes in the human brain', *Translational psychiatry*, 7(8), p. e1199. Available at: https://doi.org/10.1038/tp.2017.163.

Barnes, R.M. *et al.* (2010) 'Analysis of the Hand1 cell lineage reveals novel contributions to cardiovascular, neural crest, extra-embryonic, and lateral mesoderm derivatives.', *Developmental dynamics : an official publication of the American Association of Anatomists*, 239(11), pp. 3086–97. Available at: https://doi.org/10.1002/dvdy.22428.

Barrangou, R. *et al.* (2007) 'CRISPR provides acquired resistance against viruses in prokaryotes.', *Science (New York, N.Y.)*, 315(5819), pp. 1709–12. Available at: https://doi.org/10.1126/science.1138140.

Barron, M.E. *et al.* (2005) 'Serum response factor, an enriched cardiac mesoderm obligatory factor, is a downstream gene target for Tbx genes', *Journal of Biological Chemistry*, 280(12), pp. 11816–11828. Available at: https://doi.org/10.1074/jbc.M412408200.

Behringer, R. *et al.* (2016) 'Differentiating Mouse Embryonic Stem Cells into Embryoid Bodies by Hanging-Drop Cultures', *Cold Spring Harbor Protocols*, 2016(12), p. pdb.prot092429. Available at: https://doi.org/10.1101/pdb.prot092429.

Berge, D. ten *et al.* (2008) 'Wnt signaling mediates self-organization and axis formation in embryoid bodies', *Cell stem cell*, 3(5), p. 508. Available at: https://doi.org/10.1016/J.STEM.2008.09.013.

Bibikova, M. *et al.* (2002) 'Targeted chromosomal cleavage and mutagenesis in Drosophila using zinc-finger nucleases.', *Genetics*, 161(3), pp. 1169–75.

Blakeslee, W.W. *et al.* (2017) 'Histone Deacetylase Adaptation in Single Ventricle Heart Disease and a Young Animal Model of Right Ventricular Hypertrophy', *Pediatric research*, 82(4), p. 642. Available at: https://doi.org/10.1038/PR.2017.126.

Boheler, K.R. *et al.* (2002) 'Differentiation of pluripotent embryonic stem cells into cardiomyocytes', *Circulation Research*. Lippincott Williams & Wilkins, pp. 189–201. Available at: https://doi.org/10.1161/01.RES.0000027865.61704.32.

Boogerd, C.J.J., Moorman, A.F.M. and Barnett, P. (2009) 'Protein interactions at the heart of cardiac chamber formation.', *Annals of anatomy = Anatomischer Anzeiger : official organ of the Anatomische Gesellschaft*, 191(6), pp. 505–17. Available at: https://doi.org/10.1016/j.aanat.2009.06.004.

Borlepawar, A. *et al.* (2017) 'TRIM24 protein promotes and TRIM32 protein inhibits cardiomyocyte hypertrophy via regulation of dysbindin protein levels', *The Journal of biological chemistry*, 292(24), pp. 10180–10196. Available at: https://doi.org/10.1074/JBC.M116.752543.

Bradley, A. *et al.* (1984) ‘Formation of germ-line chimaeras from embryo-derived teratocarcinoma cell lines’, *Nature*, 309(5965), pp. 255–256. Available at: https://doi.org/10.1038/309255a0.

Brickman, J.M. and Serup, P. (2017) ‘Properties of Embryoid Bodies’, *WIREs Dev Biol*, 6(2), p. e259. Available at: https://doi.org/10.1002/wdev.259.

Brink, S.C. van den *et al.* (2014) ‘Symmetry breaking, germ layer specification and axial organisation in aggregates of mouse embryonic stem cells’, *Development (Cambridge, England)*, 141(22), p. 4231. Available at: https://doi.org/10.1242/DEV.113001.

Brownell, J.E. *et al.* (1996) ‘Tetrahymena histone acetyltransferase A: a homolog to yeast Gcn5p linking histone acetylation to gene activation.’, *Cell*, 84(6), pp. 843–51. Available at: https://doi.org/10.1016/s0092-8674(00)81063-6.

Bruneau, B.G. *et al.* (1999) ‘Chamber-specific cardiac expression of Tbx5 and heart defects in Holt-Oram syndrome.’, *Developmental biology*, 211(1), pp. 100–8. Available at: https://doi.org/10.1006/dbio.1999.9298.

Bruneau, B.G. (2008) ‘The developmental genetics of congenital heart disease.’, *Nature*, 451(7181), pp. 943–8. Available at: https://doi.org/10.1038/nature06801.

Buckingham, M., Meilhac, S. and Zaffran, S. (2005) ‘Building the mammalian heart from two sources of myocardial cells.’, *Nature reviews. Genetics*, 6(11), pp. 826–35. Available at: https://doi.org/10.1038/nrg1710.

Bui, H.-T. *et al.* (2010) ‘Effect of Trichostatin A on Chromatin Remodeling, Histone Modifications, DNA Replication, and Transcriptional Activity in Cloned Mouse Embryos1’, *Biology of Reproduction*, 83(3), pp. 454–463. Available at: https://doi.org/10.1095/biolreprod.109.083337.

Bulatovic, I. *et al.* (2016) ‘Human fetal cardiac progenitors: The role of stem cells and progenitors in the fetal and adult heart’, *Best Practice & Research Clinical Obstetrics & Gynaecology*, 31, pp. 58–68. Available at: https://doi.org/https://doi.org/10.1016/j.bpobgyn.2015.08.008.

Cahan, P. *et al.* (2014) ‘CellNet: network biology applied to stem cell engineering.’, *Cell*, 158(4), pp. 903–915. Available at: https://doi.org/10.1016/j.cell.2014.07.020.

Candido, E.P., Reeves, R. and Davie, J.R. (1978) 'Sodium butyrate inhibits histone deacetylation in cultured cells.', *Cell*, 14(1), pp. 105–13. Available at: https://doi.org/10.1016/0092-8674(78)90305-7.

Cao, D.J. *et al.* (2011) 'Histone deacetylase (HDAC) inhibitors attenuate cardiac hypertrophy by suppressing autophagy.', *Proceedings of the National Academy of Sciences of the United States of America*, 108(10), pp. 4123–8. Available at: https://doi.org/10.1073/pnas.1015081108.

Carreño, J.E. *et al.* (2006) 'Cardiac Hypertrophy: Molecular and Cellular Events', *Revista Española de Cardiología (English Edition)*, 59(5), pp. 473–486. Available at: https://doi.org/10.1016/S1885-5857(06)60796-2.

Chakraborty, S. *et al.* (2010) 'Twist1 promotes heart valve cell proliferation and extracellular matrix gene expression during development in vivo and is expressed in human diseased aortic valves', *Developmental biology*, 347(1), pp. 167–179. Available at: https://doi.org/10.1016/J.YDBIO.2010.08.021.

Chang, S. *et al.* (2004) 'Histone Deacetylases 5 and 9 Govern Responsiveness of the Heart to a Subset of Stress Signals and Play Redundant Roles in Heart Development', *Molecular and cellular biology*, 24(19), pp. 8467–8476. Available at: https://doi.org/10.1128/MCB.24.19.8467-8476.2004.

Chatterjee, A. *et al.* (2018) 'A Guide for Designing and Analyzing RNA-Seq Data', in. Humana Press, New York, NY, pp. 35–80. Available at: https://doi.org/10.1007/978-1-4939-7834-2_3.

Chen, D. *et al.* (2018) 'CRISPR/Cas9-mediated genome editing induces exon skipping by complete or stochastic altering splicing in the migratory locust', *BMC Biotechnology*, 18. Available at: https://doi.org/10.1186/S12896-018-0465-7.

Chen, J.N. and Fishman, M.C. (1996) 'Zebrafish tinman homolog demarcates the heart field and initiates myocardial differentiation.', *Development (Cambridge, England)*, 122(12), pp. 3809–16.

Chen, L. *et al.* (2017) 'Comprehensive Myocardial Proteogenomics Profiling Reveals C/EBPα as the Key Factor in the Lipid Storage of ARVC', *Journal of Proteome Research*, 16(8), pp. 2863–2876. Available at:

https://doi.org/10.1021/ACS.JPROTEOME.7B00165/SUPPL_FILE/PR7B00165_SI_007.XLSX.

Chen, M. *et al.* (2011) 'Enrichment of cardiac differentiation of mouse embryonic stem cells by optimizing the hanging drop method', *Biotechnology Letters*, 33(4), pp. 853–858. Available at: https://doi.org/10.1007/s10529-010-0494-3.

Chen, X. *et al.* (2020) 'LUM Expression and Its Prognostic Significance in Gastric Cancer', *Frontiers in Oncology*, 10. Available at: https://doi.org/10.3389/fonc.2020.00605.

Cherian, A. V. *et al.* (2016) 'N-cadherin relocalization during cardiac trabeculation', *Proceedings of the National Academy of Sciences of the United States of America*, 113(27), pp. 7569–7574. Available at: https://doi.org/10.1073/PNAS.1606385113/-/DCSUPPLEMENTAL.

Choi, S.-C. *et al.* (2004) '5-azacytidine induces cardiac differentiation of P19 embryonic stem cells', *Experimental & Molecular Medicine*, 36(6), pp. 515–523. Available at: https://doi.org/10.1038/emm.2004.66.

Choices, N. (no date) 'Congenital heart disease - NHS Choices'.

Choudhary, C. *et al.* (2014) 'The growing landscape of lysine acetylation links metabolism and cell signalling', *Nature Reviews Molecular Cell Biology*, 15(8), pp. 536–550. Available at: https://doi.org/10.1038/nrm3841.

Christoffels, V.M. *et al.* (2000) 'Chamber Formation and Morphogenesis in the Developing Mammalian Heart', *Developmental Biology*, 223(2), pp. 266–278. Available at: https://doi.org/10.1006/DBIO.2000.9753.

Chung, I.-M. and Rajakumar, G. (2016) 'Genetics of Congenital Heart Defects: The NKX2-5 Gene, a Key Player.', *Genes*, 7(2). Available at: https://doi.org/10.3390/genes7020006.

Clocchiatti, A. *et al.* (2013) 'Beside the MEF2 axis: Unconventional functions of HDAC4', *Cellular Signalling*, 25(1), pp. 269–276.

Collins, B.E. *et al.* (2019) 'Histone H3 lysine K4 methylation and its role in learning and memory 06 Biological Sciences 0604 Genetics 11 Medical and Health Sciences

1109 Neurosciences', *Epigenetics and Chromatin*. BioMed Central Ltd., pp. 1–16. Available at: https://doi.org/10.1186/s13072-018-0251-8.

Cong, L. Le *et al.* (2013) 'Multiplex genome engineering using CRISPR/Cas systems.', *Science*, 339(6121), pp. 819–23. Available at: https://doi.org/10.1126/science.1231143.

Crow, M. *et al.* (2015) 'HDAC4 is required for inflammation-associated thermal hypersensitivity', *The FASEB Journal*, 29(8), pp. 3370–3378. Available at: https://doi.org/10.1096/fj.14-264440.

Das, R. and Fernandez, J.G. (2020) 'Additive manufacturing enables production of de novo cardiomyocytes by controlling embryoid body aggregation', *Bioprinting*, 20, p. e00091. Available at: https://doi.org/10.1016/J.BPRINT.2020.E00091.

DeLaughter, D.M. *et al.* (2013) 'Spatial transcriptional profile of the chick and mouse endocardial cushions identify novel regulators of endocardial EMT in vitro', *Journal of Molecular and Cellular Cardiology*, 59, pp. 196–204. Available at: https://doi.org/10.1016/J.YJMCC.2013.03.016.

Deng, B. *et al.* (2017) 'Nkx2.5 enhances the efficacy of mesenchymal stem cells transplantation in treatment heart failure in rats.', *Life sciences*, 182, pp. 65–72. Available at: https://doi.org/10.1016/j.lfs.2017.06.014.

Deng, X. *et al.* (2015) 'Functional Analysis of Two Novel Mutations in TWIST1 Protein Motifs Found in Ventricular Septal Defect Patients.', *Pediatric cardiology*, 36(8), pp. 1602–9. Available at: https://doi.org/10.1007/s00246-015-1202-9.

Deng, Z. *et al.* (2016) 'Histone Deacetylase Inhibitor Trichostatin a Promotes the Apoptosis of Osteosarcoma Cells through p53 Signaling Pathway Activation', *International Journal of Biological Sciences*, 12(11), pp. 1298–1308. Available at: https://doi.org/10.7150/ijbs.16569.

Derrick, C.J. *et al.* (2022) 'Asymmetric Hapln1a drives regionalized cardiac ECM expansion and promotes heart morphogenesis in zebrafish development', *Cardiovascular Research*, 118(1), pp. 226–240. Available at: https://doi.org/10.1093/cvr/cvab004.

Devaiah, B.N. *et al.* (2016) 'BRD4 is a histone acetyltransferase that evicts nucleosomes from chromatin', *Nature Structural & Molecular Biology*, 23(6), pp. 540–548. Available at: https://doi.org/10.1038/nsmb.3228.

Devine, W.P. *et al.* (2014) 'Early patterning and specification of cardiac progenitors in gastrulating mesoderm', *eLife*, 3, p. 3848. Available at: https://doi.org/10.7554/ELIFE.03848.

Dhir, A. *et al.* (2018) 'Mitochondrial double-stranded RNA triggers antiviral signalling in humans', *Nature*, 560(7717), pp. 238–242. Available at: https://doi.org/10.1038/S41586-018-0363-0.

Dianatpour, S. *et al.* (2020) 'Novel Point Mutations of CITED2 Gene Are Associated with Non-familial Congenital Heart Disease (CHD) in Sporadic Pediatric Patients', *Applied biochemistry and biotechnology*, 190(3), pp. 896–906. Available at: https://doi.org/10.1007/S12010-019-03125-8.

Van Dijk, E.L., Jaszczyszyn, Y. and Thermes, C. (2014) 'Library preparation methods for next-generation sequencing: Tone down the bias', *Experimental Cell Research*. Academic Press Inc., pp. 12–20. Available at: https://doi.org/10.1016/j.yexcr.2014.01.008.

Dobin, A. *et al.* (2013) 'STAR: ultrafast universal RNA-seq aligner', *Bioinformatics*, 29(1), pp. 15–21. Available at: https://doi.org/10.1093/bioinformatics/bts635.

Dobin, A. and Gingeras, T.R. (2015) 'Mapping RNA-seq Reads with STAR', *Current Protocols in Bioinformatics*, 51(1), pp. 11.14.1-11.14.19. Available at: https://doi.org/10.1002/0471250953.bi1114s51.

Doetschman, T.C. *et al.* (1985) 'The in vitro development of blastocyst-derived embryonic stem cell lines: formation of visceral yolk sac, blood islands and myocardium.', *Journal of embryology and experimental morphology*, 87, pp. 27–45.

Dogra, D. *et al.* (2017) 'Opposite effects of Activin type 2 receptor ligands on cardiomyocyte proliferation during development and repair', *Nature Communications*, 8(1). Available at: https://doi.org/10.1038/S41467-017-01950-1.

Dong, Y., Qian, L. and Liu, J. (2021) 'Molecular and cellular basis of embryonic cardiac chamber maturation', *Seminars in cell & developmental biology*, 118, p. 144. Available at: https://doi.org/10.1016/J.SEMCDB.2021.04.022.

Doss, M.X. *et al.* (2007) 'Global transcriptome analysis of murine embryonic stem cell-derived cardiomyocytes.', *Genome biology*, 8(4), p. R56. Available at: https://doi.org/10.1186/gb-2007-8-4-r56.

Drab, M. *et al.* (1997) 'From totipotent embryonic stem cells to spontaneously contracting smooth muscle cells: a retinoic acid and db-cAMP in vitro differentiation model', *FASEB journal : official publication of the Federation of American Societies for Experimental Biology*, 11(11), pp. 905–915. Available at: https://doi.org/10.1096/FASEBJ.11.11.9285489.

Dubois, N.C. *et al.* (2011) 'SIRPA Is a Specific Cell-Surface Marker for Isolating Cardiomyocytes Derived From Human Pluripotent Stem Cells', *Nature Biotechnology*, 29(11), pp. 1011–8. Available at: https://doi.org/10.1038/nbt.2005.

Eckschlager, T. *et al.* (2017) 'Histone Deacetylase Inhibitors as Anticancer Drugs.', *International journal of molecular sciences*, 18(7). Available at: https://doi.org/10.3390/ijms18071414.

Efe, J.A. *et al.* (2011) 'Conversion of mouse fibroblasts into cardiomyocytes using a direct reprogramming strategy.', *Nature cell biology*, 13(3), pp. 215–22. Available at: https://doi.org/10.1038/ncb2164.

Egeo, A., *et al.* (2000) 'Developmental expression of the SH3BGR gene, mapping to the Down syndrome heart critical region', *Mechanisms of development*, 90(2), pp. 313–316.

Elaheh Karbassi *et al.* (2020) 'Cardiomyocyte maturation: advances in knowledge and implications for regenerative medicine', *Nature Reviews Cardiology*, 17(6), pp. 341–359.

Esteban, I. *et al.* (2022) 'Pseudodynamic analysis of heart tube formation in the mouse reveals strong regional variability and early left–right asymmetry', *Nature Cardiovascular Research 2022 1:5*, 1(5), pp. 504–517. Available at: https://doi.org/10.1038/s44161-022-00065-1.

Evans, A.L. *et al.* (2012) 'Genomic Targets of Brachyury (T) in Differentiating Mouse Embryonic Stem Cells', *PLoS ONE*, 7(3). Available at: https://doi.org/10.1371/JOURNAL.PONE.0033346.

Evans, M. and Kaufman, M. (1981) 'Establishment in Culture of Pluripotential Cells From Mouse Embryos', *Nature*, 292(5819). Available at: https://doi.org/10.1038/292154A0.

Fang, X. *et al.* (2016) 'Knockdown of DNA methyltransferase 3a alters gene expression and inhibits function of embryonic cardiomyocytes', *The FASEB Journal*, 30(9), pp. 3238–3255. Available at: https://doi.org/10.1096/FJ.201600346R.

Fatemifar, F. *et al.* (2019) 'Comparison of Biomechanical Properties and Microstructure of Trabeculae Carneae, Papillary Muscles, and Myocardium in the Human Heart', *Journal of Biomechanical Engineering*, 141(2), p. 0210071. Available at: https://doi.org/10.1115/1.4041966.

Fathi, F. *et al.* (2009) 'Cardiac differentiation of P19CL6 cells by oxytocin', *International Journal of Cardiology*, 134(1), pp. 75–81. Available at: https://doi.org/10.1016/J.IJCARD.2008.01.046.

Feinberg, A.W. *et al.* (2013) 'Functional differences in engineered myocardium from embryonic stem cell-derived versus neonatal cardiomyocytes', *Stem Cell Reports*, 1(5), pp. 387–396. Available at: https://doi.org/10.1016/j.stemcr.2013.10.004.

Ferdous, A. *et al.* (2009) 'Nkx2-5 transactivates the Ets-related protein 71 gene and specifies an endothelial/endocardial fate in the developing embryo.', *Proceedings of the National Academy of Sciences of the United States of America*, 106(3), pp. 814–9. Available at: https://doi.org/10.1073/pnas.0807583106.

Fernández Suárez, N. *et al.* (2023) 'Description of a Cohort with a New Truncating MYBPC3 Variant for Hypertrophic Cardiomyopathy in Northern Spain', *Genes (Basel)*, 14(4), p. 840.

Ferreira De Freitas, R. *et al.* (2018) 'Identification and Structure-Activity Relationship of HDAC6 Zinc-Finger Ubiquitin Binding Domain Inhibitors', *Journal of Medicinal Chemistry*, 61(10), pp. 4517–4527. Available at: https://doi.org/10.1021/acs.jmedchem.8b00258.

Festuccia, N. *et al.* (2018) 'Esrrb extinction triggers dismantling of naïve pluripotency and marks commitment to differentiation', *The EMBO Journal*, 37(21). Available at: https://doi.org/10.15252/EMBJ.201695476.

Fijnvandraat, A.C. *et al.* (2003) 'TBX5 overexpression stimulates differentiation of chamber myocardium in P19C16 embryonic carcinoma cells.', *Journal of muscle research and cell motility*, 24(2–3), pp. 211–8. Available at: https://doi.org/10.1023/a:1026063409656.

Fischer, D.D. *et al.* (2002) 'Isolation and Characterization of a Novel Class II Histone Deacetylase, HDAC10', *Journal of Biological Chemistry*, 277(8), pp. 6656–6666. Available at: https://doi.org/10.1074/jbc.M108055200.

Fischle, W., Wang, Y. and Allis, C.D. (2003) 'Histone and chromatin cross-talk', *Current Opinion in Cell Biology*, 15(2), pp. 172–183. Available at: https://doi.org/10.1016/S0955-0674(03)00013-9.

Fournier, M. *et al.* (2016) 'KAT2A/KAT2B-targeted acetylome reveals a role for PLK4 acetylation in preventing centrosome amplification', *Nature Communications*, 7(1), p. 13227. Available at: https://doi.org/10.1038/ncomms13227.

Franco, D. *et al.* (2006) 'Left and right ventricular contributions to the formation of the interventricular septum in the mouse heart', *Developmental Biology*, 294(2), pp. 366–375. Available at: https://doi.org/10.1016/J.YDBIO.2006.02.045.

Frey, N. and Olson, E.N. (2003) 'Cardiac Hypertrophy: The Good, the Bad, and the Ugly', *Annual Review of Physiology*, 65(1), pp. 45–79. Available at: https://doi.org/10.1146/annurev.physiol.65.092101.142243.

Friedland, A.E. *et al.* (2013) 'Heritable genome editing in C. elegans via a CRISPR-Cas9 system.', *Nature methods*, 10(8), pp. 741–3. Available at: https://doi.org/10.1038/nmeth.2532.

Friedman, C.E. *et al.* (2018) 'Single cell transcriptomic analysis of cardiac differentiation from human PSCs reveals HOPX-dependent cardiomyocyte maturation', *Cell stem cell*, 23(4), p. 586. Available at: https://doi.org/10.1016/J.STEM.2018.09.009.

Friedmann, D.R. and Marmorstein, R. (2013) 'Structure and mechanism of non-histone protein acetyltransferase enzymes', *FEBS Journal*, 280(22), pp. 5570–5581. Available at: https://doi.org/10.1111/febs.12373.

Fu, J.-D.J.D. *et al.* (2013) 'Direct reprogramming of human fibroblasts toward a cardiomyocyte-like state.', *Stem cell reports*, 1(3), pp. 235–47. Available at: https://doi.org/10.1016/j.stemcr.2013.07.005.

Fu, Y. *et al.* (1998) 'Vertebrate tinman homologues XNkx2-3 and XNkx2-5 are required for heart formation in a functionally redundant manner.', *Development (Cambridge, England)*, 125(22), pp. 4439–49.

Furumai, R. (2001) 'Potent histone deacetylase inhibitors built from trichostatin A and cyclic tetrapeptide antibiotics including trapoxin', *Proceedings of the National Academy of Sciences*, 98(1), pp. 87–92. Available at: https://doi.org/10.1073/pnas.011405598.

Gabant, P. *et al.* (2002) 'Alpha-fetoprotein, the major fetal serum protein, is not essential for embryonic development but is required for female fertility', *Proceedings of the National Academy of Sciences*, 99(20), pp. 12865–12870. Available at: https://doi.org/10.1073/pnas.202215399.

Gabay, O. *et al.* (2013) 'Sirt1-deficient mice exhibit an altered cartilage phenotype', *Joint, bone, spine : revue du rhumatisme*, 80(6), p. 613. Available at: https://doi.org/10.1016/J.JBSPIN.2013.01.001.

Gagnon, J.A. *et al.* (2014) 'Efficient mutagenesis by Cas9 protein-mediated oligonucleotide insertion and large-scale assessment of single-guide RNAs.', *PloS one*, 9(5), p. e98186. Available at: https://doi.org/10.1371/journal.pone.0098186.

Gallagher, J.M. *et al.* (2012) 'Dissociation of Cardiogenic and Postnatal Myocardial Activities of GATA4', *Molecular and Cellular Biology*, 32(12), pp. 2214–2223. Available at: https://doi.org/10.1128/MCB.00218-12.

Galow, A.M., Brenmoehl, J. and Hoeflich, A. (2023) 'Synergistic effects of hormones on structural and functional maturation of cardiomyocytes and implications for heart regeneration', *Cellular and Molecular Life Sciences*, 80(8), p. 240. Available at: https://doi.org/10.1007/S00018-023-04894-6.

Gan, L., Schwengberg, S. and Denecke, B. (2014) 'Transcriptome analysis in cardiomyocyte-specific differentiation of murine embryonic stem cells reveals transcriptional regulation network.', *Gene expression patterns : GEP*, 16(1), pp. 8–22. Available at: https://doi.org/10.1016/j.gep.2014.07.002.

Le Garrec, J.-F. *et al.* (2017) 'A predictive model of asymmetric morphogenesis from 3D reconstructions of mouse heart looping dynamics.', *eLife*, 6. Available at: https://doi.org/10.7554/eLife.28951.

Gatla, H.R. *et al.* (2019) 'Regulation of Chemokines and Cytokines by Histone Deacetylases and an Update on Histone Decetylase Inhibitors in Human Diseases', *International Journal of Molecular Sciences*, 20(5). Available at: https://doi.org/10.3390/IJMS20051110.

Gautel, M. and Djinović-Carugo, K. (2016) 'The sarcomeric cytoskeleton: From molecules to motion', *Journal of Experimental Biology*. Company of Biologists Ltd, pp. 135–145. Available at: https://doi.org/10.1242/jeb.124941.

Ghosh, T. *et al.* (2014) 'Studies of Genes Involved in Congenital Heart Disease', *Journal of Cardiovascular Development and Disease*, 1(1), pp. 134–145. Available at: https://doi.org/10.3390/jcdd1010134.

Ghosh, T.K. *et al.* (2001) 'Characterization of the TBX5 binding site and analysis of mutations that cause Holt-Oram syndrome.', *Human molecular genetics*, 10(18), pp. 1983–1994. Available at: https://doi.org/10.1093/hmg/10.18.1983.

Ghosh, T.K. *et al.* (2009) 'Physical interaction between TBX5 and MEF2C is required for early heart development.', *Molecular and cellular biology*, 29(8), pp. 2205–2218. Available at: https://doi.org/10.1128/MCB.01923-08.

Ghosh, T.K. *et al.* (2018) 'Acetylation of TBX5 by KAT2B and KAT2A regulates heart and limb development', *Journal of Molecular and Cellular Cardiology*, 114. Available at: https://doi.org/10.1016/j.yjmcc.2017.11.013.

Ghosh, Tushar K *et al.* (2018) 'Acetylation of TBX5 by KAT2B and KAT2A regulates heart and limb development', *Journal of molecular and cellular cardiology*, 114, pp. 185–198. Available at: https://doi.org/10.1017/CBO9781107415324.004.

Ghosh, T.K. *et al.* (2019) 'HDAC4 and 5 repression of TBX5 is relieved by protein kinase D1', *Scientific Reports*, 9(1), p. 17992. Available at: https://doi.org/10.1038/s41598-019-54312-w.

Gilda, J.E. *et al.* (2015) 'Western Blotting Inaccuracies with Unverified Antibodies: Need for a Western Blotting Minimal Reporting Standard (WBMRS)', *PLOS ONE*. Edited by F. Leng, 10(8), p. e0135392. Available at: https://doi.org/10.1371/journal.pone.0135392.

Gilsbach, R. *et al.* (2014) 'Dynamic DNA methylation orchestrates cardiomyocyte development, maturation and disease', *Nature Communications*, 5, p. 5288. Available at: https://doi.org/10.1038/ncomms6288.

Ginnan, R. *et al.* (2012) 'MEF2 is regulated by CaMKIIδ2 and a HDAC4-HDAC5 heterodimer in vascular smooth muscle cells.', *The Biochemical journal*, 444(1), pp. 105–14. Available at: https://doi.org/10.1042/BJ20120152.

Di Giorgio, E. and Brancolini, C. (2016) 'Regulation of class IIa HDAC activities: it is not only matter of subcellular localization', *Epigenomics*, 8(2), pp. 251–269. Available at: https://doi.org/10.2217/epi.15.106.

Goldman, O. *et al.* (2016) 'The mesenchymal transcription factor SNAI-1 instructs human liver specification', *Stem Cell Research*, 17(1), pp. 62–68. Available at: https://doi.org/10.1016/J.SCR.2016.05.007.

Gonçalves, S. *et al.* (2018) 'A Homozygous KAT2B Variant Modulates the Clinical Phenotype of ADD3 Deficiency in Humans and Flies', *PLoS genetics*, 14(5), p. e1007386. Available at: http://www.ncbi.nlm.nih.gov/pubmed/29768408 (Accessed: 16 October 2019).

Goswami, A. *et al.* (2019) 'Echocardiographic Evaluation of Anatomical Abnormalities of Interventricular Septum (with Special Reference to Ventricular Septal Defect) in the Population of West Bengal between 1 and 12 Years of Age', *Journal of Evolution of Medical and Dental Sciences*, 8, pp. 3599–3603. Available at: https://doi.org/10.14260/jemds/2019/777.

Grego-Bessa, J. *et al.* (2007) 'Notch signaling is essential for ventricular chamber development', *Developmental cell*, 12(3), pp. 415–429. Available at: https://doi.org/10.1016/J.DEVCEL.2006.12.011.

Gregoretti, I., Lee, Y.-M. and Goodson, H. V (2004) 'Molecular Evolution of the Histone Deacetylase Family: Functional Implications of Phylogenetic Analysis', *Journal of Molecular Biology*, 338(1), pp. 17–31. Available at: https://doi.org/10.1016/j.jmb.2004.02.006.

Grépin, C. *et al.* (1995) 'Inhibition of transcription factor GATA-4 expression blocks in vitro cardiac muscle differentiation.', *Molecular and cellular biology*, 15(8), pp. 4095–102. Available at: https://doi.org/10.1128/mcb.15.8.4095.

Greulich, F., Rudat, C. and Kispert, A. (2011) 'Mechanisms of T-box gene function in the developing heart.', *Cardiovascular research*, 91(2), pp. 212–22. Available at: https://doi.org/10.1093/cvr/cvr112.

Grozinger, C.M., Hassig, C.A. and Schreiber, S.L. (1999) 'Three proteins define a class of human histone deacetylases related to yeast Hda1p', *Proceedings of the National Academy of Sciences of the United States of America*, 96(9), pp. 4868–4873. Available at: https://doi.org/10.1073/pnas.96.9.4868.

Grozinger, C.M. and Schreiber, S.L. (2000) 'Regulation of histone deacetylase 4 and 5 and transcriptional activity by 14-3- 3-dependent cellular localization', *Proceedings of the National Academy of Sciences*, 97(14), pp. 7835–7840. Available at: https://doi.org/10.1073/pnas.140199597.

Grune, T. *et al.* (2019) 'the "MYocYteR" – convert cellular and cardiac contractions into numbers with imageJ', 9(1), p. 15112. Available at: https://doi.org/10.1038/s41598-019-51676-x.

Gryder, B.E., Sodji, Q.H. and Oyelere, A.K. (2012) 'Targeted cancer therapy: giving histone deacetylase inhibitors all they need to succeed.', *Future medicinal chemistry*, 4(4), pp. 505–24. Available at: https://doi.org/10.4155/fmc.12.3.

Guan, K. *et al.* (2001) 'Embryonic stem cell-derived neurogenesis. Retinoic acid induction and lineage selection of neuronal cells.', *Cell and tissue research*, 305(2), pp. 171–6. Available at: https://doi.org/10.1007/s004410100416.

Guan, K., Rohwedel, J. and Wobus, A.M. (1999) ‘Embryonic stem cell differentiation models: cardiogenesis, myogenesis, neurogenesis, epithelial and vascular smooth muscle cell differentiation in vitro.’, *Cytotechnology*, 30(1–3), pp. 211–26. Available at: https://doi.org/10.1023/A:1008041420166.

Guardiola, A.R. and Yao, T.P. (2002) ‘Molecular cloning and characterization of a novel histone deacetylase HDAC10’, *Journal of Biological Chemistry*, 277(5), pp. 3350–3356. Available at: https://doi.org/10.1074/jbc.M109861200.

Günthel, M., Barnett, P. and Christoffels, V.M. (2018) ‘Development, Proliferation, and Growth of the Mammalian Heart.’, *Molecular therapy : the journal of the American Society of Gene Therapy*, 26(7), pp. 1599–1609. Available at: https://doi.org/10.1016/j.ymthe.2018.05.022.

Guo, Y. *et al.* (2021) ‘Sarcomeres regulate murine cardiomyocyte maturation through MRTF-SRF signaling’, *Proceedings of the National Academy of Sciences of the United States of America*, 118(2), p. e2008861118.

Gupta, M.P. *et al.* (2008) ‘HDAC4 and PCAF bind to cardiac sarcomeres and play a role in regulating myofilament contractile activity’, *Journal of Biological Chemistry*, 283(15), pp. 10135–10146. Available at: https://doi.org/10.1074/jbc.M710277200.

Gurgul, A. *et al.* (2017) ‘The effect of histone deacetylase inhibitor trichostatin A on porcine mesenchymal stem cell transcriptome’, *Biochimie*, 139, pp. 56–73. Available at: https://doi.org/10.1016/J.BIOCHI.2017.05.015.

Habara-Ohkubo, A. (1996) ‘Differentiation of beating cardiac muscle cells from a derivative of P19 embryonal carcinoma cells.’, *Cell structure and function*, 21(2), pp. 101–10.

Haberland, M., Montgomery, R.L. and Olson, E.N. (2009) ‘The many roles of histone deacetylases in development and physiology: implications for disease and therapy’, *Nature Reviews Genetics*, 10(1), pp. 32–42. Available at: https://doi.org/10.1038/nrg2485.

Habibian, J. and Ferguson, B.S. (2018) ‘The Crosstalk between Acetylation and Phosphorylation: Emerging New Roles for HDAC Inhibitors in the Heart.’,

International journal of molecular sciences, 20(1). Available at: https://doi.org/10.3390/ijms20010102.

Hai, Y. *et al.* (2017) 'Histone deacetylase 10 structure and molecular function as a polyamine deacetylase', *Nature Communications*, 8(1), p. 15368. Available at: https://doi.org/10.1038/ncomms15368.

Hai, Y. and Christianson, D.W. (2016) 'Histone deacetylase 6 structure and molecular basis of catalysis and inhibition', *Nature Chemical Biology*, 12(9), pp. 741–747. Available at: https://doi.org/10.1038/nchembio.2134.

Halbgebauer, S., *et al.* (2022) 'Visinin-like protein 1 levels in blood and CSF as emerging markers for Alzheimer's and other neurodegenerative diseases', *Alzheimer's research & therapy*, 14(1), p. 175.

Hamamori, Y. *et al.* (1999) 'Regulation of histone acetyltransferases p300 and PCAF by the bHLH protein twist and adenoviral oncoprotein E1A', *Cell*, 96(3), pp. 405–413. Available at: https://doi.org/10.1016/S0092-8674(00)80553-X.

Han, Y. *et al.* (2015) 'Advanced applications of RNA sequencing and challenges', *Bioinformatics and Biology Insights*, 9(Suppl 1), pp. 29–46. Available at: https://doi.org/10.4137/BBI.S28991.

Hassan, A.H. *et al.* (2002) 'Function and selectivity of bromodomains in anchoring chromatin-modifying complexes to promoter nucleosomes.', *Cell*, 111(3), pp. 369–79. Available at: https://doi.org/10.1016/s0092-8674(02)01005-x.

Hayashi, Y. *et al.* (2014) 'Downregulation of rRNA Transcription Triggers Cell Differentiation', *PLoS ONE*. Edited by S.P. Deb, 9(5), p. e98586. Available at: https://doi.org/10.1371/journal.pone.0098586.

Hentze, M.W. and Kulozik, A.E. (1999) 'A Perfect Message: RNA Surveillance and Nonsense-Mediated Decay', *Cell*, 96(3), pp. 307–310. Available at: https://doi.org/10.1016/S0092-8674(00)80542-5.

van der Heyden, M.A.G. and Defize, L.H.K. (2003) 'Twenty one years of P19 cells: what an embryonal carcinoma cell line taught us about cardiomyocyte differentiation.', *Cardiovascular research*, 58(2), pp. 292–302.

Hiroi, Y. *et al.* (2001) ‘Tbx5 associates with Nkx2-5 and synergistically promotes cardiomyocyte differentiation.’, *Nature Genetics*, 28(3), pp. 276–280. Available at: https://doi.org/10.1038/90123.

Hoffman, J.I.E.E. and Kaplan, S. (2002) ‘The incidence of congenital heart disease’, *Journal of the American College of Cardiology*, 39(12), pp. 1890–1900. Available at: https://doi.org/10.1016/S0735-1097(02)01886-7.

Hohl, M. *et al.* (2013) ‘HDAC4 controls histone methylation in response to elevated cardiac load’, *Journal of Clinical Investigation*, 123(3), pp. 1359–1370. Available at: https://doi.org/10.1172/JCI61084.

HOLT, M. and ORAM, S. (1960) ‘Familial heart disease with skeletal malformations.’, *British heart journal*, 22, pp. 236–42.

Hong, J.H. and Zhang, H.G. (2022) ‘Transcription Factors Involved in the Development and Prognosis of Cardiac Remodeling’, *Frontiers in Pharmacology*, 13, p. 828549. Available at: https://doi.org/10.3389/FPHAR.2022.828549/BIBTEX.

Hoogaars, W.M.H. *et al.* (2007) ‘T-box factors determine cardiac design.’, *Cellular and molecular life sciences : CMLS*, 64(6), pp. 646–60. Available at: https://doi.org/10.1007/s00018-007-6518-z.

Hosoda, T. *et al.* (2001) ‘A novel myocyte-specific gene Midori promotes the differentiation of P19CL6 cells into cardiomyocytes.’, *The Journal of biological chemistry*, 276(38), pp. 35978–89. Available at: https://doi.org/10.1074/jbc.M100485200.

Hosseinkhani, M. *et al.* (2007) ‘Trichostatin A induces myocardial differentiation of monkey ES cells’, *Biochemical and Biophysical Research Communications*, 356(2), pp. 386–391.

Houtkooper, R.H., Pirinen, E. and Auwerx, J. (2012) ‘Sirtuins as regulators of metabolism and healthspan’, *Nature Reviews Molecular Cell Biology*. Nat Rev Mol Cell Biol, pp. 225–238. Available at: https://doi.org/10.1038/nrm3293.

Hrdlickova, R., Toloue, M. and Tian, B. (2017) ‘RNA-Seq methods for transcriptome analysis.’, *Wiley interdisciplinary reviews. RNA*, 8(1). Available at: https://doi.org/10.1002/wrna.1364.

Hu, D. *et al.* (2018) 'KDM5A Regulates a Translational Program that Controls p53 Protein Expression', *iScience*, 9, p. 84. Available at: https://doi.org/10.1016/J.ISCI.2018.10.012.

Hu, H. *et al.* (2020) 'The Role of Transcription Factor 21 in Epicardial Cell Differentiation and the Development of Coronary Heart Disease', *Frontiers in Cell and Developmental Biology*, 8. Available at: https://doi.org/10.3389/fcell.2020.00457.

Huang, J. *et al.* (2017) 'Histone/protein deacetylase 11 targeting promotes Foxp3+ Treg function', *Scientific Reports*, 7(1), p. 8626. Available at: https://doi.org/10.1038/s41598-017-09211-3.

Huangfu, D. *et al.* (2008) 'Induction of pluripotent stem cells from primary human fibroblasts with only Oct4 and Sox2.', *Nature biotechnology*, 26(11), pp. 1269–75. Available at: https://doi.org/10.1038/nbt.1502.

Hubbert, C. *et al.* (2002) 'HDAC6 is a microtubule-associated deacetylase', *Nature*, 417(6887), pp. 455–458. Available at: https://doi.org/10.1038/417455A.

Hwang, W.Y. *et al.* (2013) 'Efficient genome editing in zebrafish using a CRISPR-Cas system.', *Nature biotechnology*, 31(3), pp. 227–9. Available at: https://doi.org/10.1038/nbt.2501.

Hwang, Y.-S. *et al.* (2009) 'Microwell-mediated control of embryoid body size regulates embryonic stem cell fate via differential expression of WNT5a and WNT11', *Proceedings of the National Academy of Sciences of the United States of America*, 106(40), p. 16978. Available at: https://doi.org/10.1073/PNAS.0905550106.

Ieda, M. *et al.* (2010) 'Direct Reprogramming of Fibroblasts into Functional Cardiomyocytes by Defined Factors', *Cell*, 142(3), pp. 375–386. Available at: https://doi.org/10.1016/j.cell.2010.07.002.

Ingolia, N.T., Lareau, L.F. and Weissman, J.S. (2011) 'Ribosome Profiling of Mouse Embryonic Stem Cells Reveals the Complexity and Dynamics of Mammalian Proteomes', *Cell*, 147(4), pp. 789–802. Available at: https://doi.org/10.1016/J.CELL.2011.10.002.

Islas, J.F. *et al.* (2012) 'Transcription factors ETS2 and MESP1 transdifferentiate human dermal fibroblasts into cardiac progenitors', *Proceedings of the National Academy of Sciences*, 109(32), pp. 13016–13021. Available at: https://doi.org/10.1073/pnas.1120299109.

Isomi, M. *et al.* (2021) 'Overexpression of Gata4, Mef2c, and Tbx5 Generates Induced Cardiomyocytes Via Direct Reprogramming and Rare Fusion in the Heart', *Circulation*, 143, pp. 2123–2125. Available at: https://doi.org/10.1161/CIRCULATIONAHA.120.052799.

Itskovitz-Eldor, J. *et al.* (2000) 'Differentiation of human embryonic stem cells into embryoid bodies compromising the three embryonic germ layers.', *Molecular medicine (Cambridge, Mass.)*, 6(2), pp. 88–95.

Ivanovitch, K., Temiño, S. and Torres, M. (2017) 'Live imaging of heart tube development in mouse reveals alternating phases of cardiac differentiation and morphogenesis', *eLife*, 6. Available at: https://doi.org/10.7554/ELIFE.30668.

Iwata-Otsubo, A. *et al.* (2020) 'CBX1 variants cause a neurodevelopmental syndrome due to facultative heterochromatin dysfunction', *bioRxiv*, p. 2020.09.29.319228. Available at: https://doi.org/10.1101/2020.09.29.319228.

Jamaladdin, S. *et al.* (2014) 'Histone deacetylase (HDAC) 1 and 2 are essential for accurate cell division and the pluripotency of embryonic stem cells', *Proceedings of the National Academy of Sciences of the United States of America*, 111(27), pp. 9840–9845. Available at: https://doi.org/10.1073/PNAS.1321330111/SUPPL_FILE/PNAS.1321330111.SD01.XLSX.

Jang, D.G. *et al.* (2015) 'A thioredoxin fold protein Sh3bgr regulates Enah and is necessary for proper sarcomere formation', *Developmental Biology*, 405(1), pp. 1–9. Available at: https://doi.org/https://doi.org/10.1016/j.ydbio.2015.06.005.

Jang, J. *et al.* (2022) 'Epicardial HDAC3 Promotes Myocardial Growth Through a Novel MicroRNA Pathway', *Circulation Research*, 131(2), pp. 151–164. Available at: https://doi.org/10.1161/CIRCRESAHA.122.320785.

Jang, S. *et al.* (2017) 'Dynamics of embryonic stem cell differentiation inferred from single-cell transcriptomics show a series of transitions through discrete cell states', *eLife*, 6. Available at: https://doi.org/10.7554/ELIFE.20487.

Jasmin *et al.* (2010) 'Chemical induction of cardiac differentiation in p19 embryonal carcinoma stem cells', *Stem cells and development*, 19(3), pp. 403–411.

Jayawardena, T.M. *et al.* (2012) 'MicroRNA-mediated in vitro and in vivo direct reprogramming of cardiac fibroblasts to cardiomyocytes.', *Circulation research*, 110(11), pp. 1465–73. Available at: https://doi.org/10.1161/CIRCRESAHA.112.269035.

Jebessa, Z.H. *et al.* (2019) 'The lipid-droplet-associated protein ABHD5 protects the heart through proteolysis of HDAC4', *Nature Metabolism*, 1(11), pp. 1157–1167. Available at: https://doi.org/10.1038/s42255-019-0138-4.

Jensen, B. *et al.* (2017) 'Development of the atrial septum in relation to postnatal anatomy and interatrial communications', *Heart*, 103(6), pp. 456–462. Available at: https://doi.org/10.1136/HEARTJNL-2016-310660.

Jensen, B., Wang, T. and Moorman, A.F.M. (2019) 'Evolution and Development of the Atrial Septum', *The Anatomical Record*, 302(1), pp. 32–48. Available at: https://doi.org/10.1002/AR.23914.

Jenuwein, T. and Allis, C.D. (2001) 'Translating the histone code.', *Science (New York, N.Y.)*, 293(5532), pp. 1074–80. Available at: https://doi.org/10.1126/science.1063127.

Jeon, A.J. and Tucker-Kellogg, G. (2020) 'Bivalent genes that undergo transcriptional switching identify networks of key regulators of embryonic stem cell differentiation', *BMC Genomics*, 21(Suppl 10), p. 614. Available at: https://doi.org/10.1186/S12864-020-07009-8.

Jeong, K. *et al.* (2021) 'Fak activation promotes smc dedifferentiation via increased dna methylation in contractile genes', *Circulation Research*, 129(12), pp. E215–E233. Available at: https://doi.org/10.1161/CIRCRESAHA.121.319066.

Jiang, H. *et al.* (2020) 'Exercise improves cardiac function and glucose metabolism in mice with experimental myocardial infarction through inhibiting HDAC4 and

upregulating GLUT1 expression', *Basic Research in Cardiology*, 115(3). Available at: https://doi.org/10.1007/s00395-020-0787-1.

Jiménez-Amilburu, V. *et al.* (2016) 'In Vivo Visualization of Cardiomyocyte Apicobasal Polarity Reveals Epithelial to Mesenchymal-like Transition during Cardiac Trabeculation', *Cell Reports*, 17(10), pp. 2687–2699. Available at: https://doi.org/10.1016/j.celrep.2016.11.023.

Jin, F. *et al.* (2018) 'IL-8 regulates the stemness properties of cancer stem cells in the small-cell lung cancer cell line H446', *OncoTargets and therapy*, 11, p. 5723. Available at: https://doi.org/10.2147/OTT.S161760.

Jinek, M. *et al.* (2014) 'Structures of Cas9 endonucleases reveal RNA-mediated conformational activation.', *Science (New York, N.Y.)*, 343(6176), p. 1247997. Available at: https://doi.org/10.1126/science.1247997.

Kajol Shah *et al.* (2022) 'Calcium Channels in the Heart: Disease States and Drugs', *Cells*, 11(6), p. 943.

Kaneda, M. *et al.* (2004) 'Essential role for de novo DNA methyltransferase Dnmt3a in paternal and maternal imprinting', *Nature*, 429(6994), pp. 900–903. Available at: https://doi.org/10.1038/NATURE02633.

Kao, H.Y. *et al.* (2000) 'Isolation of a novel histone deacetylase reveals that class I and class II deacetylases promote SMRT-mediated repression.', *Genes & development*, 14(1), pp. 55–66.

Kapahnke, M., Banning, A. and Tikkanen, R. (2016) 'Random Splicing of Several Exons Caused by a Single Base Change in the Target Exon of CRISPR/Cas9 Mediated Gene Knockout.', *Cells*, 5(4). Available at: https://doi.org/10.3390/cells5040045.

Karamboulas, Christina *et al.* (2006) 'HDAC activity regulates entry of mesoderm cells into the cardiac muscle lineage.', *Journal of cell science*, 119(Pt 20), pp. 4305–14. Available at: https://doi.org/10.1242/jcs.03185.

Karamboulas, C. *et al.* (2006) 'HDAC activity regulates entry of mesoderm cells into the cardiac muscle lineage', *Journal of Cell Science*, 119(20), pp. 4305–4314. Available at: https://doi.org/10.1242/jcs.03185.

Karantzali, E. *et al.* (2008) 'Histone deacetylase inhibition accelerates the early events of stem cell differentiation: transcriptomic and epigenetic analysis.', *Genome biology*, 9(4), p. R65. Available at: https://doi.org/10.1186/gb-2008-9-4-r65.

Kardia, S.L., *et al.* (2007) 'Interactions between the adducin 2 gene and antihypertensive drug therapies in determining blood pressure in people with hypertension', *BMC medical genetics*, 8(61).

Karppinen, S. *et al.* (2018) 'Sarcoplasmic reticulum Ca2+-induced Ca2+ release regulates class IIa HDAC localization in mouse embryonic cardiomyocytes', *Physiological Reports*, 6(2). Available at: https://doi.org/10.14814/phy2.13522.

Katano, W. *et al.* (2019) 'Cardiac septation in heart development and evolution', *Development, growth & differentiation*, 61(1), pp. 114–123. Available at: https://doi.org/10.1111/DGD.12580.

Kawamura, T. *et al.* (2005) 'Acetylation of GATA-4 is involved in the differentiation of embryonic stem cells into cardiac myocytes.', *The Journal of biological chemistry*, 280(20), pp. 19682–8. Available at: https://doi.org/10.1074/jbc.M412428200.

Kee, H.J. *et al.* (2006) 'Inhibition of histone deacetylation blocks cardiac hypertrophy induced by angiotensin II infusion and aortic banding.', *Circulation*, 113(1), pp. 51–9. Available at: https://doi.org/10.1161/CIRCULATIONAHA.105.559724.

Kijima, M. *et al.* (1993) 'Trapoxin, an antitumor cyclic tetrapeptide, is an irreversible inhibitor of mammalian histone deacetylase.', *The Journal of biological chemistry*, 268(30), pp. 22429–35.

Kim, D.K. *et al.* (2014) 'Lefty1 and Lefty2 Control the Balance Between Self-Renewal and Pluripotent Differentiation of Mouse Embryonic Stem Cells', *Stem Cells and Development*, 23(5), p. 457. Available at: https://doi.org/10.1089/SCD.2013.0220.

Kim, H.-J. and Bae, S.-C. (2011) 'Histone deacetylase inhibitors: molecular mechanisms of action and clinical trials as anti-cancer drugs.', *American journal of translational research*, 3(2), pp. 166–79.

Kim, I.A.I.H. *et al.* (2005) ‘A histone deacetylase inhibitor, trichostatin A, enhances radiosensitivity by abrogating G2/M arrest in human carcinoma cells.’, *Cancer research and treatment : official journal of Korean Cancer Association*, 37(2), pp. 122–8. Available at: https://doi.org/10.4143/crt.2005.37.2.122.

King, K.R. *et al.* (2017) ‘IRF3 and Type I Interferons Fuel a Fatal Response to Myocardial Infarction’, *Nature medicine*, 23(12), p. 1481. Available at: https://doi.org/10.1038/NM.4428.

Kishino, Y. *et al.* (2020) ‘Toward the realization of cardiac regenerative medicine using pluripotent stem cells’, *Inflammation and Regeneration*, 40(1), p. 1. Available at: https://doi.org/10.1186/s41232-019-0110-4.

Kleff, S. *et al.* (1995) ‘Identification of a Gene Encoding a Yeast Histone H4 Acetyltransferase’, *Journal of Biological Chemistry*, 270(42), pp. 24674–24677. Available at: https://doi.org/10.1074/jbc.270.42.24674.

Kodo, K. and Yamagishi, H. (2017) ‘Current Insights into Genetics of Congenital Heart Diseases: GATA and T-box Cardiac Transcription Factors as the Hotspot Pathogenesis’, *Journal of Pediatric Cardiology and Cardiac Surgery*, 1(1), pp. 18–27. Available at: https://doi.org/10.24509/JPCCS.170105.

Kolossov, E. *et al.* (2005) ‘Identification and characterization of embryonic stem cell-derived pacemaker and atrial cardiomyocytes’, *The FASEB Journal*, 19(6), pp. 1–25. Available at: https://doi.org/10.1096/fj.03-1451fje.

Kook, H. and Kee, H.J. (2011) ‘Roles and targets of class I and IIa histone deacetylases in cardiac hypertrophy’, *Journal of biomedicine & biotechnology*, 2011. Available at: https://doi.org/10.1155/2011/928326.

Koopmann, T.T., *et al.* (2023) ‘Biallelic loss of LDB3 leads to a lethal pediatric dilated cardiomyopathy’, *European Journal of Human Genetics*, 31(1), pp. 97–104.

Kosicki, M., Tomberg, K. and Bradley, A. (2018) ‘Repair of double-strand breaks induced by CRISPR–Cas9 leads to large deletions and complex rearrangements’, *Nature Biotechnology*, 36(8), pp. 765–771. Available at: https://doi.org/10.1038/nbt.4192.

Kouzarides, T. (2000) 'Acetylation: a regulatory modification to rival phosphorylation?', *The EMBO journal*, 19(6), pp. 1176–9. Available at: https://doi.org/10.1093/emboj/19.6.1176.

Krämer, A. *et al.* (2014) 'Causal Analysis Approaches in Ingenuity Pathway Analysis', *Bioinformatics*, 30(4), pp. 523–30.

Krishnan, A. *et al.* (2014) 'A detailed comparison of mouse and human cardiac development', *Pediatric Research*, 76(6), pp. 500–507. Available at: https://doi.org/10.1038/pr.2014.128.

Kronlage, M., Katus, H.A. and Backs, J. (2016) 'HDAC Signaling Networks in Heart Failure', in. Springer, Cham, pp. 191–208. Available at: https://doi.org/10.1007/978-3-319-41457-7_8.

Kuales, G. *et al.* (2015) 'A Resource for the Transcriptional Signature of Bona Fide Trophoblast Stem Cells and Analysis of Their Embryonic Persistence', *Stem Cells International*. Edited by V. Kouskoff, 2015, p. 218518. Available at: https://doi.org/10.1155/2015/218518.

Kulic, I. *et al.* (2015) 'Loss of the Notch effector RBPJ promotes tumorigenesis', *Journal of Experimental Medicine*, 212(1), pp. 37–52. Available at: https://doi.org/10.1084/JEM.20121192.

Lagger, G. *et al.* (2002) 'Essential function of histone deacetylase 1 in proliferation control and CDK inhibitor repression', *EMBO*, 21(11), pp. 2672–2681. Available at: https://doi.org/10.1093/emboj/21.11.2672.

Lahm, A. *et al.* (2007) 'Unraveling the hidden catalytic activity of vertebrate class IIa histone deacetylases.', *Proceedings of the National Academy of Sciences of the United States of America*, 104(44), pp. 17335–40. Available at: https://doi.org/10.1073/pnas.0706487104.

Lalonde, S. *et al.* (2017) 'Frameshift indels introduced by genome editing can lead to in-frame exon skipping', *PLOS ONE*. Edited by A.S. Lewin, 12(6), p. e0178700. Available at: https://doi.org/10.1371/journal.pone.0178700.

Latinkić, B. V, Kotecha, S. and Mohun, T.J. (2003) 'Induction of cardiomyocytes by GATA4 in Xenopus ectodermal explants.', *Development (Cambridge, England)*, 130(16), pp. 3865–76.

Laurent, F. *et al.* (2017) 'HAND2 Target Gene Regulatory Networks Control Atrioventricular Canal and Cardiac Valve Development.', *Cell reports*, 19(8), pp. 1602–1613. Available at: https://doi.org/10.1016/j.celrep.2017.05.004.

Lee, E.J., Nam, J.H. and Choi, I. (2018) 'Fibromodulin modulates myoblast differentiation by controlling calcium channel', *Biochemical and Biophysical Research Communications*, 503(2), pp. 580–585. Available at: https://doi.org/https://doi.org/10.1016/j.bbrc.2018.06.041.

Lee, J.-H., Hart, S.R.L. and Skalnik, D.G. (2004) 'Histone deacetylase activity is required for embryonic stem cell differentiation', *genesis*, 38(1), pp. 32–38. Available at: https://doi.org/10.1002/gene.10250.

Lee, K.H. *et al.* (2010) 'A genomewide study identifies the Wnt signaling pathway as a major target of p53 in murine embryonic stem cells', *Proceedings of the National Academy of Sciences of the United States of America*, 107(1), pp. 69–74. Available at: https://doi.org/10.1073/pnas.0909734107.

Lescroart, F. *et al.* (2010) 'Clonal analysis reveals common lineage relationships between head muscles and second heart field derivatives in the mouse embryo', *Development (Cambridge, England)*, 137(19), pp. 3269–3279. Available at: https://doi.org/10.1242/DEV.050674.

Lewandowski, S.L. *et al.* (2014) 'Histone deacetylase 3 modulates Tbx5 activity to regulate early cardiogenesis', *Human Molecular Genetics*, 23(14), pp. 3801–3809. Available at: https://doi.org/10.1093/hmg/ddu093.

Li, L. *et al.* (2020) 'The role of G protein-coupled receptor kinase 4 in cardiomyocyte injury after myocardial infarction', *European Heart Journal* [Preprint]. Available at: https://doi.org/10.1093/eurheartj/ehaa878.

Li, Q. *et al.* (2012) 'Cited2 gene controls pluripotency and cardiomyocyte differentiation of murine embryonic stem cells through Oct4 gene', *The Journal of*

biological chemistry, 287(34), pp. 29088–29100. Available at: https://doi.org/10.1074/JBC.M112.378034.

Li, T. *et al.* (2018) 'Dural effects of oxidative stress on cardiomyogenesis via Gata4 transcription and protein ubiquitination article', *Cell Death and Disease*, 9(2). Available at: https://doi.org/10.1038/s41419-018-0281-y.

Li, X. *et al.* (2004) 'Phosphorylation of the histone deacetylase 7 modulates its stability and association with 14-3-3 proteins', *Journal of Biological Chemistry*, 279(33), pp. 34201–34208. Available at: https://doi.org/10.1074/jbc.M405179200.

Lieu, D.K. *et al.* (2009) 'Absence of transverse tubules contributes to non-uniform Ca2+ wavefronts in mouse and human embryonic stem cell-derived cardiomyocytes', *Stem Cells and Development*, 18(10), pp. 1493–1500. Available at: https://doi.org/10.1089/scd.2009.0052.

Lillico, R. *et al.* (2016) 'HDAC inhibitors induce global changes in histone lysine and arginine methylation and alter expression of lysine demethylases', *Journal of Proteomics*, 133, pp. 125–133. Available at: https://doi.org/10.1016/J.JPROT.2015.12.018.

Lim, S.Y. *et al.* (2013) 'Trichostatin A enhances differentiation of human induced pluripotent stem cells to cardiogenic cells for cardiac tissue engineering.', *Stem cells translational medicine*, 2(9), pp. 715–25. Available at: https://doi.org/10.5966/sctm.2012-0161.

Lin, Q. *et al.* (1997) 'Control of mouse cardiac morphogenesis and myogenesis by transcription factor MEF2C.', *Science (New York, N.Y.)*, 276(5317), pp. 1404–7.

Lindsey, S.E., Butcher, J.T. and Yalcin, H.C. (2014) 'Mechanical regulation of cardiac development.', *Frontiers in physiology*, 5, p. 318. Available at: https://doi.org/10.3389/fphys.2014.00318.

Linster, E. and Wirtz, M. (2018) 'N-terminal acetylation: an essential protein modification emerges as an important regulator of stress responses', *Journal of Experimental Botany*, 69(19), pp. 4555–4568. Available at: https://doi.org/10.1093/jxb/ery241.

Liu, F. *et al.* (2020) 'STVNA attenuates isoproterenol-induced cardiac hypertrophy response through the HDAC4 and prdx2/ROS/Trx1 pathways', *International Journal of Molecular Sciences*, 21(2). Available at: https://doi.org/10.3390/ijms21020682.

Liu, H.X. *et al.* (2001) 'A mechanism for exon skipping caused by nonsense or missense mutations in BRCA1 and other genes.', *Nature genetics*, 27(1), pp. 55–8. Available at: https://doi.org/10.1038/83762.

Liu, Y. *et al.* (2014) 'Variations of CITED2 Are Associated with Congenital Heart Disease (CHD) in Chinese Population', *PLOS ONE*, 9(5), p. e98157. Available at: https://doi.org/10.1371/JOURNAL.PONE.0098157.

Liu Zhonghao, J.X. and Ornitz, D.M. (2000) 'Temporal and spatial gradients of Fgf8 and Fgf17 regulate proliferation and differentiation of midline cerebellar structures', *Development*, 127(9), pp. 1833–1843. Available at: https://doi.org/10.1242/dev.127.9.1833.

Livigni, A. *et al.* (2009) 'Differentiation of Embryonic Stem Cells into Anterior Definitive Endoderm', *Current Protocols in Stem Cell Biology*, 10(1), pp. 1G.3.1-1G.3.10. Available at: https://doi.org/10.1002/9780470151808.sc01g03s10.

Lopaschuk, G.D. and Jaswal, J.S. (2010) 'Energy metabolic phenotype of the cardiomyocyte during development, differentiation, and postnatal maturation', *Journal of cardiovascular pharmacology*, 56(2), pp. 130–140. Available at: https://doi.org/10.1097/FJC.0B013E3181E74A14.

Lopes-Marques, M. *et al.* (2018) 'Expansion, retention and loss in the Acyl-CoA synthetase "Bubblegum" (Acsbg) gene family in vertebrate history', *Gene*, 664, pp. 111–118. Available at: https://doi.org/https://doi.org/10.1016/j.gene.2018.04.058.

López, J.E., Sullivan, E.D. and Fierke, C.A. (2016) 'Metal-dependent Deacetylases: Cancer and Epigenetic Regulators.', *ACS chemical biology*, 11(3), pp. 706–16. Available at: https://doi.org/10.1021/acschembio.5b01067.

Lu, J. *et al.* (2000) 'Regulation of skeletal myogenesis by association of the MEF2 transcription factor with class II histone deacetylases.', *Molecular cell*, 6(2), pp. 233–44. Available at: https://doi.org/10.1016/s1097-2765(00)00025-3.

Lu, Y. *et al.* (2019) 'Histone deacetylase 4 promotes type I interferon signaling, restricts DNA viruses, and is degraded via vaccinia virus protein C6', *Proceedings of the National Academy of Sciences of the United States of America*, 116(24), pp. 11997–12006. Available at: https://doi.org/10.1073/PNAS.1816399116/-/DCSUPPLEMENTAL.

De Luca, E. *et al.* (2014) 'ZebraBeat: a flexible platform for the analysis of the cardiac rate in zebrafish embryos', *Scientific Reports*, 4, pp. 835–50. Available at: https://doi.org/10.1038/srep04898.

Luo, Z. *et al.* (2019) 'Nuclear-cytoplasmic shuttling of class IIa histone deacetylases regulates somatic cell reprogramming', *Cell Regeneration*, 8(1), pp. 21–29. Available at: https://doi.org/10.1016/J.CR.2018.11.001.

Lyons, I. *et al.* (1995) 'Myogenic and morphogenetic defects in the heart tubes of murine embryos lacking the homeo box gene Nkx2-5.', *Genes & development*, 9(13), pp. 1654–66.

Ma, F. *et al.* (2019) 'A comparison between whole transcript and 3' RNA sequencing methods using Kapa and Lexogen library preparation methods', *BMC Genomics*, 20(1), p. 9. Available at: https://doi.org/10.1186/s12864-018-5393-3.

Ma, K. *et al.* (2005) 'Myocyte Enhancer Factor 2 Acetylation by p300 Enhances Its DNA Binding Activity, Transcriptional Activity, and Myogenic Differentiation', *Molecular and Cellular Biology*, 25(9), pp. 3575–3582. Available at: https://doi.org/10.1128/mcb.25.9.3575-3582.2005.

Ma, P. *et al.* (2012) 'Compensatory functions of histone deacetylase 1 (HDAC1) and HDAC2 regulate transcription and apoptosis during mouse oocyte development', *Proceedings of the National Academy of Sciences of the United States of America*, 109(8), pp. E481–E489. Available at: https://doi.org/10.1073/PNAS.1118403109/SUPPL_FILE/ST05.XLS.

Maalouf, W.E. *et al.* (2009) 'Trichostatin A treatment of cloned mouse embryos improves constitutive heterochromatin remodeling as well as developmental potential to term', *BMC Developmental Biology*, 9(1), p. 11. Available at: https://doi.org/10.1186/1471-213X-9-11.

Madsen, A. *et al.* (2020) 'An Important Role for DNMT3A-Mediated DNA Methylation in Cardiomyocyte Metabolism and Contractility', *Circulation*, 142(16), pp. 1562–1578. Available at: https://doi.org/10.1161/CIRCULATIONAHA.119.044444.

Mahmoudian, R.A. *et al.* (2019) 'MEIS1 knockdown may promote differentiation of esophageal squamous carcinoma cell line KYSE-30', *Molecular Genetics and Genomic Medicine*, 7(7). Available at: https://doi.org/10.1002/MGG3.746.

Mahmud, Z., *et al.* (2021) 'Dilated Cardiomyopathy Mutations and Phosphorylation disrupt the Active Orientation of Cardiac Troponin C', *Journal of molecular biology*, 433(13), p. 167010.

Mali, P. *et al.* (2013) 'RNA-Guided Human Genome Engineering via Cas9', *Science*, 339(6121), pp. 823–826. Available at: https://doi.org/10.1126/science.1232033.RNA-Guided.

Maltsev, V.A. *et al.* (1993) 'Embryonic stem cells differentiate in vitro into cardiomyocytes representing sinusnodal, atrial and ventricular cell types.', *Mechanisms of development*, 44(1), pp. 41–50. Available at: https://doi.org/10.1016/0925-4773(93)90015-p.

Mandrycky, C.J. *et al.* (2020) 'Engineering Heart Morphogenesis', *Trends in Biotechnology*. Elsevier Ltd, pp. 835–845. Available at: https://doi.org/10.1016/j.tibtech.2020.01.006.

Mantini, C. *et al.* (2023) 'A highly-detailed anatomical study of left atrial auricle as revealed by in-vivo computed tomography', *Heliyon*, 9(10), pp. 2405–8440. Available at: https://doi.org/10.1016/J.HELIYON.2023.E20575.

Marmorstein, R. and Zhou, M.-M. (2014) 'Writers and readers of histone acetylation: structure, mechanism, and inhibition.', *Cold Spring Harbor perspectives in biology*, 6(7), p. a018762. Available at: https://doi.org/10.1101/cshperspect.a018762.

Martin, G.R. (1981) 'Isolation of a pluripotent cell line from early mouse embryos cultured in medium conditioned by teratocarcinoma stem cells.', *Proceedings of the National Academy of Sciences of the United States of America*, 78(12), pp. 7634–8. Available at: https://doi.org/10.1073/pnas.78.12.7634.

Mathias, R.A., Guise, A.J. and Cristea, I.M. (2015) 'Post-translational Modifications Regulate Class IIa Histone Deacetylase (HDAC) Function in Health and Disease', *Molecular & Cellular Proteomics*, 14(3), pp. 456–470. Available at: https://doi.org/10.1074/mcp.O114.046565.

Mazzocco, M., *et al.* (2002) 'The identification of a novel human homologue of the SH3 binding glutamic acid-rich (SH3BGR) gene establishes a new family of highly conserved small proteins related to Thioredoxin Superfamily', *Gene*, 29(1–2), pp. 233–239.

McBurney, M.W. *et al.* (1982) 'Control of muscle and neuronal differentiation in a cultured embryonal carcinoma cell line', *Nature*, 299(5879), pp. 165–167. Available at: https://doi.org/10.1038/299165a0.

McBurney, M.W. (1993) 'P19 embryonal carcinoma cells.', *The International journal of developmental biology*, 37(1), pp. 135–40.

McBurney, M.W. *et al.* (2003) 'The mammalian SIR2alpha protein has a role in embryogenesis and gametogenesis.', *Molecular and cellular biology*, 23(1), pp. 38–54. Available at: https://doi.org/10.1128/mcb.23.1.38-54.2003.

Mccormick, J. *et al.* (2012) 'STAT1 deficiency in the heart protects against myocardial infarction by enhancing autophagy', *Journal of Cellular and Molecular Medicine*, 16(2), p. 386. Available at: https://doi.org/10.1111/J.1582-4934.2011.01323.X.

McCullough, C.E. and Marmorstein, R. (2016) 'Molecular Basis for Histone Acetyltransferase Regulation by Binding Partners, Associated Domains, and Autoacetylation', *ACS Chemical Biology*, 11(3), pp. 632–642. Available at: https://doi.org/10.1021/acschembio.5b00841.

McKinney-Freeman, S. *et al.* (2012) 'The transcriptional landscape of hematopoietic stem cell ontogeny', *Cell Stem Cell*, 11(5), pp. 701–714. Available at: https://doi.org/10.1016/j.stem.2012.07.018.

McKinsey, T.A., Zhang, C.L. and Olson, E.N. (2000) 'Activation of the myocyte enhancer factor-2 transcription factor by calcium/calmodulin-dependent protein kinase-stimulated binding of 14-3-3 to histone deacetylase 5.', *Proceedings of the*

National Academy of Sciences of the United States of America, 97(26), pp. 14400–5. Available at: https://doi.org/10.1073/pnas.260501497.

McKinsey, T.A., Zhang, C.L. and Olson, E.N. (2002) 'MEF2: a calcium-dependent regulator of cell division, differentiation and death', *Trends in biochemical sciences*, 27(1), pp. 40–47. Available at: https://doi.org/10.1016/S0968-0004(01)02031-X.

Meilhac, S.M. and Buckingham, M.E. (2018) 'The deployment of cell lineages that form the mammalian heart.', *Nature reviews. Cardiology*, 15(11), pp. 705–724. Available at: https://doi.org/10.1038/s41569-018-0086-9.

Meyer, E., Aglyamova, G. V. and Matz, M. V. (2011) 'Profiling gene expression responses of coral larvae (Acropora millepora) to elevated temperature and settlement inducers using a novel RNA-Seq procedure', *Molecular Ecology*, 20(17), pp. 3599–3616. Available at: https://doi.org/10.1111/j.1365-294X.2011.05205.x.

Mifflin, J.J. *et al.* (2018) 'Intercalated cushion cells within the cardiac outflow tract are derived from the myocardial troponin T type 2 (Tnnt2) Cre lineage', *Developmental dynamics : an official publication of the American Association of Anatomists*, 247(8), pp. 1005–1017. Available at: https://doi.org/10.1002/DVDY.24641.

Milazzo, G. *et al.* (2020) 'Histone Deacetylases (HDACs): Evolution, Specificity, Role in Transcriptional Complexes, and Pharmacological Actionability', *Genes 2020, Vol. 11, Page 556*, 11(5), p. 556. Available at: https://doi.org/10.3390/GENES11050556.

Miller, D.F.B. *et al.* (2013) 'A new method for stranded whole transcriptome RNA-seq', *Methods*, 63(2), pp. 126–134. Available at: https://doi.org/10.1016/j.ymeth.2013.03.023.

Miller, J.A. *et al.* (2014) 'Transcriptional landscape of the prenatal human brain', *Nature*, 508(7495), pp. 199–206. Available at: https://doi.org/10.1038/nature13185.

Miller, S.P. *et al.* (2007) 'Abnormal brain development in newborns with congenital heart disease.', *The New England journal of medicine*, 357(19), pp. 1928–38. Available at: https://doi.org/10.1056/NEJMoa067393.

Mitchell, J.L. and Mutch, N.J. (2019) 'Let's cross-link: diverse functions of the promiscuous cellular transglutaminase factor XIII-A', *Journal of Thrombosis and Haemostasis*, 17(1), pp. 19–30. Available at: https://doi.org/10.1111/JTH.14348.

Mitchell, S.C., Korones, S.B. and Berendes, H.W. (1971) 'Congenital heart disease in 56,109 births. Incidence and natural history.', *Circulation*, 43(3), pp. 323–32.

Miyake, Y. *et al.* (2016) 'Structural insights into HDAC6 tubulin deacetylation and its selective inhibition', *Nature Chemical Biology*, 12(9), pp. 748–754. Available at: https://doi.org/10.1038/nchembio.2140.

Miyamoto, S. *et al.* (2006) 'Histone acetyltransferase activity of p300 is required for the promotion of left ventricular remodeling after myocardial infarction in adult mice in vivo.', *Circulation*, 113(5), pp. 679–90. Available at: https://doi.org/10.1161/CIRCULATIONAHA.105.585182.

Molkentin, J.D. (2004) 'Calcineurin-NFAT signaling regulates the cardiac hypertrophic response in coordination with the MAPKs', *Cardiovascular Research*, 63(3), pp. 467–475. Available at: https://doi.org/10.1016/J.CARDIORES.2004.01.021/2/63-3-467-FIG3.GIF.

Moll, P. *et al.* (2014) 'QuantSeq 3′ mRNA sequencing for RNA quantification', *Nature Methods*, 11(12), pp. i–iii. Available at: https://doi.org/10.1038/nmeth.f.376.

Molt, S. *et al.* (2014) 'Aciculin interacts with filamin C and Xin and is essential for myofibril assembly, remodeling and maintenance', *Journal of Cell Science*, 127(16), pp. 3578–3592. Available at: https://doi.org/10.1242/JCS.152157/VIDEO-2.

Montgomery, R.L. *et al.* (2007) 'Histone Deacetylases 1 and 2 Redundantly Regulate Cardiac Morphogenesis, Growth, and Contractility', *Genes & development*, 21(14), pp. 1790–1802. Available at: https://doi.org/10.1101/gad.1563807.

Montgomery, R.L. *et al.* (2008) 'Maintenance of cardiac energy metabolism by histone deacetylase 3 in mice', *Journal of Clinical Investigation*, 118(11), pp. 3588–3597. Available at: https://doi.org/10.1172/JCI35847.

Moore, J.C. *et al.* (2004) 'A P19Cl6 GFP reporter line to quantify cardiomyocyte differentiation of stem cells.', *The International journal of developmental biology*, 48(1), pp. 47–55. Available at: https://doi.org/10.1387/ijdb.15005574.

Moorman, A. *et al.* (2003) ‘Development of the Heart : (1) Formation of the Cardiac Chambers and Arterial Trunks’, *Heart*, 89(1), pp. 806–814.

Moorman, A.F.M. and Christoffels, V.M. (2003) ‘Cardiac chamber formation: Development, genes, and evolution’, *Physiological Reviews*, 83(4), pp. 1223–1267. Available at: https://doi.org/10.1152/PHYSREV.00006.2003.

Morimoto, S. (2008) ‘Sarcomeric proteins and inherited cardiomyopathies.’, *Cardiovascular research*, 77(4), pp. 659–66. Available at: https://doi.org/10.1093/cvr/cvm084.

Morley, P. and Whitfield, J.F. (1993) ‘The differentiation inducer, dimethyl sulfoxide, transiently increases the intracellular calcium ion concentration in various cell types’, *Journal of Cellular Physiology*, 156(2), pp. 219–225. Available at: https://doi.org/10.1002/jcp.1041560202.

Mossahebi-Mohammadi, M. *et al.* (2020) ‘FGF Signaling Pathway: A Key Regulator of Stem Cell Pluripotency’, *Frontiers in Cell and Developmental Biology*, 8, p. 508125. Available at: https://doi.org/10.3389/FCELL.2020.00079/BIBTEX.

Mou, H. *et al.* (2017) ‘CRISPR/Cas9-mediated genome editing induces exon skipping by alternative splicing or exon deletion’, *Genome Biology*, 18(1), p. 108. Available at: https://doi.org/10.1186/s13059-017-1237-8.

MP, V. *et al.* (2005) ‘The Right Ventricle, Outflow Tract, and Ventricular Septum Comprise a Restricted Expression Domain Within the Secondary/Anterior Heart Field’, *Developmental biology*, 287(1). Available at: https://doi.org/10.1016/J.YDBIO.2005.08.041.

Muenks, A.G., Stiers, K.M. and Beamer, L.J. (2017) ‘Sequence-structure relationships, expression profiles, and disease-associated mutations in the paralogs of phosphoglucomutase 1’, *PLOS ONE*, 12(8), p. e0183563. Available at: https://doi.org/10.1371/JOURNAL.PONE.0183563.

Musunuru, K., Domian, I.J. and Chien, K.R. (2010) ‘Stem cell models of cardiac development and disease.’, *Annual review of cell and developmental biology*, 26, pp. 667–87. Available at: https://doi.org/10.1146/annurev-cellbio-100109-103948.

Nadadur, R. *et al.* (2017) 'Pitx2 modulates a Tbx5-dependent gene regulatory network to maintain atrial rhythm', *Science Translational Medicine*, 8(354), p. 354ra115.

Navarro, C. *et al.* (2020) 'An embryonic stem cell-specific heterochromatin state promotes core histone exchange in the absence of DNA accessibility', *Nature Communications 2020 11:1*, 11(1), pp. 1–14. Available at: https://doi.org/10.1038/s41467-020-18863-1.

Nookaew, I. *et al.* (2012) 'A comprehensive comparison of RNA-Seq-based transcriptome analysis from reads to differential gene expression and cross-comparison with microarrays: a case study in Saccharomyces cerevisiae', *Nucleic Acids Research*, 40(20), pp. 10084–10097.

Noseda, M. *et al.* (2011) 'Cardiopoietic Factors: Extracellular Signals for Cardiac Lineage Commitment', *Circulation Research*, 108(1), pp. 129–152. Available at: https://doi.org/10.1161/CIRCRESAHA.110.223792.

Nührenberg, T.G. *et al.* (2015) 'Cardiac Myocyte De Novo DNA Methyltransferases 3a/3b Are Dispensable for Cardiac Function and Remodeling after Chronic Pressure Overload in Mice', *PLoS ONE*, 10(6). Available at: https://doi.org/10.1371/JOURNAL.PONE.0131019.

Oberlin, S. *et al.* (2017) 'A genome-wide transcriptome and translatome analysis of Arabidopsis transposons identifies a unique and conserved genome expression strategy for Ty1/Copia retroelements', *Genome Research*, 27(9), pp. 1549–1562. Available at: https://doi.org/10.1101/gr.220723.117.

O'Callaghan, C. and Vassilopoulos, A. (2017) 'Sirtuins at the crossroads of stemness, aging, and cancer', *Aging Cell*, 16(6), pp. 1208–1218. Available at: https://doi.org/10.1111/acel.12685.

Ohtsu, Y. *et al.* (2005) 'Stimulation of P19CL6 with multiple reagents induces pulsating particles in vivo', *Current Medical Research and Opinion*, 21(5), pp. 795–803. Available at: https://doi.org/10.1185/030079905X41499.

Olesen, J.B. *et al.* (2011) ‘Valproate attenuates the risk of myocardial infarction in patients with epilepsy: a nationwide cohort study.’, *Pharmacoepidemiology and drug safety*, 20(2), pp. 146–53. Available at: https://doi.org/10.1002/pds.2073.

Olson, E.N. (2006) ‘Gene regulatory networks in the evolution and development of the heart.’, *Science (New York, N.Y.)*, 313(5795), pp. 1922–7. Available at: https://doi.org/10.1126/science.1132292.

Ooi, J.Y.Y. *et al.* (2015) ‘HDAC inhibition attenuates cardiac hypertrophy by acetylation and deacetylation of target genes.’, *Epigenetics*, 10(5), pp. 418–30. Available at: https://doi.org/10.1080/15592294.2015.1024406.

Orpinell, M. *et al.* (2010) ‘The ATAC acetyl transferase complex controls mitotic progression by targeting non-histone substrates.’, *The EMBO journal*, 29(14), pp. 2381–94. Available at: https://doi.org/10.1038/emboj.2010.125.

Oshlack, A. and Wakefield, M.J. (2009) ‘Transcript length bias in RNA-seq data confounds systems biology’, *Biology Direct*, 4(1), p. 14. Available at: https://doi.org/10.1186/1745-6150-4-14.

Oswald, F. *et al.* (2016) ‘A phospho-dependent mechanism involving NCoR and KMT2D controls a permissive chromatin state at Notch target genes’, *Nucleic acids research*, 44(10), pp. 4703–4720. Available at: https://doi.org/10.1093/NAR/GKW105.

Ottaviani, D., LeCain, M. and Sheer, D. (2014) ‘The role of microhomology in genomic structural variation’, *Trends in Genetics*, 30(3), pp. 85–94. Available at: https://doi.org/10.1016/J.TIG.2014.01.001.

Owen-Hughes, T. (2003) ‘Pathways for remodelling chromatin’, in *Biochemical Society Transactions*. Portland Press Ltd, pp. 893–905. Available at: https://doi.org/10.1042/bst0310893.

Padula, S.L., Velayutham, N. and Yutzey, K.E. (2021) ‘Transcriptional Regulation of Postnatal Cardiomyocyte Maturation and Regeneration.’, *International journal of molecular sciences*, 22(6). Available at: https://doi.org/10.3390/ijms22063288.

Paige, S.L. *et al.* (2012) 'A temporal chromatin signature in human embryonic stem cells identifies regulators of cardiac development.', *Cell*, 151(1), pp. 221–32. Available at: https://doi.org/10.1016/j.cell.2012.08.027.

Pajak, A. *et al.* (2019) 'Defects of mitochondrial RNA turnover lead to the accumulation of double-stranded RNA in vivo', *PLoS genetics*, 15(7). Available at: https://doi.org/10.1371/JOURNAL.PGEN.1008240.

Palmer, N.P. *et al.* (2012) 'A gene expression profile of stem cell pluripotentiality and differentiation is conserved across diverse solid and hematopoietic cancers', *Genome Biology*, 13(8), pp. 1–13. Available at: https://doi.org/10.1186/gb-2012-13-8-r71.

Palpant, N.J. *et al.* (2013) 'Transmembrane protein 88: a Wnt regulatory protein that specifies cardiomyocyte development', *Development (Cambridge, England)*, 140(18), pp. 3799–3808. Available at: https://doi.org/10.1242/DEV.094789.

Paquin, J. *et al.* (2002) 'Oxytocin induces differentiation of P19 embryonic stem cells to cardiomyocytes.', *Proceedings of the National Academy of Sciences of the United States of America*, 99(14), pp. 9550–5. Available at: https://doi.org/10.1073/pnas.152302499.

Parikh, A. *et al.* (2015) 'Signaling Pathways and Gene Regulatory Networks in Cardiomyocyte Differentiation.', *Tissue engineering. Part B, Reviews*, 21(4), pp. 377–92. Available at: https://doi.org/10.1089/ten.TEB.2014.0662.

Parikh, B.A. *et al.* (2015) 'Detailed phenotypic and molecular analyses of genetically modified mice generated by CRISPR-Cas9-mediated editing.', *PloS one*, 10(1), p. e0116484. Available at: https://doi.org/10.1371/journal.pone.0116484.

Park, S.-J. *et al.* (2019) 'Dual stem cell therapy synergistically improves cardiac function and vascular regeneration following myocardial infarction', *Nature Communications*, 10(1), p. 3123. Available at: https://doi.org/10.1038/s41467-019-11091-2.

Parmacek, M.S. and Epstein, J.A. (2013) 'An Epigenetic Roadmap for Cardiomyocyte Differentiation', *Circulation research*, 112(6), p. 881. Available at: https://doi.org/10.1161/CIRCRESAHA.113.301134.

Parthun, M.R., Widom, J. and Gottschling, D.E. (1996) 'The major cytoplasmic histone acetyltransferase in yeast: links to chromatin replication and histone metabolism.', *Cell*, 87(1), pp. 85–94. Available at: https://doi.org/10.1016/s0092-8674(00)81325-2.

Pashai, N. *et al.* (2012) 'Genome-wide profiling of pluripotent cells reveals a unique molecular signature of human embryonic germ cells', *PLoS ONE*, 7(6). Available at: https://doi.org/10.1371/journal.pone.0039088.

Patel, N. *et al.* (2019) 'HDAC2 Regulates Site-Specific Acetylation of MDM2 and Its Ubiquitination Signaling in Tumor Suppression', *iScience*, 13, pp. 43–54. Available at: https://doi.org/10.1016/J.ISCI.2019.02.008.

Pauklin, S., Pedersen, R.A. and Vallier, L. (2011) 'Mouse pluripotent stem cells at a glance.', *Journal of cell science*, 124(Pt 22), pp. 3727–32. Available at: https://doi.org/10.1242/jcs.074120.

Payan, S.M., Hubert, F. and Rochais, F. (2020) 'Cardiomyocyte proliferation, a target for cardiac regeneration', *Biochimica et biophysica acta. Molecular cell research*, 1867(3). Available at: https://doi.org/10.1016/J.BBAMCR.2019.03.008.

Peng, C.-F. *et al.* (2002) 'Microarray analysis of global changes in gene expression during cardiac myocyte differentiation', *Physiological Genomics*, 9(3), pp. 145–155. Available at: https://doi.org/10.1152/physiolgenomics.00027.2002.

Piecewicz, S.M. *et al.* (2012) 'Insulin-Like Growth Factors Promote Vasculogenesis in Embryonic Stem Cells', *PLOS ONE*, 7(2), p. e32191. Available at: https://doi.org/10.1371/JOURNAL.PONE.0032191.

Plageman, T.F. and Yutzey, K.E. (2005) 'T-box genes and heart development: putting the "T" in heart.', *Developmental dynamics : an official publication of the American Association of Anatomists*, 232(1), pp. 11–20. Available at: https://doi.org/10.1002/dvdy.20201.

Poelmann, R.E. *et al.* (2016) 'The epicardium in ventricular septation during evolution and development', *Etiology and Morphogenesis of Congenital Heart Disease: From Gene Function and Cellular Interaction to Morphology*, pp. 115–123. Available at: https://doi.org/10.1007/978-4-431-54628-3_13/FIGURES/5.

van der Pol, A. *et al.* (2020) 'Cardiac foetal reprogramming: a tool to exploit novel treatment targets for the failing heart', *Journal of Internal Medicine*, 288(5), pp. 491–506. Available at: https://doi.org/10.1111/JOIM.13094.

Poleshko, A. *et al.* (2017) 'Genome-nuclear lamina interactions regulate cardiac stem cell lineage restriction', *Cell*, 171(3), pp. 573–587.

Porter, N.J. and Christianson, D.W. (2019) 'Structure, mechanism, and inhibition of the zinc-dependent histone deacetylases', *Current Opinion in Structural Biology*, 59, pp. 9–18. Available at: https://doi.org/10.1016/J.SBI.2019.01.004.

Pradas, J.C. *et al.* (2020) 'Identification of genes and pathways regulated by lamin a in heart', *Journal of the American Heart Association*, 9(16). Available at: https://doi.org/10.1161/JAHA.119.015690.

Prall, O.W.J. *et al.* (2007) 'An Nkx2-5/Bmp2/Smad1 negative feedback loop controls heart progenitor specification and proliferation.', *Cell*, 128(5), pp. 947–59. Available at: https://doi.org/10.1016/j.cell.2007.01.042.

Price, V., Wang, L. and D'Mello, S.R. (2013) 'Conditional Deletion of Histone Deacetylase-4 in the Central Nervous System Has No Major Effect on Brain Architecture or Neuronal Viability', *Journal of neuroscience research*, 91(3), pp. 407–415.

Priest, B.T. and McDermott, J.S. (2015) 'Cardiac ion channels', *Channels (Austin)*, 9(6), pp. 352–359.

Pufahl, L. *et al.* (2012) 'Trichostatin A induces 5-lipoxygenase promoter activity and mRNA expression via inhibition of histone deacetylase 2 and 3.', *Journal of cellular and molecular medicine*, 16(7), pp. 1461–73. Available at: https://doi.org/10.1111/j.1582-4934.2011.01420.x.

Pustovit, K.B. *et al.* (2022) 'α1-adrenergic receptors accompanied by GATA4 expression are related to proarrhythmic conduction and automaticity in rat interatrial septum', *Journal of Physiology and Biochemistry*, 78(4), pp. 793–805. Available at: https://doi.org/10.1007/S13105-022-00902-8/METRICS.

Quaife-Ryan, G.A. *et al.* (2016) 'Resetting the epigenome for heart regeneration.', *Seminars in Cell & Developmental Biology*, 58, pp. 2–13. Available at: https://doi.org/10.1016/j.semcdb.2015.12.021.

Raudvere, U. *et al.* (2019) 'g:Profiler: a web server for functional enrichment analysis and conversions of gene lists (2019 update)', *Nucleic Acids Research*, 47(W1), pp. W191–W198. Available at: https://doi.org/10.1093/NAR/GKZ369.

Redman, M. *et al.* (2016) 'What is CRISPR/Cas9?', *Archives of disease in childhood. Education and practice edition* [Preprint]. Available at: https://doi.org/10.1136/archdischild-2016-310459.

Reiter, J.F. *et al.* (1999) 'Gata5 is required for the development of the heart and endoderm in zebrafish.', *Genes & development*, 13(22), pp. 2983–95.

Riggs, M.G. *et al.* (1977) 'n-Butyrate causes histone modification in HeLa and Friend erythroleukaemia cells.', *Nature*, 268(5619), pp. 462–4. Available at: https://doi.org/10.1038/268462a0.

Riley, P.R. *et al.* (2000) 'Early exclusion of hand1-deficient cells from distinct regions of the left ventricular myocardium in chimeric mouse embryos.', *Developmental biology*, 227(1), pp. 156–68. Available at: https://doi.org/10.1006/dbio.2000.9864.

Ringnér, M. (2008) 'What is principal component analysis?', *Nature Biotechnology*, 26(3), pp. 303–304. Available at: https://doi.org/10.1038/nbt0308-303.

Rius, R. *et al.* (2019) 'Clinical Spectrum and Functional Consequences Associated with Bi-Allelic Pathogenic PNPT1 Variants', *Journal of Clinical Medicine*, 8(11), p. 2020. Available at: https://doi.org/10.3390/JCM8112020.

Robertson, C., Tran, D.D. and George, S.C. (2013) 'Concise review: Maturation phases of human pluripotent stem cell-derived cardiomyocytes', *Stem Cells*. John Wiley & Sons, Ltd, pp. 829–837. Available at: https://doi.org/10.1002/stem.1331.

Romero, D. (2019) 'HDAC inhibitors tested in phase III trial', *Nature Reviews Clinical Oncology*, 16(8), pp. 465–465. Available at: https://doi.org/10.1038/s41571-019-0224-2.

Rossi, G. *et al.* (2021) 'Capturing Cardiogenesis in Gastruloids', *Cell stem cell*, 28(2), p. 230. Available at: https://doi.org/10.1016/J.STEM.2020.10.013.

Roux, M. *et al.* (2015) 'Hoxb1 regulates proliferation and differentiation of second heart field progenitors in pharyngeal mesoderm and genetically interacts with Hoxa1 during cardiac outflow tract development', *Developmental Biology*, 406(2), pp. 247–258. Available at: https://doi.org/10.1016/J.YDBIO.2015.08.015.

Rudnizky, S. *et al.* (2017) 'Nucleosome mobility and the regulation of gene expression: Insights from single-molecule studies', *Protein Science* [Preprint]. Available at: https://doi.org/10.1002/pro.3159.

de Ruijter, A.J.M. *et al.* (2003) 'Histone deacetylases (HDACs): characterization of the classical HDAC family.', *The Biochemical journal*, 370(Pt 3), pp. 737–49. Available at: https://doi.org/10.1042/BJ20021321.

Saga, Y. *et al.* (1999) 'MesP1 is expressed in the heart precursor cells and required for the formation of a single heart tube', *Development (Cambridge, England)*, 126(15), pp. 3437–3447. Available at: https://doi.org/10.1242/DEV.126.15.3437.

Sakamoto, T. *et al.* (2020) 'A Critical Role for Estrogen-Related Receptor Signaling in Cardiac Maturation.', *Circulation research* [Preprint]. Available at: https://doi.org/10.1161/CIRCRESAHA.119.316100.

Sanchez, R. and Zhou, M.-M. (2009) 'The role of human bromodomains in chromatin biology and gene transcription.', *Current opinion in drug discovery & development*, 12(5), pp. 659–65.

Sandri, C., *et al.* (2004) 'Heart morphogenesis is not affected by overexpression of the Sh3bgr gene mapping to the Down syndrome heart critical region', *Human genetics*, 114(5), pp. 517–519.

Sanosaka, T., *et al.* (2022) 'Chromatin remodeler CHD7 targets active enhancer region to regulate cell type-specific gene expression in human neural crest cells', *Scientific reports*, 12(1), p. 22648.

Sartorelli, V. *et al.* (1997) 'Molecular mechanisms of myogenic coactivation by p300: direct interaction with the activation domain of MyoD and with the MADS

box of MEF2C.', *Molecular and Cellular Biology*, 17(2), pp. 1010–1026. Available at: https://doi.org/10.1128/mcb.17.2.1010.

Schlesinger, J. *et al.* (2011) 'The Cardiac Transcription Network Modulated by Gata4, Mef2a, Nkx2.5, Srf, Histone Modifications, and MicroRNAs', *PLoS Genetics*. Edited by D. Schübeler, 7(2), p. e1001313. Available at: https://doi.org/10.1371/journal.pgen.1001313.

Schnur, N. *et al.* (2007) 'The histone deacetylase inhibitor trichostatin A mediates upregulation of 5-lipoxygenase promoter activity by recruitment of Sp1 to distinct GC-boxes', *Biochimica et Biophysica Acta (BBA) - Molecular and Cell Biology of Lipids*, 1771(10), pp. 1271–1282. Available at: https://doi.org/10.1016/j.bbalip.2007.08.003.

Schultheiss, T.M., Xydas, S. and Lassar, A.B. (1995) 'Induction of avian cardiac myogenesis by anterior endoderm.', *Development (Cambridge, England)*, 121(12), pp. 4203–14.

Seifert, W., *et al.* (2015) 'Cohen syndrome-associated protein COH1 physically and functionally interacts with the small GTPase RAB6 at the Golgi complex and directs neurite outgrowth', *The Journal of biological chemistry*, 290(6), pp. 3349–3358.

Selewa, A. *et al.* (2020) 'Systematic Comparison of High-throughput Single-Cell and Single-Nucleus Transcriptomes during Cardiomyocyte Differentiation', *Scientific Reports*, 10(1), p. 1535. Available at: https://doi.org/10.1038/s41598-020-58327-6.

Seto, E. and Yoshida, M. (2014) 'Erasers of histone acetylation: the histone deacetylase enzymes.', *Cold Spring Harbor perspectives in biology*, 6(4), p. a018713. Available at: https://doi.org/10.1101/cshperspect.a018713.

Sharma, R. *et al.* (2017) 'Bmp Signaling Maintains a Mesoderm Progenitor Cell State in the Mouse Tailbud', *Development*, 144(16), pp. 2982–2993. Available at: https://doi.org/10.1242/dev.149955.

Sheng, W. *et al.* (2013) 'Association between mRNA levels of DNMT1, DNMT3A, DNMT3B, MBD2 and LINE-1 methylation status in infants with tetralogy of Fallot', *International journal of molecular medicine*, 32(3), pp. 694–702. Available at: https://doi.org/10.3892/IJMM.2013.1427.

Shikama, N. *et al.* (2003) 'Essential function of p300 acetyltransferase activity in heart, lung and small intestine formation', *The EMBO Journal*, 22(19), pp. 5175–5185. Available at: https://doi.org/10.1093/emboj/cdg502.

Shimizu, S. *et al.* (2018) 'The GATA4 Acetylation Site Plays a Key Role in the Development of Cardiomyocyte Hypertrophy', *European Cardiology Review*, 13(2), p. 125. Available at: https://doi.org/10.15420/ecr.2018.13.2.PO6.

Shin, H.Y. *et al.* (2017) 'CRISPR/Cas9 targeting events cause complex deletions and insertions at 17 sites in the mouse genome', *Nature Communications*, 8(1), p. 15464. Available at: https://doi.org/10.1038/ncomms15464.

Sifrim, A. *et al.* (2016) 'Distinct genetic architectures for syndromic and nonsyndromic congenital heart defects identified by exome sequencing', *Nature Genetics*, 48(9), pp. 1060–1065. Available at: https://doi.org/10.1038/ng.3627.

Sirbu, I.O., Zhao, X. and Duester, G. (2008) 'Retinoic acid controls heart anteroposterior patterning by down-regulating Isl1 through the Fgf8 pathway.', *Developmental dynamics : an official publication of the American Association of Anatomists*, 237(6), pp. 1627–35. Available at: https://doi.org/10.1002/dvdy.21570.

Slepak, T.I. *et al.* (2001) 'Control of cardiac-specific transcription by p300 through myocyte enhancer factor-2D.', *The Journal of biological chemistry*, 276(10), pp. 7575–85. Available at: https://doi.org/10.1074/jbc.M004625200.

Smith, S.C. *et al.* (1987) 'The Role of Aggregation in Embryonal Carcinoma Cell Differentiation', *Journal of Cellular Physiology*, 131(1), pp. 74–84. Available at: https://doi.org/10.1002/jcp.1041310112.

Snyder, M., Huang, X.-Y. and Zhang, J.J. (2010) 'Stat3 directly controls the expression of Tbx5, Nkx2.5, and GATA4 and is essential for cardiomyocyte differentiation of P19CL6 cells.', *The Journal of biological chemistry*, 285(31), pp. 23639–46. Available at: https://doi.org/10.1074/jbc.M110.101063.

Song, K. *et al.* (2012) 'Heart repair by reprogramming non-myocytes with cardiac transcription factors.', *Nature*, 485(7400), pp. 599–604. Available at: https://doi.org/10.1038/nature11139.

Spange, S. *et al.* (2009) 'Acetylation of non-histone proteins modulates cellular signalling at multiple levels', *The International Journal of Biochemistry & Cell Biology*, 41(1), pp. 185–198. Available at: https://doi.org/10.1016/j.biocel.2008.08.027.

Spangler, A. *et al.* (2018) 'A single cell transcriptional portrait of embryoid body differentiation and comparison to progenitors of the developing embryo', *Stem Cell Research*, 31, pp. 201–215. Available at: https://doi.org/10.1016/J.SCR.2018.07.022.

Später, D. *et al.* (2014) 'How to make a cardiomyocyte.', *Development (Cambridge, England)*, 141(23), pp. 4418–31. Available at: https://doi.org/10.1242/dev.091538.

Spelke, D.P. *et al.* (2011) 'Methods for Embryoid Body Formation: The Microwell Approach', in. Humana Press, pp. 151–162. Available at: https://doi.org/10.1007/978-1-60761-962-8_10.

Sperling, S. *et al.* (2005) 'Identification and functional analysis of CITED2 mutations in patients with congenital heart defects', *Human mutation*, 26(6), pp. 575–582. Available at: https://doi.org/10.1002/HUMU.20262.

Stanley, E.G. *et al.* (2002) 'Efficient Cre-mediated deletion in cardiac progenitor cells conferred by a 3'UTR-ires-Cre allele of the homeobox gene Nkx2-5.', *The International journal of developmental biology*, 46(4), pp. 431–9.

Stefanovic, S. and Zaffran, S. (2017) 'Mechanisms of retinoic acid signaling during cardiogenesis', *Mechanisms of Development*, 143, pp. 9–19. Available at: https://doi.org/10.1016/J.MOD.2016.12.002.

Steimle, J.D. and Moskowitz, I.P. (2017) 'TBX5: A Key Regulator of Heart Development', *Current topics in developmental biology*, 122, pp. 195–221.

Stennard, F.A. and Harvey, R.P. (2005) 'T-box transcription factors and their roles in regulatory hierarchies in the developing heart.', *Development (Cambridge, England)*, 132(22), pp. 4897–910. Available at: https://doi.org/10.1242/dev.02099.

Strahl, B.D. and Allis, C.D. (2000) 'The language of covalent histone modifications', *Nature*, 403(6765), pp. 41–45. Available at: https://doi.org/10.1038/47412.

Strübing, C. *et al.* (1995) 'Differentiation of pluripotent embryonic stem cells into the neuronal lineage in vitro gives rise to mature inhibitory and excitatory neurons', *Mechanisms of Development*, 53(2), pp. 275–287. Available at: https://doi.org/10.1016/0925-4773(95)00446-8.

Sui, T. *et al.* (2018) 'CRISPR-induced exon skipping is dependent on premature termination codon mutations', *Genome Biology*, 19(1), p. 164. Available at: https://doi.org/10.1186/s13059-018-1532-z.

Sun, B. *et al.* (2021) 'Cardiac ryanodine receptor calcium release deficiency syndrome', *Science Translational Medicine*, 13(579), p. eaba7287. Available at: https://doi.org/10.1126/scitranslmed.aba7287.

Sun, W.-J. *et al.* (2012) 'Histone acetyltransferases and deacetylases: molecular and clinical implications to gastrointestinal carcinogenesis', *Acta Biochimica et Biophysica Sinica*, 44(1), pp. 80–91. Available at: https://doi.org/10.1093/abbs/gmr113.

Sylva, M., van den Hoff, M.J.B. and Moorman, A.F.M. (2014) 'Development of the human heart.', *American journal of medical genetics. Part A*, 164A(6), pp. 1347–71. Available at: https://doi.org/10.1002/ajmg.a.35896.

Szot, J.O. *et al.* (2018) 'A Screening Approach to Identify Clinically Actionable Variants Causing Congenital Heart Disease in Exome Data', *Circulation. Genomic and precision medicine*, 11(3), p. e001978. Available at: https://doi.org/10.1161/CIRCGEN.117.001978/-/DC1.

Tada, M. and Smith, J.C. (2001) 'T-targets: clues to understanding the functions of T-box proteins.', *Development, growth & differentiation*, 43(1), pp. 1–11.

Tahmasebi, S., Amiri, M. and Sonenberg, N. (2019) 'Translational Control in Stem Cells', *Frontiers in Genetics*, 9, p. 709. Available at: https://doi.org/10.3389/fgene.2018.00709.

Tai, C.I. and Ying, Q.L. (2013) 'Gbx2, a LIF/Stat3 target, promotes reprogramming to and retention of the pluripotent ground state', *Journal of Cell Science*, 126(5), pp. 1093–1098. Available at: https://doi.org/10.1242/JCS.118273/263339/AM/GBX2-A-LIF-STAT3-TARGET-PROMOTES-REPROGRAMMING-TO.

Takaya, T. *et al.* (2008) 'Identification of p300-targeted acetylated residues in GATA4 during hypertrophic responses in cardiac myocytes.', *The Journal of biological chemistry*, 283(15), pp. 9828–35. Available at: https://doi.org/10.1074/jbc.M707391200.

Tandonnet, S. and Torres, T.T. (2017) 'Traditional versus 3' RNA-seq in a non-model species.', *Genomics data*, 11, pp. 9–16. Available at: https://doi.org/10.1016/j.gdata.2016.11.002.

Tarun, A. and Antoniades, C. (2018) 'The era of cardiovascular epigenetics: Histone deacetylases and vascular inflammation', *Cardiovascular Research*. Oxford University Press, pp. 928–930. Available at: https://doi.org/10.1093/cvr/cvy099.

Teekakirikul, P., Ho, C.Y. and Seidman, C.E. (2013) 'Inherited Cardiomyopathies', *Emery and Rimoin's Principles and Practice of Medical Genetics*, pp. 1–38. Available at: https://doi.org/10.1016/B978-0-12-383834-6.00053-7.

Thomas, M. *et al.* (2019) 'Collateral damage and CRISPR genome editing', *PLOS Genetics*. Edited by L. He, 15(3), p. e1007994. Available at: https://doi.org/10.1371/journal.pgen.1007994.

Tian, P., *et al.* (2022) 'Prognostic value of high-sensitivity cardiac troponin I in patients with non-ischaemic heart failure: insights from China', *ESC heart failure*, 9(5), pp. 3345–3357.

Tompkins, J.D. *et al.* (2016) 'Mapping Human Pluripotent-to-Cardiomyocyte Differentiation: Methylomes, Transcriptomes, and Exon DNA Methylation "Memories"', *EBioMedicine*, 4, pp. 74–85. Available at: https://doi.org/10.1016/j.ebiom.2016.01.021.

Tong, J.J. *et al.* (2002) 'Identification of HDAC10, a novel class II human histone deacetylase containing a leucine-rich domain', *Nucleic Acids Research*, 30(5), pp. 1114–1123.

Travers, J.G., Hu, T. and McKinsey, T.A. (2020) 'The black sheep of class IIa: HDAC7 SIKens the heart', *Journal of Clinical Investigation*. American Society for Clinical Investigation, pp. 2811–2813. Available at: https://doi.org/10.1172/JCI137074.

Trivedi, C.M. *et al.* (2007) 'Hdac2 regulates the cardiac hypertrophic response by modulating Gsk3 beta activity.', *Nature medicine*, 13(3), pp. 324–31. Available at: https://doi.org/10.1038/nm1552.

Trivedi, C.M. *et al.* (2010) 'Hopx and Hdac2 interact to modulate Gata4 acetylation and embryonic cardiac myocyte proliferation.', *Developmental cell*, 19(3), pp. 450–9. Available at: https://doi.org/10.1016/j.devcel.2010.08.012.

Tsai, W.W. *et al.* (2010) 'TRIM24 links a noncanonical histone signature to breast cancer', *Nature*, 468(7326), p. 927. Available at: https://doi.org/10.1038/NATURE09542.

Tsaturyan, A.K., *et al.* (2023) 'De Novo Asp219Val Mutation in Cardiac Tropomyosin Associated with Hypertrophic Cardiomyopathy', *International journal of molecular sciences*, 24(1), p. 18.

Tsushima, K. *et al.* (2011) 'IRF3 regulates cardiac fibrosis but not hypertrophy in mice during angiotensin II-induced hypertension', *FASEB journal : official publication of the Federation of American Societies for Experimental Biology*, 25(5), pp. 1531–1543. Available at: https://doi.org/10.1096/FJ.10-174615.

Tu, S. and Chi, N.C. (2012) 'Zebrafish models in cardiac development and congenital heart birth defects', *Differentiation*, 84(1), pp. 4–16. Available at: https://doi.org/10.1016/j.diff.2012.05.005.

Tucker, A.C. *et al.* (2014) 'Insights into the Specificity of Lysine Acetyltransferases', *Journal of Biological Chemistry*, 289(52), pp. 36249–36262. Available at: https://doi.org/10.1074/jbc.M114.613901.

Uosaki, H. *et al.* (2015) 'Transcriptional Landscape of Cardiomyocyte Maturation', *Cell Reports*, 13(8), pp. 1705–1716.

Vanlerberghe, C. *et al.* (2019) 'Holt-Oram syndrome: clinical and molecular description of 78 patients with TBX5 variants', *European Journal of Human Genetics*. Nature Publishing Group, pp. 360–368. Available at: https://doi.org/10.1038/s41431-018-0303-3.

Váraljai, R. *et al.* (2015) 'Increased mitochondrial function downstream from KDM5A histone demethylase rescues differentiation in pRB-deficient cells', *Genes*

& development, 29(17), pp. 1817–1834. Available at: https://doi.org/10.1101/GAD.264036.115.

Vega, R.B. *et al.* (2004) 'Histone Deacetylase 4 Controls Chondrocyte Hypertrophy during Skeletogenesis', *Cell*, 119(4), pp. 555–566.

Verdin, E., Dequiedt, F. and Kasler, H.G. (2003) 'Class II histone deacetylases: versatile regulators', *Trends in Genetics*, 19(5), pp. 286–293. Available at: https://doi.org/10.1016/S0168-9525(03)00073-8.

Verdone, L. *et al.* (2006) 'Histone acetylation in gene regulation.', *Briefings in functional genomics & proteomics*, 5(3), pp. 209–21. Available at: https://doi.org/10.1093/bfgp/ell028.

Verhoeven, M.C. *et al.* (2011) 'Wnt signaling regulates atrioventricular canal formation upstream of BMP and Tbx2.', *Birth defects research. Part A, Clinical and molecular teratology*, 91(6), pp. 435–40. Available at: https://doi.org/10.1002/bdra.20804.

Villamayor, L. *et al.* (2023) 'The IFN-stimulated gene IFI27 counteracts innate immune responses after viral infections by interfering with RIG-I signaling', *Frontiers in Microbiology*, 14, p. 1176177. Available at: https://doi.org/10.3389/FMICB.2023.1176177/BIBTEX.

Vincent, S.D. and Buckingham, M.E. (2010) 'How to make a heart: the origin and regulation of cardiac progenitor cells.', *Current topics in developmental biology*, 90, pp. 1–41. Available at: https://doi.org/10.1016/S0070-2153(10)90001-X.

Vincentz, J.W., Barnes, R.M. and Firulli, A.B. (2011) 'Hand factors as regulators of cardiac morphogenesis and implications for congenital heart defects', *Birth defects research. Part A, Clinical and molecular teratology*, 91(6), p. 485. Available at: https://doi.org/10.1002/BDRA.20796.

Van Vliet, P. *et al.* (2012) 'Early cardiac development: a view from stem cells to embryos', *Cardiovascular Research*, 96(3), pp. 352–362. Available at: https://doi.org/10.1093/CVR/CVS270.

Voelter-Mahlknecht, S., Ho, A.D. and Mahlknecht, U. (2005) 'Chromosomal organization and localization of the novel class IV human histone deacetylase 11 gene.', *International journal of molecular medicine*, 16(4), pp. 589–98.

Vujic, A. *et al.* (2015) 'Experimental heart failure modelled by the cardiomyocyte-specific loss of an epigenome modifier, DNMT3B', *Journal of molecular and cellular cardiology*, 82, pp. 174–183. Available at: https://doi.org/10.1016/J.YJMCC.2015.03.007.

Waldron, L. *et al.* (2016) 'The Cardiac TBX5 Interactome Reveals a Chromatin Remodeling Network Essential for Cardiac Septation', *Developmental Cell*, 36(3), pp. 262–275. Available at: https://doi.org/10.1016/j.devcel.2016.01.009.

Wamstad, J.A. *et al.* (2012) 'Dynamic and Coordinated Epigenetic Regulation of Developmental Transitions in the Cardiac Lineage', *Cell*, 151(1), pp. 206–220. Available at: https://doi.org/10.1016/j.cell.2012.07.035.

Wang, A.H. *et al.* (2000) 'Regulation of Histone Deacetylase 4 by Binding of 14-3-3 Proteins', *Molecular and Cellular Biology*, 20(18), p. 6904. Available at: https://doi.org/10.1128/MCB.20.18.6904-6912.2000.

Wang, H. *et al.* (2013) 'One-step generation of mice carrying mutations in multiple genes by CRISPR/Cas-mediated genome engineering.', *Cell*, 153(4), pp. 910–8. Available at: https://doi.org/10.1016/j.cell.2013.04.025.

Wang, J. *et al.* (2017) 'HAND1 Loss-of-Function Mutation Causes Tetralogy of Fallot', *Pediatric Cardiology*, 38(3), pp. 547–557. Available at: https://doi.org/10.1007/s00246-016-1547-8.

Wang, L. *et al.* (2015) 'Stoichiometry of Gata4, Mef2c, and Tbx5 Influences the Efficiency and Quality of Induced Cardiac Myocyte Reprogramming', *Circulation Research*, 116(2), pp. 237–244. Available at: https://doi.org/10.1161/CIRCRESAHA.116.305547.

Wang, L. *et al.* (2018) 'Cardiomyocyte-specific deletion of Sirt1 gene sensitizes myocardium to ischaemia and reperfusion injury', *Cardiovascular Research*, 114(6), pp. 805–821. Available at: https://doi.org/10.1093/CVR/CVY033.

Wang, L. *et al.* (2021) 'Paracrine interleukin-8 affects mesenchymal stem cells through the Akt pathway and enhances human umbilical vein endothelial cell proliferation and migration', *Bioscience Reports*, 41(5). Available at: https://doi.org/10.1042/BSR20210198/228273.

Wang, W. *et al.* (2021) 'Pten Regulates Cardiomyocyte Differentiation by Modulating Non-CG Methylation via Dnmt3', *Advanced Science*, 8(17), p. 2100849. Available at: https://doi.org/10.1002/ADVS.202100849.

Wang, X. *et al.* (2020) 'Comparative analysis of cell lineage differentiation during hepatogenesis in humans and mice at the single-cell transcriptome level', *Cell Research*, 30(12), pp. 1109–1126. Available at: https://doi.org/10.1038/s41422-020-0378-6.

Wang, Y. *et al.* (2018) 'Histone variants H2A.Z and H3.3 coordinately regulate PRC2-dependent H3K27me3 deposition and gene expression regulation in mES cells', *BMC Biology*, 16(1), p. 107. Available at: https://doi.org/10.1186/s12915-018-0568-6.

Wang, Z., Qin, G. and Zhao, T.C. (2014) 'Histone Deacetylase 4 (HDAC4): Mechanism of Regulations and Biological Functions', *Epigenomics*, 6(1), p. 139. Available at: https://doi.org/10.2217/epi.13.73.

Wang, Z.-Y., Qin, W. and Yi, F. (2015) 'Targeting histone deacetylases: perspectives for epigenetic-based therapy in cardio-cerebrovascular disease.', *Journal of geriatric cardiology : JGC*, 12(2), pp. 153–64. Available at: https://doi.org/10.11909/j.issn.1671-5411.2015.02.010.

Weeks, Kate L and Avkiran, M. (2015) 'Roles and post-translational regulation of cardiac class IIa histone deacetylase isoforms.', *The Journal of physiology*, 593(8), pp. 1785–97. Available at: https://doi.org/10.1113/jphysiol.2014.282442.

Weeks, Kate L. and Avkiran, M. (2015) 'Roles and post-translational regulation of cardiac class IIa histone deacetylase isoforms', *Journal of Physiology*, 593(8), pp. 1785–1797. Available at: https://doi.org/10.1113/jphysiol.2014.282442.

Wei, J. *et al.* (2017) 'Reversal of pathological cardiac hypertrophy via the MEF2-coregulator interface', *JCI insight*, 2(17). Available at: https://doi.org/10.1172/jci.insight.91068.

Wessels, A. and Sedmera, D. (2003) 'Developmental anatomy of the heart: a tale of mice and man', *Physiological Genomics*, 15(3), pp. 165–176. Available at: https://doi.org/10.1152/physiolgenomics.00033.2003.

Williams, K.A. *et al.* (2013) 'Extracellular signal-regulated kinase (ERK) phosphorylates histone deacetylase 6 (HDAC6) at serine 1035 to stimulate cell migration', *Journal of Biological Chemistry*, 288(46), pp. 33156–33170. Available at: https://doi.org/10.1074/jbc.M113.472506.

Wobus, A.M. *et al.* (1997) 'Retinoic acid accelerates embryonic stem cell-derived cardiac differentiation and enhances development of ventricular cardiomyocytes', *Journal of molecular and cellular cardiology*, 29(6), pp. 1525–1539. Available at: https://doi.org/10.1006/JMCC.1997.0433.

Wobus, A.M., Wallukat, G. and Hescheler, J. (1991) 'Pluripotent mouse embryonic stem cells are able to differentiate into cardiomyocytes expressing chronotropic responses to adrenergic and cholinergic agents and Ca2+ channel blockers', *Differentiation; research in biological diversity*, 48(3), pp. 173–182. Available at: https://doi.org/10.1111/J.1432-0436.1991.TB00255.X.

Wolters, R. *et al.* (2021) 'Role of the Epicardium in the Development of the Atrioventricular Valves and Its Relevance to the Pathogenesis of Myxomatous Valve Disease', *Journal of Cardiovascular Development and Disease*, 8(5). Available at: https://doi.org/10.3390/JCDD8050054.

Wu, M. (2018) 'Mechanisms of trabecular formation and specification during cardiogenesis', *Pediatric cardiology*, 39(6), p. 1082. Available at: https://doi.org/10.1007/S00246-018-1868-X.

Wu, S.M. *et al.* (2006) 'Developmental origin of a bipotential myocardial and smooth muscle cell precursor in the mammalian heart', *Cell*, 127(6), pp. 1137–1150. Available at: https://doi.org/10.1016/J.CELL.2006.10.028.

Xie, L. *et al.* (2012) 'Tbx5-hedgehog molecular networks are essential in the second heart field for atrial septation.', *Developmental cell*, 23(2), pp. 280–91. Available at: https://doi.org/10.1016/j.devcel.2012.06.006.

Xie, M. *et al.* (2014) 'Histone deacetylase inhibition blunts ischemia/reperfusion injury by inducing cardiomyocyte autophagy.', *Circulation*, 129(10), pp. 1139–51. Available at: https://doi.org/10.1161/CIRCULATIONAHA.113.002416.

Xie, Z. *et al.* (2012) 'Lysine succinylation and lysine malonylation in histones.', *Molecular & cellular proteomics : MCP*, 11(5), pp. 100–7. Available at: https://doi.org/10.1074/mcp.M111.015875.

Xu, L. and Jiang, H. (2020) 'Writing and Reading Histone H3 Lysine 9 Methylation in Arabidopsis', *Frontiers in Plant Science*, 11, p. 452. Available at: https://doi.org/10.3389/fpls.2020.00452.

Xu, M. *et al.* (2014) 'CITED2 Mutation and methylation in children with congenital heart disease', *Journal of Biomedical Science*, 21(1), pp. 1–8. Available at: https://doi.org/10.1186/1423-0127-21-7/FIGURES/3.

Xu, T. *et al.* (2017) 'RBPJ/CBF1 interacts with L3MBTL3/MBT1 to promote repression of Notch signaling via histone demethylase KDM1A/LSD1', *The EMBO journal*, 36(21), pp. 3232–3249. Available at: https://doi.org/10.15252/EMBJ.201796525.

Xu, W. *et al.* (2000) 'Loss of Gcn5l2 leads to increased apoptosis and mesodermal defects during mouse development.', *Nature genetics*, 26(2), pp. 229–32. Available at: https://doi.org/10.1038/79973.

Yamagishi, H. (2021) 'Cardiac Neural Crest', *Cold Spring Harbor perspectives in biology*, 13(1), pp. 1–18. Available at: https://doi.org/10.1101/CSHPERSPECT.A036715.

Yamak, A., *et al.* (2020) 'Loss of Asb2 Impairs Cardiomyocyte Differentiation and Leads to Congenital Double Outlet Right Ventricle', *iScience*, 23(3), p. 100959.

Yamauchi, T. *et al.* (2000) 'Distinct but overlapping roles of histone acetylase PCAF and of the closely related PCAF-B/GCN5 in mouse embryogenesis', *Proceedings of*

the National Academy of Sciences, 97(21), pp. 11303–11306. Available at: https://doi.org/10.1073/pnas.97.21.11303.

Yan, Y., *et al.* (2017) 'Copy number variation of functional RBMY1 is associated with sperm motility: an azoospermia factor-linked candidate for asthenozoospermia', *Human reproduction (Oxford, England)*, 32(7), pp. 1521–1531.

Yanazume, T. *et al.* (2003) 'Cardiac p300 is involved in myocyte growth with decompensated heart failure.', *Molecular and cellular biology*, 23(10), pp. 3593–606. Available at: https://doi.org/10.1128/mcb.23.10.3593-3606.2003.

Yang, G. *et al.* (2012) 'Trichostatin a Promotes Cardiomyocyte Differentiation of Rat Mesenchymal Stem Cells after 5-Azacytidine Induction or during Coculture with Neonatal Cardiomyocytes via a Mechanism Independent of Histone Deacetylase Inhibition', *Cell Transplantation*, 21(5), pp. 985–996. Available at: https://doi.org/10.3727/096368911X593145.

Yang, G.J. *et al.* (2021) 'The emerging role of KDM5A in human cancer', *Journal of Hematology & Oncology 2021 14:1*, 14(1), pp. 1–18. Available at: https://doi.org/10.1186/S13045-021-01041-1.

Yang, Q. *et al.* (2019) 'Host HDAC4 regulates the antiviral response by inhibiting the phosphorylation of IRF3', *Journal of molecular cell biology*, 11(2), pp. 158–169. Available at: https://doi.org/10.1093/JMCB/MJY035.

Yang, X.J. *et al.* (1996) 'A p300/CBP-associated factor that competes with the adenoviral oncoprotein E1A.', *Nature*, 382(6589), pp. 319–24. Available at: https://doi.org/10.1038/382319a0.

Yang, X.-J. and Seto, E. (2007) 'HATs and HDACs: from structure, function and regulation to novel strategies for therapy and prevention', *Oncogene*, 26(37), pp. 5310–5318. Available at: https://doi.org/10.1038/sj.onc.1210599.

Yao, J. *et al.* (2016) 'Matrix Gla protein regulates differentiation of endothelial cells derived from mouse embryonic stem cells', *Angiogenesis*, 19(1), pp. 1–7. Available at: https://doi.org/10.1007/S10456-015-9484-3/METRICS.

Yelon, D. *et al.* (2000) ‘The bHLH transcription factor hand2 plays parallel roles in zebrafish heart and pectoral fin development.’, *Development (Cambridge, England)*, 127(12), pp. 2573–82.

Youn, H.D., Grozinger, C.M. and Liu, J.O. (2000) ‘Calcium regulates transcriptional repression of myocyte enhancer factor 2 by histone deacetylase 4.’, *The Journal of biological chemistry*, 275(29), pp. 22563–7. Available at: https://doi.org/10.1074/jbc.C000304200.

Zaffran, S. *et al.* (2004) ‘Right ventricular myocardium derives from the anterior heart field’, *Circulation research*, 95(3), pp. 261–268. Available at: https://doi.org/10.1161/01.RES.0000136815.73623.BE.

Zaidi, S. *et al.* (2013) ‘De novo mutations in histone-modifying genes in congenital heart disease.’, *Nature*, 498(7453), pp. 220–3. Available at: https://doi.org/10.1038/nature12141.

Zhang, C.L. *et al.* (2002) ‘Class II histone deacetylases act as signal-responsive repressors of cardiac hypertrophy.’, *Cell*, 110(4), pp. 479–88. Available at: https://doi.org/10.1016/s0092-8674(02)00861-9.

Zhang, L. *et al.* (2014) ‘Mesodermal Nkx2.5 is necessary and sufficient for early second heart field development’, *Developmental Biology*, 390(1), pp. 68–79. Available at: https://doi.org/10.1016/J.YDBIO.2014.02.023.

Zhang, L. *et al.* (2018) ‘Myocyte-specific overexpressing HDAC4 promotes myocardial ischemia/reperfusion injury’, *Molecular Medicine*, 24(1). Available at: https://doi.org/10.1186/s10020-018-0037-2.

Zhao, Y. *et al.* (2006) ‘Acetylation of p53 at Lysine 373/382 by the Histone Deacetylase Inhibitor Depsipeptide Induces Expression of p21Waf1/Cip1’, *Molecular and Cellular Biology*, 26(7), p. 2782. Available at: https://doi.org/10.1128/MCB.26.7.2782-2790.2006.

Zheng, Z. *et al.* (2012) ‘Reprogramming of human fibroblasts into multipotent cells with a single ECM proteoglycan, fibromodulin’, *Biomaterials*, 33(24), pp. 5821–5831. Available at: https://doi.org/https://doi.org/10.1016/j.biomaterials.2012.04.049.

Zhou, L. *et al.* (2017) 'Gata4 potentiates second heart field proliferation and Hedgehog signaling for cardiac septation.', *Proceedings of the National Academy of Sciences of the United States of America*, 114(8), pp. E1422–E1431. Available at: https://doi.org/10.1073/pnas.1605137114.

Zhou, X. *et al.* (2000) 'Histone deacetylase 4 associates with extracellular signal-regulated kinases 1 and 2, and its cellular localization is regulated by oncogenic Ras.', *Proceedings of the National Academy of Sciences of the United States of America*, 97(26), pp. 14329–33. Available at: https://doi.org/10.1073/pnas.250494697.

Zhou, Y.M. *et al.* (2016) 'HAND1 loss-of-function mutation associated with familial dilated cardiomyopathy', *Clinical Chemistry and Laboratory Medicine*, 54(7), pp. 1161–1167. Available at: https://doi.org/10.1515/cclm-2015-0766.

Zhu, J. *et al.* (2013) 'Genome-wide Chromatin State Transitions Associated with Developmental and Environmental Cues', *Cell*, 152(3), pp. 642–654. Available at: https://doi.org/10.1016/j.cell.2012.12.033.

Zhu, T. *et al.* (2017) 'T-box family of transcription factor-TBX5, insights in development and disease', *American Journal of Translational Research*, 9(2), pp. 442–453.

Zima, A. V. *et al.* (2007) 'IP3-dependent nuclear Ca2+ signalling in the mammalian heart', *The Journal of Physiology*, 584(2), pp. 601–611. Available at: https://doi.org/10.1113/JPHYSIOL.2007.140731.

Zou, G.L. *et al.* (2019) 'Catalpol attenuates cardiomyocyte apoptosis in diabetic cardiomyopathy via Neat1/miR-140–5p/HDAC4 axis', *Biochimie*, 165, pp. 90–99. Available at: https://doi.org/10.1016/j.biochi.2019.05.005.

Zuo, J.Y. *et al.* (2022) 'Identification and functional analysis of variants of MYH6 gene promoter in isolated ventricular septal defects', *BMC medical genomics*, 15(1), p. 213.

7 APPENDICES

7.1 Appendix 1: Full list of canonical pathways generated by IPA

Canonical Pathways	WT undiff vs WT diff B	WT undiff vs WT diff NB	WT undiff vs Hdac4 KO B	WT undiff vs Hdac4 KO NB	WT diff B vs WT diff N B	WT undiff vs TSA B	WT diff B vs Hdac4 KO B	WT diff NB vs Hdac4 KO diff NB	WT diff B vs TSA B	WT TSA B vs Hdac4 KO B
CREB Signaling in Neurons	9.935	9.815	10.839	10.604	N/A	8.066	N/A	-1.342	-3.101	4.006
Phagosome Formation	9.035	8.832	9.767	9.549	N/A	6.971	N/A	-1.606	-5.039	5.41
Cardiac Hypertrophy Signaling (Enhanced)	7.869	7.519	8.493	8.951	N/A	7.391	N/A	-0.229	-3.677	2.324

Pulmonary Fibrosis Idiopathic Signaling Pathway	7.385	7.606	8.795	8.327	N/A	6.976	N/A	0.728	-3.464	3.101
Wound Healing Signaling Pathway	8.024	8.091	7.937	7.981	N/A	7.136	N/A	0.894	-2.92	3.286
Hepatic Fibrosis Signaling Pathway	7.3	7.561	7.956	7.675	N/A	7.034	N/A	-0.447	-3.753	2.832
GP6 Signaling Pathway	6.671	6.952	6.671	6.765	N/A	5.986	N/A	2.309	-4.243	4.352
G-Protein Coupled Receptor Signaling	7.276	7.338	8.397	7.595	N/A	5.986	N/A	-1.279	-2.683	3.085
Breast Cancer Regulation by Stathmin1	7.366	7.35	8.772	7.829	N/A	6.23	N/A	-0.54	-2.54	2.929
Colorectal Cancer Metastasis Signaling	7.319	7.758	7.677	7.695	N/A	6.807	N/A	1	-3.53	1.4
Synaptogenesis Signaling Pathway	6.592	6.187	6.091	6.519	N/A	5.768	N/A	-0.577	-3.286	2.596

Cardiac Hypertrophy Signaling	6.328	6.601	6.395	6.881	N/A	6.466	N/A	1.342	-2.065	1.147
IL-8 Signaling	6.51	6.184	6.671	6.6	N/A	6.647	N/A	-0.378	-2.132	1.279
Calcium Signaling	6.455	5.612	6.119	6.35	N/A	4.636	N/A	-1.633	-1.667	2.668
Role of NFAT in Cardiac Hypertrophy	6.54	6.466	6.183	6.54	N/A	6.037	N/A	0.378	-1.5	1.147
Production of Nitric Oxide and Reactive Oxygen Species in Macrophages	5.367	5.823	5.063	5.498	N/A	5.185	N/A	0.632	-3.545	3.266
Neuroinflammation Signaling Pathway	6.582	6.237	5.635	5.942	N/A	4.87	N/A	0	-2.534	2.16
ILK Signaling	5.421	5.58	5.969	6.053	N/A	5.185	N/A	-0.378	-2.236	3
Integrin Signaling	5.009	5.356	5.085	5.662	N/A	5.341	N/A	-1	-2.683	2.4

Tumor Microenvironment Pathway	4.472	3.882	5.742	5.735	N/A	4.359	N/A	-0.775	-3	3.773
eNOS Signaling	5.88	5.798	5.252	6.021	N/A	5.374	N/A	N/A	-2.138	1.265
Oxytocin Signaling Pathway	5.364	4.666	5.613	5.757	N/A	4.9	N/A	-0.905	-1.3	2.828
STAT3 Pathway	4.907	4.901	5.485	5.555	N/A	5.217	N/A	0.447	-2.673	2.138
Adrenomedullin signaling pathway	5.444	5.607	5.208	5.208	N/A	4.391	N/A	0.378	-2.6	2.449
Signaling by Rho Family GTPases	5.814	5.59	4.95	5.277	N/A	5.812	N/A	0.447	-1.633	1.4
Neuropathic Pain Signaling In Dorsal Horn Neurons	4.992	5.443	4.992	5.374	N/A	4.323	N/A	-1.342	-1.265	2.357
Cholecystokinin/Gastrin-mediated Signaling	4.768	4.841	5.191	5.24	N/A	5.425	N/A	-0.378	-1.667	2.53
Estrogen Receptor Signaling	4.526	4.973	4.98	5.66	N/A	4.492	N/A	0.577	-1.961	2.335

Role of Pattern Recognition Receptors in Recognition of Bacteria and Viruses	4.644	5.427	4.003	4.667	N/A	4.747	N/A	0.378	-3.13	1.964
Regulation Of The Epithelial Mesenchymal Transition By Growth Factors Pathway	5.416	5.033	5.421	5.976	N/A	5.17	N/A	-0.378	-0.775	0.728
Renin-Angiotensin Signaling	4.529	4.919	4.111	5.06	N/A	4.243	N/A	-1	-2.309	2.138
IL-6 Signaling	4.629	4.899	4.919	5.032	N/A	3.893	N/A	0.333	-2	2.5
Relaxin Signaling	5.154	5.308	4.644	4.938	N/A	4.564	N/A	N/A	-2.138	1.069
Glioblastoma Multiforme Signaling	4.5	4.924	5.08	4.99	N/A	4.817	N/A	2	-1.5	0

Leukocyte Extravasation Signaling	4.276	4.542	4.185	4.41	N/A	3.91	N/A	-0.447	-2.694	2.887
White Adipose Tissue Browning Pathway	4.589	4.608	4.765	4.924	N/A	3.543	N/A	-0.447	-1	3.13
HIF1Î± Signaling	4.664	4.396	4.849	5.288	N/A	4.025	N/A	-0.707	-1.616	1.4
Pulmonary Healing Signaling Pathway	3.545	4.207	5.496	4.745	N/A	3.498	N/A	0.302	-2.837	2.132
IL-17 Signaling	4.627	4.837	4.817	4.636	N/A	4.061	N/A	-0.378	-1.789	1.528
fMLP Signaling in Neutrophils	4.768	5.126	4.459	5.096	N/A	5.209	N/A	N/A	-1.387	0.577
TREM1 Signaling	4.11	4.938	4.017	3.772	N/A	2.921	N/A	N/A	-3.3	3.5
HMGB1 Signaling	4.323	4.715	3.833	4.128	N/A	3.703	N/A	0	-2.84	2.673
P2Y Purigenic Receptor Signaling Pathway	5.078	5.422	4.533	5.27	N/A	4.423	N/A	N/A	-0.905	0.577

Neurovascular Coupling Signaling Pathway	4.315	3.702	4.005	4.357	N/A	3.138	N/A	-1.667	-1.877	3
GNRH Signaling	4.543	4.636	4.808	5.091	N/A	4.429	N/A	-1	-0.816	0.333
Ephrin Receptor Signaling	4.522	5.091	4.243	5.196	N/A	4.429	N/A	N/A	-0.707	1.155
Thrombin Signaling	4.851	5.196	4.695	4.765	N/A	5.009	N/A	-0.447	-0.277	0
Factors Promoting Cardiogenesis in Vertebrates	4.556	4.185	5.288	5.02	N/A	4.478	N/A	0	-0.728	0.853
cAMP-mediated signaling	4.217	4.417	4.529	4.859	N/A	3.074	N/A	-0.816	-1.177	1.976
GÎ±q Signaling	4.648	4.589	4.131	4.636	N/A	5.091	N/A	N/A	-1.414	0.471
RHOGDI Signaling	-4.627	-4.355	-4.061	-4.061	N/A	-4.99	N/A	-1.342	0.832	-0.5

FcÎ³ Receptor-mediated Phagocytosis in Macrophages and Monocytes	4.025	4.128	3.363	4.003	N/A	3.683	N/A	N/A	-2.668	2.668
Osteoarthritis Pathway	2.951	3.591	4.216	3.928	N/A	2.68	2	0	-1.964	3.157
RANK Signaling in Osteoclasts	4.017	3.773	4.2	4.158	N/A	3.922	N/A	N/A	-2.714	1.633
Senescence Pathway	4.392	4.233	4.121	4.6	N/A	4.631	N/A	0.378	-1.091	0.728
Gustation Pathway	4.388	5.176	4.217	4.556	N/A	4.217	N/A	0.816	0.2	0.557
Chemokine Signaling	3.9	3.651	4.158	3.922	N/A	2.132	N/A	-1	-2.53	2.673
IL-15 Production	4.715	3.983	3.883	3.883	N/A	3.883	N/A	N/A	-1.89	1.667
Nitric Oxide Signaling in the Cardiovascular System	3.647	4.33	4.041	4.323	N/A	4.111	N/A	N/A	-1.807	1.604

Role of PKR in Interferon Induction and Antiviral Response	4.743	4.938	3.592	3.651	N/A	4.218	N/A	-0.378	-1.155	-1
Acute Phase Response Signaling	4.202	4.185	4.009	4.061	N/A	3.775	N/A	0.905	-1.387	1.069
Nicotine Degradation II	4.123	3.3	4.243	3.742	N/A	3.742	N/A	N/A	-1.508	2.714
CXCR4 Signaling	4.18	4.036	3.709	4.355	N/A	4.621	N/A	N/A	-1.508	0.832
PTEN Signaling	-3.92	-3.286	-4.025	-4.217	N/A	-3.479	N/A	-0.447	1.897	-1.941
Melanocyte Development and Pigmentation Signaling	4.459	4.218	3.55	4.667	N/A	3.053	N/A	N/A	-2.121	1.134
Dopamine-DARPP32 Feedback in cAMP Signaling	4.036	4.727	3.713	4.45	N/A	4.009	N/A	-1	0.333	0.905

Ovarian Cancer Signaling	3.922	3.772	4.041	4.271	N/A	3.411	N/A	N/A	-2.333	1.342
Insulin Secretion Signaling Pathway	3.483	3.726	3.763	4.346	N/A	2.77	N/A	-1.342	-1.291	2.132
PI3K Signaling in B Lymphocytes	4.18	3.742	3.606	3.781	N/A	3.833	N/A	-0.447	-1.698	1.213
Apelin Cardiomyocyte Signaling Pathway	3.812	3.92	3.618	3.904	N/A	3.569	N/A	N/A	-1.732	1.941
FAT10 Cancer Signaling Pathway	4.264	3.922	4.082	4.146	N/A	3.545	N/A	0	-1	1.342
Estrogen-Dependent Breast Cancer Signaling	3.674	4.041	3.8	4.041	N/A	3.411	N/A	N/A	-1.633	1.633
Corticotropin Releasing Hormone Signaling	3.742	3.713	3.357	3.576	N/A	2.889	N/A	-1.633	-2.53	0.775

GPCR-Mediated Nutrient Sensing in Enteroendocrine Cells	4.131	4.481	3.969	4.371	N/A	3.983	N/A	0	0	1.213
Actin Cytoskeleton Signaling	3.457	3.15	3.474	4.106	N/A	3.775	N/A	-1	-1.604	1.342
G Beta Gamma Signaling	3.91	4.036	4.009	4.16	N/A	4.041	N/A	-0.447	0.905	-0.277
Netrin Signaling	3.656	3.212	3.656	4.218	N/A	3.656	N/A	-1	-0.707	1.667
Role of Hypercytokinemia/hyperchemokinemia in the Pathogenesis of Influenza	3.651	4.902	2.921	2.887	N/A	4.131	N/A	1.265	-1.807	0.2
IL-3 Signaling	3.889	4	3.889	4.459	N/A	4.747	N/A	N/A	-0.707	0
Glioma Signaling	3.773	3.893	4.11	4.459	N/A	3.9	N/A	N/A	-0.905	0.632

IL-17A Signaling in Airway Cells	3.9	3.962	3.3	3.771	N/A	3.606	N/A	N/A	-1.667	1.414
HOTAIR Regulatory Pathway	3.3	3.536	3.447	3.299	N/A	2.853	N/A	1.633	-2.4	0.943
Reelin Signaling in Neurons	3.13	3.063	3.162	3.618	N/A	3.317	N/A	-1.342	-1.941	1.807
Cell Cycle Control of Chromosomal Replication	-4.564	-4.564	-3.9	-3.8	N/A	-4.542	N/A	N/A	N/A	N/A
Glioma Invasiveness Signaling	3.651	4.116	3.651	3.656	N/A	3.9	N/A	N/A	-1.667	0.707
Regulation Of The Epithelial Mesenchymal Transition In Development Pathway	3.569	4.459	4.439	4.459	N/A	3.452	N/A	N/A	N/A	-0.905

Crosstalk between Dendritic Cells and Natural Killer Cells	3.273	3.657	2.858	3.411	N/A	2.132	N/A	-1	-1.897	2.496
AMPK Signaling	3.538	3.742	3.394	3.571	N/A	2.832	N/A	N/A	-1.897	1.732
Pancreatic Adenocarcinoma Signaling	3.55	3.781	3.773	3.43	N/A	3.53	N/A	N/A	-1.604	1
GDNF Family Ligand-Receptor Interactions	3.53	3.528	3.272	3.9	N/A	2.837	N/A	N/A	-2.111	1.265
Xenobiotic Metabolism PXR Signaling Pathway	3.75	3.787	2.898	2.84	N/A	2.898	N/A	1.414	-1.213	1.528
tRNA Charging	-4.359	-4	-3.873	-3.742	N/A	-4.243	N/A	N/A	N/A	N/A
Toll-like Receptor Signaling	3.13	3.266	2.982	2.668	N/A	2.236	N/A	1	-2.449	2.449
Opioid Signaling Pathway	3.2	2.886	3.384	3.881	N/A	2.222	N/A	-1.508	-0.655	2.353
Th1 Pathway	3.3	4.3	3.3	4.0	N/	3	N/	N/	-	0.7

	33	2	63	03	A		A	A	1.291	75
IGF-1 Signaling	3.413	3.333	3.182	3.889	N/A	4.082	N/A	N/A	-1.414	0.707
PCP (Planar Cell Polarity) Pathway	3.528	3.657	3.9	4.315	N/A	3.272	N/A	N/A	N/A	-1.134
p70S6K Signaling	3.328	3.775	3.266	3.501	N/A	3.507	N/A	N/A	-1.807	0.535
PAK Signaling	3.651	3.656	3.656	4.116	N/A	3.78	N/A	N/A	-0.535	-0.258
HGF Signaling	3.042	3.086	3.333	3.569	N/A	3.43	N/A	N/A	-1.897	1.134
p38 MAPK Signaling	3.13	3.606	3.571	3.795	N/A	2.188	N/A	0.447	-1.134	1.508
Apelin Liver Signaling Pathway	3.606	3.051	3.207	3.357	N/A	2.84	N/A	N/A	-2.121	1.134
Nicotine Degradation III	3.606	2.84	3.606	3.464	N/A	3.464	N/A	N/A	-0.378	1.89

Synaptic Long Term Depression	3.064	3.038	3.622	3.679	N/A	3.586	N/A	-0.378	0.535	1.279
Apelin Endothelial Signaling Pathway	3.618	3.111	3.317	3.507	N/A	3.569	N/A	N/A	-0.832	1.155
IL-9 Signaling	3.207	3.771	3.051	3.357	N/A	3.464	N/A	N/A	-1.342	0.816
SPINK1 General Cancer Pathway	3.441	3.411	2.711	3.962	N/A	3.638	N/A	N/A	-1.342	0.378
RAC Signaling	4.041	3.43	3.128	3.53	N/A	2.837	N/A	N/A	-1.265	0.632
LPS-stimulated MAPK Signaling	2.887	2.744	3.157	3.272	N/A	3.13	N/A	N/A	-1.897	1.667
JAK/STAT Signaling	3.307	3.212	3.024	3.657	N/A	3.8	N/A	N/A	-1.342	0.378
Glutamate Receptor Signaling	3.357	3.5	3.638	3.638	N/A	2.84	N/A	N/A	N/A	1.633
Dermatan Sulfate Biosynthesis	3.838	3.545	3.838	3.838	N/A	3.545	N/A	N/A	0	0

Growth Hormone Signaling	3.286	3.182	3.087	3.9	N/A	3.922	N/A	N/A	-0.816	0.333
NGF Signaling	3.452	2.777	3.363	3.781	N/A	2.058	N/A	N/A	-2.121	0.816
WNT/Ca+ pathway	3.773	3.889	3.43	3.9	N/A	2.191	N/A	N/A	N/A	1
FGF Signaling	3.087	2.333	2.744	4.004	N/A	1.915	N/A	0	-2.111	1.941
GÎ±s Signaling	2.874	3.333	3.479	3.569	N/A	2.137	N/A	-0.447	-0.707	1.414
Xenobiotic Metabolism General Signaling Pathway	2.828	2.994	3.539	3.111	N/A	2.897	N/A	0	-1.155	1.387
Synaptic Long Term Potentiation	2.885	3.606	2.832	3.647	N/A	2.359	N/A	-1.342	0	1.155
Actin Nucleation by ARP-WASP Complex	3.5	3.71	3.207	3.5	N/A	3.9	N/A	N/A	N/A	N/A
GM-CSF Signaling	2.887	2.921	3.266	2.887	N/A	2.524	N/A	N/A	-1.89	1.414

ERBB Signaling	2.921	3.212	2.874	3.182	N/A	2.6	N/A	N/A	-1.897	1
CD40 Signaling	3.3	3.411	3.153	3.3	N/A	2.673	N/A	N/A	-1	0.816
Thyroid Cancer Signaling	2.137	2.402	3.124	3.162	N/A	1.976	N/A	-1	-1.667	2.111
HER-2 Signaling in Breast Cancer	2.357	3.077	3.2	2.954	N/A	3	N/A	-0.378	-0.894	1.698
Regulation of Actin-based Motility by Rho	3.413	3.087	3.024	3.528	N/A	3.773	N/A	N/A	0	0.632
PEDF Signaling	2.921	3	3.536	3.286	N/A	3	N/A	N/A	-0.632	1
Chondroitin Sulfate Biosynthesis	3.578	3.273	3.578	3.578	N/A	3.273	N/A	N/A	0	0

Differential Regulation of Cytokine Production in Intestinal Epithelial Cells by IL-17A and IL-17F	2.449	2.828	2.236	2.449	N/A	2	N/A	-1	-2	2.236
VEGF Family Ligand-Receptor Interactions	2.401	2.967	2.92	3.43	N/A	2.414	N/A	N/A	-1.134	1.897
NF-ÎºB Activation by Viruses	2.921	2.596	3.024	3.024	N/A	3	N/A	N/A	-1.414	1.134
Lymphotoxin Î² Receptor Signaling	2.84	2.828	2.84	3	N/A	2.887	N/A	N/A	-1.633	1
Î±-Adrenergic Signaling	3.128	3.138	3	3.411	N/A	3.273	N/A	N/A	N/A	1
Thrombopoietin Signaling	2.746	3.053	3.024	3.657	N/A	3.266	N/A	N/A	-0.816	0.378
14-3-3-mediated Signaling	2.722	3.317	2.655	2.967	N/A	2.535	N/A	-0.447	-1	1.265

Fc Epsilon RI Signaling	2.214	2.771	2.287	3.244	N/A	1.859	N/A	N/A	-2.138	2.324
UVB-Induced MAPK Signaling	2.558	3	2.858	3.266	N/A	3.153	N/A	N/A	-1.134	0.816
Macropinocytosis Signaling	2.683	3.266	2.858	3.411	N/A	3.3	N/A	N/A	-0.816	0.447
FLT3 Signaling in Hematopoietic Progenitor Cells	3.272	3.307	3.053	3.651	N/A	2.6	N/A	N/A	-0.378	-0.378
PDGF Signaling	3.157	2.744	2.828	3.674	N/A	3.266	N/A	N/A	-0.632	0.333
IL-2 Signaling	2.683	3	2.683	2.985	N/A	2.5	N/A	N/A	-1.633	1.134
Differential Regulation of Cytokine Production in Macrophages and T Helper Cells by IL-17A and IL-17F	2.449	2.449	2.236	2.236	N/A	2	N/A	-1	-2	2.236

Androgen Signaling	3.333	3.244	2.828	3.307	N/A	3.053	N/A	N/A	0.447	0.378
Paxillin Signaling	2.646	3.286	2.746	3.272	N/A	2.985	N/A	N/A	-1	0.632
Prolactin Signaling	2.694	3	2.694	3.528	N/A	3.402	N/A	N/A	-0.816	0.378
Neuregulin Signaling	3.053	2.959	3.087	3.157	N/A	2.828	N/A	N/A	-1.342	N/A
Ephrin B Signaling	2.683	3.153	2.683	3.153	N/A	3.3	N/A	N/A	-0.447	1
GÎ±12/13 Signaling	3.111	2.887	3.063	3.244	N/A	2.897	N/A	0	-1	0
Chondroitin Sulfate Biosynthesis (Late Stages)	3.3	2.982	3.441	3.3	N/A	3.13	N/A	N/A	0	0
Melatonin Signaling	3.053	3.772	2.268	2.746	N/A	3.266	N/A	N/A	0	-1
Aldosterone Signaling in Epithelial Cells	3.053	3.452	2.744	3.307	N/A	2.746	N/A	N/A	0	0.707
Coronavirus Pathogenesis Pathway	1.953	0.775	2.885	2.496	N/A	1.806	N/A	-1.633	-1.698	2.711

Role of PI3K/AKT Signaling in the Pathogenesis of Influenza	2.673	3.153	2.496	2.84	N/A	2.53	N/A	N/A	-1.414	0.707
ERBB4 Signaling	2.683	2.858	2.449	3.411	N/A	2.357	N/A	N/A	-1.134	0.816
Type II Diabetes Mellitus Signaling	2.475	2.402	1.915	2.785	N/A	1.768	N/A	0.378	-1.941	1.941
CDK5 Signaling	3	2.744	2.611	3.053	N/A	3.053	N/A	N/A	0.302	0.816
IL-23 Signaling Pathway	2.357	2.985	2.065	2.524	N/A	2.324	N/A	N/A	-1.633	1.633
Kinetochore Metaphase Signaling Pathway	-3.528	-3.138	-2.785	-2.357	N/A	-3.656	N/A	N/A	N/A	N/A
Non-Small Cell Lung Cancer Signaling	2.132	2.353	3.273	3.266	N/A	2.5	N/A	N/A	-0.816	1
Amyotrophic Lateral Sclerosis Signaling	2.53	2.188	3.162	3.28	N/A	1.715	N/A	N/A	-0.832	1.604
VEGF Signaling	2.335	2.263	2.744	2.921	N/A	2.117	N/A	N/A	-1.4	1.508

									14	
IL-7 Signaling Pathway	1.89	2.828	2.711	2.858	N/A	1.706	N/A	N/A	-2.121	1.134
CNTF Signaling	2.668	2.558	2.4	3.13	N/A	2.673	N/A	N/A	-1.342	0.447
iNOS Signaling	3	2.683	2.668	2.496	N/A	3	N/A	N/A	N/A	1.342
Renal Cell Carcinoma Signaling	2.524	2.711	2.4	2.985	N/A	2.324	N/A	N/A	-1.342	0.816
Natural Killer Cell Signaling	2.286	2.255	1.94	2.474	N/A	2	N/A	-1	-1.569	1.569
ERK/MAPK Signaling	2.183	2.79	2.151	3.048	N/A	2.646	N/A	0	-1.604	0.471
Erythropoietin Signaling Pathway	1.576	1.912	2.646	3.048	N/A	2.832	N/A	-1.414	0.728	0.626
Dermatan Sulfate Biosynthesis (Late Stages)	2.84	2.5	3	2.84	N/A	2.828	N/A	N/A	0.378	-0.333
Sperm Motility	2.714	2.941	2.61	2.949	N/A	3.063	N/A	0	0	-0.333

Leptin Signaling in Obesity	1.941	2.673	2.496	2.324	N/A	2.111	N/A	N/A	-1.134	1.89
MSP-RON Signaling In Cancer Cells Pathway	2.38	2.474	3.394	3.328	N/A	2.143	N/A	N/A	0	0.832
Cyclins and Cell Cycle Regulation	-2.887	-2.887	-2.558	-2.558	N/A	-2.6	N/A	N/A	-1	N/A
Neurotrophin/TRK Signaling	2.711	2.887	2.353	3.138	N/A	1.279	N/A	N/A	-1.414	0.707
PPAR Signaling	-2.401	-2.592	-2.722	-2.535	N/A	-1.219	N/A	0	1.265	-1.732
RAN Signaling	-2.828	-2.646	-3	-2.646	N/A	-3.162	N/A	N/A	N/A	N/A
Antiproliferative Role of Somatostatin Receptor 2	1.886	2.683	2.357	2.837	N/A	2	N/A	N/A	-1.342	1.134
Small Cell Lung Cancer Signaling	1.886	1.964	2.5	2.357	N/A	2.138	N/A	N/A	-1.667	1.633

Superpathway of Inositol Phosphate Compounds	1.664	1.912	2.066	2.252	N/A	1.483	N/A	-0.816	-1.698	2.183
UVA-Induced MAPK Signaling	2.6	3.024	2.268	2.746	N/A	2.236	N/A	N/A	-0.816	0.378
Oncostatin M Signaling	2.887	2.673	2.673	2.887	N/A	2.887	N/A	N/A	N/A	N/A
Inhibition of Angiogenesis by TSP1	2.496	2.496	2.84	2.673	N/A	2.496	N/A	N/A	-1	N/A
PFKFB4 Signaling Pathway	3.441	2.558	2.357	3.3	N/A	1.789	N/A	N/A	-0.447	N/A
Xenobiotic Metabolism CAR Signaling Pathway	1.921	2.425	2.394	1.576	N/A	1.408	N/A	1.134	-0.894	2.132
Endocannabinoid Cancer Inhibition Pathway	-1.807	-2.394	-2.252	-2.782	N/A	-1.576	N/A	-1	0.832	-1.155
Huntington's Disease Signaling	2.48	2.774	2.654	2.714	N/A	2.846	N/A	N/A	-0.302	0

Dopamine Receptor Signaling	2.673	3.207	3.162	2.887	N/A	1.807	N/A	N/A	N/A	N/A
Role of IL-17F in Allergic Inflammatory Airway Diseases	2.714	1.732	1.732	2.53	N/A	1	N/A	N/A	-2	2
3-phosphoinositide Biosynthesis	1.313	1.483	2.111	2.359	N/A	1.093	N/A	-1.342	-1.807	2.138
BMP signaling pathway	3.053	2.556	2.785	2.646	N/A	2.6	N/A	N/A	0	0
Sphingosine-1-phosphate Signaling	2.598	2.941	2.359	2.412	N/A	2.714	N/A	N/A	-0.277	-0.302
Role of OCT4 in Mammalian Embryonic Stem Cell Pluripotency	-1.732	-1.265	-1.667	-2.333	N/A	-2.111	N/A	N/A	-2	2.449
Retinoate Biosynthesis I	2.496	2.309	2.138	2.673	N/A	1.732	N/A	N/A	-0.816	1.134
Estrogen Biosynthesis	2.53	2.111	2.714	2.333	N/A	1.732	N/A	N/A	-0.447	1.342

Assembly of RNA Polymerase I Complex	-2.646	-2.449	-2.828	-2.449	N/A	-2.646	N/A	N/A	N/A	N/A
TGF-Î² Signaling	2.335	1.859	2.874	2.556	N/A	2.556	N/A	N/A	0	0.816
nNOS Signaling in Neurons	2.53	1.897	2.714	2.887	N/A	1.897	N/A	N/A	N/A	1
SPINK1 Pancreatic Cancer Pathway	-2.4	-2.132	-2.858	-2.4	N/A	-1.46	N/A	N/A	0	-1.667
RHOA Signaling	2.466	1.947	2.137	2.343	N/A	1.852	N/A	1	1	0
Endothelin-1 Signaling	1.963	2.429	2.236	2.828	N/A	2.287	N/A	N/A	0.447	0.447
Xenobiotic Metabolism AHR Signaling Pathway	2.502	2.828	1.8	1.732	N/A	1.89	N/A	0	0	1.633
Interferon Signaling	2.324	2	0.832	1.508	N/A	3	N/A	N/A	N/A	-2.646
Cardiac Î²-adrenergic Signaling	1.64	1.938	1.474	2.359	N/A	1.313	N/A	N/A	-1.508	1.941
PD-1, PD-L1 cancer immunotherapy pathway	-1.976	-2.469	-1.581	-2.466	N/A	-2.596	N/A	N/A	-0.277	0.775

CCR3 Signaling in Eosinophils	1.461	2.271	1.915	2.414	N/A	1.633	N/A	N/A	-1.134	1.265
Role of MAPK Signaling in Inhibiting the Pathogenesis of Influenza	1.789	1.732	2.041	2.558	N/A	1.706	N/A	0	-1	1.265
Chondroitin and Dermatan Biosynthesis	2.449	2.449	2.449	2.449	N/A	2.236	N/A	N/A	N/A	N/A
IL-1 Signaling	2.837	2.449	2.183	2.183	N/A	2.357	N/A	N/A	N/A	N/A
Mouse Embryonic Stem Cell Pluripotency	1.067	1.155	1.982	2.655	N/A	0.156	N/A	N/A	-1.89	3.051
UVC-Induced MAPK Signaling	1.886	1.964	2.524	2.828	N/A	2.668	N/A	N/A	N/A	N/A
Telomerase Signaling	1.616	2	1.826	2.121	N/A	1.4	N/A	N/A	-1.633	1.134

Intrinsic Prothrombin Activation Pathway	1.698	1.342	2.065	1.807	N/A	1.342	N/A	N/A	-1.414	2
Regulation of Cellular Mechanics by Calpain Protease	2.53	2.324	2.333	2.333	N/A	2.138	N/A	N/A	N/A	N/A
LPS/IL-1 Mediated Inhibition of RXR Function	2.041	2.121	1.732	2.268	N/A	0.557	N/A	N/A	-1.633	1.265
IL-17A Signaling in Gastric Cells	2.236	2.646	2.236	2.236	N/A	2.236	N/A	N/A	N/A	N/A
Glycogen Degradation III	2.828	2.333	2.121	2.121	N/A	2.121	N/A	N/A	N/A	N/A
Purine Nucleotides De Novo Biosynthesis II	-2.333	-2.53	-2.333	-2.121	N/A	-2.121	N/A	N/A	N/A	N/A
Role of BRCA1 in DNA Damage Response	-2.6	-2.2	-1.964	-2	N/A	-2.646	N/A	N/A	N/A	N/A
FcÎ³RIIB Signaling in B Lymphocytes	1.886	2.236	1.414	2.236	N/A	0.832	N/A	N/A	-1.667	1.134

Endometrial Cancer Signaling	1.342	1.706	2.357	2.4	N/A	1.604	N/A	N/A	-0.816	1
Agrin Interactions at Neuromuscular Junction	2.183	2.183	1.606	2.357	N/A	1.964	N/A	N/A	-0.447	0.378
Melanoma Signaling	1.5	1.789	2	2.236	N/A	1.732	N/A	N/A	-0.816	1
Glutathione-mediated Detoxification	2.138	2.668	1.897	1.387	N/A	1.941	N/A	N/A	N/A	1
Activation of IRF by Cytosolic Pattern Recognition Receptors	2.183	2.357	0.905	1.265	N/A	2.138	N/A	0.447	0	-1.667
Autophagy	2.018	2.236	1.1	1.969	N/A	1.806	N/A	-0.816	-0.229	-0.728
Endocannabinoid Neuronal Synapse Pathway	1.432	1.313	1.953	1.838	N/A	1.457	N/A	-0.816	1.155	0.5
Inflammasome pathway	1.155	1.387	1.155	1.155	N/A	0.905	N/A	N/A	-2.4	2.236

									49	
ERB2-ERBB3 Signaling	1.342	1.633	1.528	1.877	N/A	0.728	N/A	N/A	-1.633	1.633
Th2 Pathway	1.342	2.219	1.732	2.021	N/A	0.667	N/A	N/A	-1.698	0.688
Antioxidant Action of Vitamin C	-2.058	-2.214	-1.667	-1.671	N/A	-1.461	N/A	N/A	0.378	-0.905
Folate Polyglutamylation	-2	-2	-2	-2	N/A	-2.236	N/A	N/A	N/A	N/A
Notch Signaling	1.414	2.111	2.53	1.667	N/A	0.302	N/A	N/A	-0.816	1.342
Basal Cell Carcinoma Signaling	2.117	1.8	2.449	2.4	N/A	1.4	N/A	N/A	N/A	0
Leukotriene Biosynthesis	2.236	1.89	1.342	1.633	N/A	N/A	N/A	N/A	-2	1
Death Receptor Signaling	1.715	1.761	0.707	0.756	N/A	1.029	N/A	1	-1.667	-1.387
Glycogen Degradation II	2.449	1.89	1.89	1.89	N/A	1.89	N/A	N/A	N/A	N/A

Role of NANOG in Mammalian Embryonic Stem Cell Pluripotency	1.177	1.257	0.962	1.512	N/A	0.853	N/A	N/A	-2.121	2.121
Tetrahydrofolate Salvage from 5,10-methenyltetrahydrofolate	-2	-2	-2	-2	N/A	-2	N/A	N/A	N/A	N/A
Acute Myeloid Leukemia Signaling	1.616	1.521	2.268	2.694	N/A	1.4	N/A	N/A	0	0.378
p53 Signaling	-1.183	-1.947	-1	-1.667	N/A	-1.219	N/A	N/A	1.069	-1.414
MIF Regulation of Innate Immunity	0.943	1.091	1.213	1.5	N/A	0.471	N/A	N/A	-1.633	2.646
Cardiomyocyte Differentiation via BMP Receptors	1.889	1	2.333	1.889	N/A	2.333	N/A	N/A	N/A	N/A
ATM Signaling	-1.6	-1.4	-1.1	-1.3	N/A	-1.8	N/A	N/A	-2	N/A

	16	61	34	47		59				
Heparan Sulfate Biosynthesis (Late Stages)	1.606	1.706	2.065	1.606	N/A	1.4	N/A	N/A	0.707	-0.302
Pyrimidine Deoxyribonucleotides De Novo Biosynthesis I	-2.333	-2.121	-1.667	-1.414	N/A	-1.732	N/A	N/A	N/A	0
Dilated Cardiomyopathy Signaling Pathway	1.016	1.838	0.762	1.033	1.633	0.62	N/A	1	0.378	-0.905
Gluconeogenesis I	0.816	0.816	1.414	1	N/A	-1.155	N/A	N/A	-2	1.89
GÎ±i Signaling	1.372	1.732	2.111	1.718	N/A	1.067	N/A	N/A	-0.277	0.775
Role of p14/p19ARF in Tumor Suppression	-1.265	-1.732	-1.265	-1.732	N/A	-0.707	N/A	N/A	1.134	-1
CSDE1 Signaling Pathway	1.414	1.698	2	2.673	N/A	0.894	N/A	N/A	N/A	N/A
Apelin Muscle Signaling Pathway	1.667	1.667	2.121	1.89	N/A	1.265	N/A	N/A	N/A	N/A

Glycolysis I	0	-0.378	0.333	0.447	N/A	-1.941	N/A	N/A	-2.449	3
Epithelial Adherens Junction Signaling	-0.816	-0.762	-1.905	-1.604	N/A	-0.927	N/A	0.447	-1.342	-0.632
NAD Signaling Pathway	2.101	1.069	0.962	1.387	N/A	0.535	N/A	0	-1.213	1.091
ERK5 Signaling	1.569	1.134	2.043	2.2	N/A	1.4	N/A	N/A	N/A	N/A
GPCR-Mediated Integration of Enteroendocrine Signaling Exemplified by an L Cell	1	1.183	1.667	1.768	N/A	1.414	N/A	N/A	-1.134	0
EIF2 Signaling	0	0.707	0.756	1.3	N/A	-2.534	N/A	N/A	-1.508	1.265
Endocannabinoid Developing Neuron Pathway	1.029	1.121	1.333	1.622	N/A	0.686	N/A	N/A	-1.508	0.707
Insulin Receptor Signaling	1.067	1.18	1.677	2.16	N/A	1.333	N/A	N/A	-0.277	0.302

Glucose and Glucose-1-phosphate Degradation	1.633	1.633	1.633	1.633	N/A	1.342	N/A	N/A	N/A	N/A
LXR/RXR Activation	1.109	0.651	1.361	0.729	N/A	1.54	N/A	-1	0.5	-0.943
TWEAK Signaling	2.138	1.698	1.508	1.265	N/A	1.155	N/A	N/A	N/A	N/A
Prostanoid Biosynthesis	1.342	0.816	1.633	1.633	N/A	0.816	N/A	N/A	-0.447	1
Choline Biosynthesis III	1.667	1.667	1.414	1.414	N/A	1.134	N/A	N/A	N/A	N/A
MYC Mediated Apoptosis Signaling	1.279	1.633	1	1.698	N/A	0.655	N/A	-1	0	0
VDR/RXR Activation	1.4	0.784	0.6	1	N/A	0	N/A	N/A	-1.414	1.897
tRNA Splicing	1.213	0.447	1.342	1.528	N/A	0.6	N/A	N/A	-0.816	1.134
Complement System	0.775	1.213	1	0.775	N/A	0.277	N/A	N/A	-1.134	1.633

Pyroptosis Signaling Pathway	0.324	0.885	1.151	0.507	N/A	0	N/A	-0.816	-1.414	1.5
Bladder Cancer Signaling	-0.5	-1.147	0.258	1.069	N/A	-0.243	N/A	N/A	-1.342	1.89
GDP-glucose Biosynthesis	1.342	1.342	1.342	1.342	N/A	1	N/A	N/A	N/A	N/A
Coagulation System	1.414	0.853	1.091	0.728	N/A	1.147	N/A	N/A	-1	0
Apelin Adipocyte Signaling Pathway	-0.898	-1.372	-0.962	-1.826	N/A	-1.095	N/A	N/A	0	0
Adenine and Adenosine Salvage III	-2	N/A	-2	-2	N/A	N/A	N/A	N/A	N/A	N/A
Sonic Hedgehog Signaling	-1.387	-1.155	-0.707	-0.905	N/A	-0.832	N/A	N/A	N/A	1
TNFR1 Signaling	1.414	0.655	0.775	1.069	N/A	0.775	N/A	N/A	N/A	1
The Visual Cycle	1.414	1.414	1	1.134	N/A	0.707	N/A	N/A	N/A	N/A
Ceramide Signaling	1.095	0.845	0.539	0.354	N/A	0.784	N/A	0	1.414	-0.632

Cell Cycle: G1/S Checkpoint Regulation	1.347	1.3	1.147	1.043	N/A	0.784	N/A	N/A	N/A	N/A
Apelin Cardiac Fibroblast Signaling Pathway	-0.577	-0.577	-0.302	-0.632	N/A	-1.069	N/A	N/A	-0.447	2
MSP-RON Signaling In Macrophages Pathway	0	0	0	0	N/A	-1.677	N/A	-1	-1.5	1.213
Phospholipases	0.962	1.3	0.557	0.626	N/A	0.6	N/A	N/A	1.342	0
Protein Kinase A Signaling	1.069	0.616	0.805	1.257	N/A	0.961	N/A	0.277	0.186	0.169
Inhibition of Matrix Metalloproteases	-1.213	-0.943	-0.728	-0.728	N/A	-0.775	N/A	N/A	0.816	0
BEX2 Signaling Pathway	0.522	0.354	1.257	0.539	N/A	0	N/A	N/A	-1.265	1.265
Guanosine Nucleotides Degradation III	1	1.342	1	1	N/A	0.816	N/A	N/A	N/A	N/A

MIF-mediated Glucocorticoid Regulation	-0.535	0	0	0	N/A	-0.775	N/A	N/A	-1.342	2.449
PI3K/AKT Signaling	0.493	0.617	0.801	0.667	N/A	0.707	N/A	N/A	0.302	1.414
Amyloid Processing	1.134	0.905	1.134	0.816	N/A	1	N/A	N/A	N/A	N/A
Semaphorin Neuronal Repulsive Signaling Pathway	-0.62	-1.083	0.126	0	N/A	0	N/A	N/A	1.604	-1.528
Role of CHK Proteins in Cell Cycle Checkpoint Control	-1.291	-0.728	-1	-0.832	N/A	-1	N/A	N/A	N/A	N/A
Vitamin-C Transport	0	0.632	0.816	1.633	N/A	1.633	N/A	N/A	N/A	N/A
WNT/Î²-catenin Signaling	-0.798	-0.229	-0.114	-0.236	N/A	-0.593	N/A	1.342	0.535	-0.853
Induction of Apoptosis by HIV1	1.091	0.784	0.471	0.728	N/A	-0.447	N/A	1	0	0

Pyrimidine Ribonucleotides De Novo Biosynthesis	-1.155	-1.387	-0.302	-0.333	N/A	-0.943	N/A	N/A	0	0.378
Necroptosis Signaling Pathway	-0.405	0.25	-0.143	0.289	N/A	-0.397	N/A	0.447	-1.265	1.291
Glutathione Redox Reactions I	1.387	1.069	1.155	0.277	N/A	0.535	N/A	N/A	N/A	N/A
Superpathway of Serine and Glycine Biosynthesis I	N/A	-2	N/A	-1	N/A	-1.342	N/A	N/A	N/A	N/A
Apelin Pancreas Signaling Pathway	-0.471	0	0.577	0.243	N/A	-0.277	N/A	N/A	-1	1.633
Angiopoietin Signaling	0.688	1.043	0.426	0.943	N/A	0.471	N/A	N/A	N/A	-0.378
Tryptophan Degradation X (Mammalian, via Tryptamine)	1.265	1	0.333	0.707	N/A	0.632	N/A	N/A	N/A	N/A

Aryl Hydrocarbon Receptor Signaling	-0.457	-0.295	0.156	0.324	N/A	-0.289	N/A	-0.447	0	1.89
Ethanol Degradation IV	1.155	0.905	0.577	0.905	N/A	0.302	N/A	N/A	N/A	N/A
Ferroptosis Signaling Pathway	0.156	-0.59	0	0.309	N/A	-0.447	N/A	-2	0	0.277
Neuroprotective Role of THOP1 in Alzheimer's Disease	-0.365	-0.169	0.6	0	N/A	-0.73	N/A	N/A	0.632	1.134
PPARÎ±/RXRÎ± Activation	-0.378	-0.356	-0.896	-0.64	N/A	-0.135	N/A	0	-0.816	-0.333
Noradrenaline and Adrenaline Degradation	0.535	0.535	0	0.277	N/A	0	N/A	N/A	-1	1
Pyrimidine Ribonucleotides Interconversion	-0.632	-0.905	0.333	0.378	N/A	-0.5	N/A	N/A	0	0.378
Fatty Acid Î±-oxidation	0.378	0.378	0.333	1	N/A	0	N/A	N/A	1	N/A

Putrescine Degradation III	1	0.707	0.333	0.707	N/A	0.333	N/A	N/A	N/A	N/A
Polyamine Regulation in Colon Cancer	-0.655	-1.4	-0.229	-0.218	N/A	-0.426	N/A	N/A	0	N/A
Ethanol Degradation II	0.258	0.258	-0.5	0	N/A	-0.832	N/A	N/A	-1	N/A
Histidine Degradation III	-0.447	-0.447	-0.447	-0.447	N/A	-1	N/A	N/A	N/A	N/A
UDP-N-acetyl-D-galactosamine Biosynthesis II	-0.447	-0.447	-0.447	-0.447	N/A	-1	N/A	N/A	N/A	N/A
Apoptosis Signaling	-0.2	-0.686	-0.392	-0.626	N/A	-0.365	N/A	N/A	0.378	0
Extrinsic Prothrombin Activation Pathway	N/A	-1.633	-1	N/A	N/A	N/A	N/A	N/A	N/A	N/A
Tumoricidal Function of Hepatic Natural Killer Cells	0.816	0.378	0.447	0.447	N/A	0.447	N/A	N/A	N/A	N/A

Sumoylation Pathway	0	-0.174	0.174	-0.174	N/A	-1.151	N/A	0	0	-0.816
NRF2-mediated Oxidative Stress Response	-0.354	0	0.557	0.378	N/A	-0.174	N/A	1	0	0
Unfolded protein response	-0.258	0	0.258	0.333	N/A	0.229	N/A	N/A	1.342	N/A
TNFR2 Signaling	1	-0.302	0.378	0.447	N/A	0	N/A	N/A	N/A	N/A
Pyruvate Fermentation to Lactate	N/A	N/A	N/A	N/A	N/A	-2	N/A	N/A	N/A	N/A
Î³-glutamyl Cycle	0	0	-0.447	-0.707	N/A	-0.816	N/A	N/A	N/A	N/A
1D-myo-inositol Hexakisphosphate Biosynthesis II (Mammalian)	-0.378	-0.333	0	-0.816	N/A	0.378	N/A	N/A	N/A	N/A
Histamine Degradation	0.707	0.707	0	0.378	N/A	0	N/A	N/A	N/A	N/A

Sirtuin Signaling Pathway	0	-0.243	-0.124	0	N/A	0.232	N/A	0.816	0	-0.258
Remodeling of Epithelial Adherens Junctions	N/A	N/A	N/A	N/A	N/A	1.633	N/A	N/A	N/A	N/A
Cell Cycle: G2/M DNA Damage Checkpoint Regulation	0.229	0.229	0.5	0	N/A	0.655	N/A	N/A	0	N/A
Eicosanoid Signaling	-0.277	0.5	0	0	N/A	-0.302	N/A	N/A	N/A	0.447
Purine Nucleotides Degradation II (Aerobic)	-0.378	0.378	-0.378	-0.378	N/A	0	N/A	N/A	N/A	0
Ketogenesis	0.447	0.447	0.447	0	N/A	N/A	N/A	N/A	N/A	N/A
Superpathway of Citrulline Metabolism	0	0	0.333	-0.378	N/A	0.378	N/A	N/A	N/A	N/A

Glycine Betaine Degradation	0.447	0	0.447	0	N/A	0	N/A	N/A	N/A	N/A
Superoxide Radicals Degradation	-0.447	0	0	-0.447	N/A	0	N/A	N/A	N/A	N/A
Maturity Onset Diabetes of Young (MODY) Signaling	N/A	N/A	N/A	N/A	N/A	N/A	N/A	N/A	N/A	N/A
Axonal Guidance Signaling	N/A	N/A	N/A	N/A	N/A	N/A	N/A	N/A	N/A	N/A
Urea Cycle	N/A	N/A	N/A	N/A	N/A	N/A	N/A	N/A	N/A	N/A
FAK Signaling	N/A	N/A	N/A	N/A	N/A	N/A	N/A	N/A	N/A	N/A
Threonine Degradation II	N/A	N/A	N/A	N/A	N/A	N/A	N/A	N/A	N/A	N/A
Hepatic Cholestasis	N/A	N/A	N/A	N/A	N/A	N/A	N/A	N/A	N/A	N/A
Inosine-5'-phosphate Biosynthesis II	N/A	N/A	N/A	N/A	N/A	N/A	N/A	N/A	N/A	N/A
RAR Activation	N/A	N/A	N/A	N/A	N/A	N/A	N/A	N/A	N/A	N/A

Tight Junction Signaling	N/A	N/A	N/A	N/A	N/A	N/A	N/A	N/A	N/A	N/A
Ephrin A Signaling	N/A	N/A	N/A	N/A	N/A	N/A	N/A	N/A	N/A	N/A
TR/RXR Activation	N/A	N/A	N/A	N/A	N/A	N/A	N/A	N/A	N/A	N/A
Hypusine Biosynthesis	N/A	N/A	N/A	N/A	N/A	N/A	N/A	N/A	N/A	N/A
GDP-mannose Biosynthesis	N/A	N/A	N/A	N/A	N/A	N/A	N/A	N/A	N/A	N/A
Role of Macrophages, Fibroblasts and Endothelial Cells in Rheumatoid Arthritis	N/A	N/A	N/A	N/A	N/A	N/A	N/A	N/A	N/A	N/A
Xenobiotic Metabolism Signaling	N/A	N/A	N/A	N/A	N/A	N/A	N/A	N/A	N/A	N/A
Sertoli Cell-Sertoli Cell Junction Signaling	N/A	N/A	N/A	N/A	N/A	N/A	N/A	N/A	N/A	N/A

Regulation of the Epithelial-Mesenchymal Transition Pathway	N/A	N/A	N/A	N/A	N/A	N/A	N/A	N/A	N/A	N/A
Guanine and Guanosine Salvage I	N/A	N/A	N/A	N/A	N/A	N/A	N/A	N/A	N/A	N/A
Iron homeostasis signaling pathway	N/A	N/A	N/A	N/A	N/A	N/A	N/A	N/A	N/A	N/A
Uracil Degradation II (Reductive)	N/A	N/A	N/A	N/A	N/A	N/A	N/A	N/A	N/A	N/A
Glucocorticoid Receptor Signaling	N/A	N/A	N/A	N/A	N/A	N/A	N/A	N/A	N/A	N/A
Glutamate Degradation III (via 4-aminobutyrate)	N/A	N/A	N/A	N/A	N/A	0	N/A	N/A	N/A	N/A
Cancer Drug Resistance By Drug Efflux	N/A	N/A	N/A	N/A	N/A	N/A	N/A	N/A	N/A	N/A

MSP-RON Signaling Pathway	N/A	N/A	N/A	N/A	N/A	N/A	N/A	N/A	N/A	N/A
Docosahexaenoic Acid (DHA) Signaling	N/A	N/A	N/A	N/A	N/A	N/A	N/A	N/A	N/A	N/A
Agranulocyte Adhesion and Diapedesis	N/A	N/A	N/A	N/A	N/A	N/A	N/A	N/A	N/A	N/A
Lysine Degradation V	N/A	N/A	N/A	N/A	N/A	N/A	N/A	N/A	N/A	N/A
Role of Tissue Factor in Cancer	N/A	N/A	N/A	N/A	N/A	N/A	N/A	N/A	N/A	N/A
IL-12 Signaling and Production in Macrophages	N/A	N/A	N/A	N/A	N/A	N/A	N/A	N/A	N/A	N/A
Clathrin-mediated Endocytosis Signaling	N/A	N/A	N/A	N/A	N/A	N/A	N/A	N/A	N/A	N/A
Role of JAK1 and JAK3 in Î³c Cytokine Signaling	N/A	N/A	N/A	N/A	N/A	N/A	N/A	N/A	N/A	N/A
B Cell Development	N/A	N/A	N/A	N/A	N/A	N/A	N/A	N/A	N/A	N/A

Airway Pathology in Chronic Obstructive Pulmonary Disease	N/A	N/A	N/A	N/A	N/A	N/A	N/A	N/A	N/A	N/A
G Protein Signaling Mediated by Tubby	N/A	N/A	N/A	N/A	N/A	N/A	N/A	N/A	N/A	N/A
Semaphorin Signaling in Neurons	N/A	N/A	N/A	N/A	N/A	N/A	N/A	N/A	N/A	N/A
GABA Receptor Signaling	N/A	N/A	N/A	N/A	N/A	N/A	N/A	N/A	N/A	N/A
Role of MAPK Signaling in the Pathogenesis of Influenza	N/A	N/A	N/A	N/A	N/A	N/A	N/A	N/A	N/A	N/A
Serotonin Receptor Signaling	N/A	N/A	N/A	N/A	N/A	N/A	N/A	N/A	N/A	N/A
Caveolar-mediated Endocytosis Signaling	N/A	N/A	N/A	N/A	N/A	N/A	N/A	N/A	N/A	N/A
Prostate Cancer Signaling	N/A	N/A	N/A	N/A	N/A	N/A	N/A	N/A	N/A	N/A

Pathogenesis of Multiple Sclerosis	N/A	N/A	N/A	N/A	N/A	N/A	N/A	N/A	N/A	N/A
Acyl-CoA Hydrolysis	N/A	0	N/A	0	N/A	0	N/A	N/A	N/A	N/A
Gap Junction Signaling	N/A	N/A	N/A	N/A	N/A	N/A	N/A	N/A	N/A	N/A
Human Embryonic Stem Cell Pluripotency	N/A	N/A	N/A	N/A	N/A	N/A	N/A	N/A	N/A	N/A
Circadian Rhythm Signaling	N/A	N/A	N/A	N/A	N/A	N/A	N/A	N/A	N/A	N/A
Arginine Degradation VI (Arginase 2 Pathway)	N/A	N/A	N/A	N/A	N/A	N/A	N/A	N/A	N/A	N/A
Germ Cell-Sertoli Cell Junction Signaling	N/A	N/A	N/A	N/A	N/A	N/A	N/A	N/A	N/A	N/A
L-cysteine Degradation I	N/A	N/A	N/A	N/A	N/A	N/A	N/A	N/A	N/A	N/A
Mismatch Repair in Eukaryotes	N/A	N/A	N/A	N/A	N/A	N/A	N/A	N/A	N/A	N/A

Thymine Degradation	N/A	N/A	N/A	N/A	N/A	N/A	N/A	N/A	N/A	N/A
Molecular Mechanisms of Cancer	N/A	N/A	N/A	N/A	N/A	N/A	N/A	N/A	N/A	N/A
Transcriptional Regulatory Network in Embryonic Stem Cells	N/A	N/A	N/A	N/A	N/A	N/A	N/A	N/A	N/A	N/A
nNOS Signaling in Skeletal Muscle Cells	N/A	N/A	N/A	N/A	N/A	N/A	N/A	N/A	N/A	N/A
1D-myo-inositol Hexakisphosphate Biosynthesis V (from Ins(1,3,4)P3)	N/A	N/A	N/A	N/A	N/A	N/A	N/A	N/A	N/A	N/A
IL-4 Signaling	N/A	N/A	N/A	N/A	N/A	N/A	N/A	N/A	N/A	N/A
PXR/RXR Activation	N/A	N/A	N/A	N/A	N/A	N/A	N/A	N/A	N/A	N/A

5-aminoimidazole Ribonucleotide Biosynthesis I	N/A	N/A	N/A	N/A	N/A	N/A	N/A	N/A	N/A	N/A
Mechanisms of Viral Exit from Host Cells	N/A	N/A	N/A	N/A	N/A	N/A	N/A	N/A	N/A	N/A
Role of Osteoblasts, Osteoclasts and Chondrocytes in Rheumatoid Arthritis	N/A	N/A	N/A	N/A	N/A	N/A	N/A	N/A	N/A	N/A
Atherosclerosis Signaling	N/A	N/A	N/A	N/A	N/A	N/A	N/A	N/A	N/A	N/A
Role of JAK2 in Hormone-like Cytokine Signaling	N/A	N/A	N/A	N/A	N/A	N/A	N/A	N/A	N/A	N/A
Hepatic Fibrosis / Hepatic Stellate Cell Activation	N/A	N/A	N/A	N/A	N/A	N/A	N/A	N/A	N/A	N/A
Hereditary Breast Cancer Signaling	N/A	N/A	N/A	N/A	N/A	N/A	N/A	N/A	N/A	N/A

Role of Cytokines in Mediating Communication between Immune Cells	N/A	N/A	N/A	N/A	N/A	N/A	N/A	N/A	N/A	N/A
Embryonic Stem Cell Differentiation into Cardiac Lineages	N/A	N/A	N/A	N/A	N/A	N/A	N/A	N/A	N/A	N/A
Citrulline-Nitric Oxide Cycle	N/A	N/A	0	N/A	N/A	N/A	N/A	N/A	N/A	N/A
DNA damage-induced 14-3-3Ï*f* Signaling	N/A	N/A	N/A	N/A	N/A	N/A	N/A	N/A	N/A	N/A
IL-10 Signaling	N/A	N/A	N/A	N/A	N/A	N/A	N/A	N/A	N/A	N/A
Th1 and Th2 Activation Pathway	N/A	N/A	N/A	N/A	N/A	N/A	N/A	N/A	N/A	N/A
Cellular Effects of Sildenafil (Viagra)	N/A	N/A	N/A	N/A	N/A	N/A	N/A	N/A	N/A	N/A

Glutamate Dependent Acid Resistance	N/A	N/A	N/A	N/A	N/A	N/A	N/A	N/A	N/A	N/A
Granulocyte Adhesion and Diapedesis	N/A	N/A	N/A	N/A	N/A	N/A	N/A	N/A	N/A	N/A
Adipogenesis pathway	N/A	N/A	N/A	N/A	N/A	N/A	N/A	N/A	N/A	N/A
Virus Entry via Endocytic Pathways	N/A	N/A	N/A	N/A	N/A	N/A	N/A	N/A	N/A	N/A
Chronic Myeloid Leukemia Signaling	N/A	N/A	N/A	N/A	N/A	N/A	N/A	N/A	N/A	N/A
GADD45 Signaling	N/A	N/A	N/A	N/A	N/A	N/A	N/A	N/A	N/A	N/A
Role of IL-17A in Arthritis	N/A	N/A	N/A	N/A	N/A	N/A	N/A	N/A	N/A	N/A
DNA Double-Strand Break Repair by Homologous Recombination	N/A	N/A	N/A	N/A	N/A	N/A	N/A	N/A	N/A	N/A

FXR/RXR Activation	N/A	N/A	N/A	N/A	N/A	N/A	N/A	N/A	N/A	N/A
Airway Inflammation in Asthma	N/A	N/A	N/A	N/A	N/A	N/A	N/A	N/A	N/A	N/A

7.2 Appendix 2: Full list of Tox Functions generated by IPA

Tox Functions	WT undiff vs WT diff B	WT undiff vs WT diff NB	WT undiff vs Hdac4 KO B	WT undiff vs Hdac4 KO NB	WT diff B vs WT diff NB	WT undiff vs TSA B	WT diff B vs Hdac4 KO B	WT diff NB vs Hdac4 KO diff NB	WT diff B vs TSA B	WT TSA B vs Hdac4 KO B
Congenital heart disease	-6.216	-5.694	-6.779	-6.919	N/A	-4.823	N/A	2.321	1.834	-2.997
Atrial or ventricular septal defect	-4.439	-3.945	-5.319	-5.35	N/A	-3.789	N/A	1.891	1.643	-3.398
Ventricular septal defect	-4.315	-3.893	-5.055	-5.173	N/A	-3.692	N/A	1.729	2.138	-3.432
Hydronephrosis	-5.07	-5.349	-4.66	-5.07	N/A	-4.442	N/A	N/A	1.652	-3.098
Increased Levels of Alkaline Phosphatase	4.53	4.767	5.654	4.83	N/A	3.906	N/A	-0.359	-1.309	2.633
Increased activation of alkaline phosphatase	4.501	4.821	5.503	4.65	N/A	3.931	N/A	-0.079	-1.132	2.494
Familial	-	-	-	-	N/A	-	N/A	N/A	N/	-

congenital heart disease	4.775	4.111	4.422	4.794		3.606			A	2.132
Conotruncal heart malformations	-4.562	-3.874	-4.199	-4.584	N/A	-3.349	N/A	N/A	N/A	-1.913
Activation of hepatic stellate cells	3.936	3.862	4.172	4.163	N/A	4.188	N/A	0.555	-0.415	0.696
Persistent truncus arteriosus	-4.36	-4.002	-3.964	-4.367	N/A	-3.361	N/A	N/A	N/A	-1.89
Congestive heart failure	-3.557	-3.44	-3.911	-3.5	N/A	-3.96	N/A	N/A	1.432	-1.764
Increased Levels of ALT	2.967	3.338	3.354	2.807	N/A	2.809	N/A	N/A	-2.8	2.941
Increased Levels of LDH	3.498	3.874	3.874	3.62	N/A	3.064	N/A	N/A	-1.294	1.777
Failure of heart looping	-3.761	-3.761	-3.889	-4.208	N/A	-3.499	N/A	N/A	N/A	N/A
Proliferation of kidney cells	3.06	3.183	3.275	2.944	N/A	3.448	N/A	-1.04	-0.666	1.459
Increased Levels of Red Blood Cells	2.865	2.878	3.661	4.36	N/A	2.706	N/A	-1	-0.647	0.594
Atrial septal	-	-	-	-	N/A	-	N/A	0.896	0.8	-

defect	2.781	2.504	3.502	3.421		2.424			16	2.138
Nephritis	-3.268	-3.125	-3.381	-2.428	N/A	-3.206	N/A	-2.043	-0.165	-0.614
Hypoplasia of heart ventricle	-3.853	-3.249	-3.853	-3.379	N/A	-3.842	N/A	N/A	N/A	N/A
Increased release of LDH	3.064	3.356	3.066	3.066	N/A	3.066	N/A	N/A	-1.172	1.292
Hypoplasia of heart chamber	-3.746	-3.152	-3.746	-3.277	N/A	-3.958	N/A	N/A	N/A	N/A
Proliferation of glomerular cells	3.08	3.322	3.094	2.832	N/A	3.491	N/A	N/A	-0.56	1.386
Increased Levels of Creatinine	3.115	2.867	2.867	3.077	N/A	2.719	N/A	N/A	-0.822	2.16
Proliferation of mesangial cells	2.929	3.179	3.063	2.797	N/A	3.497	N/A	-0.73	-0.26	1.134
Perimembranous ventricular septal defect	-3.478	-3.345	-3.478	-3.767	N/A	-3.478	N/A	N/A	N/A	N/A
Increased Levels of Hematocrit	2.5	2.519	3.197	3.675	N/A	2.932	N/A	-0.751	-0.199	1.127

Increased localization of ALT	2.402	2.575	2.599	2.236	N/A	1.996	N/A	N/A	-2.425	2.613
Failure of heart	-2.568	-2.655	-3.412	-2.891	N/A	-2.982	N/A	1.219	-0.187	-0.681
Damage of liver cells	2.563	2.739	2.377	2.905	N/A	2.227	N/A	N/A	-1.664	1.937
Migration of hepatic stellate cells	2.085	3.081	2.727	2.579	N/A	1.784	N/A	N/A	-2.066	2.066
Hepatic injury	2.615	3.056	1.689	2.308	N/A	1.959	N/A	0.938	-2.031	1.158
Hypoplasia of kidney	-2.771	-2.542	-2.831	-2.54	N/A	-3.235	N/A	N/A	-0.028	-1.303
Liver Damage	2.939	3.025	1.618	2.39	N/A	2.144	N/A	0.157	-1.511	0.856
Experimental autoimmune myocarditis	2.352	2.353	2.741	2.741	N/A	2.183	N/A	N/A	-2	N/A
Hepatic steatosis	-2.064	-2.062	-2.426	-1.905	N/A	-2.013	N/A	-1.556	1.173	-1.017
Atrophy of kidney	-1.9	-2.04	-2.34	-2.27	N/A	-2.0	N/A	N/A	1.109	-2.18

	68	7		1		63				6
Increased Levels of Blood Urea Nitrogen	1.921	2.287	2.287	1.612	N/A	1.408	N/A	N/A	-2	2.449
Interstitial nephritis	-2.72	-2.72	-2.72	-2.538	N/A	-3.053	N/A	N/A	N/A	N/A
Hyperplasia of kidney cells	-2.375	-2.557	-2.961	-3.124	N/A	-2.547	N/A	N/A	N/A	N/A
Proliferation of tubular cells	2.38	2.38	2.949	2.949	N/A	2.898	N/A	N/A	N/A	N/A
Focal necrosis of liver	-2.535	-3.053	-2.561	-2.173	N/A	-2.514	N/A	N/A	N/A	-0.277
Increased Levels of Albumin	1.436	1.164	2.14	2.739	N/A	0.649	N/A	N/A	-2.181	2.366
Damage of hepatocytes	1.964	1.964	1.964	2.178	N/A	1.782	N/A	N/A	-1.387	1.432
Increased clearance of creatinine	2.412	2.412	2.412	2.607	N/A	2.789	N/A	N/A	N/A	N/A
Hypoplasia of trabeculae carne	-2.585	-2.585	-2.585	-2.111	N/A	-2.36	N/A	N/A	N/A	N/A
Proliferation of heart cells	1.661	1.973	2.048	1.822	N/A	2.147	N/A	-1.281	-0.3	0.746

									45	
Cell death of kidney cells	2.536	1.869	1.943	1.916	N/A	1.31	N/A	-1.295	-0.551	0.576
Liver Regeneration	1.354	0.801	2.012	1.089	N/A	1.353	N/A	N/A	-2.55	2.8
Stenosis of cardiac valve	-2.166	-2.197	-2.491	-2.197	N/A	-2.652	N/A	N/A	N/A	N/A
Stenosis of semilunar valve	-1.937	-1.973	-2.286	-1.973	N/A	-2.286	N/A	N/A	N/A	-1.131
Systolic dysfunction	2.36	2.36	2.164	1.929	N/A	1.811	N/A	N/A	-0.816	-0.128
Hyperplasia of kidney	-2.073	-2.251	-2.358	-2.537	N/A	-2.206	N/A	N/A	N/A	N/A
Macrovesicular hepatic steatosis	-2.138	-2.345	-2.891	-1.667	N/A	-2.345	N/A	N/A	N/A	N/A
Proliferation of cardiomyocytes	1.604	1.899	1.741	1.635	N/A	1.95	N/A	-0.651	-0.787	1.103
Cell death of kidney cell lines	2.658	1.553	1.588	1.859	N/A	0.932	N/A	-0.974	-0.67	1.056
Ventricular	-	-	-	-	N/A	-	N/A	N/A	N/	N/A

fibrillation	2.433	1.982	2.433	2.219		2.219			A	
Congenital malformation of heart	-2.236	-2.236	-2.236	-2.236	N/A	-2.236	N/A	N/A	N/A	N/A
Myocarditis	1.257	1.213	1.871	1.705	N/A	1.061	N/A	N/A	-1.982	1.982
Familial ventricular septal defect	-2.178	-2.178	-2.178	-2.178	N/A	-2.178	N/A	N/A	N/A	N/A
Arrhythmia of heart ventricle	-2.248	-1.839	-2.347	-1.609	N/A	-1.994	N/A	N/A	N/A	-0.823
Increased excretion of K+	2.137	2.137	2.358	2.17	N/A	1.97	N/A	N/A	N/A	N/A
Bicuspid aortic valve	-2.191	-1.961	-2.401	-1.961	N/A	-2.191	N/A	N/A	N/A	N/A
Congenital left heart disease	-2.191	-1.961	-2.401	-1.961	N/A	-2.191	N/A	N/A	N/A	N/A
Hypoplasia of myocardium	-2.138	-2.138	-2.138	-2.138	N/A	-2.138	N/A	N/A	N/A	N/A
Atrophy of renal medulla	-1.982	-2.219	-1.982	-2.433	N/A	-1.982	N/A	N/A	N/A	N/A
Cell death of	-	-	-	-	N/A	-	N/A	N/A	-	N/A

ventricular myocytes	1.582	1.411	2.406	2.224		2.227			0.714	
Damage of kidney	1.639	2.032		1.28	1.52	N/A	1.088	N/A	-1.187	-1.429	0.325
Liver tumor	-1.259	-1.518	-0.813	-0.858	N/A	-1.193	N/A	-2.205	2.339	-0.308
Necrosis of myocardium	-2	-2	-2.236	-2.236	N/A	-2	N/A	N/A	N/A	N/A
Proliferation of cardiac fibroblasts	1.819	1.851	2.296	1.851	N/A	2.296	N/A	N/A	N/A	0.192
Apoptosis of kidney cell lines	2	1.123	1.114	1.305	N/A	0.013	N/A	-1.497	-1.162	2.029
Fibrosis of liver	1.207	1.601	1.353	1.754	N/A	1.428	N/A	-0.853	-0.95	1.031
Liver carcinoma	-1.322	-1.455	-0.832	-0.735	N/A	-0.883	N/A	-2.213	2.415	-0.249
Diastolic dysfunction	1.172	1.501	1.746	1.746	N/A	1.746	N/A	N/A	-1.109	1.026
Injury of renal glomerulus	1.709	1.709	1.526	1.798	N/A	2.148	N/A	N/A	-1.119	N/A

Congenital malformation of pulmonary valve	-2	-2	-2	-2	N/A	-2	N/A	N/A	N/A	N/A
Dysfunction of kidney	1.655	2.018	1.348	1.756	N/A	1.687	N/A	N/A	-1.192	0.283
Ventricular septal defect type 3	-1.982	-1.982	-1.982	-1.982	N/A	-1.982	N/A	N/A	N/A	N/A
Cardiac fibrillation	-1.726	-1.358	-2.209	-1.813	N/A	-1.293	N/A	N/A	-0.305	-1.205
Fibrosis of renal glomerulus	-1.067	-1.698	-1.964	-1.964	N/A	-0.97	N/A	N/A	N/A	-2.213
Increased Levels of AST	1.8	1.648	2.239	2.239	N/A	1.926	N/A	N/A	N/A	N/A
Increased Levels of Potassium	2.079	2.079	1.841	2.123	N/A	1.657	N/A	N/A	N/A	N/A
Proliferation of liver cells	0.863	0.619	1.905	1.135	N/A	1.185	N/A	0.366	-1.788	1.887
Formation of glomerular crescent	-1.51	-1.744	-1.937	-2.157	N/A	-1.195	N/A	N/A	0.555	-0.555
Necrosis of cardiac muscle	-1.884	-0.764	-2.259	-1.998	N/A	-1.656	N/A	-1.013	N/A	N/A

Failure of kidney	-2.051	-1.361	-1.297	-1.353	N/A	-1.458	N/A	-0.391	-0.346	1.259
Failure of liver	-2.114	-1.253	-1.885	-2.421	N/A	-1.632	N/A	N/A	0.105	-0.105
Proliferation of hepatic stellate cells	0.943	0.873	1.991	1.018	N/A	1.604	N/A	0.73	-2.019	0.331
Damage of renal glomerulus	2.112	2.112	1.782	2.038	N/A	N/A	N/A	N/A	-1.461	N/A
Glomerulonephritis	-1.628	-1.516	-1.367	-0.925	N/A	-1.817	N/A	-1.51	-0.501	-0.219
Increased localization of AST	1.58	1.342	2.007	2.007	N/A	1.668	N/A	N/A	0.106	0.689
Apoptosis of ventricular myocytes	-1.576	-1.382	-2.257	-2.09	N/A	-2.084	N/A	N/A	N/A	N/A
Injury of kidney	1.074	1.295	1.029	1.061	N/A	1.421	N/A	-1.911	-0.92	0.526
Hepatocellular carcinoma	-1.228	-1.263	-0.522	-0.519	N/A	-0.793	N/A	-2.213	2.415	-0.249
Perivascular fibrosis of artery	1.929	1.929	1.929	1.929	N/A	1.411	N/A	N/A	N/A	N/A

Quantity of hepatocytes	1.976	2.538	1.943	1.238	N/A	1.414	N/A	N/A	N/A	N/A
Cell death of heart	-1.953	-0.752	-2.268	-2.048	N/A	-1.693	N/A	N/A	N/A	0.378
Fibrosis of heart	-1.041	-1.145	-1.437	-1.268	N/A	-1.774	N/A	-0.931	-1.29	0.16
Acute renal failure	0.799	1.854	1.584	1.584	N/A	0.479	N/A	N/A	-1.067	1.664
Endocardial cushion defect	-1.689	-1.924	-1.924	-2.051	N/A	-1.383	N/A	N/A	N/A	N/A
Increased release of ALT	1.477	1.981	1.981	1.491	N/A	2.035	N/A	N/A	N/A	N/A
Primum atrial septal defect	-1.633	-1.89	-1.89	-1.89	N/A	-1.633	N/A	N/A	N/A	N/A
Liver cancer	-1.153	-1.488	-0.463	-0.364	N/A	-1.077	N/A	-2.198	2.103	-0.06
Myocardial infarction	-1.155	-0.958	-1.11	-1.316	N/A	-1.492	N/A	0.73	-0.715	1.41
Arrhythmia	-1.094	-0.763	-1.742	-1.241	N/A	-1.479	N/A	0.905	-0.491	-1.043

Familial cardiac septal defect	-2.178	N/A	-2.178	-2.178	N/A	-2.178	N/A	N/A	N/A	N/A
Bleeding of liver	-1.546	-1.649	-1.923	-1.058	N/A	-1.058	N/A	N/A	-0.447	1
Inflammation of cardiac muscle	1.744	1.709	1.744	1.452	N/A	1.97	N/A	N/A	N/A	N/A
Apoptosis of glomerular cells	1.116	1.478	1.239	1.191	N/A	1.919	N/A	-1.285	-0.305	-0.055
Dilation of heart chamber	1.056	0.771	1.007	1.852	N/A	1.559	N/A	-0.75	-0.946	0.547
Reperfusion injury of kidney	1.362	1.476	1.218	0.793	N/A	1.155	N/A	N/A	-1.195	1.195
Apoptosis of cardiomyocytes	-1.496	-0.591	-2.009	-1.616	N/A	-1.296	N/A	-0.994	0.045	-0.313
Liver Hypoplasia	-1.155	-1.201	-2.068	-2.068	N/A	-1.664	N/A	N/A	N/A	-0.152
Infection by Hepatitis C virus	-1.725	-1.42	-1.725	-1.297	N/A	-2.019	N/A	N/A	N/A	N/A
Stenosis of aortic valve	-1.134	-1.195	-1.463	-1.195	N/A	-1.463	N/A	N/A	N/A	-1.715

Survival of glomerular cells	1.768	1.768	1.532	1.532	N/A	1.532	N/A	N/A	N/A	N/A
Common atrium	-1.387	-1.387	-1.982	-1.982	N/A	-1.387	N/A	N/A	N/A	N/A
Cell death of heart ventricle	-1.189	-1.017	-1.991	-1.955	N/A	-1.96	N/A	N/A	N/A	N/A
Cell death of cardiomyocytes	-1.515	-0.441	-1.87	-1.595	N/A	-1.347	N/A	-1.244	-0.046	0.035
Cortical renal glomerulopathies	-1.387	-1.387	-1.664	-1.664	N/A	-1.912	N/A	N/A	N/A	N/A
Sinus arrhythmia	-2	N/A	-2	-2	N/A	-2	N/A	N/A	N/A	N/A
Sinus bradycardia	-2	N/A	-2	-2	N/A	-2	N/A	N/A	N/A	N/A
Inflammation of liver	-1.673	-1.254	-1.492	-1.086	N/A	-1.07	N/A	-0.957	0.097	-0.324
Atrophy of renal tubule	-1.463	-1.463	-1.526	-1.526	N/A	-1.757	N/A	N/A	N/A	N/A
Apoptosis of kidney cells	0.699	1.342	1.373	1.025	N/A	1.224	N/A	-1.581	-0.083	-0.331
Damage of	1.3	1.34	1.04	1.34	N/A	1.3	N/A	N/A	-	N/A

kidney cells	4		1			94			1.179	
Interstitial fibrosis of heart	1.178	1.15	1.314	1.114	N/A	0.728	N/A	-0.128	-1.219	0.757
Apoptosis of heart ventricle	-1.212	-1.017	-1.892	-1.721	N/A	-1.712	N/A	N/A	N/A	N/A
Ventricular extrasystole	-1.698	-1.067	-1.964	-1.254	N/A	-1.51	N/A	N/A	N/A	N/A
Cirrhosis	-1.62	-1.294	-1.62	-1.294	N/A	-1.62	N/A	N/A	N/A	N/A
Supraventricular arrhythmia	-1.001	-0.802	-1.935	-1.697	N/A	-0.765	N/A	N/A	-0.305	-0.923
Cirrhosis of liver	-1.617	-1.286	-1.617	-1.286	N/A	-1.617	N/A	N/A	N/A	N/A
Dysfunction of left ventricle	0.862	1.632	0.567	1.31	N/A	0.135	N/A	N/A	-1.89	0.956
Stenosis of pulmonary valve	-1.254	-1.254	-1.698	-1.254	N/A	-1.698	N/A	N/A	N/A	N/A
Inflammation of myocardium	1.432	1.387	1.432	1.067	N/A	1.698	N/A	N/A	N/A	N/A
Dilation of	-	-	-	-	N/A	-	N/A	N/A	N/	N/A

kidney	1.387	1.387	1.387	1.387		1.387			A	
Injury of podocytes	1.38	1.38	1.034	1.38	N/A	1.761	N/A	N/A	N/A	N/A
Viral hepatitis	-1.485	-1.142	-1.485	-1.027	N/A	-1.776	N/A	N/A	N/A	N/A
Carditis	0.84	0.789	1.609	1.12	N/A	0.877	N/A	N/A	-0.788	0.788
Dysfunction of heart	0.159	1.335	0.504	0.373	N/A	-0.28	N/A	-0.701	-2.232	1.152
Infarction of heart	-0.817	-0.622	-0.766	-0.839	N/A	-1.064	N/A	N/A	-0.978	1.631
Liver metastasis	1.175	0.954	1.308	1.308	N/A	0.791	N/A	N/A	-0.277	-0.896
Transposition of great vessels	-1.912	-1.129	-1.211	-1.912	N/A	-0.493	N/A	N/A	N/A	N/A
Cell viability of kidney cells	1.772	1.772	1.539	1.539	N/A	N/A	N/A	N/A	N/A	N/A
Proliferation of renal tubular epithelial cells	1.461	1.461	N/A	1.964	N/A	1.715	N/A	N/A	N/A	N/A
Fibrosis of coronary artery	1.114	1.114	1.114	1.114	N/A	0.963	N/A	N/A	-1.1	N/A

									14	
Cell proliferation of kidney cell lines	-1.063	-1.001	-0.678	-1.122	N/A	-0.939	N/A	-0.137	-0.141	-1.451
Apoptosis of podocytes	0.968	0.83	1.264	1.235	N/A	1.546	N/A	N/A	-0.046	-0.6
Dilation of left ventricle	0.943	0.548	0.823	1.781	N/A	1.544	N/A	N/A	-0.625	0.218
Development of hepatocellular carcinoma	-0.454	-0.22	0.174	0.518	N/A	-0.1	N/A	-2.213	2.621	0.113
Damage of podocytes	1.662	1.662	1.34	1.662	N/A	N/A	N/A	N/A	N/A	N/A
Apoptosis of renal glomerulus	0.524	0.915	0.69	0.617	N/A	1.355	N/A	-1.536	0.13	-0.382
Damage of heart	-0.901	-1.055	-1.209	-0.921	N/A	-0.898	N/A	-0.213	0.513	-0.404
Apoptosis of heart cells	-1.549	-0.542	-2.066	-1.669	N/A	N/A	N/A	N/A	-0.084	-0.196
Injury of renal tubule	1.339	1.339	1.339	1.105	N/A	0.943	N/A	N/A	N/A	N/A
Cell death of liver cell lines	1.002	1.697	1.118	0.894	N/A	1.349	N/A	N/A	N/A	N/A

Dilation of heart ventricle	1.14	0.829	0.863	1.761	N/A	1.449	N/A	N/A	N/A	N/A
Quantity of hepatocellular carcinoma	-1.342	-1	-1	-1.342	N/A	-1.342	N/A	N/A	N/A	N/A
Fibrosis of kidney	-0.123	-0.838	-0.515	-0.763	N/A	-0.071	N/A	0.555	0.831	-2.19
Atrioventricular septal defect and common atrioventricular junction	-1.066	-1.32	-1.32	-1.463	N/A	-0.711	N/A	N/A	N/A	N/A
Cell death of heart cells	-1.553	-0.385	-1.847	-1.633	N/A	N/A	N/A	N/A	-0.166	0.276
Carbon tetrachloride-induced liver fibrosis	1.253	1.253	1.516	1.253	N/A	0.537	N/A	N/A	N/A	N/A
Focal segmental glomerulosclerosis	1.109	1.109	1.408	1.408	N/A	0.762	N/A	N/A	N/A	N/A
Single ventricle defect	-0.816	-0.816	-1.633	-1.633	N/A	-0.816	N/A	N/A	N/A	N/A
Apoptosis of hepatocytes	-0.457	-0.301	-0.852	-0.678	N/A	0.176	N/A	-1.126	1.864	-0.242

Growth of liver tumor	-1.393	-1.629	-0.416	-0.78	N/A	-0.47	N/A	N/A	0.842	-0.142
Double outlet right ventricle	-1.131	-1.131	-1.131	-1.131	N/A	-1.131	N/A	N/A	N/A	N/A
Injury of heart	-0.945	-1.179	-0.468	-0.945	N/A	-0.713	N/A	N/A	0.695	-0.686
Situs inversus totalis	-1.414	-1	-1.667	-1.265	N/A	0	N/A	N/A	N/A	N/A
Interstitial fibrosis of kidney	-1.075	-1.25	-0.787	-0.913	N/A	-1.035	N/A	N/A	-0.036	0.218
Chronic renal failure	-1.075	-1.25	-0.787	-0.913	N/A	-1.035	N/A	N/A	-0.036	0.218
End stage renal disease	-1.075	-1.25	-0.787	-0.913	N/A	-1.035	N/A	N/A	-0.036	0.218
Crescentic glomerulonephritis	-1.387	-1.387	-1	-1.387	N/A	N/A	N/A	N/A	N/A	N/A
Cell death of renal tubule	0.565	1.174	1.527	1.063	N/A	0.791	N/A	N/A	N/A	N/A
Microvesicular hepatic steatosis	-0.669	-0.628	-1.112	-1.625	N/A	-1.077	N/A	N/A	N/A	N/A

Apoptosis of mesangial cells	0.327	1.035	0.317	0.317	N/A	0.992	N/A	-1.931	-0.13	N/A
Apoptosis of hepatic stellate cells	-0.397	-0.666	-0.445	-0.666	N/A	-0.915	N/A	0.655	0.6	-0.686
Inflammation of heart	-0.868	-1.164	-0.955	-0.75	N/A	0.025	N/A	0.577	-0.027	-0.599
Cell death of hepatocytes	-0.21	0.034	-0.579	-0.152	N/A	0.615	N/A	-1.202	1.805	0.298
Necrosis of liver	-0.417	-0.007	-0.843	-0.132	N/A	-0.032	N/A	-1.906	0.919	0.609
Conjugation of glutathione	1.109	1.357	1.109	0.656	N/A	0.129	N/A	N/A	0.186	-0.304
Apoptosis of renal tubular epithelial cells	0.259	0.532	0.823	0.545	N/A	-0.384	N/A	N/A	-1.276	1
Proliferation of liver cancer cells	-1.414	-0.905	-1.265	-1	N/A	0.149	N/A	N/A	N/A	N/A
Proliferation of hepatocytes	0.208	0.089	1.031	0.633	N/A	0.4	N/A	0.374	-0.319	1.66
Apoptosis of liver cell lines	0.679	1.463	0.869	0.615	N/A	1.086	N/A	N/A	N/A	N/A

Apoptosis of liver cells	-0.347	-0.237	-0.826	-0.727	N/A	-0.005	N/A	-0.905	1.408	0.108
Apoptosis of renal tubule	0.295	0.778	1.386	0.85	N/A	0.514	N/A	N/A	-0.65	0.042
Survival of podocytes	1.109	1.109	0.762	0.762	N/A	0.762	N/A	N/A	N/A	N/A
Steatohepatitis	0.907	1.192	0.968	0.73	N/A	0.681	N/A	N/A	N/A	N/A
Glomerulosclerosis	-0.283	-0.755	-0.424	-0.604	N/A	0.071	N/A	0.323	0.367	-1.613
Dysplasia of kidney	-0.816	-0.816	-0.816	-0.816	N/A	-1.134	N/A	N/A	N/A	0
Development of liver tumor	-0.402	-0.376	-0.066	-0.005	N/A	-0.531	N/A	N/A	2.804	-0.213
Necrosis of renal tubule	0.375	1.018	1.225	0.693	N/A	0.531	N/A	N/A	-0.471	-0.081
Necrosis of renal glomerulus	0.583	0.973	0.746	0.675	N/A	1.415	N/A	N/A	N/A	N/A
Damage of cardiac muscle	-0.455	-0.229	-0.659	-0.24	N/A	-0.416	N/A	-1.109	1.254	N/A
Lupus nephritis	0.2	0.19	0.37	1.89	N/A	-	N/A	N/A	-	0.37

	13	4	8			0.447			0.816	8
Perivascular fibrosis of heart	0.935	0.563	0.794	0.286	N/A	0.038	N/A	-0.152	-1.477	N/A
Oxidative stress response of heart	-0.762	-0.277	-0.806	0.555	N/A	1.067	N/A	N/A	N/A	-0.497
Dextrocardia	-0.847	0.088	-1.461	-1.029	N/A	0.487	N/A	N/A	N/A	N/A
Cell death of renal tubular epithelial cells	0.173	0.889	1.206	0.676	N/A	0.07	N/A	N/A	-0.895	N/A
Cell death of liver cells	0.117	0.492	-0.228	-0.06	N/A	0.643	N/A	-1.02	0.667	0.66
Degeneration of liver	-1.098	-0.929	-1.252	-0.301	N/A	0.124	N/A	N/A	N/A	0.152
Fibrosis of myocardium	0.705	-0.211	0.35	-0.225	N/A	-0.338	N/A	N/A	-1.412	0.463
Liver hyperplasia	-0.742	-0.742	-0.742	-1.452	N/A	N/A	N/A	N/A	N/A	N/A
Atrial fibrillation	-0.431	-0.431	-1.056	-0.718	N/A	-0.164	N/A	N/A	N/A	-0.847

Cholestasis	-0.431	-0.388	-0.961	-0.522	N/A	-1.32	N/A	N/A	N/A	N/A
Ventricular dysfunction	-0.071	0.57	0.212	0.27	N/A	-0.349	N/A	N/A	-1.486	0.615
Hepatocellular adenoma	1	0.895	-0.236	0.294	N/A	1	N/A	N/A	N/A	N/A
Perivascular fibrosis	0.664	0.362	0.247	0.052	N/A	-0.152	N/A	N/A	-1.72	-0.193
Fibrosis of heart chamber	1.04	0.803	0.619	0.585	N/A	0.325	N/A	N/A	N/A	N/A
Myocardial fibrosis	0.478	0.478	0.478	0.478	N/A	1.195	N/A	N/A	N/A	0.152
Left ventricular dysfunction	-0.376	0.213	0.061	-0.066	N/A	-0.503	N/A	-1.158	-0.747	0.121
Apoptosis of proximal tubule cells	-0.647	-0.647	-0.647	-0.647	N/A	-0.647	N/A	N/A	N/A	N/A
Apoptosis of tubular cells	-0.046	0.5	1.179	0.314	N/A	-0.017	N/A	N/A	-0.699	0.437
Cell death of proximal tubule cells	N/A	N/A	-1.04	-1.04	N/A	-1.04	N/A	N/A	-0.068	N/A

Atrial fibrillation or flutter	-0.505	-0.5055	-1.113	-0.786	N/A	-0.243	N/A	N/A	N/A	N/A
Cell death of tubular cells	-0.097	0.773	1.237	0.237	N/A	0.089	N/A	N/A	-0.718	N/A
Pulmonary Hypertension	0.313	0.313	-0.606	-0.017	N/A	-0.517	N/A	N/A	-0.519	-0.849
Thrombosis of renal glomerulus	-0.555	-0.5555	-0.97	-0.555	N/A	0.447	N/A	N/A	N/A	N/A
Arrhythmia of atrium	-0.302	-0.302	-1.351	-1.056	N/A	-0.059	N/A	N/A	N/A	N/A
Damage of renal tubule	0.233	0.169	0.169	0.176	N/A	-0.916	N/A	N/A	-0.391	1
Rupture of heart	0.728	0.728	0.391	0.728	N/A	0.342	N/A	N/A	N/A	N/A
Hepatotoxicity	0.726	0.201	0.219	1.081	N/A	0.41	N/A	N/A	0.254	N/A
Quantity of glutathione in liver	0.333	0.707	1.134	0.378	N/A	0.333	N/A	N/A	N/A	N/A
Left ventricular fibrosis	0.534	0.38	0.497	0.033	N/A	0.106	N/A	-1.103	-0.129	0.092

Quantity of peroxisomes	0.44	0.44	0.44	0.44	N/A	1.101	N/A	N/A	N/A	N/A
Bleeding of heart	N/A	-1.131	-0.283	-0.283	N/A	-1.131	N/A	N/A	N/A	N/A
Proliferation of biliary epithelial cells	-0.218	-0.788	-0.788	-0.478	N/A	-0.493	N/A	N/A	N/A	N/A
Remodeling of left ventricle	0	0.761	0.761	0.761	N/A	0.479	N/A	N/A	N/A	N/A
Benign neoplasm of liver	1.081	0.618	-0.267	0.132	N/A	0.66	N/A	N/A	N/A	N/A
Proliferation of oval cells	0.586	0.297	0.433	0.586	N/A	-0.464	N/A	N/A	0.132	N/A
Increased excretion of albumin	N/A	N/A	N/A	1.103	N/A	0.254	N/A	N/A	-1.103	N/A
Nonalcoholic fatty liver disease	-0.563	-0.563	-0.64	-0.64	N/A	-0.048	N/A	N/A	N/A	N/A
Pulmonary hypertensive arterial disease	-0.391	-0.391	-0.479	-0.842	N/A	-0.301	N/A	N/A	N/A	N/A
Fibrosis of heart ventricle	0.757	0.439	0.703	0.289	N/A	0.185	N/A	N/A	N/A	N/A
Disorder of	0.3	0.37	0.37	0.01	N/A	0.3	N/A	N/A	0.0	-

coronary artery	79	9	9	4		9			38	0.751
Bradycardia	0.274	0.491	0.065	0.47	N/A	0	N/A	N/A	-0.699	-0.301
Decreased Levels of Albumin	1.091	0.6	0.6	0	N/A	0	N/A	N/A	N/A	N/A
Increased uptake of albumin	1.091	0.6	0.6	0	N/A	0	N/A	N/A	N/A	N/A
Quantity of liver tumor	0.168	-0.41	-0.41	-0.387	N/A	-0.901	N/A	N/A	N/A	N/A
Damage of myocardium	0.103	0.094	-0.196	-0.513	N/A	0.094	N/A	N/A	0.651	-0.555
Acute kidney injury	-0.128	-0.113	-0.788	-0.128	N/A	-0.896	N/A	N/A	N/A	-0.152
Diastolic dysfunction of heart	N/A	N/A	1.067	1.067	N/A	N/A	N/A	N/A	N/A	N/A
Degeneration of kidney	-0.389	-0.359	-0.389	0.213	N/A	-0.389	N/A	N/A	0.391	N/A
Nephrosis	N/A	N/A	-1	-1.091	N/A	N/A	N/A	N/A	N/A	N/A
Hypoplasia of	N/	N/A	N/A	N/A	N/A	-2	N/A	N/A	N/	N/A

renal medulla	A								A	
Glomerular endotheliosis	N/A	-0.655	-0.655	-0.655	N/A	N/A	N/A	N/A	N/A	N/A
Fibrosis of atrium	N/A	1.235	0.269	N/A	N/A	0.404	N/A	N/A	N/A	N/A
Tachycardia	0.372	0.372	0.354	0.357	N/A	-0.218	N/A	N/A	0.152	0.022
Cell death of renal glomerulus	0.039	0.451	0.235	0.145	N/A	0.89	N/A	N/A	N/A	N/A
Apoptosis of liver	-0.227	-0.027	-0.703	-0.599	N/A	0.201	N/A	N/A	N/A	N/A
Pulmonary embolism	-0.302	0.038	0.038	-0.302	N/A	-0.986	N/A	N/A	N/A	N/A
Proliferation of cholangiocytes	-0.113	-0.478	-0.478	-0.128	N/A	-0.426	N/A	N/A	N/A	N/A
Cell death of liver	-0.326	0.291	-0.761	-0.05	N/A	0.129	N/A	N/A	N/A	N/A
Secretion of bile acid	N/A	N/A	0.762	N/A	N/A	0.762	N/A	N/A	N/A	N/A
Fibrosis of cardiac muscle	0.705	-0.211	0.35	-0.225	N/A	N/A	N/A	N/A	N/A	N/A

Ventricular tachycardia	-0.282	0	-0.262	0.399	N/A	-0.1	N/A	N/A	N/A	-0.371
Glomerulopathy of mesangium	0.277	0.277	0.277	0.277	N/A	0.277	N/A	N/A	N/A	N/A
Interstitial fibrosis of left ventricle	0.456	0.317	0.397	0.084	N/A	0.09	N/A	N/A	N/A	N/A
Autoimmune glomerulonephritis	-0.447	0.447	N/A	N/A	N/A	-0.447	N/A	N/A	N/A	N/A
Injury of myocardium	N/A	0.068	0.068	N/A	N/A	0.44	N/A	N/A	0.747	N/A
Hepatic adenocarcinoma	0.058	0.058	-0.326	-0.326	N/A	0.433	N/A	N/A	N/A	N/A
Perivascular fibrosis of coronary artery	N/A	N/A	N/A	N/A	N/A	1.091	N/A	N/A	N/A	N/A
Left ventricular diastolic dysfunction	N/A	N/A	N/A	N/A	N/A	N/A	N/A	N/A	N/A	1.067
Damage of heart ventricle	-0.152	-0.152	-0.152	N/A	N/A	-0.555	N/A	N/A	N/A	N/A
Dysfunction of cardiomyocytes	N/A	1	N/A	N/A	N/A	N/A	N/A	N/A	N/A	N/A
Hyperplasia of	-	0.23	-	0	N/A	0	N/A	N/A	N/	N/A

heart	0.128	9	0.478						A	
Cell death of hepatic stellate cells	N/A	N/A	N/A	-0.267	N/A	-0.515	N/A	N/A	N/A	N/A
Erythropoiesis of liver	N/A	0.762	N/A	N/A	N/A	N/A	N/A	N/A	N/A	N/A
Nonalcoholic steatohepatitis	0.128	0.128	0.152	0.152	N/A	0.128	N/A	N/A	N/A	N/A
Cell viability of cardiomyocytes	0.072	0.072	0.072	0.072	N/A	-0.141	N/A	N/A	N/A	-0.056
Chronic hepatitis	N/A	-0.277	N/A	N/A	N/A	N/A	N/A	N/A	N/A	N/A
Coronary occlusion	N/A	N/A	N/A	N/A	N/A	-0.243	N/A	N/A	N/A	N/A
Inflammation of renal glomerulus	N/A	N/A	-0.218	N/A	N/A	N/A	N/A	N/A	N/A	N/A
Perivascular fibrosis of left ventricle	N/A	N/A	-0.117	N/A	N/A	N/A	N/A	N/A	N/A	N/A
Nonsyndromic renal hypodysplasia 1	N/A	N/A	N/A	N/A	N/A	N/A	N/A	N/A	N/A	N/A
Hypertrophy of cardiac-like	N/A	N/A	N/A	N/A	N/A	N/A	N/A	N/A	N/A	N/A

myocytes										
Stable disease stage ischemic heart failure	N/A	N/A	N/A	N/A	N/A	N/A	N/A	N/A	N/A	N/A
Double inlet heart left ventricle	N/A	N/A	N/A	N/A	N/A	N/A	N/A	N/A	N/A	N/A
Histopathological change of liver	N/A	N/A	N/A	N/A	N/A	N/A	N/A	N/A	N/A	N/A
Hepatomegaly	N/A	N/A	N/A	N/A	N/A	N/A	N/A	N/A	N/A	N/A
Nephrotic syndrome type 4	N/A	N/A	N/A	N/A	N/A	N/A	N/A	N/A	N/A	N/A
Cardiorenal syndrome	N/A	N/A	N/A	N/A	N/A	N/A	N/A	N/A	N/A	N/A
Dilated cardiomyopathy	N/A	N/A	N/A	N/A	N/A	N/A	N/A	N/A	N/A	N/A
Familial focal segmental glomerulosclerosisrosis	N/A	N/A	N/A	N/A	N/A	N/A	N/A	N/A	N/A	N/A
Right ventricular hypertrophy	N/A	N/A	N/A	N/A	N/A	N/A	N/A	N/A	N/A	N/A
Severe alcoholic hepatitis	N/A	N/A	N/A	N/A	N/A	N/A	N/A	N/A	N/A	N/A
Advanced liver cholangiocarcinoma	N/A	N/A	N/A	N/A	N/A	N/A	N/A	N/A	N/A	N/A

Sudden cardiac death	N/A	N/A	N/A	N/A	N/A	N/A	N/A	N/A	N/A	N/A
Secretion of bile salt	N/A	N/A	N/A	N/A	N/A	N/A	N/A	N/A	N/A	N/A
Paroxysmal supraventricular tachycardia	N/A	N/A	N/A	N/A	N/A	N/A	N/A	N/A	N/A	N/A
Arrest in growth of kidney cell lines	N/A	N/A	N/A	N/A	N/A	N/A	N/A	N/A	N/A	N/A
Coronary artery disease	N/A	N/A	N/A	N/A	N/A	N/A	N/A	N/A	N/A	N/A
Associated pulmonary arterial hypertension	N/A	N/A	N/A	N/A	N/A	N/A	N/A	N/A	N/A	N/A
Chronic atrial flutter	N/A	N/A	N/A	N/A	N/A	N/A	N/A	N/A	N/A	N/A
Acute decompensated heart failure	N/A	N/A	N/A	N/A	N/A	N/A	N/A	N/A	N/A	N/A
Advanced stage cirrhosis	N/A	N/A	N/A	N/A	N/A	N/A	N/A	N/A	N/A	N/A
Proximal tubular toxicity	N/A	N/A	N/A	N/A	N/A	N/A	N/A	N/A	N/A	N/A
Mild dilated cardiomyopathy	N/A	N/A	N/A	N/A	N/A	N/A	N/A	N/A	N/A	N/A
Thrombosis of	N/	N/A	N/A	N/A	N/A	N/	N/A	N/A	N/	N/A

glomerular capillary	A					A			A	
Renal adysplasia	N/A	N/A	N/A	N/A	N/A	N/A	N/A	N/A	N/A	N/A
Double aortic arch	N/A	N/A	N/A	N/A	N/A	N/A	N/A	N/A	N/A	N/A
Acute inflammation of liver	N/A	N/A	N/A	N/A	N/A	N/A	N/A	N/A	N/A	N/A
Severe heart failure	N/A	N/A	N/A	N/A	N/A	N/A	N/A	N/A	N/A	N/A
New York Heart Association class IV heart failure	N/A	N/A	N/A	N/A	N/A	N/A	N/A	N/A	N/A	N/A
Bile duct proliferation	N/A	N/A	N/A	N/A	N/A	N/A	N/A	N/A	N/A	N/A
Recurrent myocardial infarction	N/A	N/A	N/A	N/A	N/A	N/A	N/A	N/A	N/A	N/A
Infection by hepatitis B virus	N/A	N/A	N/A	N/A	N/A	N/A	N/A	N/A	N/A	N/A
Primary dilated cardiomyopthy	N/A	N/A	N/A	N/A	N/A	N/A	N/A	N/A	N/A	N/A
Child-Pugh class A hepatocellular carcinoma	N/A	N/A	N/A	N/A	N/A	N/A	N/A	N/A	N/A	N/A
Severe dilated cardiomyopathy	N/A	N/A	N/A	N/A	N/A	N/A	N/A	N/A	N/A	N/A

Decreased excretion of albumin	N/A	N/A	N/A	N/A	N/A	N/A	N/A	N/A	N/A	N/A
Acute glomerulonephritis	N/A	N/A	N/A	N/A	N/A	N/A	N/A	N/A	N/A	N/A
Chronic active hepatitis	N/A	N/A	N/A	N/A	N/A	N/A	N/A	N/A	N/A	N/A
Generation of reactive oxygen species in liver	N/A	N/A	N/A	N/A	N/A	N/A	N/A	N/A	N/A	N/A
Severely symptomatic disease stage atrial fibrillation or flutter	N/A	N/A	N/A	N/A	N/A	N/A	N/A	N/A	N/A	N/A
Hypertrophy of cardiac muscle	N/A	N/A	N/A	N/A	N/A	N/A	N/A	N/A	N/A	N/A
Familial atrial fibrillation type 9	N/A	N/A	N/A	N/A	N/A	N/A	N/A	N/A	N/A	N/A
Dilation of proximal convoluted tubule	N/A	N/A	N/A	N/A	N/A	N/A	N/A	N/A	N/A	N/A
Minimal change nephrotic syndrome	N/A	N/A	N/A	N/A	N/A	N/A	N/A	N/A	N/A	N/A
Longstanding	N/	N/A	N/A	N/A	N/A	N/	N/A	N/A	N/	N/A

persistent atrial fibrillation	A					A			A	
Symptomatic toxin induced pulmonary arterial hypertension	N/A	N/A	N/A	N/A	N/A	N/A	N/A	N/A	N/A	N/A
Congenital malformation of aortic valve	N/A	N/A	N/A	N/A	N/A	N/A	N/A	N/A	N/A	N/A
Oxidative stress response of myocardium	N/A	N/A	N/A	N/A	N/A	N/A	N/A	N/A	N/A	N/A
Familial ventricular arrhythmia	N/A	N/A	N/A	N/A	N/A	N/A	N/A	N/A	N/A	N/A
Tetralogy of Fallot	N/A	N/A	N/A	N/A	N/A	N/A	N/A	N/A	N/A	N/A
Severe hepatic steatosis	N/A	N/A	N/A	N/A	N/A	N/A	N/A	N/A	N/A	N/A
Nonsyndromic arrhythmogenic right ventricular cardiomyopathy	N/A	N/A	N/A	N/A	N/A	N/A	N/A	N/A	N/A	N/A
Mitogenesis of hepatic stellate cells	N/A	N/A	N/A	N/A	N/A	N/A	N/A	N/A	N/A	N/A
ST-elevation myocardial	N/A	N/A	N/A	N/A	N/A	N/A	N/A	N/A	N/A	N/A

infarction										
Finnish congenital nephrotic syndrome	N/A	N/A	N/A	N/A	N/A	N/A	N/A	N/A	N/A	N/A
Adhesion of liver cells	N/A	N/A	N/A	N/A	N/A	N/A	N/A	N/A	N/A	N/A
Hereditary Wolff-Parkinson-White syndrome	N/A	N/A	N/A	N/A	N/A	N/A	N/A	N/A	N/A	N/A
Kidney graft failure	N/A	N/A	N/A	N/A	N/A	N/A	N/A	N/A	N/A	N/A
Alport syndrome or thin basement membrane nephropathy	N/A	N/A	N/A	N/A	N/A	N/A	N/A	N/A	N/A	N/A
Recessive dilated cardiomyopathy	N/A	N/A	N/A	N/A	N/A	N/A	N/A	N/A	N/A	N/A
Metastatic liver cholangiocarcinoma	N/A	N/A	N/A	N/A	N/A	N/A	N/A	N/A	N/A	N/A
Oxidative stress response of cardiac muscle	N/A	0	0	N/A	N/A	N/A	N/A	N/A	N/A	N/A
Dilated cardiomyopathy 1z	N/A	N/A	N/A	N/A	N/A	N/A	N/A	N/A	N/A	N/A

Increased localization of alkaline phosphatase	N/A	N/A	N/A	N/A	N/A	N/A	N/A	N/A	N/A	N/A
Moderately differentiated hepatocellular carcinoma	N/A	N/A	N/A	N/A	N/A	N/A	N/A	N/A	N/A	N/A
Child-Pugh class A primary hepatocellular carcinoma	N/A	N/A	N/A	N/A	N/A	N/A	N/A	N/A	N/A	N/A
Familial atrial fibrillation	N/A	N/A	N/A	N/A	N/A	N/A	N/A	N/A	N/A	N/A
Autosomal recessive renal tubular dysgenesis	N/A	N/A	N/A	N/A	N/A	N/A	N/A	N/A	N/A	N/A
Unilateral renal agenesis	N/A	N/A	N/A	N/A	N/A	N/A	N/A	N/A	N/A	N/A
Focal necrosis of liver cells	N/A	N/A	N/A	N/A	N/A	N/A	N/A	N/A	N/A	N/A
Expansion of hepatocytes	N/A	N/A	N/A	N/A	N/A	N/A	N/A	N/A	N/A	N/A
Shortened PR interval	N/A	N/A	N/A	N/A	N/A	N/A	N/A	N/A	N/A	N/A
Hypertrophy of renal glomerulus	N/A	N/A	N/A	N/A	N/A	N/A	N/A	N/A	N/A	N/A

Hypertrophy of heart chamber	N/A	N/A	N/A	N/A	N/A	N/A	N/A	N/A	N/A	N/A
Immune complex nephritis	N/A	N/A	N/A	N/A	N/A	N/A	N/A	N/A	N/A	N/A
Enlargement of ventricular myocytes	N/A	N/A	N/A	N/A	N/A	N/A	N/A	N/A	N/A	N/A
Familial sudden cardiac death	N/A	N/A	N/A	N/A	N/A	N/A	N/A	N/A	N/A	N/A
Lesioning of liver	N/A	N/A	N/A	N/A	N/A	N/A	N/A	N/A	N/A	N/A
Stable disease stage cardiomyopathic heart failure	N/A	N/A	N/A	N/A	N/A	N/A	N/A	N/A	N/A	N/A
Well-differentiated hepatocellular carcinoma	N/A	N/A	N/A	N/A	N/A	N/A	N/A	N/A	N/A	N/A
Familial primary pulmonary hypertension	N/A	N/A	N/A	N/A	N/A	N/A	N/A	N/A	N/A	N/A
Persistent fetal circulation syndrome	N/A	N/A	N/A	N/A	N/A	N/A	N/A	N/A	N/A	N/A
Spontaneous coronary artery dissection	N/A	N/A	N/A	N/A	N/A	N/A	N/A	N/A	N/A	N/A

Susceptibility to noncryptogenic cirrhosis	N/A	N/A	N/A	N/A	N/A	N/A	N/A	N/A	N/A	N/A
Non-ST elevation myocardial infarction	N/A	N/A	N/A	N/A	N/A	N/A	N/A	N/A	N/A	N/A
New York Heart Association class III heart failure	N/A	N/A	N/A	N/A	N/A	N/A	N/A	N/A	N/A	N/A
Invasion of hepatocellular carcinoma	N/A	N/A	N/A	N/A	N/A	N/A	N/A	N/A	N/A	N/A
Increased release of AST	N/A	N/A	N/A	N/A	N/A	N/A	N/A	N/A	N/A	N/A
Abnormal morphology of podocytes	N/A	N/A	N/A	N/A	N/A	N/A	N/A	N/A	N/A	N/A
Heritable pulmonary artery hypertension	N/A	N/A	N/A	N/A	N/A	N/A	N/A	N/A	N/A	N/A
Familial arrhythmogenic right ventricular dysplasia type 2	N/A	N/A	N/A	N/A	N/A	N/A	N/A	N/A	N/A	N/A
Hypertrophy of kidney	N/A	N/A	N/A	N/A	N/A	N/A	N/A	N/A	N/A	N/A
Multiple types congenital heart	N/A	N/A	N/A	N/A	N/A	N/A	N/A	N/A	N/A	N/A

defects type 7										
Cardiotoxicity	N/A	N/A	N/A	N/A	N/A	N/A	N/A	N/A	N/A	N/A
Hyperplasia of distal tubule	N/A	N/A	N/A	N/A	N/A	N/A	N/A	N/A	N/A	N/A
Primary liver cirrhosis	N/A	N/A	N/A	N/A	N/A	N/A	N/A	N/A	N/A	N/A
Unresectable hepatocellular carcinoma	N/A	N/A	N/A	N/A	N/A	N/A	N/A	N/A	N/A	N/A
Variant angina	N/A	N/A	N/A	N/A	N/A	N/A	N/A	N/A	N/A	N/A
Nephrotoxic acute renal failure	N/A	N/A	N/A	N/A	N/A	N/A	N/A	N/A	N/A	N/A
Familial dilated cardiomyopathy	N/A	N/A	N/A	N/A	N/A	N/A	N/A	N/A	N/A	N/A
Symptomatic stage hypertensive heart failure	N/A	N/A	N/A	N/A	N/A	N/A	N/A	N/A	N/A	N/A
Familial nephrotic syndrome	N/A	N/A	N/A	N/A	N/A	N/A	N/A	N/A	N/A	N/A
Autosomal recessive benign recurrent intrahepatic cholestasis 1	N/A	N/A	N/A	N/A	N/A	N/A	N/A	N/A	N/A	N/A

Left ventricular noncompaction type 2	N/A	N/A	N/A	N/A	N/A	N/A	N/A	N/A	N/A	N/A
Thrombosis of heart	N/A	N/A	N/A	N/A	N/A	N/A	N/A	N/A	N/A	N/A
Mesocardia	N/A	N/A	N/A	N/A	N/A	N/A	N/A	N/A	N/A	N/A
Apoptosis of cardiac fibroblasts	N/A	N/A	N/A	N/A	N/A	N/A	N/A	N/A	N/A	N/A
Symptomatic stage atrial flutter	N/A	N/A	N/A	N/A	N/A	N/A	N/A	N/A	N/A	N/A
Chronic heart failure stable disease stage heart failure	N/A	N/A	N/A	N/A	N/A	N/A	N/A	N/A	N/A	N/A
Left ventricular noncompaction type 10	N/A	N/A	N/A	N/A	N/A	N/A	N/A	N/A	N/A	N/A
Dilated cardiomyopathy 1d	N/A	N/A	N/A	N/A	N/A	N/A	N/A	N/A	N/A	N/A
Sinoatrial node dysfunction and deafness	N/A	N/A	N/A	N/A	N/A	N/A	N/A	N/A	N/A	N/A
Familial left ventricular noncompaction	N/A	N/A	N/A	N/A	N/A	N/A	N/A	N/A	N/A	N/A

Monogenic nephrotic syndrome	N/A	N/A	N/A	N/A	N/A	N/A	N/A	N/A	N/A	N/A
Familial hypoplastic left heart syndrome	N/A	N/A	N/A	N/A	N/A	N/A	N/A	N/A	N/A	N/A
Familial sinus bradycardia	N/A	N/A	N/A	N/A	N/A	N/A	N/A	N/A	N/A	N/A
Deafness, congenital heart defects, and posterior embryotoxon	N/A	N/A	N/A	N/A	N/A	N/A	N/A	N/A	N/A	N/A
Hepatitis B surface antigen-negative hepatitis C virus negative hepatocellular carcinoma	N/A	N/A	N/A	N/A	N/A	N/A	N/A	N/A	N/A	N/A
Chronic hepatitis C virus genotype 4	N/A	N/A	N/A	N/A	N/A	N/A	N/A	N/A	N/A	N/A
Severe ventricular arrhythmia	N/A	N/A	N/A	N/A	N/A	N/A	N/A	N/A	N/A	N/A
Severe experimental autoimmune	N/A	N/A	N/A	N/A	N/A	N/A	N/A	N/A	N/A	N/A

myocarditis										
Acute phase crescentic glomerulonephritis	N/A	N/A	N/A	N/A	N/A	N/A	N/A	N/A	N/A	N/A
End-stage chronic kidney disease	N/A	N/A	N/A	N/A	N/A	N/A	N/A	N/A	N/A	N/A
Arrhythmogenic right ventricular dysplasia familial 9	N/A	N/A	N/A	N/A	N/A	N/A	N/A	N/A	N/A	N/A
Adhesion of hepatocytes	N/A	N/A	N/A	N/A	N/A	N/A	N/A	N/A	N/A	N/A
Q-wave acute myocardial infarction	N/A	N/A	N/A	N/A	N/A	N/A	N/A	N/A	N/A	N/A
Familial dilated cardiomyopathy with left ventricular noncompaction	N/A	N/A	N/A	N/A	N/A	N/A	N/A	N/A	N/A	N/A
Permanent atrial fibrillation	N/A	N/A	N/A	N/A	N/A	N/A	N/A	N/A	N/A	N/A
Renal agenesis or hypodysplasia	N/A	N/A	N/A	N/A	N/A	N/A	N/A	N/A	N/A	N/A
Idiopathic and/or familial pulmonary	N/A	N/A	N/A	N/A	N/A	N/A	N/A	N/A	N/A	N/A

arterial hypertension										
Progression of hepatocellular carcinoma	0	0	0	0	N/A	N/A	N/A	N/A	N/A	N/A
Brugada syndrome type 1	N/A	N/A	N/A	N/A	N/A	N/A	N/A	N/A	N/A	N/A
Degeneration of nephron	N/A	N/A	N/A	N/A	N/A	N/A	N/A	N/A	N/A	N/A
Stenosis of coronary artery	N/A	N/A	N/A	N/A	N/A	N/A	N/A	N/A	N/A	N/A
Nephrotic syndrome type 7	N/A	N/A	N/A	N/A	N/A	N/A	N/A	N/A	N/A	N/A
IgA nephropathy	N/A	N/A	N/A	N/A	N/A	N/A	N/A	N/A	N/A	N/A
Damage of tubulointerstitium	N/A	N/A	N/A	N/A	N/A	N/A	N/A	N/A	N/A	N/A
Refractory hemodynamically unstable ventricular tachycardia	N/A	N/A	N/A	N/A	N/A	N/A	N/A	N/A	N/A	N/A
Cardiorespiratory arrest	N/A	N/A	N/A	N/A	N/A	N/A	N/A	N/A	N/A	N/A
Paroxysmal familial ventricular fibrillation type	N/A	N/A	N/A	N/A	N/A	N/A	N/A	N/A	N/A	N/A

1										
Bradyasystolic cardiac arrest	N/A	N/A	N/A	N/A	N/A	N/A	N/A	N/A	N/A	N/A
Thrombosis of atrium	N/A	N/A	N/A	N/A	N/A	N/A	N/A	N/A	N/A	N/A
Dilated cardiomyopathy type 1DD	N/A	N/A	N/A	N/A	N/A	N/A	N/A	N/A	N/A	N/A
Familial renal agenesis or hypodysplasia	N/A	N/A	N/A	N/A	N/A	N/A	N/A	N/A	N/A	N/A
Symptomatic stage ischemic heart failure	N/A	N/A	N/A	N/A	N/A	N/A	N/A	N/A	N/A	N/A
Cardiac death	N/A	N/A	N/A	N/A	N/A	N/A	N/A	N/A	N/A	N/A
Syndromic arrhythmia	N/A	N/A	N/A	N/A	N/A	N/A	N/A	N/A	N/A	N/A
Acute pulmonary embolism	N/A	N/A	N/A	N/A	N/A	N/A	N/A	N/A	N/A	N/A
Decreased Levels of Potassium	N/A	N/A	N/A	N/A	N/A	N/A	N/A	N/A	N/A	N/A
Decreased production of albumin	N/A	N/A	N/A	N/A	N/A	N/A	N/A	N/A	N/A	N/A
Catecholaminerg	N/	N/A	N/A	N/A	N/A	N/	N/A	N/A	N/	N/A

ic polymorphic ventricular tachycardia or long QT syndrome	A					A			A	
Sustained ventricular tachycardia	N/A	N/A	N/A	N/A	N/A	N/A	N/A	N/A	N/A	N/A
Experimental crescentic glomerulonephritis	N/A	N/A	N/A	N/A	N/A	N/A	N/A	N/A	N/A	N/A
Sinus-node dysfunction	N/A	N/A	N/A	N/A	N/A	N/A	N/A	N/A	N/A	N/A
Collagen type IV inherited nephropathy	N/A	N/A	N/A	N/A	N/A	N/A	N/A	N/A	N/A	N/A
Pressure overload hypertrophy	N/A	N/A	N/A	N/A	N/A	N/A	N/A	N/A	N/A	N/A
Atrophy of renal cortex	N/A	N/A	N/A	N/A	N/A	N/A	N/A	N/A	N/A	N/A
Inoperable chronic thromboembolic pulmonary hypertension	N/A	N/A	N/A	N/A	N/A	N/A	N/A	N/A	N/A	N/A
Advanced chronic heart	N/A	N/A	N/A	N/A	N/A	N/A	N/A	N/A	N/A	N/A

failure										
Metastatic liver tumor	N/A	N/A	N/A	N/A	N/A	N/A	N/A	N/A	N/A	N/A
T wave changes	N/A	N/A	N/A	N/A	N/A	N/A	N/A	N/A	N/A	N/A
Primary biliary cirrhosis	N/A	N/A	N/A	N/A	N/A	N/A	N/A	N/A	N/A	N/A
Recurrent hepatocellular carcinoma	N/A	N/A	N/A	N/A	N/A	N/A	N/A	N/A	N/A	N/A
Hypoplasia of mesangial cells	N/A	N/A	N/A	N/A	N/A	N/A	N/A	N/A	N/A	N/A
Early stage myocardial infarction	N/A	N/A	N/A	N/A	N/A	N/A	N/A	N/A	N/A	N/A
Hypertrophy of left ventricle	N/A	N/A	N/A	N/A	N/A	N/A	N/A	N/A	N/A	N/A
Child-Pugh class A advanced hepatocellular carcinoma	N/A	N/A	N/A	N/A	N/A	N/A	N/A	N/A	N/A	N/A
Familial glomerulopathy	N/A	N/A	N/A	N/A	N/A	N/A	N/A	N/A	N/A	N/A
Stage IV primary biliary cirrhosis	N/A	N/A	N/A	N/A	N/A	N/A	N/A	N/A	N/A	N/A
Hypertrophy of ventricular wall	N/A	N/A	N/A	N/A	N/A	N/A	N/A	N/A	N/A	N/A
Chronic allograft	N/	N/A	N/A	N/A	N/A	N/	N/A	N/A	N/	N/A

nephropathy	A					A			A	
Non-valvular atrial fibrillation	N/A	N/A	N/A	N/A	N/A	N/A	N/A	N/A	N/A	N/A
Chronic hepatitis C	N/A	N/A	N/A	N/A	N/A	N/A	N/A	N/A	N/A	N/A
Cardiac valvular form autosomal recessive Ehlers-Danlos syndrome	N/A	N/A	N/A	N/A	N/A	N/A	N/A	N/A	N/A	N/A
Brugada syndrome	N/A	N/A	N/A	N/A	N/A	N/A	N/A	N/A	N/A	N/A
Focal glomerulonephritis	N/A	N/A	N/A	N/A	N/A	N/A	N/A	N/A	N/A	N/A
Familial steroid-resistant nephrotic syndrome	N/A	N/A	N/A	N/A	N/A	N/A	N/A	N/A	N/A	N/A
Catecholaminergic polymorphic ventricular tachycardia type 1	N/A	N/A	N/A	N/A	N/A	N/A	N/A	N/A	N/A	N/A
Primary pulmonary hypertension	N/A	N/A	N/A	N/A	N/A	N/A	N/A	N/A	N/A	N/A
Anthracycline-induced	N/A	N/A	N/A	N/A	N/A	N/A	N/A	N/A	N/A	N/A

cardiotoxicity										
Nephromegaly	N/A	N/A	N/A	N/A	N/A	N/A	N/A	N/A	N/A	N/A
Hepatorenal syndrome	N/A	N/A	N/A	N/A	N/A	N/A	N/A	N/A	N/A	N/A
Cardiomyopathy of left ventricle	N/A	N/A	N/A	N/A	N/A	N/A	N/A	N/A	N/A	N/A
Acute myocarditis	N/A	N/A	N/A	N/A	N/A	N/A	N/A	N/A	N/A	N/A
Severe renal hypodysplasia	N/A	N/A	N/A	N/A	N/A	N/A	N/A	N/A	N/A	N/A
Catecholaminergic polymorphic ventricular tachycardia type 2	N/A	N/A	N/A	N/A	N/A	N/A	N/A	N/A	N/A	N/A
Acyanotic congenital heart disease	N/A	N/A	N/A	N/A	N/A	N/A	N/A	N/A	N/A	N/A
Hepatitis C virus-related hepatocellular carcinoma	N/A	N/A	N/A	N/A	N/A	N/A	N/A	N/A	N/A	N/A
Stable disease stage heart failure	N/A	N/A	N/A	N/A	N/A	N/A	N/A	N/A	N/A	N/A
End-stage renal failure	N/A	N/A	N/A	N/A	N/A	N/A	N/A	N/A	N/A	N/A

Lipidosis of renal glomerulus	N/A	N/A	N/A	N/A	N/A	N/A	N/A	N/A	N/A	N/A
Cryptogenic cirrhosis	N/A	N/A	N/A	N/A	N/A	N/A	N/A	N/A	N/A	N/A
Progressive hepatocellular carcinoma	N/A	N/A	N/A	N/A	N/A	N/A	N/A	N/A	N/A	N/A
Hypertrophy of heart septum	N/A	N/A	N/A	N/A	N/A	N/A	N/A	N/A	N/A	N/A
Familial ventricular fibrillation	N/A	N/A	N/A	N/A	N/A	N/A	N/A	N/A	N/A	N/A
Inoperable hepatocellular carcinoma	N/A	N/A	N/A	N/A	N/A	N/A	N/A	N/A	N/A	N/A
Congenitally corrected transposition of the great arteries	N/A	N/A	N/A	N/A	N/A	N/A	N/A	N/A	N/A	N/A
Symptomatic stage iodine-refractory liver metastasis	N/A	N/A	N/A	N/A	N/A	N/A	N/A	N/A	N/A	N/A
Diastolic heart failure	N/A	N/A	N/A	N/A	N/A	N/A	N/A	N/A	N/A	N/A
Familial pulmonary hypertension	N/A	N/A	N/A	N/A	N/A	N/A	N/A	N/A	N/A	N/A

Dilated cardiomyopathy 3B	N/A	N/A	N/A	N/A	N/A	N/A	N/A	N/A	N/A	N/A
Intrahepatic cholestasis	N/A	N/A	N/A	N/A	N/A	N/A	N/A	N/A	N/A	N/A
Frasier syndrome	N/A	N/A	N/A	N/A	N/A	N/A	N/A	N/A	N/A	N/A
Alcoholic cirrhosis	N/A	N/A	N/A	N/A	N/A	N/A	N/A	N/A	N/A	N/A
Alcoholic steatohepatitis	N/A	N/A	N/A	N/A	N/A	N/A	N/A	N/A	N/A	N/A
Expansion of mesangial cells	N/A	N/A	N/A	N/A	N/A	N/A	N/A	N/A	N/A	N/A
Primary glomerulonephritis	N/A	N/A	N/A	N/A	N/A	N/A	N/A	N/A	N/A	N/A
Hepatotoxicity of hepatocytes	N/A	N/A	N/A	N/A	N/A	N/A	N/A	N/A	N/A	N/A
Paroxysmal atrial flutter	N/A	N/A	N/A	N/A	N/A	N/A	N/A	N/A	N/A	N/A
Sick sinus syndrome type 2 with cardiac noncompaction and ascending aorta dilation	N/A	N/A	N/A	N/A	N/A	N/A	N/A	N/A	N/A	N/A
Nonsyndromic congenital heart	N/A	N/A	N/A	N/A	N/A	N/A	N/A	N/A	N/A	N/A

disease										
Galloway-Mowat syndrome 7	N/A	N/A	N/A	N/A	N/A	N/A	N/A	N/A	N/A	N/A
Lupus nephritis WHO class III/IV	N/A	N/A	N/A	N/A	N/A	N/A	N/A	N/A	N/A	N/A
Congestion of glomerular capillary	N/A	N/A	N/A	N/A	N/A	N/A	N/A	N/A	N/A	N/A
Small cell undifferentiated hepatoblastoma	N/A	N/A	N/A	N/A	N/A	N/A	N/A	N/A	N/A	N/A
Familial sick sinus syndrome	N/A	N/A	N/A	N/A	N/A	N/A	N/A	N/A	N/A	N/A
Primary pulmonary hypertension 1	N/A	N/A	N/A	N/A	N/A	N/A	N/A	N/A	N/A	N/A
Dysfunction of liver	N/A	N/A	N/A	N/A	N/A	N/A	N/A	N/A	N/A	N/A
Atrial flutter	N/A	N/A	N/A	N/A	N/A	N/A	N/A	N/A	N/A	N/A
Congenital long QT syndrome	N/A	N/A	N/A	N/A	N/A	N/A	N/A	N/A	N/A	N/A
Recurrent tachyarrhythmia	N/A	N/A	N/A	N/A	N/A	N/A	N/A	N/A	N/A	N/A
Shprintzen syndrome	N/A	N/A	N/A	N/A	N/A	N/A	N/A	N/A	N/A	N/A

Dilated cardiomyopathy type 1EE	N/A	N/A	N/A	N/A	N/A	N/A	N/A	N/A	N/A	N/A
Symptomatic stage chronic systolic heart failure	N/A	N/A	N/A	N/A	N/A	N/A	N/A	N/A	N/A	N/A
Systemic lupus erythematosus nephritis	N/A	N/A	N/A	N/A	N/A	N/A	N/A	N/A	N/A	N/A
Moderate hepatic fibrosis	N/A	N/A	N/A	N/A	N/A	N/A	N/A	N/A	N/A	N/A
Non-obstructive coronary artery disease	N/A	N/A	N/A	N/A	N/A	N/A	N/A	N/A	N/A	N/A
Paroxysmal atrial fibrillation	N/A	N/A	N/A	N/A	N/A	N/A	N/A	N/A	N/A	N/A
Abnormal morphology of mesangial cells	N/A	N/A	N/A	N/A	N/A	N/A	N/A	N/A	N/A	N/A
Dilated cardiomyopathy 1A	N/A	N/A	N/A	N/A	N/A	N/A	N/A	N/A	N/A	N/A
Hypertrophy of cardiac anterior wall	N/A	N/A	N/A	N/A	N/A	N/A	N/A	N/A	N/A	N/A
Left ventricular noncompaction	N/A	N/A	N/A	N/A	N/A	N/A	N/A	N/A	N/A	N/A

BCLC stage C hepatocellular carcinoma	N/A	N/A	N/A	N/A	N/A	N/A	N/A	N/A	N/A	N/A
Calcific aortic valve stenosis	N/A	N/A	N/A	N/A	N/A	N/A	N/A	N/A	N/A	N/A
Dysplasia of hepatocytes	N/A	N/A	N/A	N/A	N/A	N/A	N/A	N/A	N/A	N/A
Locally advanced hepatocellular carcinoma	N/A	N/A	N/A	N/A	N/A	N/A	N/A	N/A	N/A	N/A
Dilated cardiomyopathy with left ventricular noncompaction type 1c	N/A	N/A	N/A	N/A	N/A	N/A	N/A	N/A	N/A	N/A
Glomerulosclerosis of mesangium	N/A	N/A	N/A	N/A	N/A	N/A	N/A	N/A	N/A	N/A
Dilated cardiomyopathy type 1JJ	N/A	N/A	N/A	N/A	N/A	N/A	N/A	N/A	N/A	N/A
Systolic heart failure	N/A	N/A	N/A	N/A	N/A	N/A	N/A	N/A	N/A	N/A
Catecholaminergic polymorphic ventricular tachycardia	N/A	N/A	N/A	N/A	N/A	N/A	N/A	N/A	N/A	N/A

Hepatosplenic T-cell lymphoma	N/A	N/A	N/A	N/A	N/A	N/A	N/A	N/A	N/A	N/A
Quantity of apoptotic kidney cell lines	N/A	N/A	N/A	N/A	N/A	N/A	N/A	N/A	N/A	N/A
Focal nodular hyperplasia	N/A	N/A	N/A	N/A	N/A	N/A	N/A	N/A	N/A	N/A
Neoplasia of hepatocytes	N/A	N/A	N/A	N/A	N/A	N/A	N/A	N/A	N/A	N/A
Wolff-Parkinson-White syndrome	N/A	N/A	N/A	N/A	N/A	N/A	N/A	N/A	N/A	N/A
Mild hepatic fibrosis	N/A	N/A	N/A	N/A	N/A	N/A	N/A	N/A	N/A	N/A
Acute myocardial infarction	N/A	N/A	N/A	N/A	N/A	N/A	N/A	N/A	N/A	N/A
BCLC stage B primary hepatocellular carcinoma	N/A	N/A	N/A	N/A	N/A	N/A	N/A	N/A	N/A	N/A
Autosomal 2 visceral heterotaxy	N/A	N/A	N/A	N/A	N/A	N/A	N/A	N/A	N/A	N/A
Biliary cirrhosis	N/A	N/A	N/A	N/A	N/A	N/A	N/A	N/A	N/A	N/A
Atresia of tricuspid valve	N/A	N/A	N/A	N/A	N/A	N/A	N/A	N/A	N/A	N/A

Dominant dilated cardiomyopathy	N/A	N/A	N/A	N/A	N/A	N/A	N/A	N/A	N/A	N/A
Stable chronic heart failure	N/A	N/A	N/A	N/A	N/A	N/A	N/A	N/A	N/A	N/A
Increased synthesis of CRP	N/A	N/A	N/A	N/A	N/A	N/A	N/A	N/A	N/A	N/A
Severe hepatitis	N/A	N/A	N/A	N/A	N/A	N/A	N/A	N/A	N/A	N/A
Nephrotoxicity	N/A	N/A	N/A	N/A	N/A	N/A	N/A	N/A	N/A	N/A
Primary hepatocellular carcinoma	N/A	N/A	N/A	N/A	N/A	N/A	N/A	N/A	N/A	N/A
Acute ST-elevation myocardial infarction	N/A	N/A	N/A	N/A	N/A	N/A	N/A	N/A	N/A	N/A
Progressive familial intrahepatic cholestasis type 1	N/A	N/A	N/A	N/A	N/A	N/A	N/A	N/A	N/A	N/A
Bleeding of renal glomerulus	N/A	N/A	N/A	N/A	N/A	N/A	N/A	N/A	N/A	N/A
Pulmonary hypertension WHO functional class IV chronic	N/A	N/A	N/A	N/A	N/A	N/A	N/A	N/A	N/A	N/A

thromboembolic pulmonary hypertension										
Symptomatic stage bradycardia	N/A	N/A	N/A	N/A	N/A	N/A	N/A	N/A	N/A	N/A
C3 glomerulopathy	N/A	N/A	N/A	N/A	N/A	N/A	N/A	N/A	N/A	N/A
Inherited primary arrhythmia syndrome	N/A	N/A	N/A	N/A	N/A	N/A	N/A	N/A	N/A	N/A
Enlargement of cardiomyocytes	N/A	N/A	N/A	N/A	N/A	N/A	N/A	N/A	N/A	N/A
Increased Levels of Bilirubin	N/A	N/A	N/A	N/A	N/A	N/A	N/A	N/A	N/A	N/A
Mild glomerulonephritis	N/A	N/A	N/A	N/A	N/A	N/A	N/A	N/A	N/A	N/A
Initiation of regeneration of liver	N/A	N/A	N/A	N/A	N/A	N/A	N/A	N/A	N/A	N/A
Brugada syndrome type 8	N/A	N/A	N/A	N/A	N/A	N/A	N/A	N/A	N/A	N/A
Congenital anomaly of aortic arch	N/A	N/A	N/A	N/A	N/A	N/A	N/A	N/A	N/A	N/A
Enlargement of heart ventricle	N/A	N/A	N/A	N/A	N/A	N/A	N/A	N/A	N/A	N/A

Left ventricular dilation	N/A	N/A	N/A	N/A	N/A	N/A	N/A	N/A	N/A	N/A
Postoperative pulmonary embolism	N/A	N/A	N/A	N/A	N/A	N/A	N/A	N/A	N/A	N/A
Repetitive paroxysmal supraventricular tachycardia	N/A	N/A	N/A	N/A	N/A	N/A	N/A	N/A	N/A	N/A
Enlargement of left ventricle	N/A	N/A	N/A	N/A	N/A	N/A	N/A	N/A	N/A	N/A
Familial arrhythmia	N/A	N/A	N/A	N/A	N/A	N/A	N/A	N/A	N/A	N/A
Cell death of Kupffer cells	N/A	N/A	N/A	N/A	N/A	N/A	N/A	N/A	N/A	N/A
Dilated cardiomyopathy type 1MM	N/A	N/A	N/A	N/A	N/A	N/A	N/A	N/A	N/A	N/A
Sick sinus syndrome type 3	N/A	N/A	N/A	N/A	N/A	N/A	N/A	N/A	N/A	N/A
Abnormal morphology of mesangium	N/A	N/A	N/A	N/A	N/A	N/A	N/A	N/A	N/A	N/A
Recurrent ventricular fibrillation	N/A	N/A	N/A	N/A	N/A	N/A	N/A	N/A	N/A	N/A
Short QT syndrome	N/A	N/A	N/A	N/A	N/A	N/A	N/A	N/A	N/A	N/A

Recurrent chronic thromboembolic pulmonary hypertension	N/A	N/A	N/A	N/A	N/A	N/A	N/A	N/A	N/A	N/A
Proliferation of hepatoblasts	N/A	N/A	N/A	N/A	N/A	N/A	N/A	N/A	N/A	N/A
Acute tubular necrosis	N/A	N/A	N/A	N/A	N/A	N/A	N/A	N/A	N/A	N/A
Short-QT syndrome 3	N/A	N/A	N/A	N/A	N/A	N/A	N/A	N/A	N/A	N/A
Hypertrophy of distal tubule	N/A	N/A	N/A	N/A	N/A	N/A	N/A	N/A	N/A	N/A
Familial isolated autosomal dominant noncompaction of left ventricular myocardium	N/A	N/A	N/A	N/A	N/A	N/A	N/A	N/A	N/A	N/A
Membranous glomerulonephritis	N/A	N/A	N/A	N/A	N/A	N/A	N/A	N/A	N/A	N/A
Hyperplasia of renal tubule	N/A	N/A	N/A	N/A	N/A	N/A	N/A	N/A	N/A	N/A
Stage III primary biliary cirrhosis	N/A	N/A	N/A	N/A	N/A	N/A	N/A	N/A	N/A	N/A
Wolff Parkinson White syndrome	N/A	N/A	N/A	N/A	N/A	N/A	N/A	N/A	N/A	N/A

with hypertrophic cardiomyopathy										
Hepatoblastoma	N/A	N/A	N/A	N/A	N/A	N/A	N/A	N/A	N/A	N/A
Nonfatal myocardial infarction	N/A	N/A	N/A	N/A	N/A	N/A	N/A	N/A	N/A	N/A
Early-onset premature coronary artery disease	N/A	N/A	N/A	N/A	N/A	N/A	N/A	N/A	N/A	N/A
Inherited arrhythmia syndrome	N/A	N/A	N/A	N/A	N/A	N/A	N/A	N/A	N/A	N/A
Enlargement of right ventricle	N/A	N/A	N/A	N/A	N/A	N/A	N/A	N/A	N/A	N/A
Hypoplasia of right heart	N/A	N/A	N/A	N/A	N/A	N/A	N/A	N/A	N/A	N/A
Atrial septal defect type 3	N/A	N/A	N/A	N/A	N/A	N/A	N/A	N/A	N/A	N/A
Chronic autoimmune hepatitis	N/A	N/A	N/A	N/A	N/A	N/A	N/A	N/A	N/A	N/A
Stage II acute myocardial infarction	N/A	N/A	N/A	N/A	N/A	N/A	N/A	N/A	N/A	N/A
Poorly differentiated	N/A	N/A	N/A	N/A	N/A	N/A	N/A	N/A	N/A	N/A

hepatocellular carcinoma										
Interrupted aortic arch	N/A	N/A	N/A	N/A	N/A	N/A	N/A	N/A	N/A	N/A
Electrical alternation of heart	N/A	N/A	N/A	N/A	N/A	N/A	N/A	N/A	N/A	N/A
Acute congestive heart failure	N/A	N/A	N/A	N/A	N/A	N/A	N/A	N/A	N/A	N/A
Metastatic hepatocellular carcinoma	N/A	N/A	N/A	N/A	N/A	N/A	N/A	N/A	N/A	N/A
Myocytolysis of heart	N/A	N/A	N/A	N/A	N/A	N/A	N/A	N/A	N/A	N/A
Stage V chronic kidney disease	N/A	N/A	N/A	N/A	N/A	N/A	N/A	N/A	N/A	N/A
Child-Pugh class A recurrent hepatocellular carcinoma	N/A	N/A	N/A	N/A	N/A	N/A	N/A	N/A	N/A	N/A
Persistent chronic thromboembolic pulmonary hypertension	N/A	N/A	N/A	N/A	N/A	N/A	N/A	N/A	N/A	N/A
Local hepatocellular carcinoma	N/A	N/A	N/A	N/A	N/A	N/A	N/A	N/A	N/A	N/A
Interauricular	N/	N/A	N/A	N/A	N/A	N/	N/A	N/A	N/	N/A

communication	A					A			A	
Left ventricular noncompaction type 3	N/A	N/A	N/A	N/A	N/A	N/A	N/A	N/A	N/A	N/A
Symptomatic stage atrial fibrillation	N/A	N/A	N/A	N/A	N/A	N/A	N/A	N/A	N/A	N/A
Oxidative stress response of cardiomyocytes	N/A	N/A	N/A	N/A	N/A	N/A	N/A	N/A	N/A	N/A
Ann Arbor stage I-IV hepatosplenic T-cell lymphoma	N/A	N/A	N/A	N/A	N/A	N/A	N/A	N/A	N/A	N/A
Severe acute renal failure	N/A	N/A	N/A	N/A	N/A	N/A	N/A	N/A	N/A	N/A
Andersen syndrome	N/A	N/A	N/A	N/A	N/A	N/A	N/A	N/A	N/A	N/A
Autosomal dominant pulmonary arterial hypertension	N/A	N/A	N/A	N/A	N/A	N/A	N/A	N/A	N/A	N/A
Dilated cardiomyopathy type 1AA	N/A	N/A	N/A	N/A	N/A	N/A	N/A	N/A	N/A	N/A
Familial isolated dilated cardiomyopathy	N/A	N/A	N/A	N/A	N/A	N/A	N/A	N/A	N/A	N/A

Dilated cardiomyopathy 2a	N/A	N/A	N/A	N/A	N/A	N/A	N/A	N/A	N/A	N/A
Apoptosis of proximal tubule epithelial cells	N/A	N/A	N/A	N/A	N/A	N/A	N/A	N/A	N/A	N/A
Suppression of hepatocellular carcinoma	N/A	N/A	N/A	N/A	N/A	N/A	N/A	N/A	N/A	N/A
BCLC stage B hepatocellular carcinoma	N/A	N/A	N/A	N/A	N/A	N/A	N/A	N/A	N/A	N/A
Myocardial hypertrophy	N/A	N/A	N/A	N/A	N/A	N/A	N/A	N/A	N/A	N/A
Renal hypodysplasia/aplasia type 3	N/A	N/A	N/A	N/A	N/A	N/A	N/A	N/A	N/A	N/A
Pulmonary hypertension WHO functional class III pulmonary hypertension	N/A	N/A	N/A	N/A	N/A	N/A	N/A	N/A	N/A	N/A
Size of liver tumor	N/A	N/A	N/A	N/A	N/A	N/A	N/A	N/A	N/A	N/A
Abnormal morphology of glomerular capillary	N/A	N/A	N/A	N/A	N/A	N/A	N/A	N/A	N/A	N/A

Refractory ventricular fibrillation	N/A	N/A	N/A	N/A	N/A	N/A	N/A	N/A	N/A	N/A
Type 1 hepatorenal syndrome	N/A	N/A	N/A	N/A	N/A	N/A	N/A	N/A	N/A	N/A
Unresectable liver cholangiocarcinoma	N/A	N/A	N/A	N/A	N/A	N/A	N/A	N/A	N/A	N/A
Increased release of albumin	N/A	N/A	N/A	N/A	N/A	N/A	N/A	N/A	N/A	N/A
Agenesis of kidney	N/A	N/A	N/A	N/A	N/A	N/A	N/A	N/A	N/A	N/A
Steroid dependent nephrotic syndrome	N/A	N/A	N/A	N/A	N/A	N/A	N/A	N/A	N/A	N/A
Familial arrhythmogenic right ventricular dysplasia type 1	N/A	N/A	N/A	N/A	N/A	N/A	N/A	N/A	N/A	N/A
Spontaneous coronary artery disease	N/A	N/A	N/A	N/A	N/A	N/A	N/A	N/A	N/A	N/A
Stenosis of pulmonary artery	N/A	N/A	N/A	N/A	N/A	N/A	N/A	N/A	N/A	N/A
Mild to moderate stage heart	N/A	N/A	N/A	N/A	N/A	N/A	N/A	N/A	N/A	N/A

failure										
Susceptibility to myocardial infarction	N/A	N/A	N/A	N/A	N/A	N/A	N/A	N/A	N/A	N/A
Chronic viral hepatitis	N/A	N/A	N/A	N/A	N/A	N/A	N/A	N/A	N/A	N/A
Acute hepatitis	N/A	N/A	N/A	N/A	N/A	N/A	N/A	N/A	N/A	N/A
Abnormal morphology of coronary artery	N/A	N/A	N/A	N/A	N/A	N/A	N/A	N/A	N/A	N/A
Abnormal morphology of renal glomerulus	N/A	N/A	N/A	N/A	N/A	N/A	N/A	N/A	N/A	N/A
Calcification of aortic valve	N/A	N/A	N/A	N/A	N/A	N/A	N/A	N/A	N/A	N/A
Symptomatic stage heart failure	N/A	N/A	N/A	N/A	N/A	N/A	N/A	N/A	N/A	N/A
Familial atrial septal defect	N/A	N/A	N/A	N/A	N/A	N/A	N/A	N/A	N/A	N/A
Right ventricular dysfunction	N/A	N/A	N/A	N/A	N/A	N/A	N/A	N/A	N/A	N/A
Sick sinus syndrome 2 with cardiac noncompaction	N/A	N/A	N/A	N/A	N/A	N/A	N/A	N/A	N/A	N/A
Brugada	N/	N/A	N/A	N/A	N/A	N/	N/A	N/A	N/	N/A

syndrome type 9	A					A			A	
Cardiac decompensation	N/A	N/A	N/A	N/A	N/A	N/A	N/A	N/A	N/A	N/A
Chronic heart failure acute decompensated disease stage heart failure	N/A	N/A	N/A	N/A	N/A	N/A	N/A	N/A	N/A	N/A
Nonischemic dilated cardiomyopathy	N/A	N/A	N/A	N/A	N/A	N/A	N/A	N/A	N/A	N/A
Pyelonephritis	N/A	N/A	N/A	N/A	N/A	N/A	N/A	N/A	N/A	N/A
Experimentally induced cirrhosis	N/A	N/A	N/A	N/A	N/A	N/A	N/A	N/A	N/A	N/A
Enlargement of heart chamber	N/A	N/A	N/A	N/A	N/A	N/A	N/A	N/A	N/A	N/A
Arrhythmogenic right ventricular cardiomyopathy	N/A	N/A	N/A	N/A	N/A	N/A	N/A	N/A	N/A	N/A
Hypertrophy of cardiomyocytes	N/A	N/A	N/A	N/A	N/A	N/A	N/A	N/A	N/A	N/A
Autosomal recessive Finnish congenital nephrotic syndrome	N/A	N/A	N/A	N/A	N/A	N/A	N/A	N/A	N/A	N/A
Liver cholangiocarcino	N/A	N/A	N/A	N/A	N/A	N/A	N/A	N/A	N/A	N/A

ma										
Alcoholic hepatitis	N/A	N/A	N/A	N/A	N/A	N/A	N/A	N/A	N/A	N/A
Chronic heart failure	N/A	N/A	N/A	N/A	N/A	N/A	N/A	N/A	N/A	N/A
Fatal myocardial infarction	N/A	N/A	N/A	N/A	N/A	N/A	N/A	N/A	N/A	N/A
Child-Pugh class A metastatic hepatocellular carcinoma	N/A	N/A	N/A	N/A	N/A	N/A	N/A	N/A	N/A	N/A
Survival of mesangial cells	N/A	N/A	N/A	N/A	N/A	N/A	N/A	N/A	N/A	N/A
Child-Pugh class B7 advanced hepatocellular carcinoma	N/A	N/A	N/A	N/A	N/A	N/A	N/A	N/A	N/A	N/A
Atrophy of renal glomerulus	N/A	N/A	N/A	N/A	N/A	N/A	N/A	N/A	N/A	N/A
Congenital atrioventricular valve abnormality	N/A	N/A	N/A	N/A	N/A	N/A	N/A	N/A	N/A	N/A
Right ventricular dilatation	N/A	N/A	N/A	N/A	N/A	N/A	N/A	N/A	N/A	N/A
Pulmonary arterial hypertension associated with	N/A	N/A	N/A	N/A	N/A	N/A	N/A	N/A	N/A	N/A

congenital heart disease										
Dilated cardiomyopathy type 1FF	N/A	N/A	N/A	N/A	N/A	N/A	N/A	N/A	N/A	N/A
Transformation of kidney cells	N/A	N/A	N/A	N/A	N/A	N/A	N/A	N/A	N/A	N/A
Decreased localization of albumin	N/A	N/A	N/A	N/A	N/A	N/A	N/A	N/A	N/A	N/A
Susceptibility to hepatitis C virus	N/A	N/A	N/A	N/A	N/A	N/A	N/A	N/A	N/A	N/A
Vasospasm of coronary artery	N/A	N/A	N/A	N/A	N/A	N/A	N/A	N/A	N/A	N/A
X-linked dilated cardiomyopathy	N/A	N/A	N/A	N/A	N/A	N/A	N/A	N/A	N/A	N/A
Hepatitis B virus-related hepatocellular carcinoma	N/A	N/A	N/A	N/A	N/A	N/A	N/A	N/A	N/A	N/A
Postmyocardial infarction syndrome	N/A	N/A	N/A	N/A	N/A	N/A	N/A	N/A	N/A	N/A
Focal segmental glomerulosclerosis type 9	N/A	N/A	N/A	N/A	N/A	N/A	N/A	N/A	N/A	N/A
Dilation of glomerular capsule	N/A	N/A	N/A	N/A	N/A	N/A	N/A	N/A	N/A	N/A

Advanced hepatocellular carcinoma	N/A	N/A	N/A	N/A	N/A	N/A	N/A	N/A	N/A	N/A
Heart failure with preserved ejection fraction	N/A	N/A	N/A	N/A	N/A	N/A	N/A	N/A	N/A	N/A
Autosomal recessive progressive familial intrahepatic cholestasis type 1	N/A	N/A	N/A	N/A	N/A	N/A	N/A	N/A	N/A	N/A
Delay in autoimmune glomerulonephritis	N/A	N/A	N/A	N/A	N/A	N/A	N/A	N/A	N/A	N/A
Susceptibility to hepatitis B virus	N/A	N/A	N/A	N/A	N/A	N/A	N/A	N/A	N/A	N/A
Metastasis of hepatocellular carcinoma	N/A	N/A	N/A	N/A	N/A	N/A	N/A	N/A	N/A	N/A
Hypertrophy of heart	N/A	N/A	N/A	N/A	N/A	N/A	N/A	N/A	N/A	N/A
Ventricular hypertrophy	N/A	N/A	N/A	N/A	N/A	N/A	N/A	N/A	N/A	N/A
Abnormal morphology of mesangial matrix	N/A	N/A	N/A	N/A	N/A	N/A	N/A	N/A	N/A	N/A

Paroxysmal familial ventricular fibrillation	N/A	N/A	N/A	N/A	N/A	N/A	N/A	N/A	N/A	N/A
Hypertrophy of heart cells	N/A	N/A	N/A	N/A	N/A	N/A	N/A	N/A	N/A	N/A
Rupture of left ventricle	N/A	N/A	N/A	N/A	N/A	N/A	N/A	N/A	N/A	N/A
Hypertrophy of renal tubule	N/A	N/A	N/A	N/A	N/A	N/A	N/A	N/A	N/A	N/A
Pulmonary hypertension WHO functional class III chronic thromboembolic pulmonary hypertension	N/A	N/A	N/A	N/A	N/A	N/A	N/A	N/A	N/A	N/A
Hypertrophy of myocardium	N/A	N/A	N/A	N/A	N/A	N/A	N/A	N/A	N/A	N/A
WHO functional class II pulmonary arterial hypertension	N/A	N/A	N/A	N/A	N/A	N/A	N/A	N/A	N/A	N/A
Atrial hypertrophy	N/A	N/A	N/A	N/A	N/A	N/A	N/A	N/A	N/A	N/A
BCLC stage C advanced hepatocellular	N/A	N/A	N/A	N/A	N/A	N/A	N/A	N/A	N/A	N/A

carcinoma										
Symptomatic stage cardiomyopathic heart failure	N/A	N/A	N/A	N/A	N/A	N/A	N/A	N/A	N/A	N/A
Decreased synthesis of albumin	N/A	N/A	N/A	N/A	N/A	N/A	N/A	N/A	N/A	N/A
Pulmonary hypertension WHO functional class III pulmonary hypertensive arterial disease	N/A	N/A	N/A	N/A	N/A	N/A	N/A	N/A	N/A	N/A
Symptomatic drug induced pulmonary arterial hypertension	N/A	N/A	N/A	N/A	N/A	N/A	N/A	N/A	N/A	N/A
Increased release of alkaline phosphatase	N/A	N/A	N/A	N/A	N/A	N/A	N/A	N/A	N/A	N/A
Proliferative glomerulonephritis	N/A	N/A	N/A	N/A	N/A	N/A	N/A	N/A	N/A	N/A
Hyperplasia of cardiomyocytes	N/A	N/A	N/A	N/A	N/A	N/A	N/A	N/A	N/A	N/A
Decreased	N/	N/A	N/A	N/A	N/A	N/	N/A	N/A	N/	N/A

activation of albumin	A					A			A	
Interstitial fibrosis of myocardium	N/A	N/A	N/A	N/A	N/A	N/A	N/A	N/A	N/A	N/A
Compensated cirrhosis	N/A	N/A	N/A	N/A	N/A	N/A	N/A	N/A	N/A	N/A
Eisenmenger complex	N/A	N/A	N/A	N/A	N/A	N/A	N/A	N/A	N/A	N/A
Hepatosplenomegaly	N/A	N/A	N/A	N/A	N/A	N/A	N/A	N/A	N/A	N/A
Familial ventricular tachycardia	N/A	N/A	N/A	N/A	N/A	N/A	N/A	N/A	N/A	N/A
Enlargement of heart	N/A	N/A	N/A	N/A	N/A	N/A	N/A	N/A	N/A	N/A
Early stage hepatocellular carcinoma	N/A	N/A	N/A	N/A	N/A	N/A	N/A	N/A	N/A	N/A
WHO functional class I pulmonary arterial hypertension	N/A	N/A	N/A	N/A	N/A	N/A	N/A	N/A	N/A	N/A
Dysfunction of podocytes	N/A	N/A	N/A	N/A	N/A	N/A	N/A	N/A	N/A	N/A
Primary liver cancer	N/A	N/A	N/A	N/A	N/A	N/A	N/A	N/A	N/A	N/A

Enlargement of heart cells	N/A	N/A	N/A	N/A	N/A	N/A	N/A	N/A	N/A	N/A
Proliferation of proximal tubule cells	N/A	N/A	N/A	N/A	N/A	N/A	N/A	N/A	N/A	N/A
Advanced liver tumor	N/A	N/A	N/A	N/A	N/A	N/A	N/A	N/A	N/A	N/A
Non-rheumatic aortic stenosis	N/A	N/A	N/A	N/A	N/A	N/A	N/A	N/A	N/A	N/A
Acute alcoholic hepatitis	N/A	N/A	N/A	N/A	N/A	N/A	N/A	N/A	N/A	N/A
Toxin induced pulmonary arterial hypertension	N/A	N/A	N/A	N/A	N/A	N/A	N/A	N/A	N/A	N/A
Invasive hepatocellular carcinoma	N/A	N/A	N/A	N/A	N/A	N/A	N/A	N/A	N/A	N/A
Intrahepatic cholestasis of pregnancy type 1	N/A	N/A	N/A	N/A	N/A	N/A	N/A	N/A	N/A	N/A
Familial coronary artery disease	N/A	N/A	N/A	N/A	N/A	N/A	N/A	N/A	N/A	N/A
Infantile cholestatic hepatitis syndrome	N/A	N/A	N/A	N/A	N/A	N/A	N/A	N/A	N/A	N/A

Hyperbilirubinemia	N/A	N/A	N/A	N/A	N/A	N/A	N/A	N/A	N/A	N/A
Regeneration of myocardium	N/A	N/A	N/A	N/A	N/A	N/A	N/A	N/A	N/A	N/A
Dilated cardiomyopathy 1S	N/A	N/A	N/A	N/A	N/A	N/A	N/A	N/A	N/A	N/A
Stable disease stage hypertensive heart failure	N/A	N/A	N/A	N/A	N/A	N/A	N/A	N/A	N/A	N/A
Left ventricular noncompaction type 6	N/A	N/A	N/A	N/A	N/A	N/A	N/A	N/A	N/A	N/A
Long-QT syndrome	N/A	N/A	N/A	N/A	N/A	N/A	N/A	N/A	N/A	N/A
Acute heart failure	N/A	N/A	N/A	N/A	N/A	N/A	N/A	N/A	N/A	N/A
Drug-induced hepatotoxicity	N/A	N/A	N/A	N/A	N/A	N/A	N/A	N/A	N/A	N/A
Symptomatic stage systolic heart failure	N/A	N/A	N/A	N/A	N/A	N/A	N/A	N/A	N/A	N/A
Vasodilation of renal artery	N/A	N/A	N/A	N/A	N/A	N/A	N/A	N/A	N/A	N/A
Acute deep vein thrombosis with pulmonary	N/A	N/A	N/A	N/A	N/A	N/A	N/A	N/A	N/A	N/A

embolism										
Hypertrophy of ventricular myocytes	N/A	N/A	N/A	N/A	N/A	N/A	N/A	N/A	N/A	N/A
Familial renal hypoplasia	N/A	N/A	N/A	N/A	N/A	N/A	N/A	N/A	N/A	N/A
Decreased hematocrit of organism	N/A	N/A	N/A	N/A	N/A	N/A	N/A	N/A	N/A	N/A
Dilated cardiomyopathy 1g	N/A	N/A	N/A	N/A	N/A	N/A	N/A	N/A	N/A	N/A
Stable coronary artery disease	N/A	N/A	N/A	N/A	N/A	N/A	N/A	N/A	N/A	N/A
BCLC stage B advanced hepatocellular carcinoma	N/A	N/A	N/A	N/A	N/A	N/A	N/A	N/A	N/A	N/A
Dilated cardiomyopathy secondary to drug	N/A	N/A	N/A	N/A	N/A	N/A	N/A	N/A	N/A	N/A
Progressive liver metastasis	N/A	N/A	N/A	N/A	N/A	N/A	N/A	N/A	N/A	N/A
Hypodysplasia of kidney	N/A	N/A	N/A	N/A	N/A	N/A	N/A	N/A	N/A	N/A
Endocarditis	N/A	N/A	N/A	N/A	N/A	N/A	N/A	N/A	N/A	N/A

BCLC stage C primary hepatocellular carcinoma	N/A	N/A	N/A	N/A	N/A	N/A	N/A	N/A	N/A	N/A
Hereditary nephritis	N/A	N/A	N/A	N/A	N/A	N/A	N/A	N/A	N/A	N/A
Hypoplasia of aortic arch	N/A	N/A	N/A	N/A	N/A	N/A	N/A	N/A	N/A	N/A
Decompensated cirrhosis of liver	N/A	N/A	N/A	N/A	N/A	N/A	N/A	N/A	N/A	N/A
Chronic New York Heart Association class II-IV heart failure	N/A	N/A	N/A	N/A	N/A	N/A	N/A	N/A	N/A	N/A
Left ventricular systolic dysfunction	N/A	N/A	N/A	N/A	N/A	N/A	N/A	N/A	N/A	N/A
Size of glomerular crescent	N/A	N/A	N/A	N/A	N/A	N/A	N/A	N/A	N/A	N/A
Vasodilation of kidney	N/A	N/A	N/A	N/A	N/A	N/A	N/A	N/A	N/A	N/A
Persistent atrial fibrillation	N/A	N/A	N/A	N/A	N/A	N/A	N/A	N/A	N/A	N/A
Severe hepatic fibrosis	N/A	N/A	N/A	N/A	N/A	N/A	N/A	N/A	N/A	N/A
New York Heart	N/	N/A	N/A	N/A	N/A	N/	N/A	N/A	N/	N/A

Association class II heart failure	A					A			A	
Pericarditis	N/A	N/A	N/A	N/A	N/A	N/A	N/A	N/A	N/A	N/A
Long QT syndrome 1	N/A	N/A	N/A	N/A	N/A	N/A	N/A	N/A	N/A	N/A
Advanced stage intrahepatic cholestasis	N/A	N/A	N/A	N/A	N/A	N/A	N/A	N/A	N/A	N/A
Familial atrial fibrillation type 7	N/A	N/A	N/A	N/A	N/A	N/A	N/A	N/A	N/A	N/A
Supraventricular tachycardia	N/A	N/A	N/A	N/A	N/A	N/A	N/A	N/A	N/A	N/A
Nephrotic syndrome type 11	N/A	N/A	N/A	N/A	N/A	N/A	N/A	N/A	N/A	N/A
Hepatitis subtype infantile hepatitis syndrome	N/A	N/A	N/A	N/A	N/A	N/A	N/A	N/A	N/A	N/A